



City Research Online

City, University of London Institutional Repository

Citation: McGuinness Abdollahi, Zahra (2015). Intra-operative optical monitoring of bowel tissue viability based on photoplethysmography and laser doppler flowmetry. (Unpublished Doctoral thesis, City University London)

This is the accepted version of the paper.

This version of the publication may differ from the final published version.

Permanent repository link: <https://openaccess.city.ac.uk/id/eprint/13684/>

Link to published version:

Copyright: City Research Online aims to make research outputs of City, University of London available to a wider audience. Copyright and Moral Rights remain with the author(s) and/or copyright holders. URLs from City Research Online may be freely distributed and linked to.

Reuse: Copies of full items can be used for personal research or study, educational, or not-for-profit purposes without prior permission or charge. Provided that the authors, title and full bibliographic details are credited, a hyperlink and/or URL is given for the original metadata page and the content is not changed in any way.

City Research Online:

<http://openaccess.city.ac.uk/>

publications@city.ac.uk

INTRA-OPERATIVE OPTICAL MONITORING OF BOWEL TISSUE VIABILITY BASED ON PHOTOPLETHYSMOGRAPHY AND LASER DOPPLER FLOWMETRY

A thesis submitted for the degree of
Doctor of Philosophy at City University London

ZAHRA MCGUINNESS ABDOLLAHI

Biomedical Engineering Research Centre,
School of Engineering and Mathematical Sciences,
City University London,
Northampton Square, London, EC1V 0HB

March 2015



THE FOLLOWING PARTS OF THIS THESIS HAVE BEEN REDACTED FOR COPYRIGHT REASONS:

p26: Fig 2.1
p28: Fig 2.2
p29: Fig 2.3, Fig 2.4
p31: Fig 2.5
p32: Fig 2.6
p41: Fig 3.1
p43: Fig 3.2, Fig 3.3
p44: Fig 3.4
p45: Fig 3.5
p51: Fig 3.7
p52: Fig 3.8, 3.9
p53: Fig 3.10
p54: Fig 3.11
p55: Fig 3.12
p56: Fig 3.13
p71: Fig 5.1
p72: Fig 5.2
p79: Fig 5.5
p84: Fig 6.1
p99: Fig 7.5 (a)
p101: Fig 7.5

THE FOLLOWING PREVIOUSLY PUBLISHED PAPERS HAVE BEEN REDACTED FOR COPYRIGHT REASONS:

pp219-221:

Z. Abdollahi, J. P. Phillips, Kyriacou, P.A. (2015), Evaluation of the optical interference in a combined measurement system used for assessment of tissue blood flow. In *SPIE Proceedings* Vol. 9315.

doi: [10.1117/12.2079760](https://doi.org/10.1117/12.2079760)

pp223-225:

Abdollahi, Z., Phillips, J.P. Kyriacou, P.A. (2013), Evaluation of a combined photoplethysmography (PPG) and laser Doppler flowmetry (LDF) measurement system for simultaneously monitoring blood flow at different pressure. In *Engineering in Medicine and Biology Society (EMBC), 2013 35th Annual International Conference of the IEEE*, pp1728-1731.

url: <http://dx.doi.org/10.1109/EMBC.2013.6609853>

Determination of bowel viability in patients undergoing bowel resection is essential in gastrointestinal surgery. One of the most common operations in gastrointestinal surgery is *bowel resection* for patients who have different kinds of bowel cancer or any other occlusion in which anastomosis has to be carried out following the removal of an unhealthy segment of the bowel. Monitoring blood flow in abdominal surgery especially intraoperatively would be a valuable tool for prevention of a postoperative anastomosis complication (e.g. anastomotic leak, which is the main complication after colorectal resection).

The development of a continuous method for monitoring perfusion of bowel tissue would assist in early detection of inadequate blood supply which then help to reduce the occurrence of an anastomosis complication. Although various monitoring techniques have been proposed to assess intestinal viability intraoperatively, none of these techniques have proved to be reliable enough to replace visual observation. Therefore, to date there is no widely accepted and readily available intraoperative technique to reliably assess the viability of bowel tissue.

The aim of this study was to combine the established techniques, laser Doppler flowmetry (LDF) and Photoplethysmography (PPG), into one probe intended for assessment of perfusion in abdominal tissue during bowel resection intraoperatively. In PPG, changes in transmission of light through tissue due to pulsation of small arteries can be monitored whereas in LDF microcirculatory blood cell velocity and flux can be studied. Such a probe could alert the surgeon immediately of any compromise in blood flow so further investigation and, if necessary, therapeutic steps can be applied immediately to prevent severe consequences. Therefore, custom reflectance PPG along with LDF sensor was designed and built in the form of a probe to investigate the changes in blood volume, blood flow and arterial oxygen saturation in patients undergoing bowel resection.

The instrumentation was designed successfully and the data was saved for the further analysis. Twenty-four patients undergoing bowel resection were recruited for monitoring of perfusion and blood flow intraoperatively; twenty had undergone laparoscopy and the remainder had a laparotomy operation. Eight different measurements were performed during each trial. The results revealed that the probe could be an indicator of evaluating perfusion and blood flow changes at different stages of the surgery. The results also suggest that laser Doppler is more sensitive to artefact compared to PPG. Differences in amplitude of PPG between different measurements reveal that the sensor does detect changes in blood volume and flow confirming that it has the ability to verify that pulsatile flow is being preferentially preserved at the last step of the resection procedure (at the edges of the anastomosis sites after anastomosis is been constructed).

Abstract2
Table of Contents4
List of Figures10
List of Tables.....18
Acknowledgments20
Declaration21
Glossary22

Chapter One

Introducton23
 1.1 Thesis outlines24

Chapter Two

Review Of Anatomy And Physiology Of Gastrointestinal Tract .26
 2.1 Overview of the gastrointestinal tract.....26
 2.2 Peritoneum27
 2.3 Stomach.....27
 2.4 Small intestine28
 2.4.1 Duodenum, Jejunum and Ileum30
 2.5 Large intestine31
 2.6 Blood Supply of the stomach and intestine.....32
 2.6.1 The celiac artery33
 2.6.2 Superior Mesenteric Artery (SMA)33
 2.6.3 Inferior Mesenteric Artery (IMA)34
 2.6.4 Marginal Artery34
 2.6.5 Griffiths' Point and Sudeck's point.....34
 2.7 Veins.....36
 2.7.1 Portal Vein.....36
 2.7.2 The tributaries of the portal vein.....36
 2.8 Differences between small and large intestine38
 2.9 Internal differences38

Chapter Three

Bowel Resection40

3.1 Definition of the bowel resection	40
3.1.1 Small Bowel Resection	40
3.1.2 Large Bowel Resection	40
3.2 Bowel Obstruction (BO)	41
3.2.1 Small Bowel Obstruction (SMO).....	41
Adhesions	42
Hernias	43
Tumours	44
3.2.2 Large Bowel Obstruction (LBO)	44
Colorectal Cancer	44
Volvulus.....	44
Diverticular disease	45
3.3 Colorectal Cancer (CRC)	45
Symptoms	46
Treatment	46
3.4 Bowel Resection for Colorectal Cancer	46
3.5 Surgical Techniques for Bowel Resection	47
3.5.1 Laparoscopic and Laparotomy Procedures	47
3.5.2 Anastomosis.....	48
3.6 Types of Surgical Operation for Bowel Resection for CRC	49
3.7 Surgical Treatment for Colon Cancer	50
3.7.1 Right Hemi-Colectomy	50
3.7.2 Extended Right Hemi-Colectomy	51
3.7.3 Transverse Colectomy	52
3.7.4 Left Hemi-Colectomy.....	53
3.7.5 Sigmoid Colectomy	53
3.8 Surgical Treatment for Rectal Cancer	54
3.8.1 High Anterior Resection	54
3.8.2 Low Anterior Resection	54
3.8.3 Abdominoperineal Resection	55

Chapter Four

Intraoperative Determination of Intestinal Viability	57
4.1 Introduction	57
4.2 Monitoring Methods for the Detection of Intestinal Viability	59
4.3 First Group.....	59
4.3.1 Polagraphic Measurements of Oxygen Tension	59
4.3.2 Doppler Ultrasound	59
4.3.3 Hydrogen Gas Clearance.....	60
4.3.4 Radioisotope Studies	61
4.3.5 Bowel Wall Contractility Measurements	61
4.4 Second Group	61
4.4.1 Pulse Oximetry	61
4.4.2 Near Infrared and Visible Light Spectrophotometry (NIRS & VLS)	62
4.4.3 Intravital Microscopy (IVM).....	64
4.4.4 Fluorometry and Laser Fluorescence Angiography	64

4.4.5 Infrared Imaging	65
4.4.6 Laser Doppler Flowmetry	65
4.4.7 pH Monitoring	66
4.4.8 Microdialysis	67
4.5 Discussion	67

Chapter Five

Photoplethysmography and Pulse Oximetry	69
5.1 Introduction	69
5.2 Photoplethysmography	69
5.3 History of Photoplethysmography	70
5.4 The Photoplethysmographic Waveform	70
5.5 Photoplethysmography Operation	72
5.6 Pulse Oximetry	73
5.7 Pulse Oximeter and Blood Oxygen Saturation	75
5.8 Light Emitting Diode (LEDs)	76
5.9 Photodetector	78
5.10 Principle of the Pulse Oximeter	78
5.10.1 Beer-Lambert law	79
5.11 Typical Photoplethysmographic Waveform	80
5.12 Calibration of Pulse Oximeters	81
5.13 Pulse Oximetry Limitations	82

Chapter Six

Laser Doppler Flowmetry	83
6.1 Introduction	83
6.2 Principle of LDF	85
6.3 Light Source	88
6.4 LDF Techniques	90
6.4.1 Laser Doppler Perfusion Monitoring (LDPM)	90
6.4.2 Laser Doppler Perfusion Imaging (LDPI)	91
6.4.3 CMOS Imager	93
6.5 Limitation of LDF	94
6.5.1 Calibration Standard	94
6.5.2 Biological Zero	94
6.5.3 Motion Artefacts	95
6.5.4 Multiple Doppler Shifts: a theoretical limitation	95

Chapter Seven

Development of a Combined PPG/LDF Optical Probe	96
--	-----------

7.1 Introduction	96
7.2 Combined Sensor: Design and Construction for the PPG probe.....	96
7.2.1 PPG sensor	97
Light sources (LEDs)	97
Photo-detector.....	99
7.2.2 Sensor construction	100
7.3 Combined sensor: Laser Doppler probe and monitor.....	101
7.4 Probe sheath	102
7.5 Evaluation of the combined sensor.....	103
7.5.1 First volunteer study	104
Experimental Method	104
Data Analysis and Statistics.....	104
Results	105
Discussion and Conclusion	107
7.5.2 Second volunteer study.....	107
Experimental Method	108
<i>a. First study</i>	108
<i>b. Second study</i>	108
<i>c. Third study</i>	108
Data Analysis	109
Results	109
Discussion and Conclusion	110
7.6 Thermal evaluation on the combined sensor.....	111
7.6.1 Thermal Safety Testing	111
7.6.2 Experimental Methods	112
7.6.3 Results	112
7.7 Sensor design and safety test summary.....	113

Chapter Eight

Development and Evaluation of the Combined Measurement System	114
8.1 Introduction	114
8.2 Instrumentation	114
PPG unit.....	115
Block Diagram of the System.....	116
Timing Circuit	118
Multiplexer/Driver of two Wavelengths.....	120
Transimpedance Amplifier.....	123
De-multiplexer	124
Band-pass Filter (Low and High pass Filter)	127
Amplifier	127
8.3 Laser Doppler Monitor	127

Chapter Nine

Data Acquisition and Development of Virtual Instrument (VIs) for Signal Processing, Data Storage and Display	130
9.1 Introduction to LabVIEW	130
The front panel	131
The block diagram	131
9.2 Two Wavelengths and laser Doppler Signal Acquisition VI	132
NI-DAQmx	132
DAQmx Create Channel.....	134
DAQmx Timing (Sample Clock)	135
DAQmx Start Task	135
9.3 Algorithm for continuous signal display	135
While-Loop.....	135
For-Loop.....	136
DAQmx Read	137
9.4 Estimation of the bowel tissue SpO ₂	139
DAQmxBase Clear Task VI	141
9.5 VI for Data Storage	143
9.6 Front panel of the VI	144

Chapter Ten

Intra-operative PPG-LDF Assessment of Bowel Tissue Viability	147
10.1 Introduction	147
10.2 Methods	148
10.2.1 Patients	148
10.2.2 Measurements	148
10.3 Intraoperative Measurements	152
10.3.1 Mobilization	152
10.3.2 Over Tumour	152
10.3.3 Pre-Ligation	152
10.3.4 Post-Ligation	153
10.3.5 Pre Anastomosis Proximal and Distal	153
10.3.6 Post Anastomosis Proximal and Distal	153
10.4 Methods of Analysing the Acquired Data.....	154
10.4.1 Filtration and Normalisation of the Acquired Signals	156
10.5 Results of Analysing the Acquired Data	158
10.5.1 Mobilisation Measurements	158
10.5.2 Over Tumour Measurements	159
10.5.3 Pre and Post Ligation Measurements	161
10.5.4 Pre and Post Anastomosis Measurements	164
10.6 Comparison PPG amplitude between all measurements	169
10.7 Comparison of LDF Flux between all measurements	176
10.8 Arterial Blood Oxygen Saturation (SpO ₂) Estimations	178

10.9 Statistical Analysis179

Chapter Eleven

Discussion, Conclusion and Future Work183
11.1 Discussions and Conclusions183
11.2 Future Work187
 A: Initial Study188
 B: Follow-up Study189
 C: Final Study.....190

References 191

Appendices

Appendix A

Technical Specification for Potoplethysmographic System208

Appendix B

Technical Specification for laser Doppler monitor and probe210

Appendix C

Ethical Approval Confirmation212

Own Publications 217

LIST OF FIGURES

Figure 2.1 Picture of the gastrointestinal (GI) tract starts from the mouth and proceeds to the pharynx, oesophagus, stomach, duodenum, jejunum, intestines (small and large), rectum and finally the anal canal (4).	26
Figure 2.2 Picture of the major abdominal organs including stomach, small and large intestines (10).....	28
Figure 2.3 The internal structure of stomach, from outer to inner including: the serous (peritoneal), muscular, submucous and mucous coats (12).....	29
Figure 2.4 Picture of small and large intestine, the small bowel is placed in the central and lower part of the abdominal cavity surrounded by the large intestine (10).....	29
Figure 2.5 The structure of villi: microscopic finger-like projections. Villi help nutrients in the food absorb more efficiently into the body (16).	31
Figure 2.6 Parts of large intestine including Ascending Colon, Descending Colon, Sigmoid and Rectum (17)	32
Figure 2.7 The arterial blood supply of stomach including five main arteries: left gastric, right gastric, right gastro-epiploic, left gastro-epiploic and short gastric (19).....	33
Figure 2.8 Arterial blood supply to the colon including: the celiac artery, superior mesenteric artery (SMA), inferior mesenteric artery (IMA), and branches of the intestinal iliac artery (IIA) (21).....	34
Figure 2.9 Marginal arteries and Griffith's along with Sudeck's points that is indicated by shaded areas (27).....	35
Figure 2.10 Formation of portal vein behind neck of pancreas made up by the union of superior mesenteric vein and splenic vein (28).	37
Figure 2.11 Veins of portal circulation including: Splenic veins, Inferior mesenteric vein, Superior mesenteric vein, Left gastric vein, Right gastric and Cystic veins (28).....	37

Figure 2.12 Some external and internal differences between the small and large intestine (28).....	39
Figure 3.1 Left side: a blockage in the small intestine as a result of scar tissue (adhesions) right side: a partial blockage in the colon caused by a tumour (cancer) (37).....	41
Figure 3.2 One example of blockage in small and large bowel (43)	43
Figure 3.3 Hernia in small bowel in which a segment of the small intestine sticks out through this weakened area (43)	43
Figure 3.4 Large bowel obstructions are caused by colorectal cancer (43).....	44
Figure 3.5 Large bowel obstructions are caused by volvulus in which a segment of intestinal twists around itself (50)	45
Figure 3.6 An example of anastomosis, an end-to-end anastomosis, in which the ends of the bowel are joining together to create an anastomosis using the stiches (64).....	49
Figure 3.7 A right hemi-colectomy, A: tumour in cecum, B: ileocolic anastomosis (65).....	51
Figure 3.8 Extended right colectomy, A: tumour in splenic flexure, B: ileocolic anastomosis (63).....	52
Figure 3.9 Transverse colectomy, A: tumour in transverse colon, B: anastomosis of ascending and descending colon (65)	52
Figure 3.10 Left hemi-colectomy, A: tumour in descending colon, B: anastomosis of transverse and sigmoid colon (65).....	53
Figure 3.11 Sigmoid colectomy, A: tumour in sigmoid colon, b: anastomosis of the upper rectum and descending colon (65).....	54
Figure 3.12 Low anterior resection: A: tumour in rectum, B: anastomosis of the anus and the rest of sigmoid colon (65).....	55
Figure 3.13 Abdominoperineal resection, A: tumour in rectum, B: colostomy (65)	56
Figure 5.1 PPG: the origin of the signal (AC, DC) and absorbed light (151).....	71

Figure 5.2 Two main operations of sending light, (right) transmission method, (left) Reflectance method (154).....	72
Figure 5.3 Pulse oximeter device	76
Figure 5.4 Absorption levels of oxygenated and deoxygenated (169).....	77
Figure 5.5 Pulsatile signals observed during pulse oximetry (173).....	79
Figure 5.6 Light of intensity i_0 enters the medium is transmitted with intensity with i_t , l is the path with the path length through the medium	80
Figure 5.7 Dicrotic notch in a normal arterial pulsation waveform	81
Figure 6.1 Principles of operation in laser Doppler flowmetry. A laser beam is directed into a target tissue. Light waves are reflected and scattered after contacting with moving objects like red blood cells. The backscattered light (both unshifted and Doppler shifted) then can be detected and received by a photodetector (190).....	84
Figure 6.2 The Doppler effect: The frequency of the light scattered by the moving objects (RBC) with velocity v in the direction defined by α_s is shifted in frequency by an amount Δf compared to that of the light of frequency f_i , which hits the RBC at an angle α_i (179).....	86
Figure 6.3 Laser Doppler perfusion monitoring system (194)	87
Figure 6.4 The volume of light penetration is generally 1 mm^3 or smaller (193)..	89
Figure 6.5 A diagram of (a) LDPM and (b) LDPI geometries on a tissue model. LD laser diode, PD photodetector (191).....	92
Figure 6.6 Schematic illustrations of the various LDF modalities, LDPM (a), LDPI (b), and CMOS imager (c).....	93
Figure 7.1 A schematic of the combined PPG -LDF probe, including the photodiode, two LEDs and laser Doppler with 8 mm outside diameter.....	97
Figure 7.2 Left R LED (221) and Right IR LED (222).....	99
Figure 7.3 The photodiode used for the PPG part (BPW 43 s) (223)	99
Figure 7.4 The three-dimensional concept of the combined probe.....	100

Figure 7.5 The vp8c titanium disc probe (224) (a) and the laser Doppler monitor (b).....	101
Figure 7.6 Photograph of the combined probe with two LEDs, one photodiode and the laser Doppler probe tip of 8 mm in diameter	102
Figure 7.7 The sterile probe ready to use for measurement	103
Figure 7.8 (a) IR_{AC} , (b) R_{AC} and (c) laser Doppler signals at zero mmhg for 10 second.....	106
Figure 7.9 (a) IR_{AC} , (b) R_{AC} and (c) laser doppler signals at 75 mmhg for 10 second.....	106
Figure 7.10 (a) IR_{AC} , (b) R_{AC} and (c) laser doppler signals at 135 mmhg for 10 second.....	106
Figure 7.11 R_{AC} amplitude at various pressure from zero to 135 mmhg.....	106
Figure 7.12 IR_{AC} amplitude at various pressure from zero to 135 mmhg.....	106
Figure 7.13 Laser Doppler amplitude at various pressure from zero to 135 mmhg06	106
Figure 7.14 Blood oxygen saturation (SpO_2) during hypoperfusion from zero to 135 mmhg	107
Figure 7.15 Graph showing changes in temperature induced on skin by the combined probe	112
Figure 8.1 A simple block diagram of PPG/LDF process system	114
Figure 8.2 Instrumentation: box containing data acquisition card, PCB board, power supply and the connection to computer and probe	115
Figure 8.3 Photograph of the back panel of monitoring system.....	116
Figure 8.4 Photograph of the front panel of monitoring system	116
Figure 8.5 The circuit of PPG measurement system	117
Figure 8.6 The block diagram of the PPG/LDF system.....	118
Figure 8.7 A schematic of the entire measurement system	119
Figure 8.8 Generating the timing pulses for pulse oximeters (227)	120

Figure 8.9 (a) Functional and (b) Timing diagram for HEF4520B	121
Figure 8.10 (c) HEF5420B 4-bit binary counter used in this circuit, CP1 is the clock signal as the input and counter produces three signals Q1, Q2 and Q3. Q1 has frequency $f_{CP1}/2$, Q2 has frequency $f_{CP1}/4$ and Q3 has frequency $f_{CP1}/8$	121
Figure 8.11 Schematic drawing of the LEDs current driver circuit	122
Figure 8.12 Light source timing diagram	123
Figure 8.13 Transimpedance amplifier circuit	124
Figure 8.14 Sample and hold IC pin out diagram,	125
Figure 8.15 The de-multiplexer circuit. The pins on the LF398 sample-and-hold chip are: pin 3 (photodiode output/analogue input), pin 8 (logic input) and pin 5 (analogue output)	126
Figure 8.16 Timing diagram for the de-multiplexer. The dotted lines indicate the times when sampling of the photodetector output occurs	126
Figure 8.17 Photograph of Laser Doppler Flowmetry monitor	128
Figure 8.18 Photograph of measurement system. Note: in the photograph the distal tip of the probe is being held between thumb and forefinger.....	128
Figure 9.1 Block diagram of the PPG/LDF processing system and the connection with the VI.....	130
Figure 9.2 Simple diagram of the virtual instrument (VI).....	133
Figure 9.3 Basic DAQmx used in the VI developed to continuously acquire PPG and LDF signals	134
Figure 9.4 Diagram of DAQmx create Virtual Channel	134
Figure 9.5 Diagram of DAQmx Timing	135
Figure 9.6 Diagram of DAQmx Start Task.....	135
Figure 9.7 While-loop	136
Figure 9.8 For-loop.....	137
Figure 9.9 Algorithm for continuous signal display.....	138
Figure 9.10 Diagram of DAQmx Read	138

Figure 9.11 Index Array Function	139
Figure 9.12 Array Max and Min Functions	140
Figure 9.13 Mean function	140
Figure 9.14 Illustration of the algorithm used for calculating R_R and SpO_2 for the PPG.....	142
Figure 9.15 Diagram of DAQmx Base Clear Task VI.....	143
Figure 9.16 Array to Spreadsheet String Function.....	143
Figure 9.17 Write to Text File Function	143
Figure 9.18 Get Date/Time String Function	144
Figure 9.19 The VI used to save all the acquired analogue signals.....	144
Figure 9.20 Front panel of the virtual instrument	146
Figure 10.1 <i>in vivo</i> monitoring for anastomosis measurement during laparoscopy	154
Figure 10.2 Selected period of the data for analysis	156
Figure 10.3 Raw signals with noise artefact (a) and after filtration (b).....	157
Figure 10.4 10-second sample of red and infrared ac PPGs and LDF obtained atypical mobilisation measurements (case No 6).....	158
Figure 10.5 10-second sample of typical red and infrared ac PPGs and LDF obtained at over tumour measurements (case No 7).....	160
Figure 10.6 10-second sample of typical red and infrared AC PPGs and LDF at pre ligation measurements (case No 7)	162
Figure 10.7 10-second sample of typical red and infrared AC PPGs and LDF at post ligation measurements (case No 7).....	162
Figure 10.8 mean (\pm SD) of normalised AC IR PPG amplitudes averaged for all patients for (a) pre-ligation IR (n=10), post-ligation IR (n=16), (b) pre-ligation R (n=6), and post-ligation R (n=12)	164
Figure 10.9 10-second sample of typical PPG and LDF signals at pre anastomosis measurement at the proximal end (case No 5).....	165

Figure 10.10 10-second sample of typical PPG and LDF signals at pre-anastomosis measurement from the distal end (case No 5).....	165
Figure 10.11 10-second sample of typical PPG and LDF signals at post-anastomosis measurement from the proximal end (case No 21).....	166
Figure 10.12 10-second sample of typical PPG and LDF signals at post-anastomosis measurement from the distal end (case No 21).....	166
Figure 10.13 Mean (\pm SD) for normalised AC IR PPG amplitudes averaged for all patients in pre-anastomosis-proximal (n=16), pre-anastomosis-distal (n=4), post anastomosis-proximal (n=14) and post-anastomosis distal (n=9).....	169
Figure 10.14 Mean (\pm SD) for normalised AC R PPG amplitudes averaged for all patients in pre anastomosis-proximal (n=10), pre-anastomosis-distal (n=3), post anastomosis-proximal (n=10) and post-anastomosis distal (n=7).....	169
Figure 10.15 Bar graph of the mean (\pm SD) normalised R and IR across all the measurements averaged for all patients	171
Figure 10.16 Percentage change for IR PPG amplitudes for all measurements in all patients. Reference; 1: mobilisation, 2: over tumour, 3: pre-ligation, 4: post-ligation, 5: pre-anastomosis proximal, 6: pre-anastomosis distal, 7: post-anastomosis proximal, 8: post-anastomosis distal	172
Figure 10.17 Mean R PPG amplitudes with the percentage change for all measurements in all patients. Reference; 1: mobilisation, 2: over tumour, 3: pre-ligation, 4: post-ligation, 5: pre-anastomosis proximal, 6: pre anastomosis distal, 7: post-anastomosis-proximal, 8: post-anastomosis distal.....	173
Figure 10.18 percentage change in amplitude for (a) normalised IR and (b) normalised R PPG in pre and post ligation	174
Figure 10.19 percentage change in amplitude for normalised IR PPG in pre and post anastomosis in proximal and distal site	174
Figure 10.20 Percentage change in amplitude for normalized R PPG in pre and post anastomosis in proximal and distal site	175
Figure 10.21 Amplitude of DC IR in all measurements showing the blood volume	175

Figure 10.22 Detected signals, showing that LDF was more sensitive to motion artefacts than PPG	176
Figure 10.23 Mean (\pm SD) flux (PU) for all measurements averaged for all patients	177
Figure 10.24 Percentages change in PU across all the measurements	177
Figure 10.25 Mean (\pm SD) SpO ₂ estimated values by sensor from bowel compared to the values measured with the commercial device, from the finger for all measurements averaged for all patients	179

LIST OF TABLES

Table 3.1 Causes of Small Bowel Obstruction (40)	42
Table 3.2 Types of colorectal resection (57)	50
Table 5.1 Factors that affects pulse oximetry	82
Table 6.1 Laser Doppler applications.....	88
Table 7.1 R LED specifications and electrical/optical characteristics (220)	98
Table 7.2 IR LED specifications and electrical/optical characteristics (221)	98
Table 7.3 Characteristic and maximum rating of the photodiode used on the PPG part (BPW 43 S) (222).....	100
Table 7.4 Mean values from measurements in the first study (a), second study (b) and in the third study (c).....	109
Table 7.5 Temperature change with LEDs of and on.....	113
Table 10.1 Details of all patients recruited to the study including the measurements for each trial. Reference; 1: Mobilisation, 2: Over Tumour, 3: Pre Ligation, 4: Post Ligation, 5: Pre Anastomosis Proximal, 6: Pre Anastomosis Distal, 7: Post Anastomosis Proximal, 8: Post Anastomosis Distal measurement (Measurements will be explained in detail in the following section)	151
Table 10.2: Mean normalised AC PPG amplitudes and LDF flux from all subjects at mobilisation	159
Table 10.3 Mean normalised PPG AC amplitudes and LDF flux from all subjects at over tumour.....	161
Table 10.4 Mean normalised PPG AC amplitudes and LDF flux from all subjects at pre and post ligation	163
Table 10.5 Mean normalised PPG AC amplitudes and LDF flux from all subjects at pre and post anastomosis (proximal)	167
Table 10.6 Mean normalised PPG AC amplitudes and LDF flux from all subjects at pre and post anastomosis (distal)	168
Table 10.7 The percentage change in all measurements for R and IR. Reference; 1: Mobilisation, 2: Over Tumour, 3: Pre-Ligation, 4: Post-Ligation, 5: Pre-Anastomosis Proximal, 6: Pre-Anastomosis Distal, 7: Post-Anastomosis Proximal,	

8: Post-Anastomosis Distal	173
Table 10.8 The percentage change in all measurements for R and IR. Reference; 1: Mobilisation, 2: Over Tumour, 3: Pre-Ligation, 4: Post-Ligation, 5: Pre- Anastomosis Proximal, 6: Pre-Anastomosis Distal, 7: Post-Anastomosis Proximal, 8: Post-Anastomosis Distal	178
Table 10.9 Paired T-test between pre and post ligation for AC R and IR amplitudes.....	180
Table 10.10 Paired T-test between pre and post anastomosis in proximal and distal for AC IR amplitudes.....	180
Table 10.11 Paired T-test between pre and post anastomosis in proximal and distal for AC R amplitudes.....	181
Table 10.12 Paired T-test between pre and post ligation for DC R and IR amplitudes.....	181
Table 10.13 Paired T-test between pre and post anastomosis in proximal and distal for DC IR amplitudes.....	181
Table 10.14 Paired T-test between pre and post anastomosis in proximal and distal for DC R amplitudes.....	182
Table 10.15 Paired T-test between pre and post ligation for LDF flux	182
Table 1.16 Paired T-test between pre and post anastomosis in proximal and distal for LDF flux	182

ACKNOWLEDGMENTS

My sincere appreciation and wholehearted gratitude to my supervisor Dr. Justin Phillips for his warm support, great advice and constant inspiration at various stages of the research project. I will forever be thankful to him.

I would like to specially thank my co-supervisor Professor Panayiotis Kyriacou for his diligent academic and professional supervision, valuable guidance, and encouragement during my studies.

Sincere thanks to Mr. Mohamed Thaha of Royal London Hospital for his generous support throughout the project, his kind assistance in recruiting patients for my clinical trials and his great advice when carrying out these trials.

Thanks are also due to Mr. Anthony Rmasanahie of Royal London Hospital for his great cooperation and assistance when carrying out measurements in theatre for the trials. Extra thanks goes to Mr. Shafi Ahmed at same for his help and assistance during these clinical trials.

To all the patients who participated in the project I extend my warmest regards and untold thanks for their contribution. Without their cooperation this project would not have been possible.

I thank the nurses and clinicians at Royal London Hospital Barts, Theatre 1 and 2, especially Victoria and Mary for their kind cooperation.

I would like to acknowledge the support of the City University Doctoral Studentships for the financial assistance offered, and the City University Future Fund for their additional contributions.

I thank my colleagues and friends in the Biomedical Engineering Research Group for sharing their knowledge and this experience with me, with special thanks extended to Tina and James for being there for me when I needed them.

I owe a deep debt of gratitude to my beloved brother, Abbas, as it was his idea that spawned this research project. He provided such great support and advice during the last four years.

To my wonderful husband Mark, I thank him for his steady patience, faithful support, and constant motivation during the inevitable highs and lows of the PhD experience. His enduring love and support throughout the experience was my rock.

Finally I thank my family and parents for their unconditional love, inspiration, moral strength and financial support. Without their endless help my entire academic career would not have been possible.

DECLARATION

I hereby declare that this thesis "*Intra-operative optical monitoring of bowel tissue viability based on photoplethysmography and laser Doppler flowmetry*" is my own work and has been prepared by me under the guidance of Dr. Justin Phillips, Biomedical Engineering Research Group, School of Engineering and Mathematical Sciences, during the years 2010-2014 and has not been submitted anywhere else.

Zahra McGuinness Abdollahi
March 2015

AC	Alternating Current
BZ	Biological Zero
DAQ	Data Acquisition
DC	Direct Current
ECM	Electronic Contractility Meter
Hb	Haemoglobin (also referred to as deoxyhaemoglobin)
HbO ₂	Oxyhaemoglobin
HGC	Hydrogen Gas Clearance
IR	Infrared light
IVM	Intravital Microscopy
LED	Light Emitting Diode
LDF	Laser Doppler Flowmetry
LDPI	Laser Doppler Perfusion Imaging
LDPM	Laser Doppler Perfusion Monitoring
LFA	Laser Fluorescence Angiography
NIRS	Near Infrared Spectrophotometry
PCB	Printed Circuit Board
pCO ₂	Carbon dioxide partial pressure
PPG	Photoplethysmography
PtO ₂	Tissue Oxygen Tension
R	Red light
S _a O ₂	Arterial Oxygen Saturation measured using a haemoximeter
SpO ₂	Arterial blood Oxygen Saturation
StO ₂	Tissue Oxygen Saturation
VI	Virtual Instrument
VLS	Visible Light Spectrophotometry

Introduction

Having a continuous method for monitoring perfusion of bowel tissue is very important and desirable in gastrointestinal surgery since it can assist in the early detection of inadequate blood supply, which can help to reduce the complication and the length of the hospital stay after an operation and also to reduce postoperative morbidity and mortality (1, 2). Several techniques and monitoring devices have been applied for assessing bowel tissue perfusion intraoperatively however each of them have their limitations, some of these limitations include; not easy to use for the operator, are time consuming, invasive and/or expensive. These limitations prevent their routine application in clinical practice for monitoring perfusion in bowel operation. Therefore, to date there is no widely accepted and readily available intraoperative technique to reliably assess the viability of bowel tissue.

This project sets out to develop a new technique for the continuous monitoring of bowel viability. A new processing system was developed utilising the combination of two techniques, photoplethysmography (PPG) along with laser Doppler flowmetry (LDF), suitable for intraoperative monitoring of bowel perfusion, a new combined PPG/LDF sensor was also designed. The goal of this work is to demonstrate that this novel probe may have the capability of continuously and noninvasively monitoring the perfusion of bowel tissue intraoperatively by detecting any changes in volume of arterial blood pulsating and estimating the oxygen saturation using PPG along with estimating the blood flow (the flux) using LDF.

This thesis describes the design, construction and evaluation of the combined system. *In vivo* evaluation was performed in 24 patients at The Royal London Hospital. The methodology of the clinical trials is described. The results from the trials in all patients undergoing bowel resection are presented.

1.1 Thesis Outline

A brief summary of each of the chapters contained in this thesis is presented below.

Chapter 2 presents a review of the anatomy and physiology of the gastrointestinal tract; an emphasis has been given to the intestine, as it is the main part of investigation for this project. The blood supply of the intestine is also presented in detail to give a better explanation of the perfusion of the intestine, which would provide a better understanding of intraoperative measurements in bowel resection.

Chapter 3 presents the different kinds of bowel resection. Bowel obstruction in both small and large intestine is described and more attention has been given to the main large bowel obstruction, colorectal cancer. Surgical treatments for colorectal cancer are presented in more detail, as this was the main focus of this study. And different types of surgical operations for bowel colorectal cancer are presented as well.

Chapter 4 describes a review of the basic principles of photoplethysmography and pulse oximetry. The technology of the pulse oximeter has been explained along with principle of operation, applications of the technique; also limitation of the technique is presented in brief. The two probe configurations utilised in pulse oximetry are described as well.

Chapter 5 covers the basic principle of laser Doppler flowmetry (LDF) technique. Types of perfusion measurements, limitation of the system and LDF application in the gastrointestinal area is also presented.

Chapter 6 discusses which techniques for monitoring the bowel have been taken from the earliest recorded study in 1976 until now. Past and current techniques for intraoperative determination of intestinal viability have been presented, which is the main focus of this project, an overview of the technique is provided for each, followed by the advantages and limitations associated with its use.

[Chapter 7](#) describes the design and development of a new combined sensor for perfusion monitoring of the intestine intraoperatively. The design considerations, construction and optical component selection of a combined dual-wavelength photoplethysmography and LDF are set out in this chapter. Since the sensor will be introduced in theatre to patient's abdomen, sterilisation issues of the probe prior to each trial, which was very important, are also discussed. The two evaluations that were conducted in the laboratory on healthy volunteers are presented as well. These experiments are: (1) Investigation of the optical interference between LDF and PPG, (2) Evaluation of the system's ability to differentiate between states of normal and compromised perfusion.

[Chapter 8](#) goes on to describe the development of a new processing system, which compromises two techniques, photoplethysmographic (PPG) and LDF. Details of the schematic design, choice of components and the construction of the circuits are reviewed. The evaluation has been performed and the results presented as well.

[Chapter 9](#) describes the developed virtual instrument for use in conjunction with the new combined sensor. The LabVIEW software described is used to acquire, display and store the obtained PPG and LDF signals. Details of the algorithms used for estimating SpO₂ values are also covered in this chapter.

[Chapter 10](#) presents the results obtained from all clinical trials on 24 patients undergoing bowel resection performed in The Royal London Hospital. These results include the PPG and LDF amplitude analysis along with the outcome of SpO₂ calculations from all patients.

[Chapter 11](#) presents the conclusions drawn from these studies along with suggestions for future work.

Review Of Anatomy And Physiology Of Gastrointestinal Tract

2.1 Overview of the gastrointestinal tract

The human gastrointestinal (GI) tract refers to all the structures from the mouth to the anus. In fact, the GI starts with the mouth and proceeds to the pharynx, oesophagus, stomach, duodenum, jejunum, intestines (small and large), rectum and finally the anal canal (Figure 2.1). This muscular tube is about 9 m in length (in an adult) and it is under control of the autonomic nervous system (3).

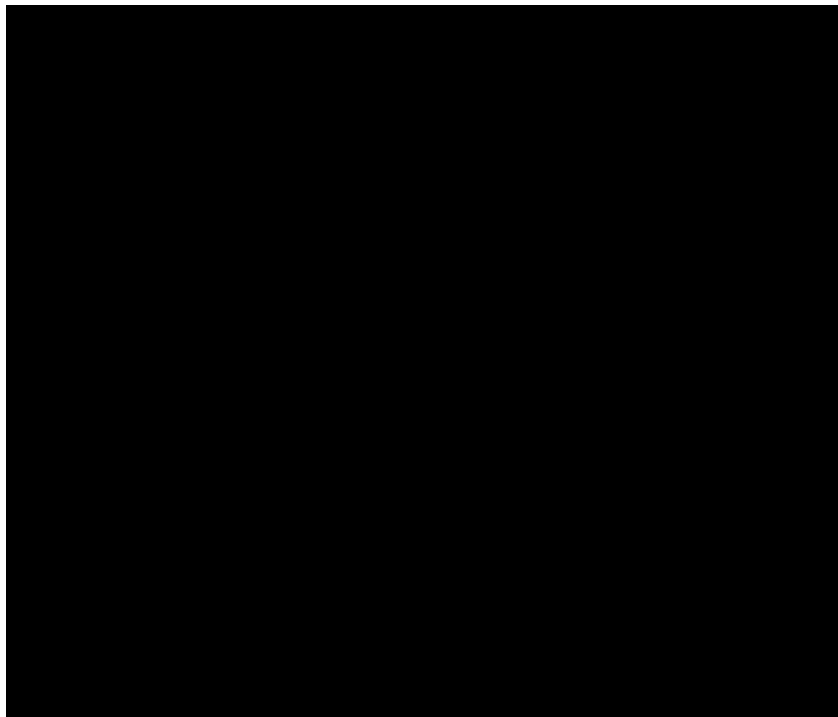


Figure 2.1: Picture of the gastrointestinal (GI) tract starts from the mouth and proceeds to the pharynx, oesophagus, stomach, duodenum, jejunum, intestines (small and large), rectum and finally the anal canal (4).

The responsibility of the GI tract is the breakdown of the food, digestion and absorption of nutrients, and excretion of solid waste. Ingested food cannot be absorbed into the body, in fact food need to break down physically then larger

molecules (e.g. starches) has to be converted to nutrients in order to be absorbed into the blood and then the nutrients are carried to cells throughout the body. This is the initial role of the GI system. So when food is eaten, it moves through each part of the GI tract and then the various digestive fluids and enzymes will mix with it. The salivary glands begin secreting as soon as food is inserted into the mouth, and as the food passes throughout the GI, enzymes secrete in the stomach, small intestine, pancreas and the liver in order for the digestion to continue. The small and large intestines play important roles in digestion with different functions. The most important part of digestion occurs in the small intestine while the responsibility of the large intestine is to absorb water and the excretion of solid waste material (5, 6).

2.2 Peritoneum

The peritoneum is a thin semi-transparent membrane and is multi-layered. It coats the abdominal wall, pelvic cavity and the organs within it. The peritoneum has a shiny surface and secretes a lubricative liquid known as serous fluid. The peritoneum is in two parts: *The parietal peritoneum*, which lines the abdominal wall and *the visceral peritoneum* that covers the external surface of internal organs (viscera). A lot of blood vessels, lymph vessels and nerves supply the peritoneum. The peritoneum forms ligaments, mesenteries, omenta, pouches, pits, and folds while it passes from one organ to another organ and from the organs to the body wall (7).

The mesentery is a fold of two peritoneal layers and is the part of the visceral membrane that connects a membrane-encapsulated organ to the abdominal wall or to another organ (7).

2.3 Stomach

The stomach is one of the main organs of digestion. It has a sac-like shape; and is located between the oesophagus and the intestines (8). It can be seen in Figure 2.2.

Four layers make up the stomach wall, from outer to inner including: the serous (peritoneal), muscular, submucous and mucous coats. The serous, or the peritoneal coat, is a thin layer of loose connective tissue made up by the peritoneum. It is attached to the subjacent muscular coat which is located just under the peritoneal coat and has three layers of non-striated muscles, consisting of outer longitudinal, middle circular and inner oblique layers respectively from outer to inner (8, 9). The internal structure of stomach can be seen in Figure 2.3.

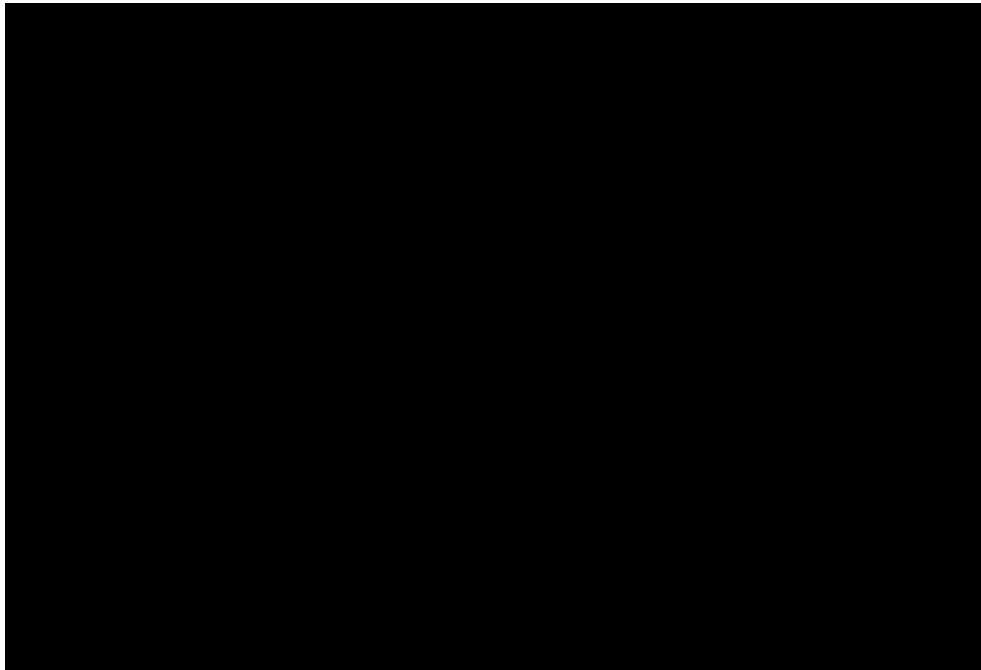


Figure 2.2: Picture of the major abdominal organs including stomach, small and large intestines (10).

2.4 Small Intestine

The longest section of the gastrointestinal (GI) tract is the small intestine (or small bowel). Although it is referred to as small, in fact it is a lot longer than the large bowel (4.3 meter on average). It is thin (or narrow) compared to the large bowel and about 20 mm in diameter. The small bowel is a convoluted tube and a vital organ involved in nutrient absorption, starts from the pylorus and ends at the colic valve. Its length is approximately 7 meters but it diminishes in size. As it can be

seen in Figure 2.4 the small bowel is placed in the central and lower part of the abdominal cavity surrounded by the large intestine (11).

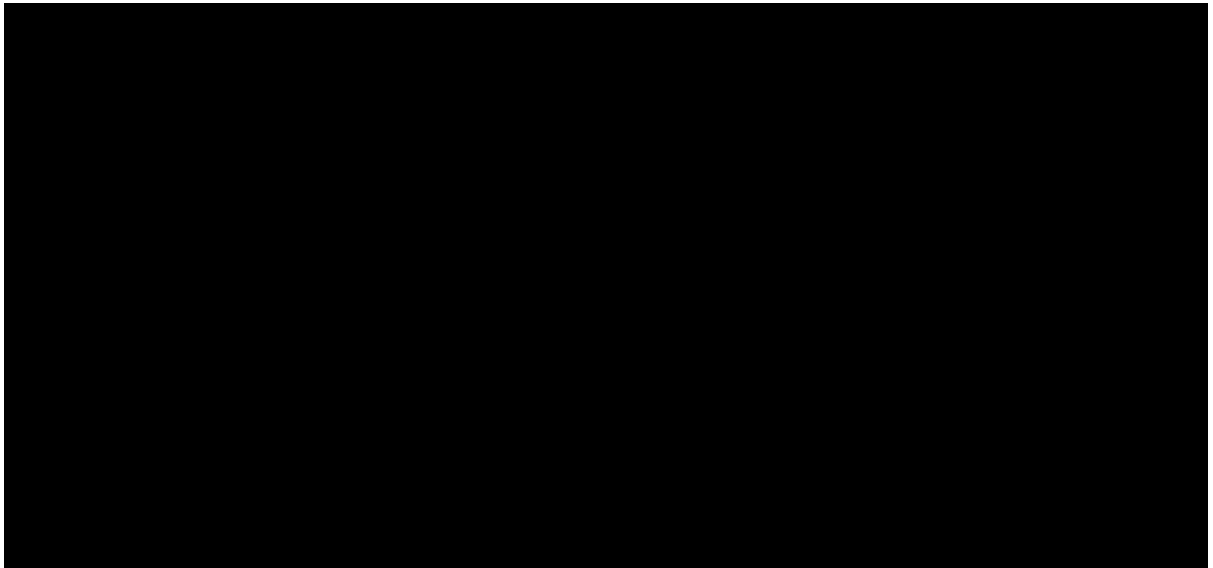


Figure 2.3: The internal structure of stomach, from outer to inner including: the serous (peritoneal), muscular, submucous and mucous coats (12).

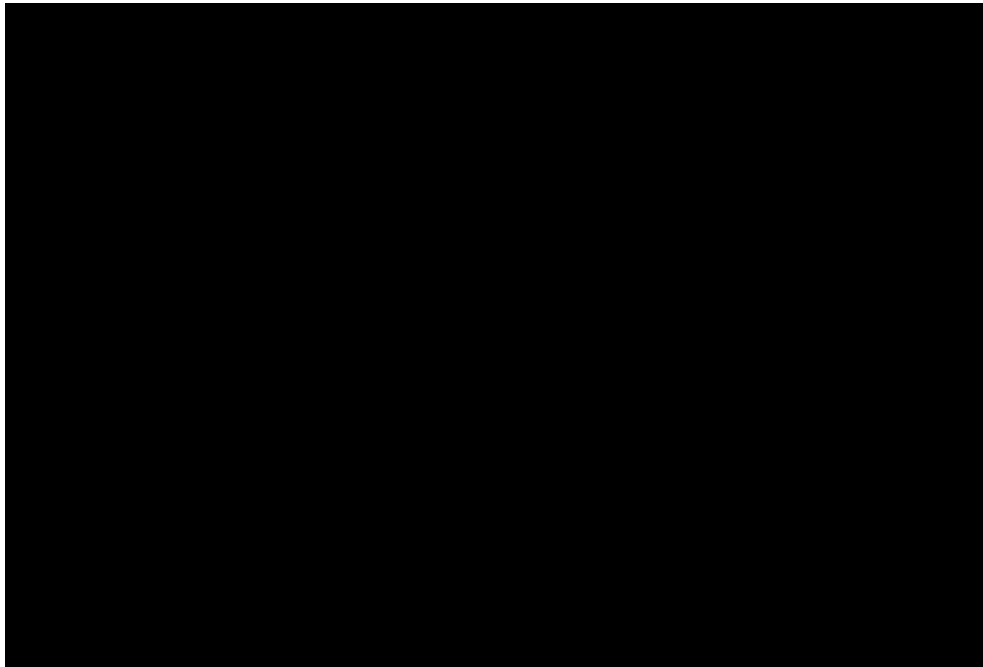


Figure 2.4: Picture of small and large intestine, the small bowel is placed in the central and lower part of the abdominal cavity surrounded by the large intestine (10).

The small intestine wall is made up of four coats (in fact, most of the GI tract is similarly composed of these four layers): serous, muscular, areolar, and mucous. The mucosal and submucosal layers of the small intestine are modified and consist of many glands known as the intestinal glands. The small intestine wall is protected from the action of acid by gastric juice secreted by the intestinal glands. The surface of mucosa has millions of villi giving it a soft velvety appearance. Villi (singular: villus) are microscopic finger-like projections, helping nutrients in the food absorb more efficiently into the body. There are about 20–40 villi per square millimetre. The serous coat, the external layer, is originated from peritoneum and the entire surface of the small bowel is coated with that. The muscular layer is located under the serous layer comprised of two distinct layers of muscle fibres: an outer longitudinal and an inner circular (11).

2.4.1 Duodenum, Jejunum and Ileum

The small intestine is divided into three segments including the duodenum, jejunum and ileum. The smallest segment of the small intestine, the duodenum, is approximately 25 cm long and starts from the pylorus and ends at the duodenal jejunal flexure. This area connects the rest of the intestine to the stomach and it can be anatomically divided into four parts: superior, descending, horizontal, and ascending. It curves around the head of the pancreas and is also the most immobile part of the small bowel (13).

Jejunum is the middle segment of the small intestine, which is wider and thicker than the duodenum. The jejunum is about 2.5 m long and the ileum, which is the last segment of the small intestine, is about 3.6 m long (14). The mesentery, an extensive fold of peritoneum, attaches itself to the posterior abdominal wall and allows jejunum and ileum to have the greatest motion (13). The ileum ends with the ileocecal valve (sphincter) and enters into the wall of the large intestine. The ileocecal valve regulates the movement of chyme into the large intestine and prevents backward flow of the contents from the large intestine. No structural or functional margin exists between the three segments of small intestine (15). Figure 2.5 shows the structure of villi in the small intestine.

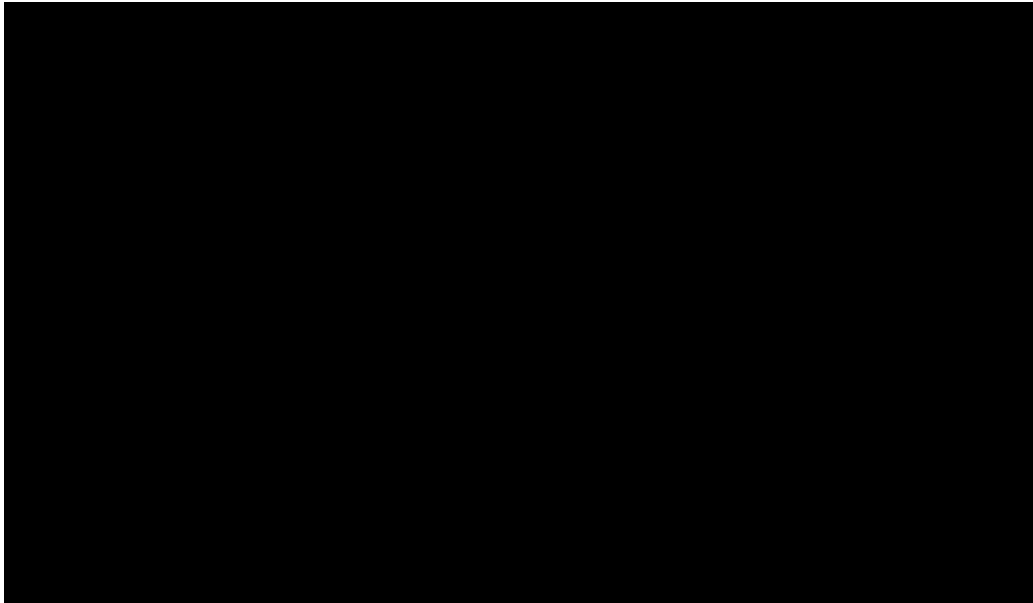


Figure 2.5: The structure of villi: microscopic finger-like projections. Villi help nutrients in the food absorb more efficiently into the body (16).

While food is passed from the small intestine to the large intestine all of its nutrients along with most of the water are extracted from the food (11).

2.5 Large Intestine

When all nutrients have been absorbed in the small intestine via the villi, the watery waste then enters the last part of the gastrointestinal tract, the large intestine. In fact, the key function of the large intestine is to absorb water from the waste and compresses it into a form so that it's easy to discharge from the body. As the chyme slowly passes through the colon, the water is removed and it is mixed with mucus and bacteria and at the end is converted into faeces (11).

The large intestine has two sections including the colon and rectum. The colon is the longest part of the large bowel, which is sub-divided into four sections including: the ascending colon, the transverse colon, the descending colon and the sigmoid colon. The last segment of the colon is known as the rectum (11). See Figures 2.4 and 2.6.

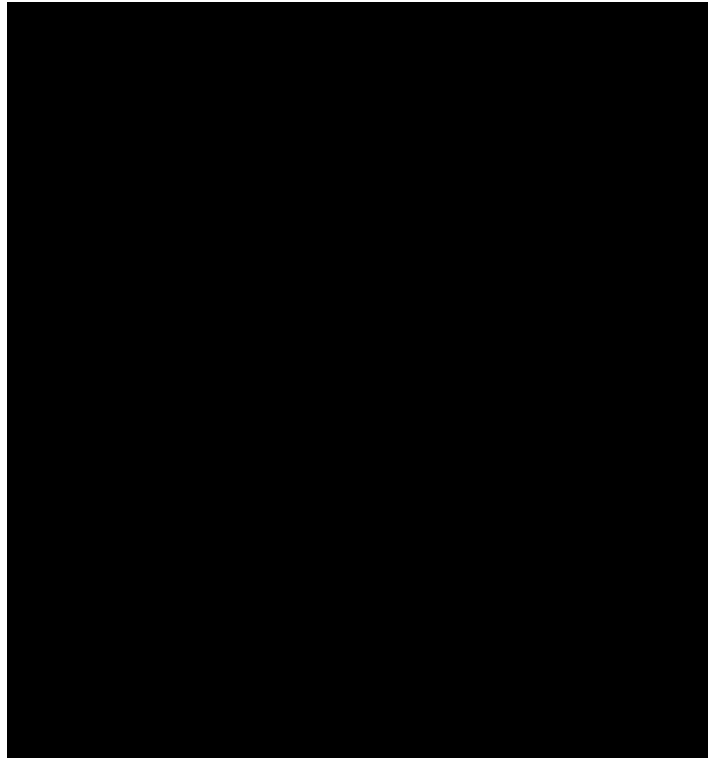


Figure 2.6: Parts of large intestine including Ascending Colon, Descending Colon, Sigmoid and Rectum (17).

2.6 Blood Supply of the stomach and intestine

The stomach has a rich blood supply; five main arteries are left gastric, right gastric, right gastro-epiploic, left gastro-epiploic and short gastric (18) as shown in Figure 2.7.

Three branches from abdominal aorta provide blood supply to the intestine, which include the celiac artery, superior mesenteric artery (SMA), inferior mesenteric artery (IMA), and branches of the intestinal iliac artery (IIA) (18). See Figure 2.8.

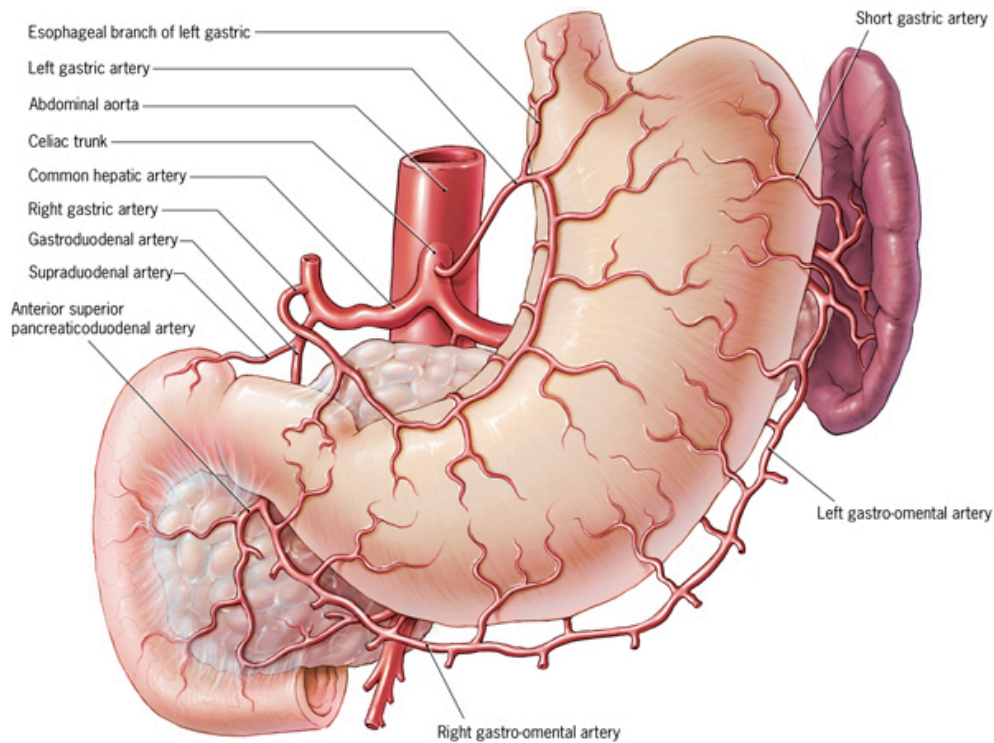


Figure 2.7: The arterial blood supply of stomach including five main arteries: left gastric, right gastric, right gastro-epiploic, left gastro-epiploic and short gastric (19).

This research project focuses on the intestines, so blood supply for the small and large intestines will be described in more detail.

2.6.1 The Celiac Artery

The celiac artery or trunk, which is very short about 1 cm to 2 cm long, comes from the aorta through a diaphragm. This artery supplies the foregut and it has three terminal branches including: the left gastric, splenic, and hepatic arteries (20).

2.6.2 Superior Mesenteric Artery (SMA)

Superior mesenteric artery is the main blood vessel in the digestive system, which branches off from the abdominal aorta. This artery supplies the pancreas and the lower parts of the intestine including the distal part of duodenum, the jejunum, ileum, cecum, appendix, ascending colon, and the transverse colon (20).

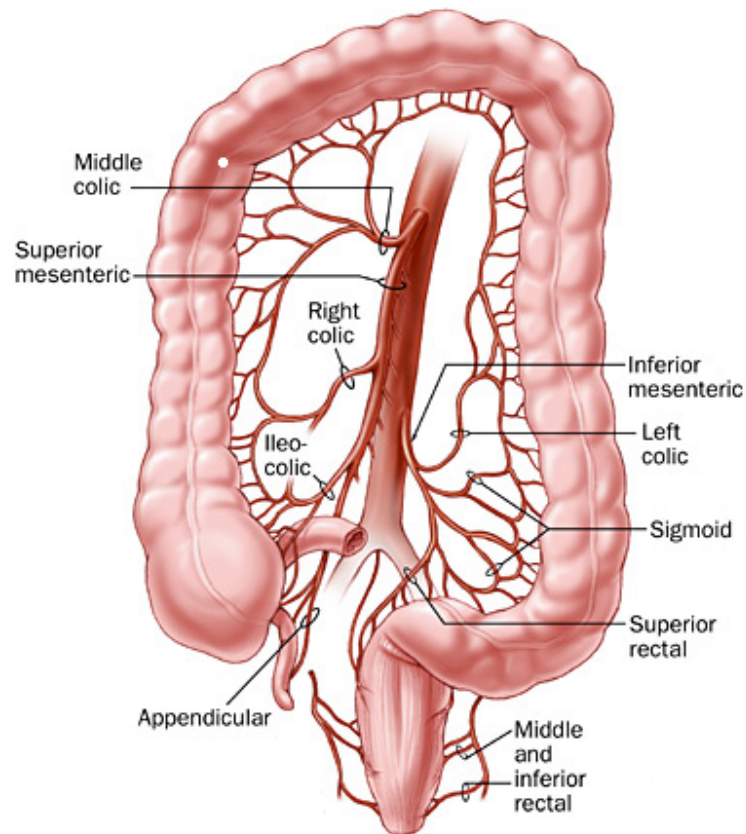


Figure 2.8: Arterial blood supply to the colon including: the celiac artery, superior mesenteric artery (SMA), inferior mesenteric artery (IMA), and branches of the intestinal iliac artery (IIA) (21).

2.6.3 Inferior Mesenteric Artery (IMA)

The inferior mesenteric artery provides the blood supply to the left third segment of the transverse colon, descending colon, sigmoid colon, rectum and also the upper half of the anal canal. The IMA then branches into the left colic, the superior rectal arteries, and the sigmoid branches (22).

2.6.4 Marginal Artery

The anastomoses of the connected branches of the colic artery form a continuous arterial loop or arcade near the inner border of the large intestine known as the marginal artery (23). See Figure 2.9.

2.6.5 Griffiths' Point and Sudeck's point

A watershed is a weak point in the colonic blood supply, which results from incomplete anastomoses of the marginal arteries. Several watershed areas can

be seen in the colonic blood supply and they are frequently susceptible to ischemia. These areas include Griffiths' point at the splenic flexure and Sudeck's point at the sigmoid colon (24) (Figure 2.9, indicated by shaded area).

Griffiths' point is at the splenic flexure and at the junction of the SMA and IMA territories. Anastomoses (the connections between the blood vessels) here might be weak or even absent, therefore the marginal artery at this area are poorly developed along the right side of the colon, explaining the reason that the splenic flexure is susceptible to ischaemia (25).

The point of origin of the last sigmoidal artery, originated from the inferior mesenteric artery (IMA) is called Sudeck's critical point (26).

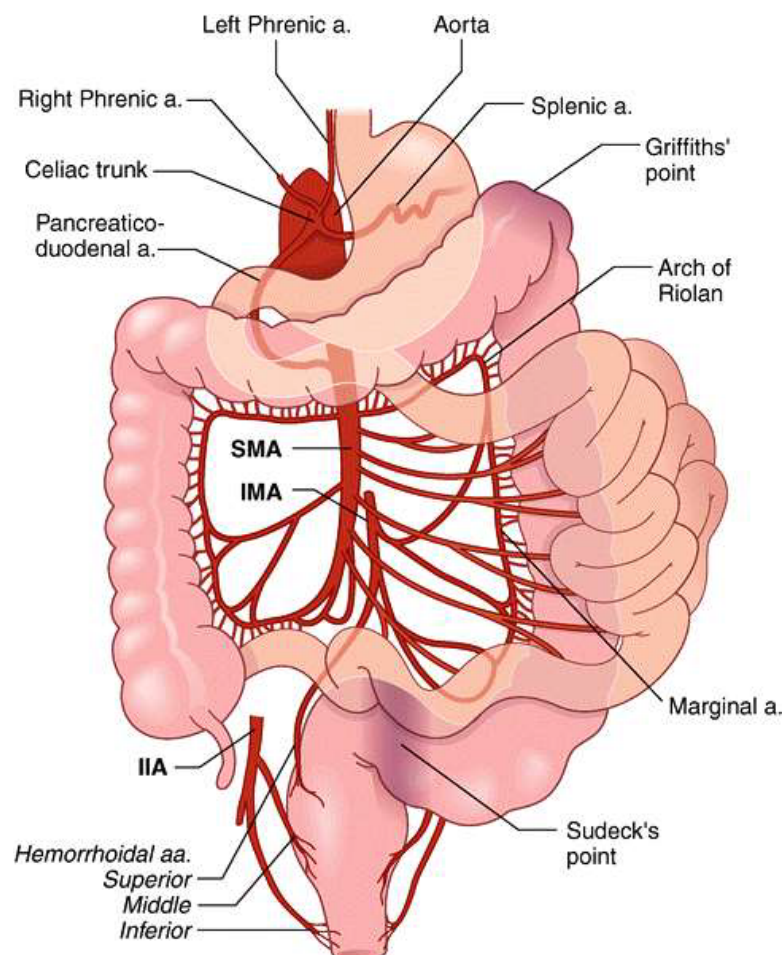


Figure 2.9: Marginal arteries and Griffith's along with Sudeck's points that is indicated by shaded areas (27).

2.7 Veins

The portal venous system is the system of veins containing multiple veins and tributaries, which drains blood from the greater sections the gastrointestinal tract (28).

2.7.1 Portal Vein

The portal vein is the vein of the gut that brings blood from the abdominal part of the gastrointestinal tract from the lower third of esophagus to halfway down the anal canal including: spleen, pancreas and gall bladder then delivers it to the liver (28). The portal vein is an important vein, about 8 cm long and made up by the union of superior mesenteric vein and splenic vein at the back of the neck of the pancreas (29) (Figure 2.10). It runs to the right behind the first part of the duodenum then inserts into the lesser omentum. After entering through the porta hepatis it then divides into two terminal branches: right and left branches. Further these terminal branches break up into a system of microscopic vessels known as sinusoids. After adding nutrients to the blood or removing them from it, then hepatic veins collect the blood from the sinusoid (29).

2.7.2 The tributaries of the portal vein

There are a few direct tributaries of the portal vein including: Splenic veins, Inferior mesenteric vein, Superior mesenteric vein, Left gastric vein, Right gastric and Cystic veins. Figure 2.11 shows all these veins (28).

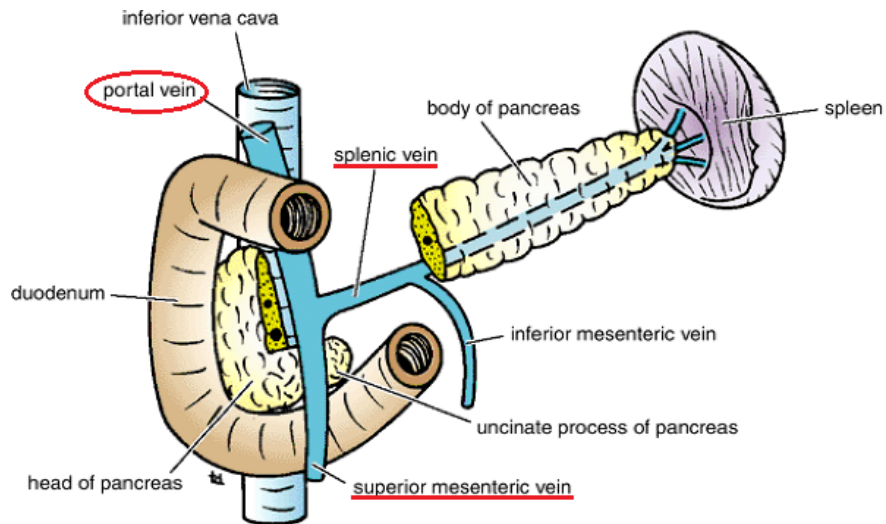


Figure 2.10: Formation of portal vein behind neck of pancreas made up by the union of superior mesenteric vein and splenic vein (28).

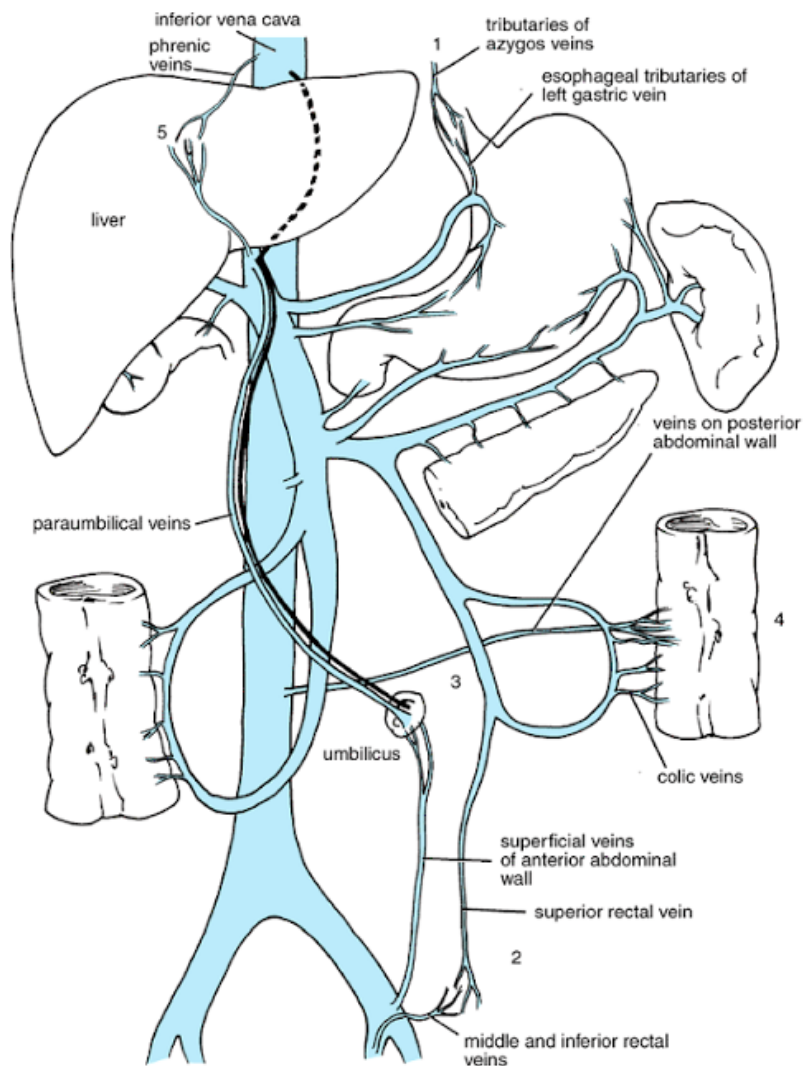


Figure 2.11: Veins of portal circulation including: Splenic veins, Inferior mesenteric vein, Superior mesenteric vein, Left gastric vein, Right gastric and Cystic veins (28).

2.8 Differences between the small and large intestine

The small and large intestines are important sections of the human digestive system. Although there is continuity between both there are some noticeable differences between them, some of the main differences are explained below. Some of these differences have been shown in Figure 2.12.

Mobility: The mobility of the small and large intestine are not the same in fact; most segments of the small intestine (apart from of duodenum) are mobile, while most of the colon is fixed in place by mesenteric (30).

Calibre: The calibre of the small intestine when full is normally less than the caliber of the large intestine when full (28).

Longitudinal muscle: In the small intestine a continuous layer has been formed around the intestine with the longitudinal muscle. But the longitudinal muscle in the large bowel is seen as three separate bands known as teniae coli (30).

Fatty tags: On the wall of large intestine there are fat filled tags called the *appendices epiploicae*, however these fatty tags are not present in the small intestine (28).

Smoothness: The small intestine wall has a smooth outer surface, but that of the large intestine becomes sacculated (having sac-like expansion) (31).

2.9 Internal Differences

Mucous membrane: The mucous sheath of the small intestine (see Figure 2.4) contains plicae circulars. These are not seen in the large intestine; instead occasional incomplete folds can be seen (30).

Villi: The mucous sheath of small intestine (see Figure 2.5) is characterised by the presence of numerous villi. However, the large intestine has no villi (30).

Lymphoid tissue: Throughout the mucous sheath of the small intestine (see Figure 2.4) masses of lymphoid tissue can be seen known as Peyer's patches. Cells and organs that form the lymphatic system (like white blood cells, bone marrow etc.) are called lymphoid tissue. These are not present in the large intestine (31).

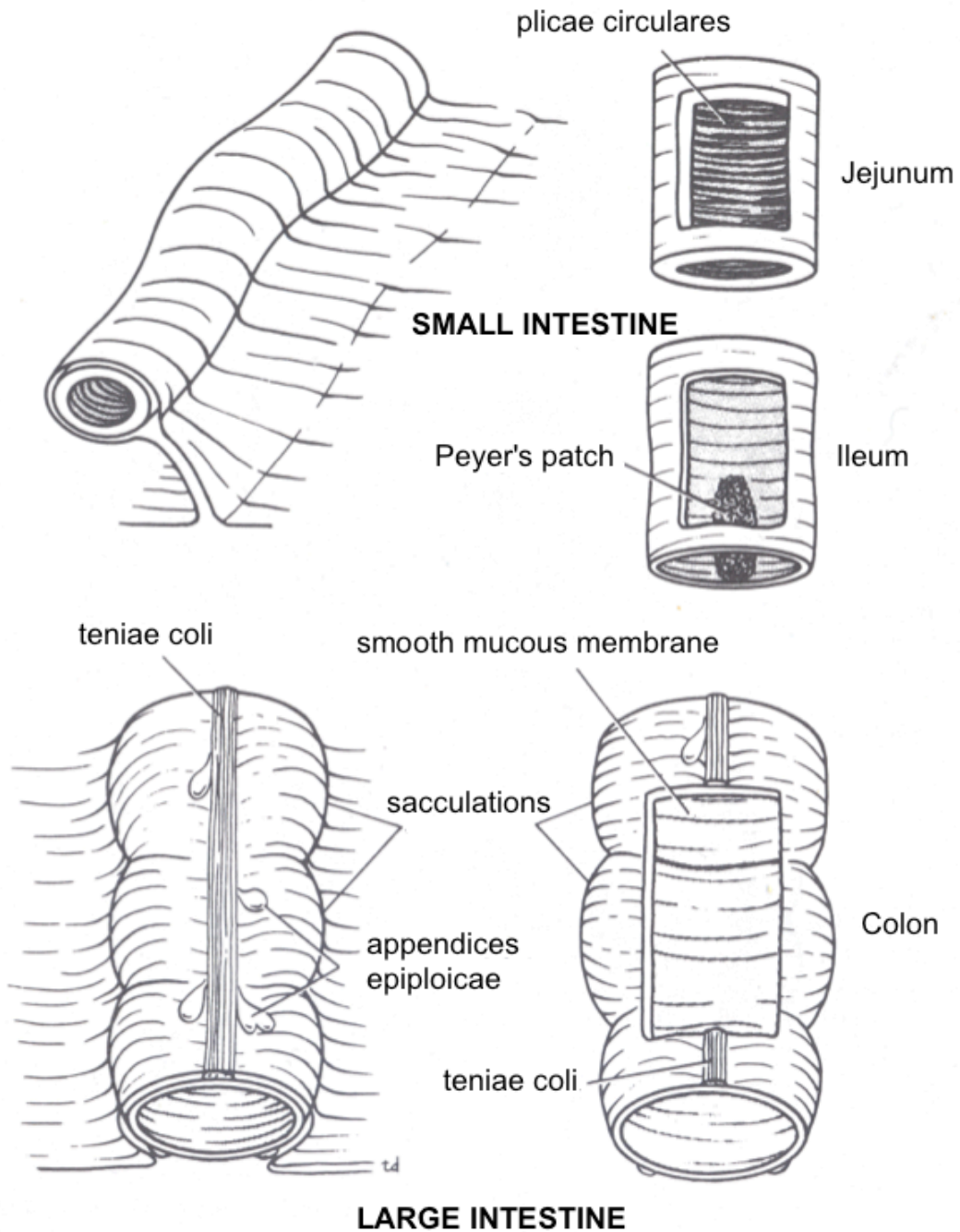


Figure 2.12: some external and internal differences between the small and large intestine (28).

Different kinds of bowel resection will be discussed in the following chapter.

Bowel Resection

3.1 Definition of the bowel resection

Resection is another name for any operation that removes tissue or part of an organ. Bowel resection is a surgical procedure to remove part of, or the entire bowel (32). It is carried out when part of the small or large bowel is blocked, damaged or diseased. The goal of bowel resection is to treat the condition while preserving normal bowel function. Proctocolectomy is the removal of the entire colon and the rectum while in subtotal colectomy, part or all of the colon but not the rectum is removed (33).

3.1.1 Small Bowel Resection

Small bowel resection may be recommended for blockage of the small intestine (small intestinal obstruction) due to scar tissue, hernia or other causes, bleeding, infection or ulcers due to inflammation of the small intestine (regional ileitis, regional enteritis, Crohn's disease), injuries, cancer, precancerous polyps (nodes), carcinoid tumour and ischaemia (34).

3.1.2 Large Bowel Resection

This operation is also known as colectomy, colon removal, colon resection, or resection of part of the large intestine. Some of the conditions that can be treated with large bowel resection include blockage in the large intestine (large intestinal obstruction) due to scar tissue or other causes, colon cancer, Crohn's disease, ulcerative colitis, precancerous polyps (nodes), familia polyposis, ischaemia (35). Since bowel obstructions are more common than other causes for bowel resection in both small and large intestine, they will be discussed in Section 3.2 in more detail.

3.2 Bowel Obstruction (BO)

When a bowel obstruction (also known as intestinal obstruction) occurs, a blockage inhibits the contents (food, fluids, and gas) of the intestines to pass freely through the digestive tract. There are two types of intestinal obstructions, mechanical; which means there is a physical obstruction and non-mechanical (functional). A mechanical bowel obstruction might be a partial or complete blockage depending on whether any bowel contents can pass normally through the obstructed area (32). Mechanical obstructions can have many causes including tumours, scar tissues (adhesion), or twisting or narrowing of the intestines etc. Treatment for mechanical obstruction is mostly carried out by removing the source of the blockage (36). Examples of blockage in the small and large bowel are shown in Figure 3.1.

BO can happen in any section along the small intestine or large intestine (colon), which will be discussed in Sections 3.2.1 and 3.2.2 respectively.

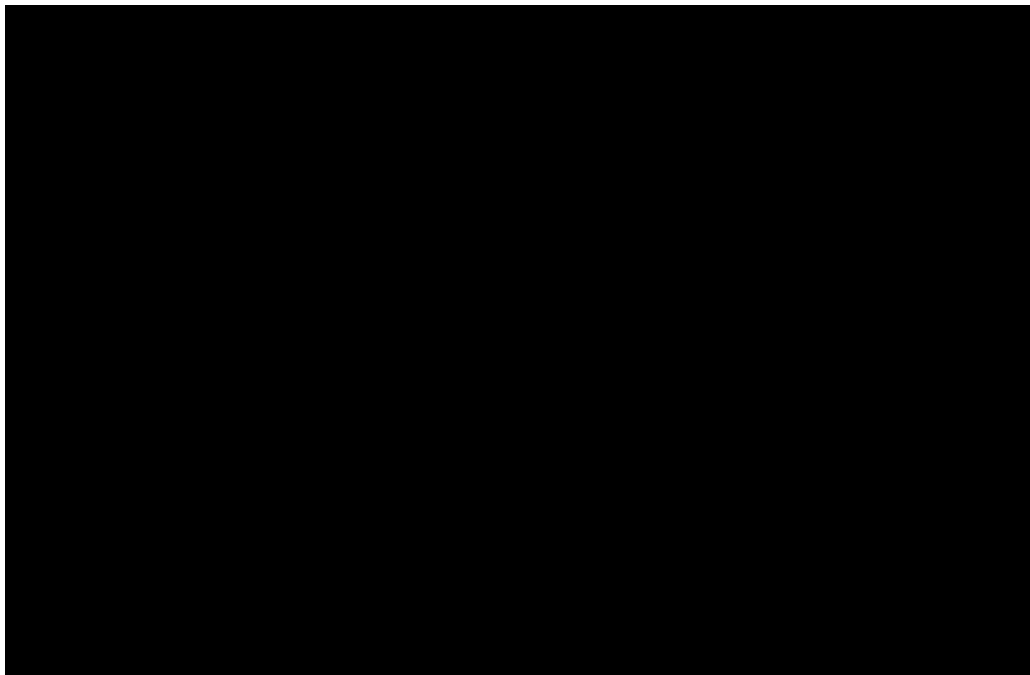


Figure 3.1: Left side: a blockage in the small intestine as a result of scar tissue (adhesions) Right side: a partial blockage in the colon caused by a tumour (cancer) (37).

3.2.1 Small Bowel Obstruction (SMO)

Small bowel obstruction (SBO) is a common clinical condition requiring hospitalisation and surgical consultation, which is a reason for approximately

20% of surgical admissions of patients with acute abdominal conditions (38). SMO can occur partially or completely and prevents normal transit of the contents and blood flow through the small bowel (39, 40). In Table 3.1 the most common causes of small bowel obstruction with their incidence percentage is listed and some will be discussed. Intestinal obstructions are more common in the small intestine and they can cause severe pain.

Table 3.1 Causes of Small Bowel Obstruction (41).

Cause	Incidence
Adhesion	60%
Malignant tumour	20%
Hernia	10%
Inflammatory bowel disease	5%
Volvulus	3%
Others	2%

Adhesions — the main cause of bowel obstruction is adhesions caused by scar tissue, which is usually related to prior laparotomy. Abdominal adhesions are bands of fibrous scar tissue; they can form on part of tissue inside the abdomen, causing the tissues to bind to each other or to the wall of the abdomen. See Figure 3.2. Sometimes this condition of adhesions blocks the intestines either completely or partially. If this obstruction happens it might lead to death in about 5% of cases (42).

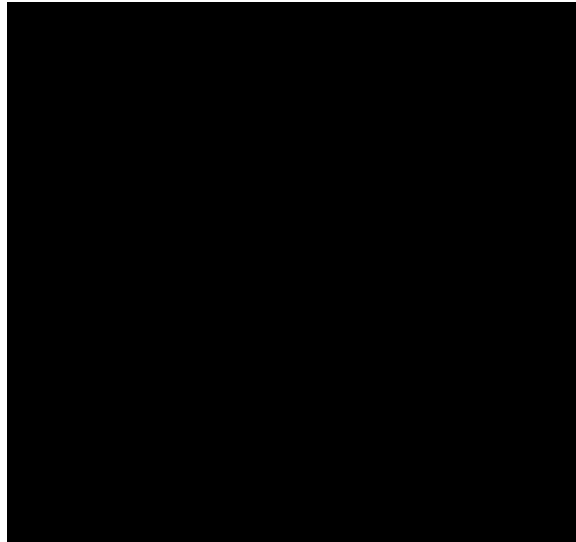


Figure 3.2: One example of blockage in the small and large bowel (43).

Hernia – hernia reports account for 10% of small bowel obstructions (44), which can twist or narrow the intestine. A hernia might happen when there is a structural weakness in the tissue of the abdominal wall, in which a segment of the small intestine may stick out through this weakened area. It can appear as a lump under the skin. This segment of intestine is called a hernia, which can block the small intestine and the blood supply might be cut off as well (44). A sample of hernia has been shown in Figure 3.3. Hernia can occur in many areas in the body but it mostly happens in the small intestine (44).

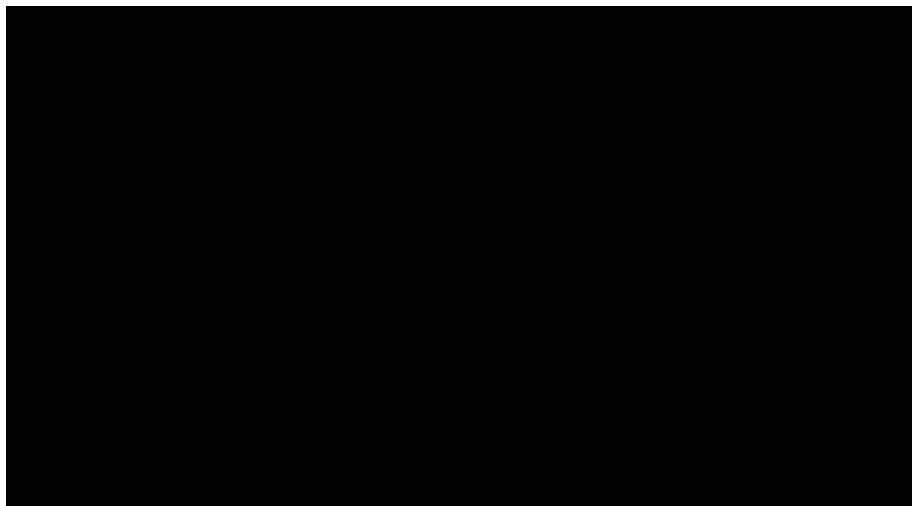


Figure 3.3: Hernia in small bowel in which a segment of the small intestine sticks out through this weakened area (43).

Tumours – Cancerous tumours can cause small bowel obstruction although it accounts for a small percentage of all small bowel obstructions. Growing within the wall of the intestine they might gradually block its inner passageway after some time (46).

3.2.2 Large Bowel Obstruction (LBO)

The obstruction can be complete or partial like in small obstruction. LBO can occur due to many causes, most often as a result of primary carcinoma, volvulus or diverticulitis (47).

Colorectal Cancer – between 10 % and 30 % of patients with colorectal cancer present large bowel obstruction. Colorectal cancer is the reason for about half of all large bowel obstructions. If colon and also rectal cancer is not diagnosed this may lead to the gradual narrowing of the large intestine's inner passageway. Single-staged operation including resection and anastomosis are common procedures to be performed on an obstructed segment of the bowel (48). In Figure 3.4 LBO can be seen as a result of colorectal cancer. Since this study has been performed on patients undergoing bowel resection for colorectal cancer, the main focus will be on this, and the procedure will be discussed separately in more detail in the following sections.

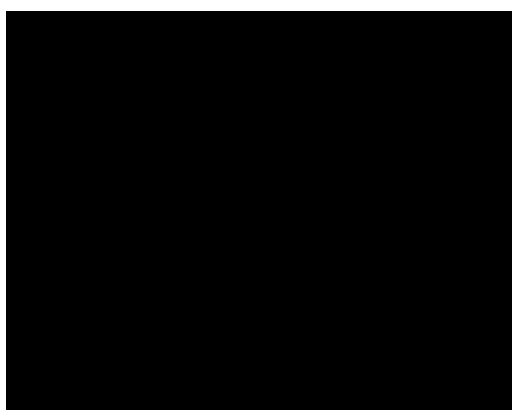


Figure 3.4: Large bowel obstructions are caused by colorectal cancer (43).

Volvulus – Colon Volvulus (CV) is an abnormal twisting or rotation of a segment of intestinal around itself, which produces a closed loop of bowel with a pinched

base, this causes intestinal obstruction and vascular compromise (see Figure 3.5). CV is a frequent condition that happens in people over the age of 65 (49).

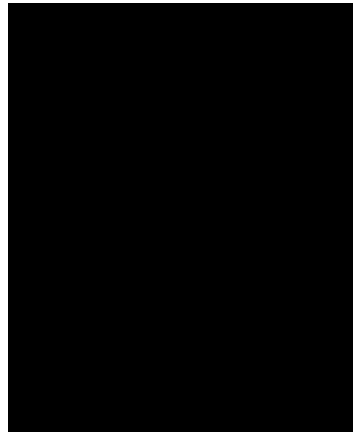


Figure 3.5: Large bowel obstructions are caused by volvulus in which a segment of intestinal twists around itself (50).

Diverticular disease – Diverticula, are small bags that may protrude from the wall of the intestine. Having these pouches called diverticulosis, is more common in elderly people. About half of all people over age 60 might experience this disease. If the pouches become inflamed or infected then it is called diverticulitis. It might cause a blockage in the colon by gradually narrowing the intestine (51).

3.3 Colorectal Cancer (CRC)

Colorectal cancer (CRC) is a kind of cancer that forms in either the large intestine (colon) or the rectum (end of the colon) (52). Worldwide, It is the third most common cancer, which affects more than 940,000 patients annually (53). In the UK it's the second biggest cancer killer, and around 40,000 people are diagnosed with colorectal cancer in men and women each year. About two thirds of all CRCs occur in the colon and one third is located in the rectum. Caught early, it is often curable. Colorectal cancer can begin in either the tissues of any of sections of the colon or the rectum. When cells that line either of these organs become abnormal and grow out of control, a cancerous tumour forms. This cancer in most cases develops slowly over a period of several years (54, 55).

It is more common in people over the age of 50, and the risk increases with age. Also people more likely to get it if they have: polyps - growths inside the colon and rectum that may become cancerous, a diet high in fat and meat, high alcohol intake, family history or personal history of colorectal cancer, ulcerative colitis or Crohn's diseases (55, 56).

Symptoms

Symptoms may include blood in the stool, narrower stools, change in bowel habit, abdominal pain and tenderness in the lower abdomen, weight loss and general stomach discomfort. Colonoscopy and sigmoidoscopy are screening tests for colorectal cancer (56).

Treatment

Treatment for CRC depends mostly on the stage and location of the cancer, however surgery is usually the most common treatment for all stages of colorectal cancer. Especially if detected early, surgery is often effective. The goal of bowel resection is to take out the affected part of the colon or rectum. Additional treatments are sometimes indicated including chemotherapy, radiotherapy and biotherapy or a combination of these (56).

3.4 Bowel Resection for Colorectal Cancer

In CRC, the tumour and part of the colon or rectum on either side is removed by a bowel resection procedure. After removal of the diseased part, the healthy ends of the colon or rectum are re-joined together (see Figure 3.6) with the aim of restoring normal function to the colon.

Bowel resection plays an important role in colorectal cancer. In early-stage cancer, surgery is done to remove as much cancer as possible to give the greatest chance of survival. And in cases of advanced colorectal cancer when it has spread (metastasized) to other parts of the body, bowel resection is still required to remove tumours that are blocking the intestine or causing bleeding (57, 58).

Treatment after bowel resection may include radiotherapy, which uses high-energy radiation, usually X-rays to kill cancerous cells, and also chemotherapy, which uses drugs, given either as pills or through injection, to selectively destroy them. Follow-up care is essential because colorectal cancer may come back after surgery, especially if it was not discovered in the early stages.

3.5 Surgical Techniques for Bowel Resection

Bowel resection surgery can be performed by one of two techniques: 1) laparoscopy or 2) open laparotomy.

3.5.1 Laparoscopic and Laparotomy Procedures

The first attempt to laparoscopic colectomy for cancer was made in the early 1990s (59). Laparoscopy, also known as keyhole or minimally invasive surgery, is a method that requires 5-6 small incisions in the abdomen, one for a laparoscopic camera and the rest for other tools, along with a small incision of 35–45 mm for the anastomosis (60). While in laparotomy, the operation is carried out through a large incision on the abdomen. Laparoscopic operations have become extremely popular recently, and have been widely employed for almost all kind of resection operations in patients with different stages of colorectal cancer (60, 33).

Laparoscopic operations have been of more interest than open laparotomy, this is due to the benefits of laparoscopy which include; less pain from the incisions after the operation, faster return of the normal bowel function, quicker healing of the wound, less scarring on the bowel and shorter stay in hospital (61). Also during the operation a magnified perspective of the operation can be viewed on a monitor by the surgical team leading to safer surgery, while in laparotomy the surgical team is not able to view the entire surgical field for the whole time of the surgery (62). As a result laparoscopic surgery is the most common procedure performed in the clinical area for bowel operation.

Even in laparoscopy, the anastomosis has to be performed while that part of the colon is out of the bowel through an abdominal incision (the one made at 35-45 mm), which the surgeon creates prior to the anastomosis (63).

These two procedures were performed for bowel resection for the patients that were included in this study, with the majority having colon cancer, out of them, 20 of the patients were treated laparoscopically, and for the remaining 4, open laparotomy was performed.

3.5.2 Anastomosis

The creation of a joint between two ends of the bowel is called *anastomosis*, which is needed after removing the dead/diseased part. In fact, an anastomosis is a surgical procedure between two structures and can refer to a connection that is created between any tubular structures including intestine or blood vessels (55).

The construction of an anastomosis depends on the kind of the resection. Different kinds of anastomosis can be performed, such as end-to-end, side-to-end and side-to-side anastomosis in which different staplers can be used to create the desired anastomosis (64). Figure 3.6 shows an end-to-end anastomosis as an example.

The following sections will discuss and outline the general principles in bowel resection operations.

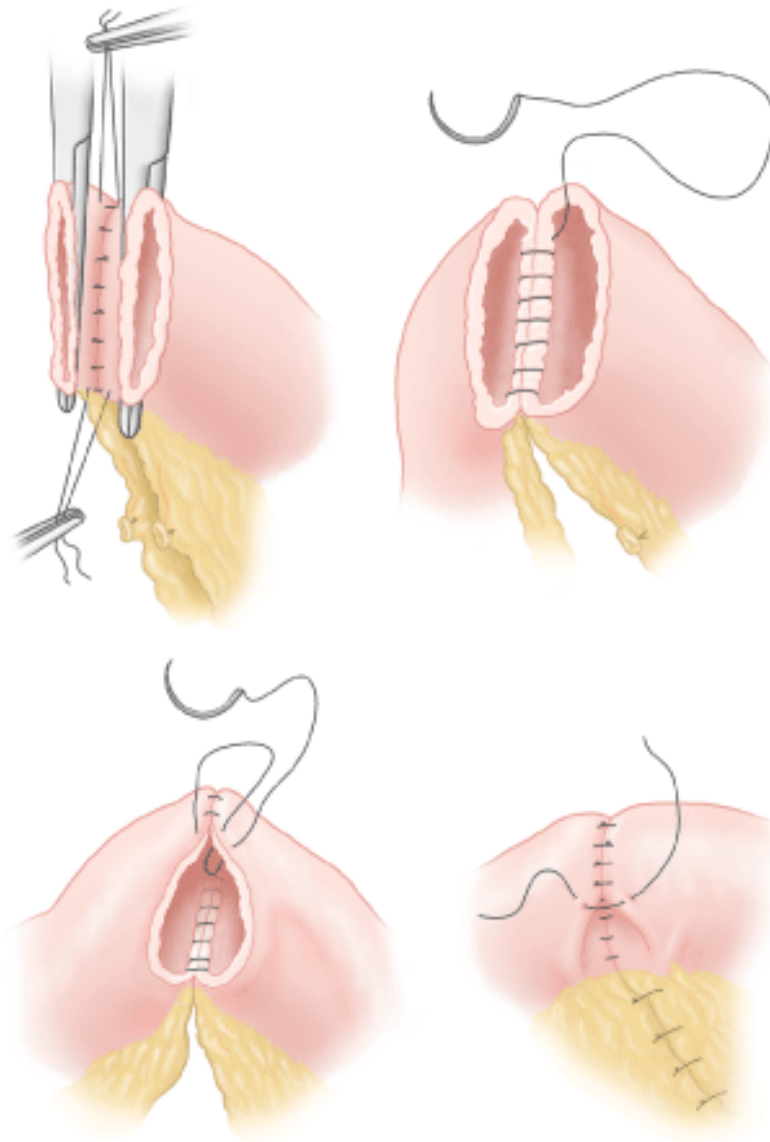


Figure 3.6: An example of anastomosis, an end-to-end anastomosis, in which the ends of the bowel are joining together to create an anastomosis using the stitches (64).

3.6 Types of Surgical Operation for Bowel Resection for CRC

A **colectomy** is the name of an operation in which part of the colon has to be removed. As mentioned in Chapter 2, the colon has several parts (Figure 2.5). Depending on where the tumour is, one or more specific parts may be removed. Table 3.2 describes the type of different resections according to their location in the bowel (59). Each cancer operation is aimed to remove all the cancer along with enough part of the healthy normal tissue around it, to ensure that the risk of

the cancer returning in that area is as low as possible. Colectomy is performed to treat one of these bowel cancers:

Table 3.2: Types of colorectal resection (59)

Type of Operation	Location of Tumour
Right Hemi-Colectomy	Caecum, right colon, hepatic flexure
Extended Right Hemi-Colectomy	Transverse colon or splenic flexure
Transverse Colectomy	Transverse colon
Left Hemi-Colectomy	Splenic flexure or left colon
Sigmoid Colectomy	Sigmoid colon
High Anterior Resection	Recto-sigmoid, upper third rectum
Low Anterior Resection	Middle third rectum
Abdominoperineal Resection	Distal third rectum

The next sections explain different types of colorectal resection.

3.7 Surgical Treatment for Colon Cancer

3.7.1 Right Hemi-Colectomy

A right hemi-colectomy is the usual operation when the tumour is in the right side of the colon, so the right side of the colon has to be removed, which is called right hemi colectomy. The first step in all bowel resection is mobilisation of the colon and its mesentery, and then ligation of the appropriate vessels at their origin has to be performed. Since right colic vessels are the vessels that supply the right part of the colon, these specific vessels have to be ligated (Chapter 2). With the colon mobilised and after the ligation, the segment of the colon to be resected is ready to be removed and anastomosis can be constructed. For that, the ends of the remaining parts of the colon are re-joined to each other. Anastomosis (Section 3.5.2) can be performed with hand sutures or using staples (59). Figure 3.7 shows a right hemi-colectomy and the anastomosis.

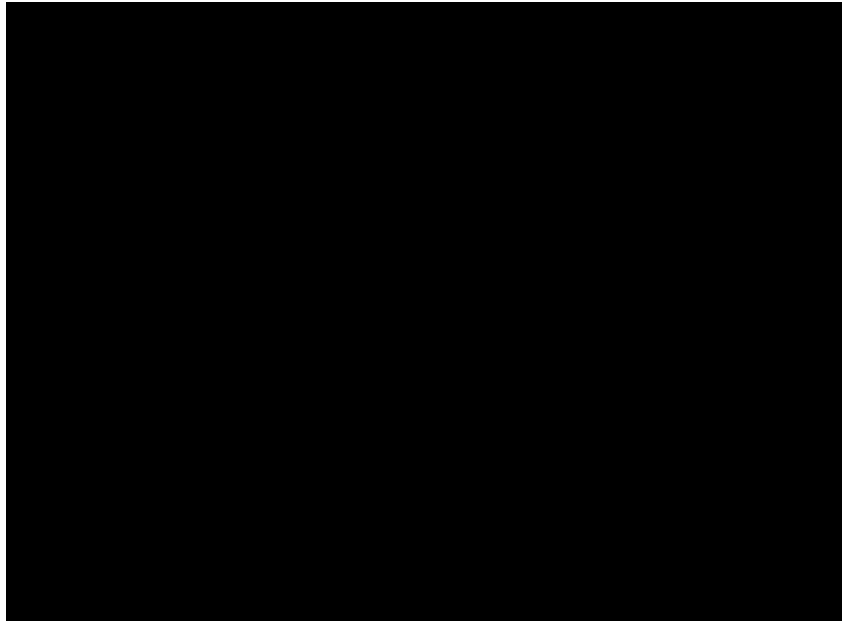


Figure 3.7: A right hemi-colectomy, A: tumour in cecum, B: ileocolic anastomosis (65).

3.7.2 Extended Right Hemi-Colectomy

When the tumour is in the mid transverse colon or splenic flexure, the treatment can be managed by an extended right hemi-colectomy (Figure 3.8). This operation will remove the terminal ileum, cecum, ascending colon, hepatic flexure and a portion of the transverse colon. When the tumour is in the transverse colon, the middle colic artery, which comes from superior mesenteric artery, has to be ligated. And if the tumour is in splenic flexure, the left colic artery, which comes from the inferior mesenteric artery (IMA) has to be ligated (59).

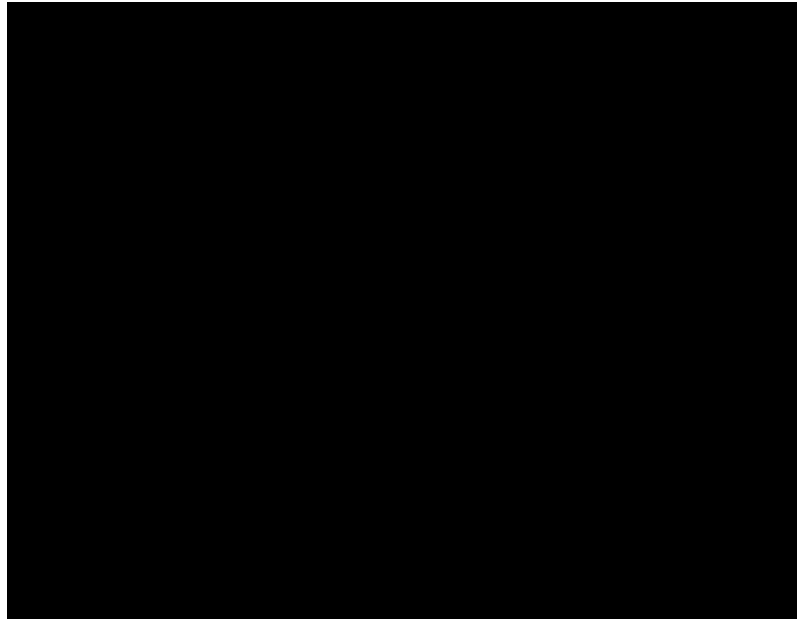


Figure 3.8: Extended right colectomy, A: tumour in splenic flexure, B: ileocolic anastomosis (65).

3.7.3 Transverse Colectomy

If the middle part of the bowel is removed (the transverse colon), it is called a transverse colectomy. In which the middle colic artery has to be ligated then two ends of the remaining colon (the ascending and descending colon) can be rejoined to create the anastomosis (66). See Figure 3.9.

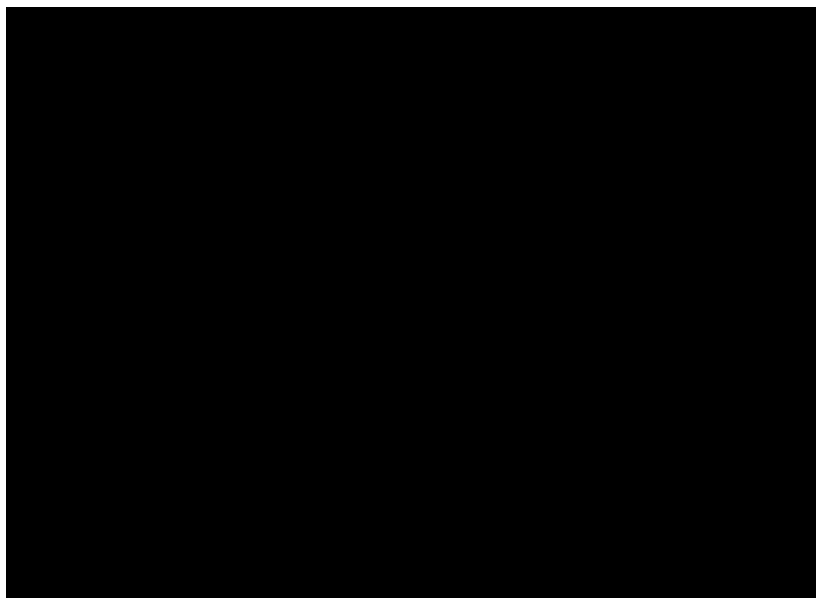


Figure 3.9: Transverse colectomy, A: tumour in transverse colon, B: anastomosis of ascending and descending colon (65).

3.7.4 Left Hemi-Colectomy

This operation is performed for tumours of the descending colon, in which the left colic artery has to be ligated, the splenic flexure and descending colon should be removed and the rest of the colon (the transverse and upper sigmoid colon) can be rejoined to create the anastomosis (67). See Figure 3.10.

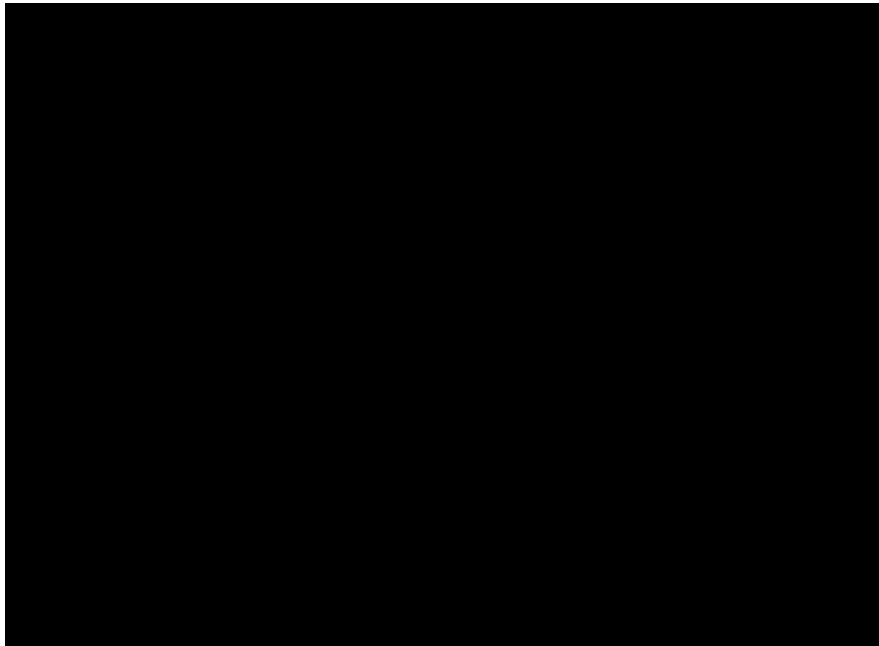


Figure 3.10: Left hemi-colectomy, A: tumour in descending colon, B: anastomosis of transverse and sigmoid colon (65).

3.7.5 Sigmoid Colectomy

If the sigmoid colon is removed it is called a sigmoid colectomy. After removal of the cancerous segment the upper rectum and descending colon can be rejoined to make the anastomosis (68). In some patients a colostomy needs to be performed for drainage of waste through an opening in the abdomen (stoma) (69). A colostomy is considered in some cases to divert digestive waste away from the affected areas of the colon allowing them a greater chance of healing. Once the areas are healed the anastomosis can be treated (59). See Figure 3.11.



Figure 3.11: Sigmoid colectomy, A: tumour in sigmoid colon, B: anastomosis of the upper rectum and descending colon (65).

3.8 Surgical Treatment for Rectal Cancer

3.8.1 High Anterior Resection

Anterior resection is performed for treatment of rectal tumours, high anterior resection involves the removal of the sigmoid colon, the upper rectum and a variable portion of the left colon. For anterior resection the sigmoid artery, which comes from the inferior mesenteric artery has to be ligated after the bowel is mobilised (70).

3.8.2 Low Anterior Resection

To treat rectal cancer and cancers in the upper third of the rectum low anterior resection is considered. After removing the cancerous part of the rectum, the colon can be reattached to the remaining part of the rectum (71). See Figure 3.12.

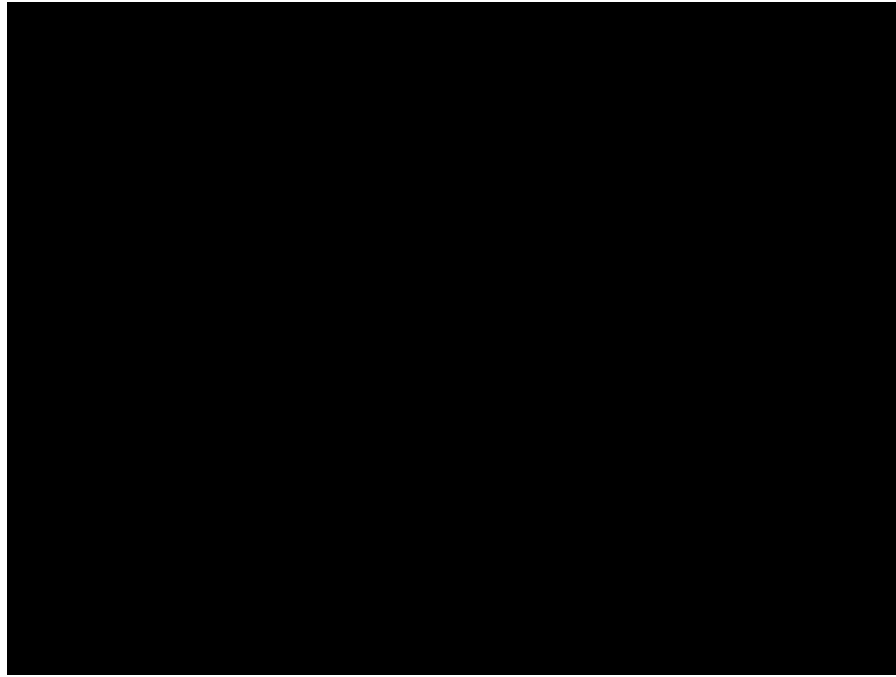


Figure 3.12: Low anterior resection: A: tumour in rectum, B: anastomosis of the anus and the rest of sigmoid colon (65).

3.8.3 Abdominoperineal Resection

Abdominoperineal resection (APR) is a standard surgical treatment for patients with a tumour in the distal third of the rectum (i.e. when the cancer is located very low in the rectum or anus). For this treatment the anus, rectum and sigmoid colon have to be removed leading to a permanent iliac colostomy. Ligation of the superior rectal artery has to be performed before resection (72). See Figure 3.13.

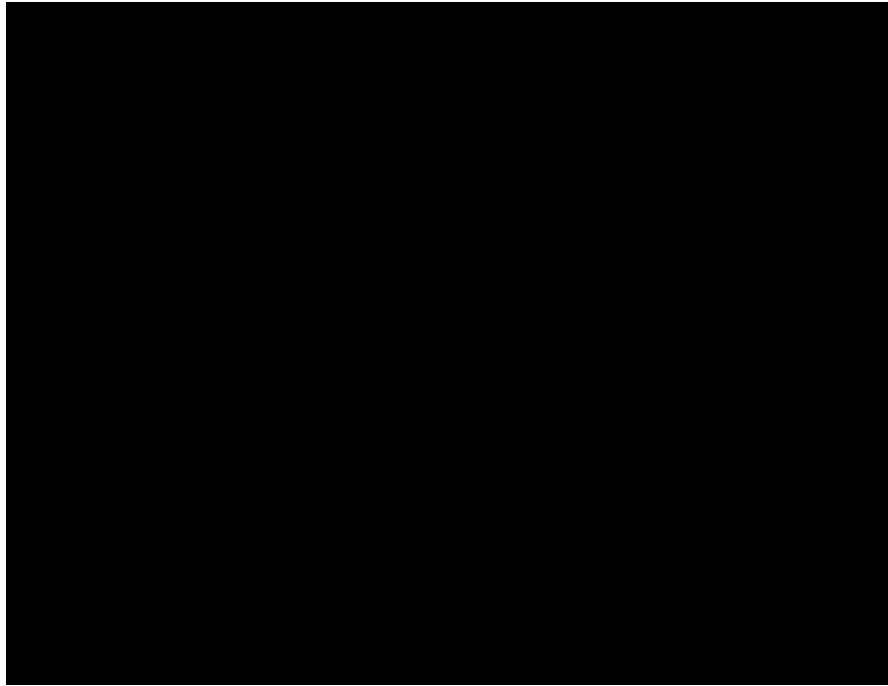


Figure 3.13: Abdominoperineal resection, A: tumour in rectum, B: colostomy (65).

The next chapter presents a summary of previous research in intra-operative determination of intestinal viability.

Intraoperative Determination of Intestinal Viability

4.1 Introduction

As mentioned in Chapter three, one of the most common operations in gastrointestinal surgery is *bowel resection* for patients who have different kinds of bowel cancer or any other occlusion in which anastomosis has to be carried out following the removal of an unhealthy segment of the bowel. The most common complication after the anastomosis is anastomotic leakage, which unfortunately has remained a problem (73). Despite some developments in techniques like new stapling methods for anastomosis and modalities in bowel operation, anastomotic leakage after bowel resection is still a major concern and the occurrence has not decreased significantly over the last decade (74). In order to avoid anastomotic leak or any other complications like intestinal ischemia or necrosis, which can happen in any bowel surgery, intraoperative viability of the bowel must be evaluated regularly during any gastrointestinal operation. In order to have successful healing of an anastomosis, a sufficient blood supply is needed, which then helps to decrease the anastomotic leakage, intestinal ischemia and necrosis (75, 76). Having a successful anastomosis greatly improves the patient's recovery stay in hospital after an operation and also reduces postoperative morbidity and mortality. The incidence of anastomotic leakage has been reported between 1.2% and 19.2%, nearly 32% of these patients die due to postoperative complication (77). Unfortunately in clinical practice it is not easy to judge whether the intestine remains viable after the procedure, and determination of the bowel viability has remained a dilemma for surgeons (78-81). In many cases, second-look operation, decided by the surgeon, is carried out to be sure the surgery was a success (82, 83). This procedure has become more common in some mesenteric surgery especially when uncertain intestinal viability is observed during the primary

surgery. Some surgeons believe that the second-look laparotomy is a gold standard for determining future bowel viability (84).

Intestinal microcirculation and viability in the clinical site is usually estimated on the basis of clinical findings such as the intestinal colour tone of the serosal surface (Chapter 2), the presence of bowel peristalsis (muscle contractions), arterial pulsation and also bleeding from the marginal arteries. These clinical features of the bowel viability do not relate consistently to bowel survival, and also they are subjectively based on the experience of the surgeon (78, 75), so human error is possible. For example a dark colour does not always indicate a serious problem, as the bowel might be in fact viable; the reason for the dark colour may be due to transient venous insufficiency. The colour may seem normal in early arterial occlusion. Absence or lack of mesenteric pulsation does not necessarily mean that the tissue is not viable; hypotension or spasm might be a reason for this. Also even in a totally ischemic bowel, peristalsis may continue. Therefore visual signs are unreliable indicators for assessment of intestinal microcirculation and should not be the sole basis for clinical decision making. As a result, there is a need to have a more reliable method for determination of intestinal viability (78, 85) during gastrointestinal operations. To address this need, a wide variety of methods have been proposed, each having advantages and disadvantages. Studies to assess the intra-operative and/or peri-operative intestinal blood flow using sensors have a long history, dating back to 1976. To date just a few of these methods are applicable in surgical practice for use in tissue of doubtful viability, although none of them are employed routinely in clinical practice (78).

Some methods have been shown to increase the accuracy of intestinal viability assessment and have been the subject of research studies. These techniques have shown potential to be of some value, although they are subject to certain drawbacks and limitations.

4.2 Monitoring Methods for the Detection of Intestinal Viability

As mentioned, to date, various methods have been proposed to assess intestinal blood flow or intestinal viability, most of which are discussed below.

All methods for the detection of monitoring of the bowel have been divided into two groups based on old and new techniques with some still under research:

First Group: methods, which are old or no longer in use.

Second Group: methods, which are new or have been of great interest in the last decade.

In the following sections, all the monitoring methods will be described according to these two groups.

4.3 First Group

This group of monitoring methods comprises of all methods involving those, which are no longer employed or of no interest at present, either in clinical use or in research.

4.3.1 Polagraphic Measurement of Oxygen Tension

Tissue oxygen tension (PtO_2), measures the local partial pressure of oxygen in a specific tissue in the body using a Clark electrode (86). There is some controversy regarding the usefulness of employing this method in the intestinal tissue. One study showed that the decreased PtO_2 level in intestinal tissue can predict anastomotic leakage (87), while another study showed that no increase in anastomotic leakage was associated with a decrease in PtO_2 (88). A result of these conflicting findings has been a decline in the use of the technique.

4.3.2 Doppler Ultrasound

In earlier studies it was believed that intraoperative Doppler ultrasound of the marginal arteries was a reliable method for predicting the intestinal viability intraoperatively, an economical and easy to use technique (89). In a study in 1979

by Cooperman, Doppler ultrasound was used successfully to determine the adequacy of blood supply at the edge of anastomosis of resection for patients undergoing intestinal resection (90). In a more recent study in patients undergoing colorectal resections, only 1% incidence of anastomotic leakage at the edge of the resected site was observed when they were assessed with Doppler ultrasound (91).

The drawbacks of Doppler ultrasound for assessing bowel viability have been discussed widely and include being sensitive to the signals from nearby large vessels and requiring tissue contact, which can impair local blood flow (92). Also Rotering *et al.* in a comparison study in 1982 demonstrated that laser Doppler has superior sensitivity, ease of use and objectivity compared to ultrasound (93). In 1988, Lynch TG *et al.* presented a comparison study between Doppler ultrasound, laser Doppler, and perfusion fluorometry in bowel ischemia, results have revealed that the sensitivity of Doppler ultrasound in detecting intestinal viability is 86% which is significantly lower than that of two other methods (the sensitivity of laser Doppler index was 94%, and of perfusion fluorometry was 95%) (94).

4.3.3 Hydrogen Gas Clearance (HGC)

Hydrogen gas clearance (HGC) was applied for assessment of microcirculation in intestinal studies in earlier experimental studies, which were mostly studied between 1964 and 1990 (95). This technique is based on the method of inserting a positively polarised electrode into the tissue of interest, administering hydrogen gas (H₂) which can be done by respiration or intra-arterially, allowing the H₂ to be cleared from arterial blood, and at the end the exponential clearance rate of H₂ from the target tissue, can be monitored.

A 1980 review article concluded that HGC was a valid and important method for monitoring blood flow, despite some drawbacks (96). HGC has been performed for measuring blood flow in different organs, in fact any tissue in which a small electrode can be implanted, however this technique is not used routinely in clinical application for evaluation of intestinal blood flow mostly because of its invasiveness, inconvenience and inadequate reliability (75, 97).

4.3.4 Radioisotope Studies

Radioisotope methods have been used in earlier studies in human and animal research to monitor blood perfusion at anastomotic or ischemic sites. In these methods, injections of radioisotopes were applied to monitor blood flow in regions where ischemia was suspected. These methods have some disadvantages, the main one being exposure to radiation for both the patient and medical personnel. Also storage and disposal of radioisotopes are expensive and impractical. Therefore these techniques are no longer in clinical or research use at present (98, 99). These studies were mostly performed between 1976 and 1985.

4.3.5 Bowel Wall Contractility Measurements

In 1986, a new method called the electronic contractility meter (ECM) was proposed to measure contractile activity of the ischemic part of the bowel. This technique comprises two main components including a special probe and an electronic control part. The probe was clipped to the surface of the bowel and the electromyogram (tracing representing electrical activity in muscle) reflecting peristalsis (muscle contractions) of the small intestine, was measured in millivolts using a computer algorithm. Low values of electromyography (EMG) are attributed to ischemic damage of the site under study (100). In a later study by Brolin *et al.* it was observed that the electronic contractility meter (ECM) is capable of providing a quantitative assessment of ischemic damage in the bowel and that EMG was a sensitive indicator of ischemic damage (81). However this technique did not find a wider clinical acceptance mostly due to the complexity of the technique.

4.4 Second Group

This group of monitoring methods covers all methods involving those which have been of more interest in the last decade, and still are of interest today in clinical practice or research area.

4.4.1 Pulse Oximetry

DeNobile *et al.* and Erikoglu *et al.* measured the oxygen saturation of the bowel using pulse oximetry in 1990 and 2005 respectively. The results of both studies

concluded that using pulse oximetry for intraoperative evaluation of intestinal viability could provide an idea of the degree of the pathological changes in the investigation area (78). Also MacDonald *et al.* in 1993 suggested that a pulse oximeter is capable of being used in intestinal blood flow assessment intraoperatively (101). One year later in 1994, Gardner *et al.* using reflectance pulse oximetry in an animal model showed that pulse oximetry can be a useful and a simple method for continuously monitoring the blood flow of the distal colon intraoperatively and might also be useful when there is doubt about the adequacy of blood flow to the distal colon (102). In 2001 a study suggested that pulse oximetry can help preserve bowel of doubtful viability (103). In a study in 2008, Phillips *et al.* introduced a novel reflectance pulse oximetry method for intraoperative measurements of SpO₂ in the oesophagus and large bowel and suggested that this method is able to measure SpO₂ continuously in patients with compromised peripheral perfusion (104).

Although pulse oximetry is widely accepted there are some limitations. Hadley and Mars in 2003 stated that although pulse oximeters measure oxygen saturation and give an indication of perfusion, they do not measure blood flow or tissue viability (105). Also Dyess *et al.* in 1991 believed that by using pulse oximetry, there is a high rate of false-negative and false-positive evaluations (106).

4.4.2 Near Infrared and Visible Light Spectrophotometry (NIRS & VLS)

The principle of spectrophotometry is based on the amount of light absorbed or transmitted as it passes through the target tissue in order to measure the concentrations of different types of haemoglobin and/or 'tissue oxygen saturation' (StO₂). Visible light spectrophotometry (VLS) relies on locally absorbed, shallow-penetrating visible light of 475-625 nm for monitoring microvascular hemoglobin oxygen saturation (StO₂) in small thin tissue volumes and has a penetration of about 2 mm into the tissue. NIRS with wavelengths typically beginning at 700-730 nm can penetrate more deeply compared to visible light. Unlike pulse oximetry, these techniques do not use photoplethysmography to discriminate between the pulsating arterial blood and the other blood components. Near Infrared Spectrophotometry (NIRS) therefore provides assessment of oxygenation in all

vascular compartments including arterial, venous and capillary, while VLS generally is able to measure the StO_2 in the capillaries due to its shallower penetration depth (107).

VLS and NIRS have been employed recently in some studies. Benaron *et al.* in 2005 suggested that VLS is a suitable method for monitoring the localized subsurface hemoglobin oxygen saturation in the microvascular tissue (108). In 2006 Hirano *et al.* successfully measured bowel StO_2 using NIRS at the anastomosis site of the bowel in patients undergoing colorectal resection. They demonstrated that low StO_2 on the anastomosis site could be a warning of an increased risk of anastomosis complications (109). Recently the evaluation of the estimated value of VLS for anastomotic leakage has been performed for the colon and rectum by Karliczek *et al.* in 2010. According to the result of this study on patients undergoing colorectal resections, StO_2 levels in colonic tissue were stable and reproducible while these values increased at the anastomotic site of the bowel after the creation of the anastomosis. An increase in the value of StO_2 was interpreted as a sign of leakage in the anastomosis (110).

It is believed that one advantage of VLS is the shallow penetration of the light in this technique, which is considered more appropriate than NIRS for the measurements of bowel wall oxygenation (102). Although the most important advantage of VLS compared to other techniques like polarographic (or tonometry measurements), NIRS or laser Doppler flowmetry (LDF) is that there is no need for tissue contact since the instrument corrects for an uneven baseline and the full light spectrum is analysed (110).

There are some drawbacks, for example the specific level of StO_2 that can lead to intestinal ischemia has not yet been defined. Also there is a lack of reproducibility in StO_2 values measured by different algorithms by different oximetry systems. Another drawback is that presence of solids (like stool and food) inside the intestine can affect the results. Also the probe needs to be held perpendicular to the tissue surface, a different angle can affect the accuracy of the measurements. In colorectal anastomoses, measurements are not easily performed, and finally, spectrophotometry systems are expensive. However it seems that VLS is an

auspicious method for bowel oxygenation measurement and has been recently the main subject of the majority of studies in this area.

4.4.3 Intravital Microscopy (IVM)

Intravital microscopy (IVM) is one of the most recent developments and has been recommended as a gold standard in 2008 by Duchs and Fiotzik in a study for microcirculatory research, since it can directly visualise and quantify changes in blood flow at the capillary level (111). In an animal study by Yasumura *et al.* this method showed that it could be a useful indicator of bowel viability. However the technique has not yet been applied to human studies, mostly due to the time consuming nature of the method (78).

4.4.4 Fluorometry and Laser Fluorescence Angiography

Fluorescence methods, namely perfusion fluorometry and laser fluorescence angiography (LFA), have both been performed in the evaluation of intestinal viability. Lynch *et al.* in 1988 in a comparison study between Doppler ultrasound, laser Doppler and perfusion fluorometry in bowel ischemia showed that the sensitivity of perfusion fluorometry in detecting intestinal viability is 95%, which was the greatest of these three methods (94). Later in 1992, Horgan mentioned in his work that perfusion fluorometry is a reliable technique for assessing areas of particularly doubtful viability (112).

The main disadvantage of fluorometry is that the measurements are not repeatable as the fluorescein remains in the tissue of interest for a significant period following injection (113). Also the results show a large standard deviation. Some believe that the viability of the tissue cannot be measured directly by this method, moreover it can also give a false prediction of non-viability and might lead to unnecessary secondary surgery (78).

Recently laser fluorescence angiography (LFA) has been applied for intestinal microcirculation assessment, which is based on intravenous injection of fluorescent dye (indocyanine green). In this technique the target tissue is then illuminated using laser light. The system in this technique has been proved to be

reliable and the measurements are repeatable, which is an advantage compared to conventional perfusion fluorometry (114).

4.4.5 Infrared Imaging

Small differences in the temperature between adjacent structures can be measured by thermal or infrared imaging, which has been used for assessment of the intestinal blood flow in some studies.

The first study dates back to 1978 when Moss *et al.* were working on reactive hyperemia (the transient increase in blood flow in tissue following haemostasis). They demonstrated that thermographic assessment could be of value in assessing bowel viability during surgery (115). Later in 2000, Brooks *et al.* introduced thermal imaging for detection of bowel ischemia intraoperatively (116). They compared thermal imaging with three other methods including visual inspection, Doppler ultrasound and fluorescence. All techniques showed a higher sensitivity to detect differences between vascularized and devascularized bowel than visual inspection. Also in 1997 another study by Robert *et al.* concluded that infrared imaging is a good method for localising anatomic structures. They also showed in an animal model that this technique is useful in tissue viability assessment during laparoscopy procedures (117). Later Cadeddu *et al.* in 2001 (118), Nishikawa *et al.* in 2006 (119), Shussman *et al.* in 2011 (120), found that intraoperative thermal imaging provided useful information regarding bowel viability.

The limitation of infrared imaging is that this technique is not a direct indicator of the blood perfusion and oxygenation; also the measurements depend on ambient temperature (121).

4.4.6 Laser Doppler Flowmetry

In this technique direct information about oxygen, nutrient or waste metabolite exchange in the adjacent tissue could not be obtained. Many researchers have employed LDF in their studies. Vignali *et al.* in 2000 concluded that LDF measurements can be a valuable tool intra-operatively in predicting the

occurrence of anastomotic leak in patients with colorectal cancer (122). Their study shows that LDF can show blood flow reduction during different stages of large bowel resection. In 2002, Nakatsuka used LDF and gastric tonometry to measure colonic tissue blood flow and gastric mucosal pH respectively to compare which of these methods is more reliable in reflecting changes in intestinal microcirculation (123). In this comparison study the results proved that LDF is a better method in preventing postoperative ischemia. In another study by Seike *et al.* in 2007, the colonic blood flow was measured intraoperatively in large bowel resection (124). In this study using LDF blood flow measurements showed a significance decrease by clamping the arteries. LDF measurements have also been applied by others in cancer of the rectum and sigmoid colon, also for assessing bowel serosal and mucosal oxygenation in colon surgery. It has been proved that LDF measurements can be a valuable technique in the detection of ischemia from the serosal surface of the bowel (125). Recently in 2012, Kaser *et al.* showed that laser Doppler flowmetry and spectrometry have an important role on clinical outcome since they are potentially valuable methods in order to assist the surgeon to make the right decision in critical venous mesenteric perfusion (126).

However, like every other technique there are some limitations for LDF: it is a time consuming method, movement artefacts affect the results, the perfusion units are subjective and rather qualitative, large standard deviation can be observed in measurements of the bowel surface and the cut-off level of flow indicative of intestinal ischemia is not specific (in different studies it was not the same). Also measurements require tissue contact, which might affect the local blood flow (78).

4.4.7 pH Monitoring

Tonometry, a noninvasive technique to measure pH using a tonometer, is a method for monitoring the changes in intramucosal pH (pHi) after ischemia. A tonometer is a balloon catheter filled with a isotonic sodium chloride solution, which is placed into the lumen (the inside space of the intestine) allowing the free diffusion of carbon dioxide (CO₂). After an equilibration period, pCO₂ inside the balloon is proportional to the intestinal mucosal pCO₂ so using the Henderson-

Hasselbach equation, the intramucosal pH can be calculated (127, 128). According to the study of Hernandez *et al.* in 1996 pH monitoring is a valuable method to detect early ischemia, they believe that fast and significant changes in pHi occurs after arterial and venous ischemia (129). Millan, in 2006 demonstrated that pHi<7.28 is associated with the high risk of anastomotic leak, the study was performed on 90 patients who underwent colorectal resections (130). One year later in 2007, Kamiya *et al.* used tonometry to observe pHi levels in the intestinal lumen intra and postoperatively on 35 patients (131). According to the results from this study there was a good connection between intramucosal pH and ischemic occurrences. Furthermore, using pHi measurements with tonometry was useful for finding vascular problems in the intestine.

4.4.8 Microdialysis

Microdialysis is a well-known method for measuring metabolism in various tissues such as the brain, muscle and the subcutis during different circumstances. The possibility of using this method in the digestive system has been reported. In a study in 1999 by Tenhunen *et al.* it was confirmed that by monitoring metabolic markers like measurements of glucose, lactate and glycerol from the jejunal wall, intestinal microdialysis can be used as an indicator of intestinal ischaemia (132) with high sensitivity and specificity (133). In another study in 2008 a microdialysis analyser was applied to measure glucose and lactate levels intraoperatively in the bowel tissue of several subjects when they were been resected, the results from this study showed this technique in clinical practice is feasible (134).

4.5 Discussion

The survivability of the gastrointestinal serosal (refer to Chapter 2) in an abnormal condition is of great importance, for that reason methods enabling measurement of gastric blood flow are of great interest. One important factor in a successful gastro-surgical program is to have an effective method of monitoring blood perfusion (135).

As discussed in this chapter, quantitative evaluation of intestinal viability through

objective measurement has been attempted, using various methods to find an easy and reliable method of monitoring bowel viability, probably dating back to the first study in 1976. Subsequent investigations have continuously been introduced to new methods in the hope of finding an ideal monitoring technique in the assessment of bowel viability. To date however, no ideal monitoring method has been found, since none of the mentioned methods can fulfil the criteria of the ideal monitoring method for bowel viability; some are invasive and others are time consuming or unreliable. The ideal bowel monitoring method should be reliable, fast, easy to use, accurate with least false negative results, be non-invasive, safe, cheap, objective and reproducible.

Among various monitoring techniques to date, just a few have found wide acceptance and clinical applicability including laser Doppler flowmetry. Good correlation has been obtained between the LDF signal and intestinal blood flow. The laser Doppler flowmeter still is a promising technique for studying gastric perfusion during operation and endoscopy (158). LDF has been employed as one of the two techniques in this study. The other technique is pulse oximetry. So in order to investigate a potentially ideal method for monitoring bowel viability intraoperatively a combined PPG/LDF probe was proposed.

Several studies investigated the combination of laser Doppler flowmetry (LDF) and photoplethysmography (PPG) measurements. Examples include the characterisation of scleroderma and primary Raynaud's phenomenon by Rosato *et al.* (136), pressure ulcer research by Bergstrand (137), assessment of peripheral blood flow at different vascular depths by Hagblad (138) and detection of colonic ischaemia in dogs by Avino *et al.* (139).

The following chapter presents the basic principle of photoplethysmography and pulse oximetry.

Photoplethysmography and Pulse Oximetry

5.1 Introduction

Measurement of arterial blood oxygen saturation is one of the most important factors in clinical physiological monitoring. The oxygen saturation describes the percentage of haemoglobin binding sites in the bloodstream occupied by oxygen. Photoplethysmography is an optical technique that provides a means to measure the oxygen saturation noninvasively, namely pulse oximetry (140). The pulse oximeter is now an indispensable monitoring device in anaesthesia, critical care and other areas of medicine (141).

5.2 Photoplethysmography

Photoplethysmography (PPG) is a non-invasive electro-optical method developed by Hertzman (142). PPG can provide information on the blood volume changes in the body, caused by cardiovascular pulsations in the target tissue (143). A photoplethysmogram, is achieved by illuminating a portion of the living tissue of interest and detecting the reflected or transmitted light. Photoplethysmography requires two basic forms of optoelectronic components: one for emitting visible or near-infrared light into tissue and the other for detecting the intensity of the transmitted or reflected (backscattered) light, i.e. the portion of light that is not absorbed by tissue and blood. Variation in the signal correlates to pulsatile changes in blood volume, from which blood flow may be inferred (144).

Various ranges of tissue depths can be investigated using suitable combinations of distances between the light source and the photo detector and suitable choice of

wavelength. By using a short distance from a green LED (560 nm) to a photo detector, a shallow penetration depth can be achieved. On the other hand, using near-infrared light (810 nm) placed at a further distance from the sensor, e.g. 25 mm, can measure a deeper penetration (145, 146).

5.3 History of Photoplethysmography

In 1937, Alrick B. Hertzman *et al.* (147) demonstrated that blood volume changes when it is induced by exercise or exposure to cold. In 1940 Hertzman and Dillon (148) separated the pulsatile and static components using separate electronic amplifiers and used them to monitor vasomotor activity. Hertzman believed that movement of the measurement probe against the skin could be avoided; which led to the development of elaborate positioning devices. To create this device, Hertzman used a battery powered torch lamp, which was not ideal due to its relatively wide spectrum, and the widespread illumination. Moreover, using the torch lamp, constant light intensity could not be guaranteed. The improvements in optoelectronics and also medical instrumentation led to the development of photoplethysmography equipment, which was small, reliable, low-cost and user friendly (140, 146). Considerable improvements in the size, sensitivity, reliability and reproducibility of PPG recording and the design of PPG sensors were possible due to development in semiconductor technology. Computer-based digital signal processing and pulse wave analysis have since undergone significant developments. All these developments have contributed to the adoption and success of pulse oximetry as a clinical tool (149).

5.4 The Photoplethysmographic Waveform

The PPG signal consists of two components: a static DC part and a pulsatile AC part (Figure 4.1). The AC component is a periodic waveform, which represents the pulsing of the blood in the arteries while the DC component, which dominates the total signal, is produced by the partial transmission or backscattering of light from the

non-pulsing arterial blood, the venous and capillary blood and also other tissues. The AC part may be separated from the DC part using a high pass filter and amplifier stage. Since a large portion of light from the source, passes through the tissue without any contact with blood vessels, the DC part is bigger compared to the very small AC components (produced as a result of light passing through arterial blood vessels). Immediately after systole, the amount of blood in the arteries increases leading to an increase of the absorbance of light by the blood (which is highly absorbing due to the high concentration of haemoglobin present), and as a result, the intensity of light reaching the photo detector is reduced. During diastole, the amount of blood in the arteries decreases, resulting in an increase in the light transmission (143, 150). Thus the part of the detected signal due to the arterial blood appears pulsatile in nature, synchronous with the heart rate, as shown in Figure 5.1.

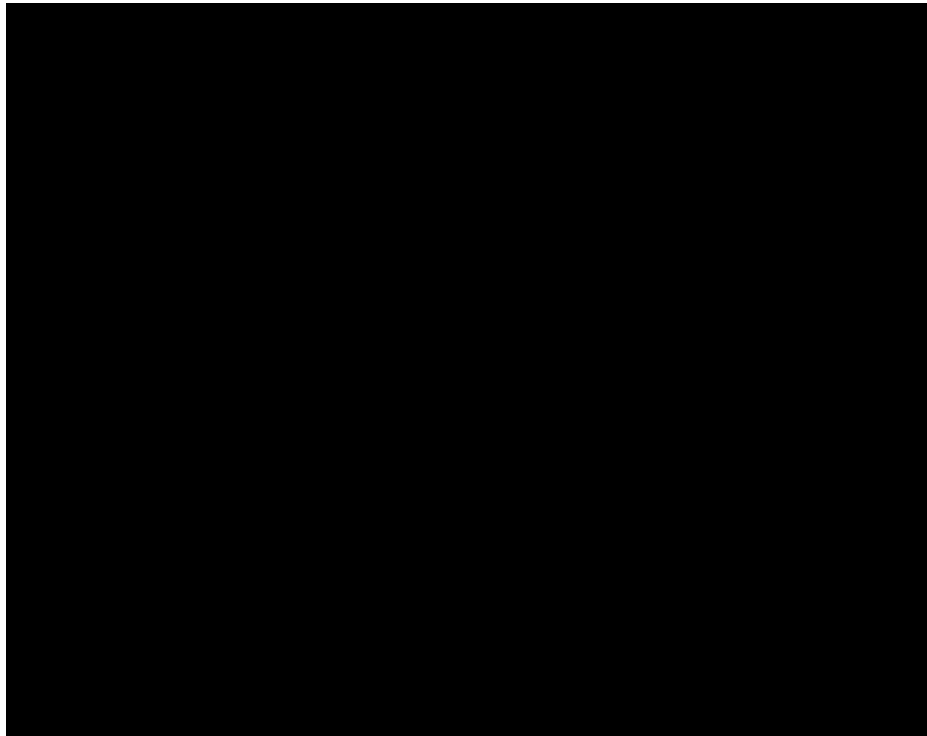


Figure 5.1: PPG: The origin of the signal (AC, DC) and absorbed light (151).

5.5 Photoplethysmography Operation

LEDs and the detector can be placed in one of two configurations. In transmission mode operation, the target tissue (e.g. fingertip) is placed between the light source and the photo detector, while in reflection mode operation, the light source and the detector are placed next to each other as shown in Figure 5.2 (152).

In order to decrease the possible motion artefact, the PPG sensor needs to be held in place avoiding movement. Other sources of artefact including ambient light interference must be considered. Artefact can be minimised in several ways including using a suitable probe attached to the skin, shielding of the measurement site from ambient light and using electronic filtering (153).

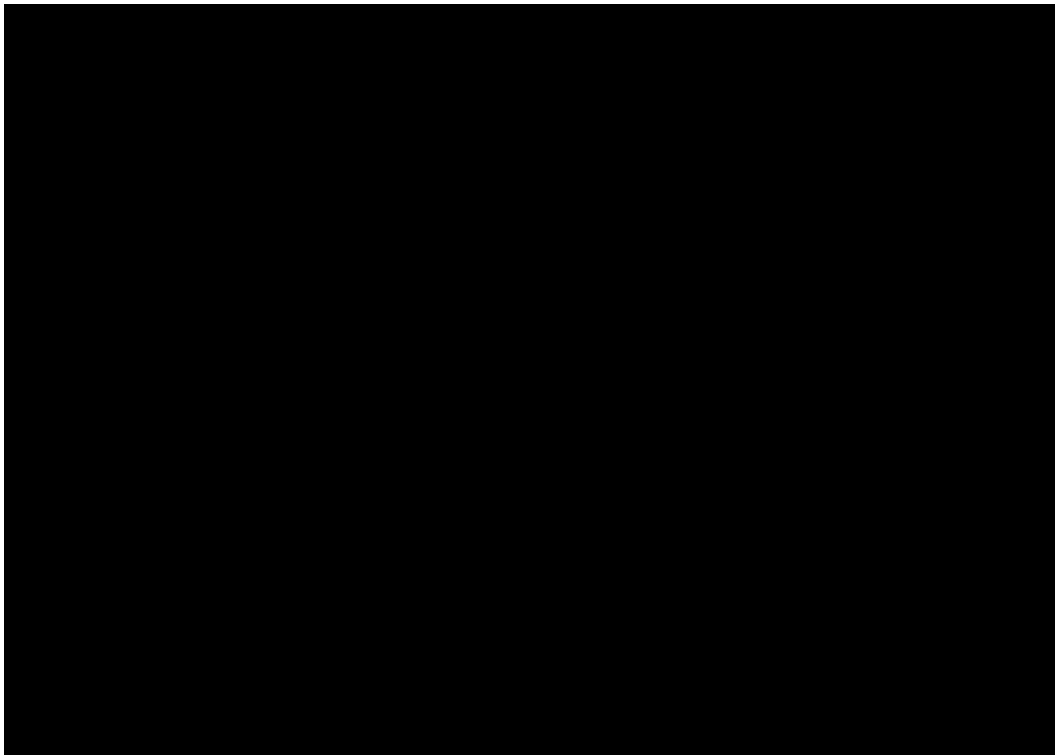


Figure 5.2: Two main operations of sending light, (right) Transmission method, (left) Reflectance method (154).

5.6 Pulse Oximetry

Measurement of oxygen saturation using the optical principles dates back to the 1930s, when it was demonstrated by Karl Matthes, that red light passes readily through oxyhaemoglobin but reduced haemoglobin absorbs it more strongly (155). Karl Matthes constructed the first device to measure blood oxygen saturation in vivo continuously. Two wavelengths of light were used in his device, one sensitive to oxygen saturation and the other, in the infrared range, was used to compensate for changes in tissue thickness and light intensity. This method was useful in following trends in saturation, but it was difficult to calibrate, thus limiting its application. In the early 1940s, Millikan developed an instrument named an “oximeter” to measure arterial oxygen saturation from the ear of World War II pilots (156). Since his ear oximeter was not calibrated Millikan had to guess the normal saturation for each case. Then Goldie, Wood and Geraci worked on Millikan’s ear oximeter which resulted in important subsequent improvements of the device (157).

In 1949, the monitoring of SaO_2 (arterial oxygen saturation measured using a haemoximeter) was described by Brinkman and Zijlstra, which was based upon skin reflectance spectroscopy from the forehead. Their idea was based on using light reflection instead of tissue transillumination, resulted in monitoring of SaO_2 from almost any part of the body (158). Their idea was followed by a more advanced photoelectric method suggested by Sekelj *et al.* for SaO_2 determination (159). Later the fiber optic catheter oximeter was proposed by Polanyi and Hehir (160), which is in fact the basis for the modern oximeter. Others like Robert Shaw in 1964 and Hewlett-Packard in the early 1970s worked to improve the ear oximeters (161). They tried to mount a sensor in the ear and light delivered via a fiberoptic cable with a heating element in order to keep the tissue locally perfused with blood. Significant progresses were added by Cohen and Wardsworth by a non-invasive reflectance oximetry (162).

In 1972 Takuo Aoyagi designed the modern two-wavelength pulse oximetry while he

was working on an experiment to measure the light passing through the earlobe, instead he noticed that light transmitting through the earlobe was able to show pulsatile variations. He tried to eliminate or remove these variations, and then he realized that the ratio of pulsatile signals measured at two different wavelengths could be related to oxygen saturation in the arterial blood. Later the OLV-5100, the first pulse oximeter, was presented by him and his team in March 1974. The number of wavelengths necessary for the measurement of arterial oxygen saturation reduced from eight (used in the HP instrument) to two (163). However, all these early instruments suffered from a number of disadvantages including lack of suitable calibration method, difficulty in distinguishing tissue, arterial blood and venous blood or error due to unknown optical path length (164).

In the late 1970s, several scientific groups began working on refinements to pulse oximetry. Advances in semiconductor technology, solid state devices such as LEDs, photodiodes and microprocessors led to the development of modern pulse oximetry. LEDs emit a very narrow band of wavelengths that can massively improve the signal quality and therefore the accuracy of pulse oximeters. In 1981, two companies, Nellcor and Ohmeda, presented commercial pulse oximeters using LEDs and a photodiode. These LEDs and photodiode were small in size and both can be mounted directly on the sensor probe applied to the patient's finger (165). Many manufacturers currently produce pulse oximeters that give clinicians high levels of confidence in the readings of oxygen saturation.

On the 1st January 1990, the American Society of Anesthesiologists (ASA) made pulse oximetry a standard for use intraoperatively. Since then, pulse oximetry has become the standard method for monitoring oxygenation during sedation, anaesthesia, post anaesthesia intensive care including neonatal intensive care, and recovery from anaesthesia (166).

5.7 Pulse Oximeter and Blood Oxygen Saturation

As described in the last section, a pulse oximeter is a routine medical device that estimates the oxygen saturation of a patient's arterial blood noninvasively (since it measures oxygen saturation without the need of a blood sample) using a dual wavelength spectrophotometer by transmitting light through a pulsating arterial vascular bed. It is the most common method to measure and display oxygenation in the human body. The pulse oximeter displays the oxygen saturation (SpO_2), the percentage of hemoglobin in the arterial circulation that is bound to oxygen (141).

A pulse oximeter can be a useful device in any situation where normal oxygenation is doubtful, unstable or at risk, including intensive care, surgery, recovery, emergency and hospital ward settings, for general assessment of a patient's oxygenation, and also to determine if supplemental oxygen is needed (140).

Pulse oximeters operate in two modes, either by reflection or transmission, the mode determining the design of the sensor or probe. The accuracy of pulse oximetry may be compromised by dyshaemoglobinaemias, poor peripheral pulse and other physiological states, and it is not reliable at low saturation level. Despite these limitations, pulse oximetry is perhaps the most significant recent development in clinical physiological monitoring (141). A typical portable commercial oximeter is shown in Figure 5.3.



Figure 5.3: Pulse Oximeter device.

5.8 Light Emitting Diodes (LEDs)

A light emitting diode is a light source that produces and emits light when an electric current is applied in the forward bias direction of the device. The principle of pulse oximetry is based on the emission of light by two LEDs with different wavelengths as light sources usually red and infrared (the wavelength for red is around 660 nm, and for infrared, typically are 905, 910, or 940 nm) through the cutaneous vascular beds in peripheral regions such as the finger, toe or earlobe. A photo detector in the probe detects the reflected or transmitted light. The absorption spectrum of oxyhaemoglobin varies significantly from that of deoxyhaemoglobin as can be seen in Figure 5.4. The extinction coefficient of deoxyhemoglobin is much higher than for that of oxyhaemoglobin in the red region of the spectrum (around 660 nm), meanwhile at 940 nm, oxyhemoglobin has a higher absorption. Once the absorption levels are detected, the ratio of absorption between oxyhemoglobin and

deoxyhemoglobin can be determined (152, 167 and 168). Melanin and other skin pigments absorb a great amount of light at wavelengths shorter than 600 nm, while water strongly absorbs wavelengths longer than 1 μm . Since the light absorption of oxyhaemoglobin and deoxyhaemoglobin are not the same at red and infrared, the amplitudes of the red and infrared AC signals (Section 5.3) are sensitive to changes in SpO_2 (144).

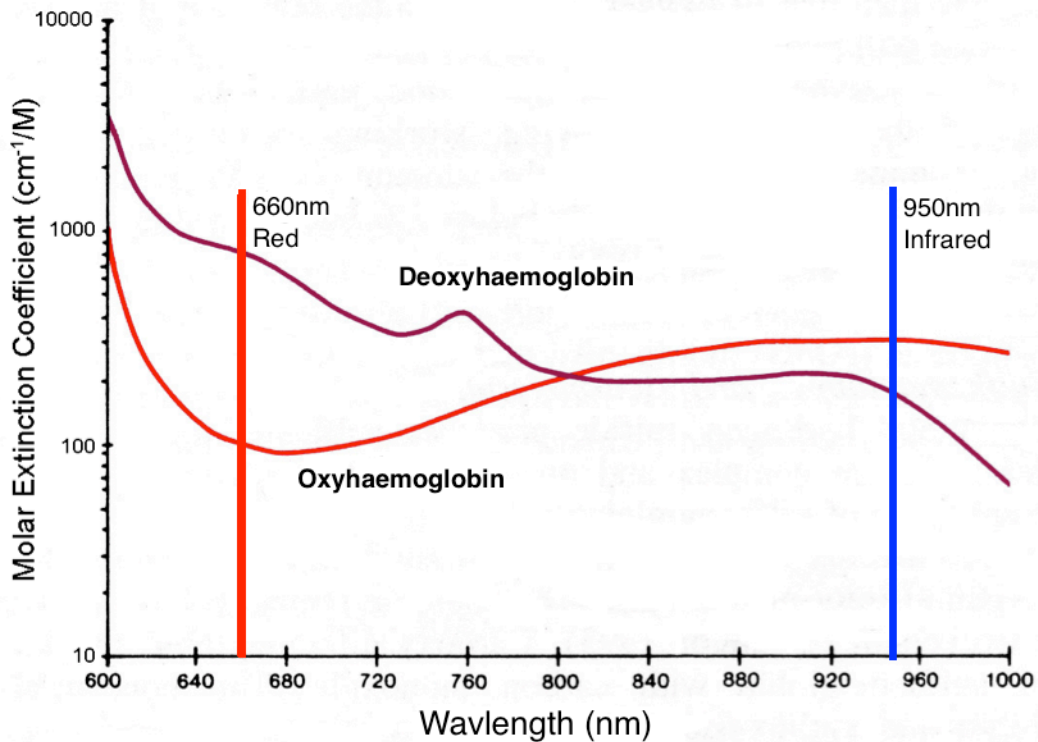


Figure 5.4: Absorption levels of oxygenated and deoxygenated (169).

From the normalised amplitude ratios (AC/DC) for each wavelength, SpO_2 can be estimated. The absorbance of oxyhemoglobin and deoxyhemoglobin is equal for the wavelengths of 590 and 805 nm (isosbestic point); in some earlier oximeters these wavelengths were used for correction of hemoglobin concentration. The monitored signal is synchronous with the heart beat due to arterial blood vessels expanding and contracting in response to periodic variations in blood pressure over the cardiac cycle (143).

5.9 Photodetector

The photodetector is used to convert light energy into an electrical current. There are many types of photodetectors such as photodiodes, phototransistors and photoresistors. The photodiode has been chosen as a photodetector for many reasons including: it has an excellent linearity of output current as a function of incident light, it is sensitive, has fast response times and has a spectral response from 190 nm to 1100 nm (170).

5.10 Principles of Pulse Oximetry

The principle of pulse oximetry is based on the fact that oxygenated and deoxygenated haemoglobin absorb the red (R) and infrared (IR) light at different wavelengths with different absorption levels. Haemoglobin (Hb) absorbs relatively more light at 660 nm than oxyhaemoglobin (HbO_2), while HbO_2 absorbs more light at 940 nm than Hb. Thus comparisons of the absorbencies at different wavelengths allow the estimation of the relative concentrations of HbO_2 and Hb (i.e. saturation)(171). The detector measures the intensity of the transmitted light at each wavelength and the changes in light absorption during the arterial pulsatile flow can be analysed, and the arterial oxygen saturation (SpO_2) is derived by the ratio between the red light and the infrared light (172).

With each heartbeat the left ventricle contracts and pumps blood into the systemic arterial system, this leads to a pressure increase in the arteries (systolic pressure) followed by a decrease in pressure (diastolic pressure). As a result the blood volume in the arteries including the peripheral arteries will increase leading to more light absorption during systole. The photoplethysmographic signal recorded by the pulse oximeter at a peripheral site resembles the shape of a peripheral arterial pressure waveform. The pulsatile waveform consists of AC and DC components as can be seen from Figure 5.5 (140).



Figure 5.5: Pulsatile signals observed during pulse oximetry (173).

In order to find the percentage of blood oxygen saturation, the ratio of ratios R_R is used (169). AC and DC components from each of the wavelengths need to be measured and taken as a ratio as follows:

$$R_R = \frac{R_{AC}/R_{DC}}{IR_{AC}/IR_{DC}} \quad \text{Equation 5.1}$$

Where R_{AC} and IR_{AC} are the AC components of red and infrared light sources, respectively, while, R_{DC} and IR_{DC} are DC components of red and infrared light sources, respectively. The SpO_2 values can be obtained using the following formula:

$$SpO_2 = 110 - 25 (R_R) \quad \text{Equation 5.2}$$

Normal arterial oxygen saturation values in a healthy individual are 95% to 99% (174).

5.10.1 Beer-Lambert law

The intensity I_t of light transmitted through a medium is given by the Beer-Lambert

law:

$$I_t = I_0 \exp(-\alpha(\lambda)cl)$$

Equation 5.3

Where I_0 is the intensity of incident light that enters the medium, $\alpha(\lambda)$ is a wavelength-dependent absorbance coefficient, l is the distance the light travels through the media and c is molar concentration of the absorbing species (see Figure 5.6) (175).

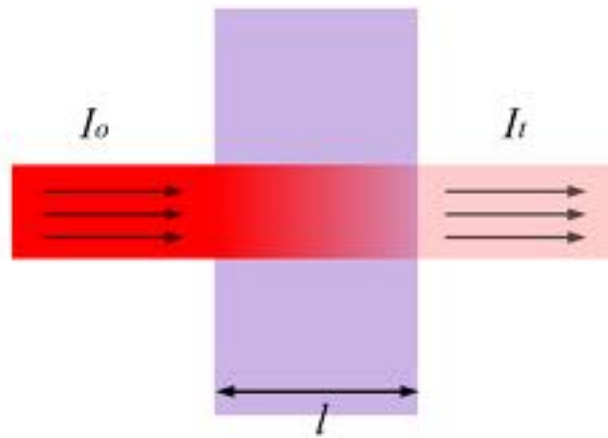


Figure 5.6: light of intensity I_0 enters the medium and is transmitted with intensity I_t , l is the path with the path length through the medium.

5.11 Typical Photoplethysmographic Waveform

A typical PPG signal is shown in Figure 5.7. The PPG signal contains additional information in its shape, height, timing, some of which may be used to extract clinically useful information. A recognizable feature is the “dicrotic notch” which is a sudden drop in pressure after systolic contraction. The dicrotic notch represents the closure of the aortic valve after the end of systole (176). The period of the waveform can be used to calculate the heart rate.

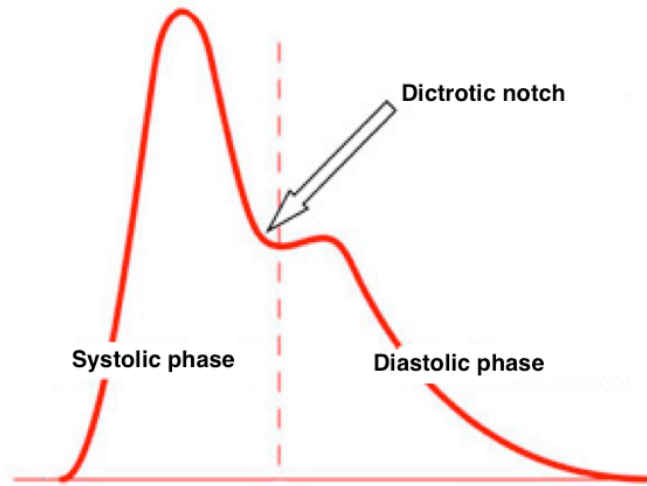


Figure 5.7: Dicrotic notch in a normal arterial pulsation waveform.

5.12 Calibration of Pulse Oximeters

The first pulse oximeters, manufactured in the early 1980s, used Equation 5.2 to calibrate the value of S_aO_2 , which is based on the Beer-Lambert law. However all manufactures use the empirical calibration as right conditions for using Beer-Lamberts law since the Beer-Lambert law does not consider the multiple scattering of light by the red blood cell.

There are two definitions for oxygen saturation: functional oxygen saturation and fractional oxygen saturation (175). Functional saturation considers only haemoglobin species capable of binding with oxygen:

$$\text{Functional } S_aO_2 = \frac{HbO_2}{HbO_2+Hb} \times 100\% \quad \text{Equation 5.4}$$

Fractional saturation includes dysfunctional haemoglobins, the most common being carboxyhaemoglobin (HbCO) and methaemoglobin (MetHb) (175):

$$\text{Fractional } S_a O_2 = \frac{\text{Hb}O_2}{\text{Hb}O_2 + \text{Hb} + \text{HbCO} + \text{MetHb}} \times 100\%$$

Equation 5.5

5.13 Pulse Oximetry Limitations

There are some factors that interfere with accurate determination of SpO₂ and should be considered with its use. These factors include ambient light, body movement, skin pigmentation, hypoperfusion, administration of vasopressors and hypothermia and more (177). Table 5.1 shows factors that have an affect on pulse oximetry (178).

Table 5.1 Factors that affect pulse oximetry

Factors	Effect on Pulse Oximetry
Emergent	
Cardiac arrest	Poor signal
Respiratory arrest	Poor signal
Shock	Poor signal
Physiologic	
Jaundice	No interference
Anemia	No interference
Cardiac arrhythmia	Poor signal
Environmental	
Bright light or sunshine	False increase in signal (overreading)
Shivering, tremors, rigors, motion	Poor signal
Electrical frequencies	Interference with signal
Mechanical interference with Poor signal circulation (blood pressure cuff, tourniquet, arterial line)	Poor signal

The following chapter presents the principle of laser Doppler flowmetry (LDF) technique.

Laser Doppler Flowmetry

6.1 Introduction

The Austrian physicist Christian Doppler was the first to describe in 1842 the apparent shift in frequency of sound waves when their source is approaching or receding from an observer. When a source of waves and the receiver are approaching each other, the frequency of the detected waves increases and the wavelength is shortened; sounds are detected with higher pitch and, in the case of light waves, light appears bluer. On the other hand if the sender and receiver are moving apart, detected sounds become lower pitched and light appears redder. The apparent frequency shift is known as the Doppler effect (179).

The Doppler effect is employed in laser Doppler flowmeters for measuring microvascular blood flow. In brief, a beam of laser light, transferred by a fibre-optic probe, interacts with moving components of tissue such as red blood cells and is Doppler shifted while light interacting with static objects is unchanged (see Figure 6.1) (179). The light is then scattered and partially absorbed by the tissue under investigation. A returning fibre picks up the light, converts into an electrical signal and the output signal provides an estimation of blood flow. The 'flux' is commonly used in order to describe the blood flow measured by the laser Doppler technique. And it is the product of the velocity and the number of red cells in the volume of tissue interrogated by the probe (180). The principle of LDF will be presented in the next section.

In 1955 Forrester *et al.* (181) was the first to determine the basis for LDF and tried to improve his theory later (182), then this principle for LDF was developed by Cummins and Swinney (183) during the 1960s. Later in 1975 Stern successfully introduced LDF into the field of biomedical engineering by presenting *in vivo* measurements (184). After that LDF progressed rapidly with improvements like introducing the first fibre-optic based laser Doppler perfusion

monitoring (LDPM) by Holloway and Watkins in 1977 (185). Again in 1980 this was improved by Nilsson *et al.* (186). Continuous improvements were made in later years (187, 188), the first imaging system was also introduced in 1989 by Nilsson *et al.* (189), these techniques will be discussed in Section 6.4.

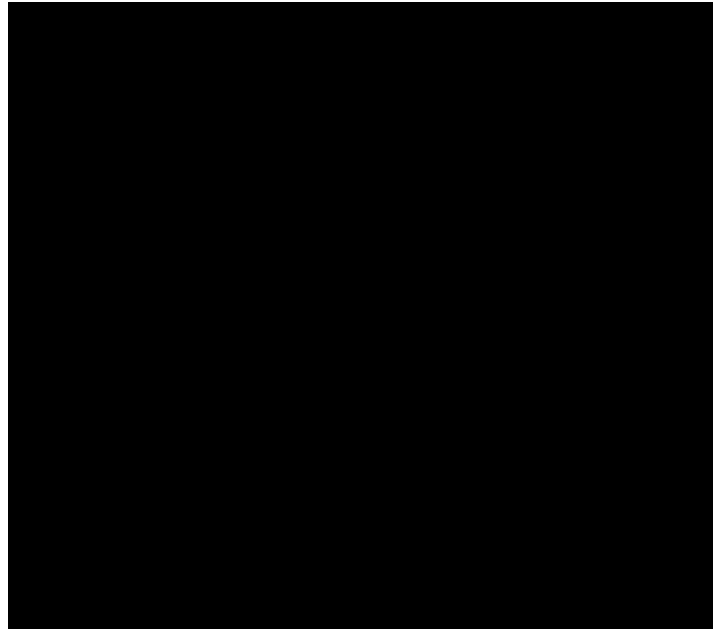


Figure 6.1: Principles of operation in laser Doppler flowmetry. A laser beam is directed into a target tissue. Light waves are reflected and scattered after contacting with moving objects like red blood cells. The backscattered light (both unshifted and Doppler shifted) then can be detected and received by a photodetector (190).

Various methods for measuring skin blood flow have been studied; such as fluorescent traces, thermography, laser Doppler flowmetry, Doppler ultrasound etc. Of these techniques, laser Doppler flowmetry (LDF) has been of great interest in studies and research as well as clinical settings. Generally speaking, the main advantage of this technique is its non-invasiveness, the ability to measure the microcirculation of the tissue and the ability to resolve small changes very quickly. Since the commercialisation of the technique (in 1980), LDF has undergone a lot of improvement in perfusion monitoring.

Since then the number of peer-reviewed articles, which have used LDF in their research has increased (191). Although, like most monitoring techniques, LDF

has some drawbacks, which will be discussed later. The principle of LDF is discussed in the following section.

6.2 Principle of LDF

Laser Doppler flowmetry (LDF) is a method for estimating the measurement of microvascular red blood cells (or erythrocytes) perfusion in tissue including capillaries, arterioles, venules and shunting vessels. The technique is based on the emission of laser light carried by a fibre-optic probe attached to or inserted into the target tissue. Laser light from this fibre, transmits photons into the tissue, which then are scattered and reflected within the tissue and eventually some are scattered back to the probe. Another optical fibre collects the backscattered light from the target tissue (see Figure 6.1). At which stage the photodiode receives the photons and converts them into current. Every photon that encounters a moving red blood cell (RBC) or any other moving particle undergoes a shift in frequency, the magnitude of which depend on the velocity of the moving cells (192), this small frequency shift is the basics of LDF theory (190, 191). Figure 6.2 shows a laser beam of single frequency f_i colliding with a single object as a RBC moving at velocity v at an angle α_i in the direction of v , and scattered by the RBC in different directions. The frequency of this light differs from f_i in the direction of the detector with the angel defined as α_s . This small frequency shift Δf can be obtained using Equation 6.1 (179).

$$\Delta f = v (\cos \alpha_s - \cos \alpha_i) \frac{n}{\lambda} \quad \text{Equation 6.1}$$

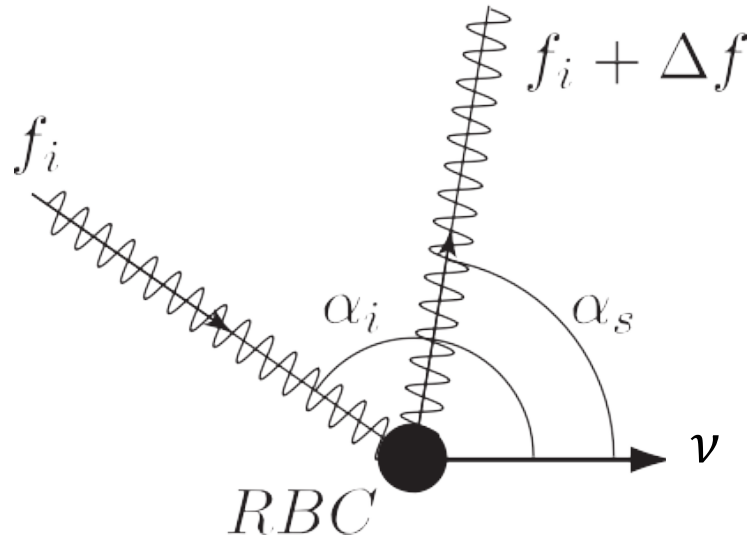


Figure 6.2: The Doppler effect: The frequency of the light scattered by the moving objects (RBC) with velocity ν in the direction defined by α_s is shifted in frequency by an amount Δf compared to that of the light of frequency f_i , which hits the RBC at an angle α_i (179).

The backscattered light from the target tissue is analysed to retrieve information about the blood flow in the microcirculation, by analysing the frequency shift of the backscattered light, conclusions about the amount and velocity of the blood flow can be illustrated (193). The principle of LDF shown in Figure 6.1 and Figure 6.3 shows a laser Doppler perfusion monitoring system.

The flux is proportional to the average velocity (proportional to the beat frequency) and number of red blood cells in the area of investigation (proportional to the intensity of the Doppler shifted light), which can be calculated using Equation 6.2 (179).

$$Flux = k \times \nu \times Vol \quad \text{Equation 6.2}$$

Where k is proportionality constant, ν is the mean speed of the RBCs in the sampling volume (proportional to the mean Δf) and Vol is the concentration of moving RBCs in this volume.

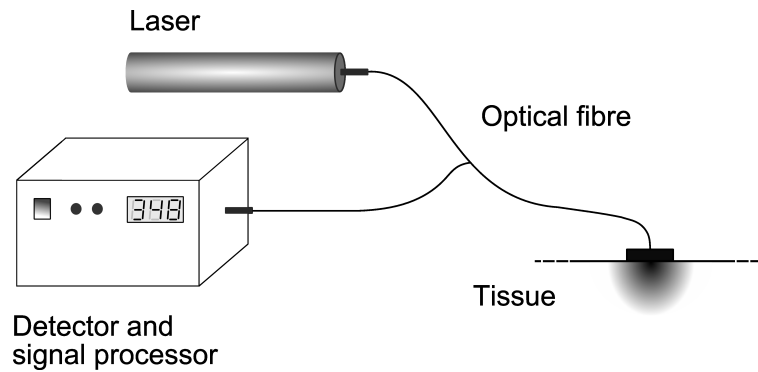


Figure 6.3: Laser Doppler perfusion monitoring system (194).

LDF is a non-invasive technique for assessment the blood perfusion in the microcirculation that has been proven as a useful measurement in most organ systems (195, 196). LDF is currently used in a variety of fields in medicine, especially in biomedical research and clinical settings including wound healing (197), assessment of burn wound depth (198), skin tumour characterisation (199), amputation level determination (200, 201), neurosurgery (202), and breast reconstruction (203). Other clinical researches such as cerebral monitoring, flap transfer surgery, transplantation surgery and vital organ monitoring, pharmacology, and also peripheral vascular disease research have been used by the means of LDF (194). A list of laser Doppler applications is provided in Table 6.1.

Laser Doppler flowmetry has some limitations: the tissues' optical properties might have an affect on the perfusion signal, noise caused by motion artefact, lack of knowledge of the depth of measurement, lack of quantitative units for perfusion and also the biological zero signal (perfusion measured when there is no flow condition)(191). Also it is impossible to determine exact measurements of blood flow because the plasma component of blood is not detected and so does not contribute to the Doppler shift. Since LDF cannot give the absolute measurement of blood perfusion, this limits its application in the clinical setting. The direction of movement of the blood cells relative to the probe is also not known, as the frequency difference between Doppler shifted and un-shifted light is always positive, regardless of whether the actual frequency shift is positive or negative (194). Although, regardless of all these limitations, LDF remains in high

demand for monitoring microcirculatory blood flow, is routinely used in some areas of medicine and has found application in many areas of research such as monitoring small-vessel perfusion in kidneys, liver, muscles, intestines, brain and heart (191). Some of these limitations will be discussed in details in Section 6.6.

Table 6.1: Laser Doppler applications

Angiogenesis
Burn depth assessment
Cardiovascular monitoring
Dentistry
Dermatology
Gastroenterology
Impotence
Ischemia
Neurology/cerebral blood flow
Oncology
Ophthalmology
Otology
Rheumatology

6.3 Light Source

The incident laser light beam used in LDF must be monochromatic (light of a specific wavelength). It has a penetration depth of approximately 1 mm however in blood-rich organs like the kidney or the liver, the measuring depth will be considerably decreased to less than one millimetre. If the blood supply to a region is limited for any reason, the measuring depth will increase due to the lack of blood permits increased passage of light in the area. The penetration depth of light is influenced by the path that light takes through the skin. The penetration depth is limited by some factors, like absorption and scattering effects of the area of tissue. The measuring depth depends also on the structure of the capillary beds and their density, oxygenation, etc. The wavelength of the laser light and the distance between the sending and receiving fibres in the laser Doppler probe

used, also affects on the measurement depth (203). The volume of light penetration is generally 1 mm³ or smaller (194) (Figure 6.4).

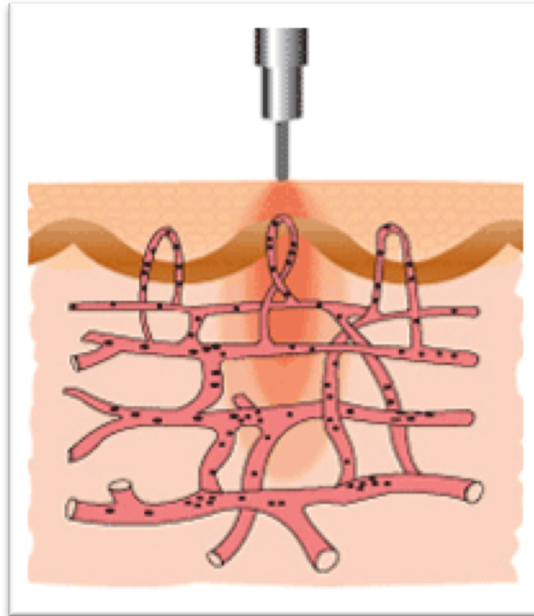


Figure 6.4: The volume of light penetration is generally 1 mm³ or smaller (193).

Although laser Doppler has undergone significant improvement since it was first introduced, there is still no current LDF instrument that can provide absolute perfusion values (e.g. ml/min/100 gram tissue). Measurements are stated as Perfusion Units (PU), which are arbitrary, as the laser Doppler instrument cannot show blood flux in absolute values (203).

The actual frequency of the light is too high to be measured using low cost electronics (being of the order of 10^{14} Hz), instead the Doppler shifted light interferes with light scattered from static objects to produce a modulation ('beat' frequency) equal to the difference in frequency between the frequency shifted and incident light. The beat frequency is typically in the range 0-8 kHz, so may be readily measured using simple circuitry (194).

The techniques of laser Doppler are presented in the following section.

6.4 LDF Techniques

As mentioned earlier in this chapter, typically there are two kinds of perfusion measurements, single point (LDPM) and imaging (LDPI) systems. Laser Doppler perfusion monitoring (LDPM) measures the perfusion in just one point of sample tissue. On the other hand laser Doppler perfusion imaging (LDPI) instruments is able to provide perfusion monitoring for a larger area in which the laser beam is scanned over the area of interest (191, 205). In this section, the special characteristics of these systems, as well as an advanced type of imaging systems based on fast CMOS cameras, are described. LDPM and LDPI instruments are both commercially available.

6.4.1 Laser Doppler Perfusion Monitoring (LDPM)

In laser Doppler perfusion monitor, a fibre optic probe with one multimode fibre has been used, which delivers the laser light to the target tissue. Another multimode fibre is used to detect the back-scattered photons (Figure 6.5 (a)). In this technique the perfusion of one point of target tissue in real time is recorded. The wavelength and the fibre separation used in the instrument indicate the measurement depth and sampling volume. According to this the measuring depth in normal skin with a probe fibre separation 0.25 mm (which is a standard probe separation) and 780 nm wavelengths is between 0.5 to 1 millimetre and the measurement volume is about 1 mm³ (191).

For laser Doppler instruments the main manufacturers are Perimed AB (Stockholm, Sweden), Moor Instruments Ltd. (Axminster, UK), Transonic Systems Inc. (Ithaca, New York, USA), Oxford Optronix Ltd (Oxford, UK) and LEA Medizintechnik (Giessen, Germany). The wavelengths typically used by these manufactures are mostly 630 nm, 780 nm and 830 nm, with approximately fibre-to-fibre distances of 0.25 mm, 0.5 mm and 0.78 mm (apart from the instruments by LEA) (191).

There are many different types of probes available for different applications such as fibre probe systems (206) and integrated probe systems (207).

The advantage of LDPM compared to other monitoring methods in the measurement of microvascular blood perfusion is the fact that it is able to recognize even small changes in local blood perfusion very quickly (less than 0.1 s), making it useful for continuous perfusion monitoring. Another advantage is that it is non-invasive since the probe does not need to touch the surface of the tissue and as a result the normal physiological state of the microcirculation won't be affected. Furthermore, the small dimension of the probe means it can be used in experimental environments that are hard to access (191).

This technique has its limitations. Since it has been designed to record tissue perfusion at a single point over time, any information regarding the surrounding perfusion area is not gathered (208, 209). Another issue with this technique is that the results of the measurements are proportional to blood flow and since the factor of proportionality are not the same for different tissues and tissues sites means that the system does not present exact measurements of blood flow. The flux measured in commercial LDPM systems is generally referred to by the manufacturers as 'perfusion', and expressed in Perfusion Units (PU), or similar (191).

6.4.2 Laser Doppler Perfusion Imaging (LDPI)

The need to study perfusion over larger tissue areas was the next evolution in laser Doppler, which led to the construction of LDPI, in which a laser Doppler perfusion imaging instrument is able to map the perfusion from a larger area in which the laser beam is scanned over the area of interest to form an image. The scanning procedure lasts for a couple of minutes to form an entire image of the tissue, since in each scanning position for each pixel value the perfusion value has to be calculated and transformed to form an entire image (191). In Figure 6.5(b) the schematic of a scanning laser Doppler perfusion imager is shown. Like LDPM it's a non-invasive technique, however it provides the perfusion for a larger area, with this the average perfusion in heterogeneous tissue can be provided in one measurement (191). Another advantage is that this technique is non-contact so it can be used in clinical situations with hard accessible tissue (191).

This technique has some advantages over the single-probe technique; one is that the blood flow is measured over an area rather than at a single site as in DLPM, so it can remove some of the difficulties that arise in the LDPM technique such as movement artefacts and site-to-site perfusion variations due to the heterogeneous nature of tissue. This technique has special limitations, one is the length of time taken to complete a full scan is extensive; examining a rapid change in blood flow cannot be done over short periods (191). However some studies have been made to reduce these limits. Also the distance between the imager and the tissue might affect the measurements, as in if this distance changes between the subsequent measurements it can affect the results (210).

Perimed AB and Moor Instruments Ltd are the major manufacturers of laser Doppler perfusion imagers.

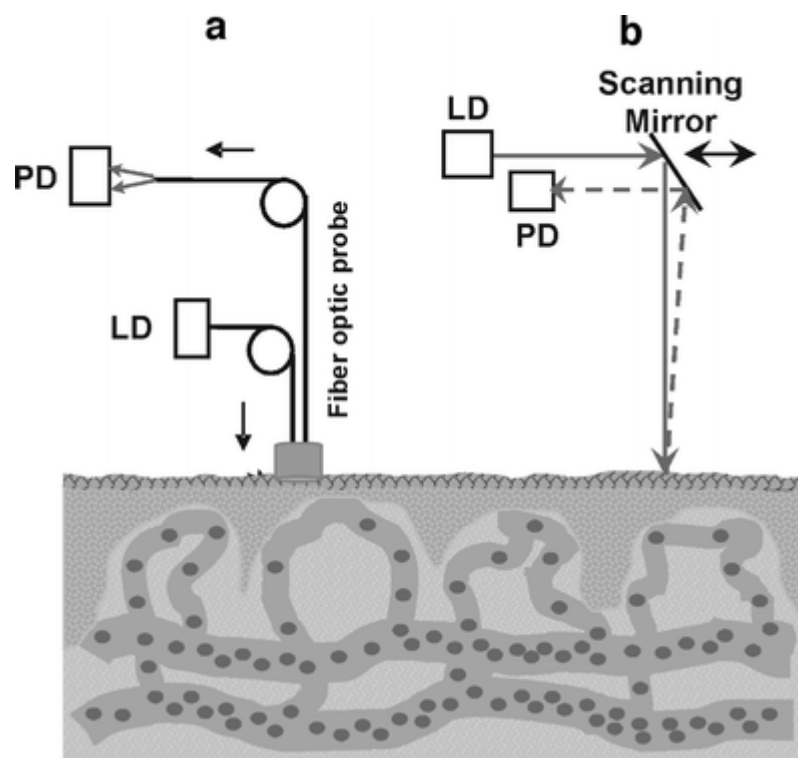


Figure 6.5: A diagram of (a) LDPM and (b) LDPI geometries on a tissue model. *LD* laser diode, *PD* photodetector (191).

6.4.3 CMOS Imager

As mentioned, LDPI system have some drawbacks, one is that it is slow, and the other is the estimated perfusion value is affected by the spot size of backscattered light. To address these drawbacks a new generation LDPI system, suggested by Serov *et al*, was presented, which is based on fast CMOS cameras to make imaging procedure faster (211-213). The complementary metal oxide semiconductor (CMOS) technology was introduced and a new generation laser Doppler perfusion imaging (214, 215) in which the backscattered light is focused on a detector array. In this system every pixel in the array is used to calculate a perfusion value from the part of the tissue that the pixel sees (Figure 6.6c). So by simultaneously illuminating the whole target tissue, the pixels in the complete image will be obtained simultaneously and the tissue can be mapped using the processing signal obtained by each pixel in time, faster than scanning the area point to point like in LDPI. Movement artefacts can be avoided in this new system, as there is no scanning in the system (191). The disadvantage of this system is that the cameras are not yet fast enough (205).

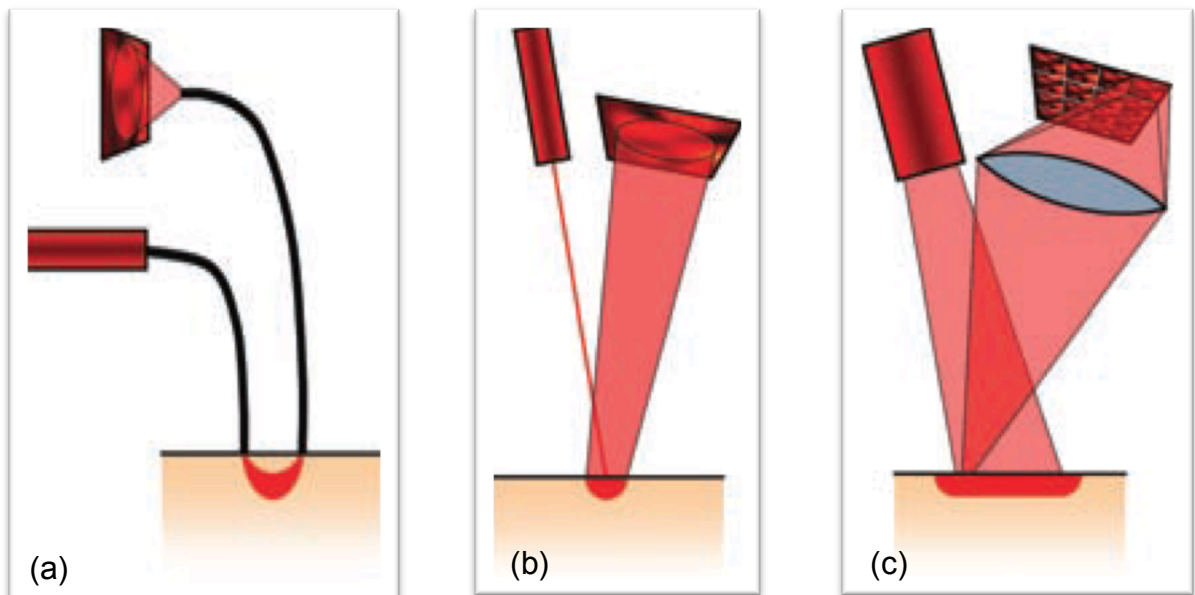


Figure 6.6: Schematic illustrations of the various LDF modalities, LDPM (a), LDPI (b), and CMOS imager (c).

6.5 Limitations of LDF

6.5.1 Calibration Standards

The laser Doppler perfusion signal is a comparative measure of flux, so the measurements need to be standardised. A proper calibration system has been under investigation from the early days of introducing LDF.

To date there is no gold standard available for calibration of LDF in relation to absolute blood flow per unit volume of tissue, due to the varied and heterogeneous distribution of blood vessels in the tissue. Several studies have been performed in the hope of designing and developing a calibration device but the use of these devices has been limited to research. Therefore an ideal calibration system is still under investigation and seems rather difficult to realise (191).

6.5.2 Biological Zero

When a laser Doppler probe is used with tissue in which haemostasis has been applied (e.g. by applying a tight tourniquet to a limb), a residual flux signal is still reported, even when there is no blood flow. Tenland *et al.* (210) was first to suggest that this signal should be called “biological zero” (BZ) and needs to be subtracted from the total output signal. The origin of BZ probably arises from several sources including small involuntary muscle movement, and random movement of red cells and other tissue partly due to Brownian motion (218, 219).

In some clinical applications, the BZ is measured in each experiment and the value subtracted from the normal perfusion value, this might be more important especially when there is very low perfusion in the tissue (220–222). Some studies have been performed to a better understanding of BZ, according to the result of Fagrell and Nilsson (223), the BZ is caused by residual movement of entangled blood cells and other moving components of living tissue, such as vessel wall activity, hair follicles and sweat gland production. In another study by Kernick *et al.* (224), they strongly suggest that since BZ changes with temperature in both in vivo and in vitro measurements, the original BZ signal in the measurement of the skin comes from the Brownian motion of the tissue structure and macromolecules

in the interstitial spaces. Although Kernick *et al.* had shown that temperature might affect BZ, the accuracy of the idea is still under question (191, 224).

6.5.3 Motion Artefacts

One of the important drawbacks of LDF is that the movement artefact has affect on the output signals. Tissue movement or fibre movement both might cause the motion artefact. It has been suggested by Gush and King that some modifications of fibre-optic probes can reduce the movement artefacts. They believe that by using small aperture fibres and keeping the fibre close to the skin can reduce the motion artefacts to some extent (225).

The effect of tissue movement on the blood flow signal in laser Doppler devices was studied by Öberg (225). The results of his study showed that by increasing the tissue movement, the flow signal increases linearly. Other study suggests that motion artefacts have more effect when the measurement device is not in contact with the tissue (like LDPI) compared to the devices that their probe can be fixed on the target tissue (227).

6.5.4 Multiple Doppler Shifts: a theoretical limitation

The theoretical model of laser Doppler perfusion monitors and imagers is based on single Doppler shifted photons for the calculation of blood flow; however, in reality, many of photons might interact with more than one moving object, this might happen mostly in the tissue with high perfusion (191).

These limitations of the laser Doppler technique were addressed by the researchers and many improvements have been obtained. However, some of these limitations given still need to be considered. Although there are still some unsolved limitation, LDF techniques is still of great interest for microcirculatory blood flow measurements.

The design and development of this new combined sensor for intraoperative perfusion monitoring of the intestine will be presented in the next chapter.

Development of a Combined PPG/LDF Optical Probe

7.1 Introduction

A new combined PPG/LDF system has been developed to detect and pre-process the red and infrared photoplethysmographic (PPG) along with Laser Doppler Flowmetry (LDF) signals. Chapter 8 presents the details of the construction of the PPG/LDF instrumentation. This chapter outlines the various stages taken in the design and development of the combined PPG/LDF sensor, which include the choice of components for the PPG probe, the choice of LDF probe, the dimensions and configuration of the sensor, the mechanical construction and also infection control considerations. Finally, evaluation tests were carried out in the laboratory to determine the effectiveness of the sensor as a means of transmitting and receiving light for PPG and LDF measurement.

7.2 Combined Sensor: Design and Construction for the PPG probe

In this study the optical components for the PPG probe were configured in the reflectance mode. This mode was chosen instead of transmission mode to measure the PPG signals from the bowel (refer to Chapter 4 for an explanation of reflectance and transmission modes), since in transmission mode the tissue needs to be placed between the light sources and the photo detector, which would have restricted the choice of monitoring site. A schematic of the combined PPG/LDF probe, based on a printed circuit board design, is shown in Figure 7.1.

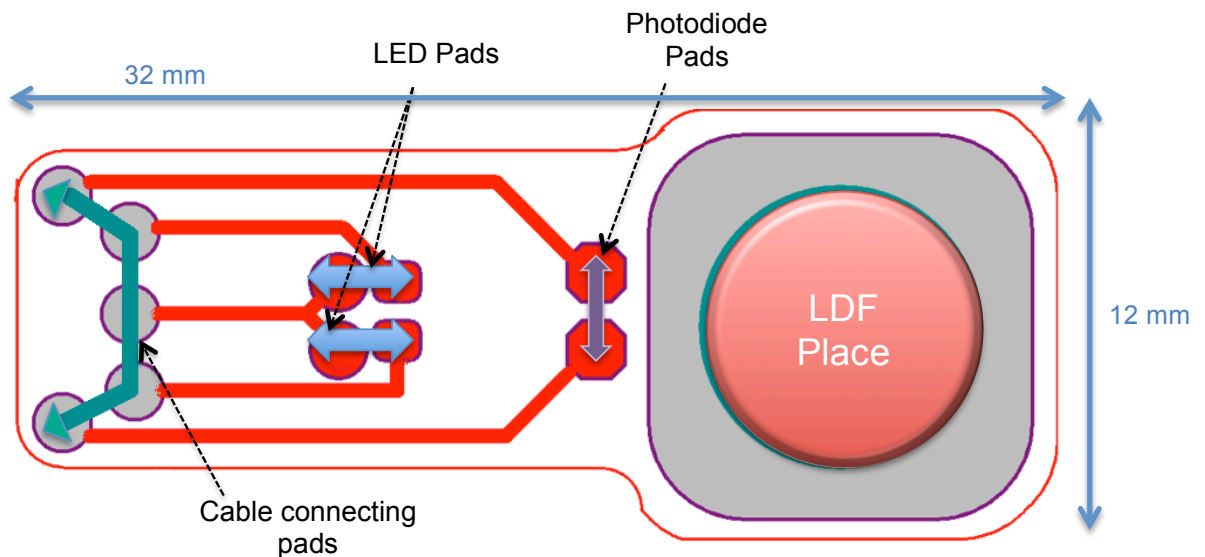


Figure 7.1: A schematic of the combined PPG/LDF probe, including the photodiode, two LEDs and laser Doppler with 8 mm outside diameter.

The shape of the sensor was designed in a rectangular shape and small enough (a width of 12 mm) to be inserted into the Trocar (a sharp-pointed surgical instrument that is placed through the abdomen during laparoscopic surgery as a portal for the subsequent placement of other instruments, such as graspers, scissors, staplers, etc.) for the measurements during the operation. The combined sensor is connected to the processing system by a multicore cable.

7.2.1 PPG Sensor

The PPG part of the sensor consists of a central photo detector surrounded by two light sources for PPG and also incorporates an LDF fibre tip that can be placed on the bowel surface. Details of the choice of light sources and photodetector used will be discussed in the following sections.

Light sources (LEDs)

In order to measure the blood oxygen saturation by oximetry, two wavelengths (usually red and near infrared) are required (Section 4.8). LEDs are ideal for pulse oximeters as light sources as they are cheap (so can be used even in disposable probes), very compact (can fit into very small probes), emit light in a narrow range of wavelengths and do not produce excessive amounts of heat during use (so they do not damage the tissue) (228).

A combination of wavelengths of light sources was used in this study, and both sources were mounted the same distance from the photo detector (7 mm). Surface mounted ceramic type red LED (CR 60 R, PerkinElmer, Inc., USA) was used with a peak emission wavelength of 628 nm. The dimensions of the LED were 3.00 mm x 1.27 mm x 0.60 mm. The optical and electronics characteristics are shown in Table 7.1.

Table 7.1: R LED specifications and electrical/optical characteristics (229).

Parameter	Value	Unit
LED Colour	Red	
Light Emission Angle	100	°
Continuous Forward Current	60	mA
LED Mounting	SMD	
Lens Shape	Rectangular	
Peak Emission Wavelength	628	nm
Forward Voltage	2.0	V
Luminous Intensity Min	100	Mcd
Luminous Intensity Type	140	Mcd
Operating Temperature Max	80	°C
Operating Temperature Min	-20	°C
Soldering Temperature	240	°C
Reverse Leakage Current Max	10	µA

The infrared LED used in this study was a surface mounted ceramic device (AP2012F3C, Kingbright, USA) with a peak emission wavelength of 940 nm. The dimensions of the LED was 2.00 mm x 1.25 mm x 1.1 mm. The optical and electronics characteristics are shown in Table 7.2.

Table 7.2: IR LED specifications and electrical/optical characteristics (230).

Parameter	Value	Unit
Peak Wavelength	940	nm
Forward Current I_f (AV)	20	mA
Radiant Intensity	3	mW/Sr
Viewing Angle	120	°
Forward Voltage V_f Max	1.6	V
Operating Temperature Min	-40	°C
Operating Temperature Max	85	°C
Operating Temperature Range	-40 to +85	°C
Weight	0.000003	kg

The two LEDs chosen for the sensor are shown in Figure 7.2. Each LED was mounted on the PCB board manually.

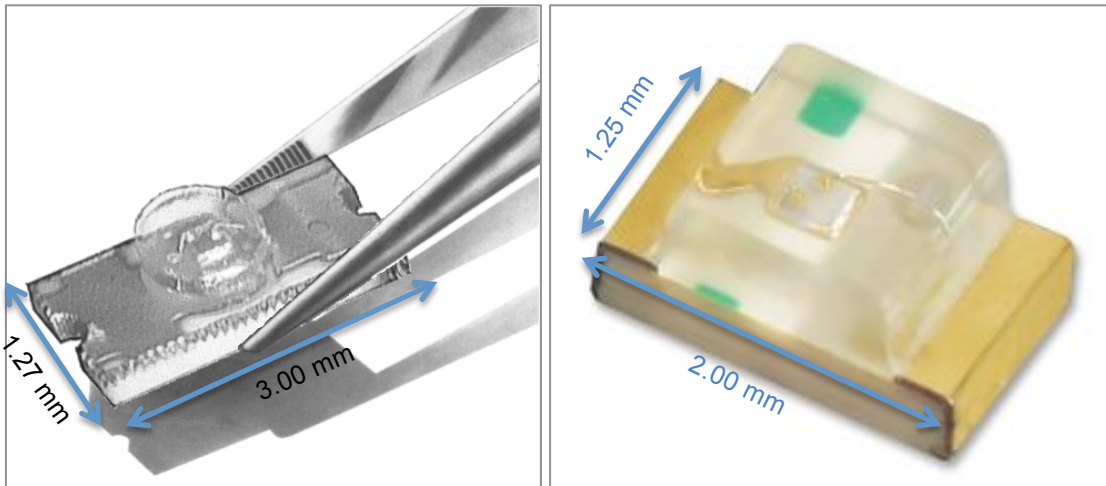


Figure 7.2: Left R LED (229) and Right IR LED (230).

Photo-detector

The detector used in this sensor to detect the backscattered light from bowel tissue is a surface mounted silicon PIN photodiode (BPW 34 S) sensitive to light in the 400 nm to 1100 nm range. This wide range of detection allows detection of both LED wavelengths using a single photo detector. The radiant sensitive area is 7 mm^2 with the dimension of $4.5 \text{ mm} \times 4.0 \text{ mm} \times 1.2 \text{ mm}$. Figure 7.3 shows a picture of the photodiode while Table 7.3 presents characteristic and maximum rating of the photodiode used in this study.

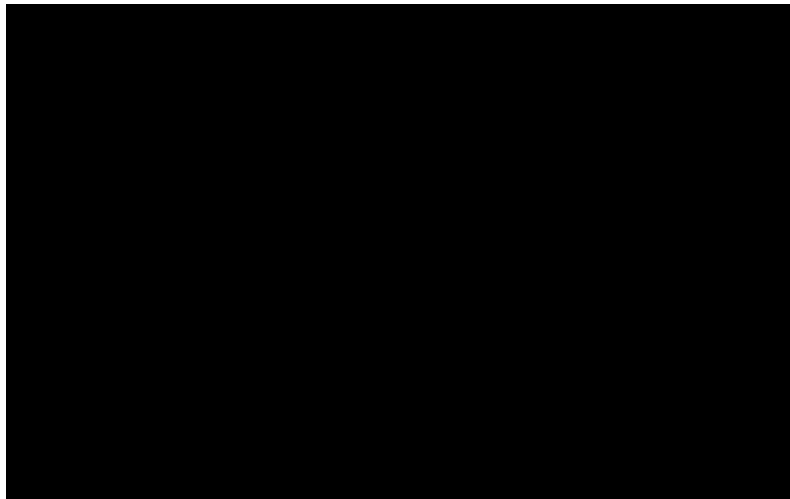


Figure 7.3: The photodiode used for the PPG part (BPW 43 S) (231).

Table 7.3: Characteristic and maximum rating of the photodiode used on the PPG part (BPW 43 S) (231).

Parameter	Value	Unit
Operating and storage temperature range	-40.... +100	°C
Reverse Voltage	32	V
Total power dissipation	150	mW
Wavelength of max. sensitivity	850	nm
Spectral range of sensitivity	400_110	nm
Dimension of radiant sensitive area	2.65 × 2.65	mm × mm
Rise and fall time of the photocurrent	20	ns

The LEDs were placed at a distance of 7 mm from the centre of the photodiode. The distance between Photodiode and the LDF tip is 7 mm (note that the laser Doppler tip is effectively a combined emitter and detector, i.e. the photodiode on the probe is solely for PPG measurement). A three-dimensional concept of the combined probe construction is shown in Figure 7.4.

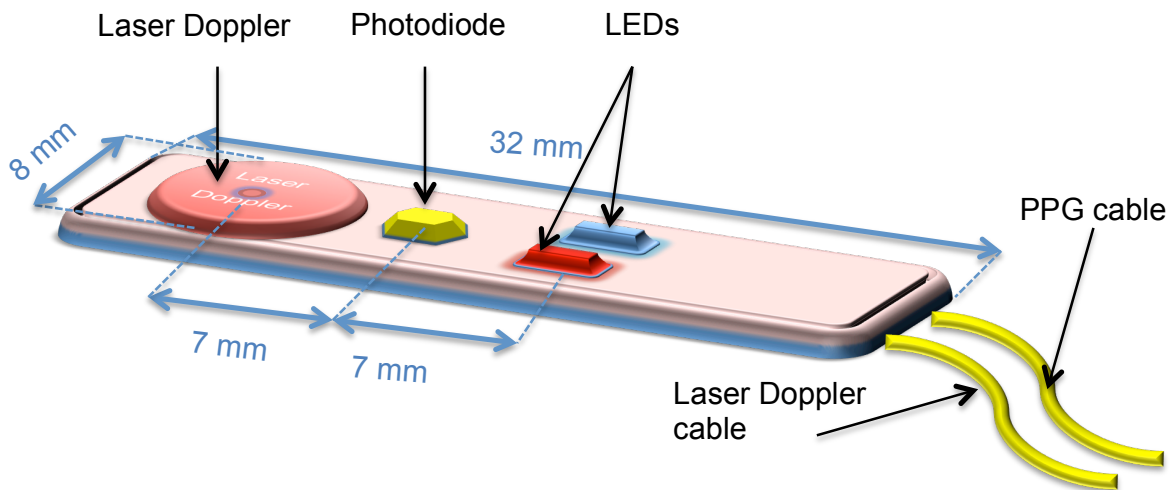


Figure 7.4: The three-dimensional concept of the combined probe.

7.2.2 Sensor construction

Commercial software Altium Designer (Altium limited, Sydney, Australia) was used to design the probe printed circuit board (PCB). Using a laser printer with high resolution, the desirable circuit was printed out first on a transparent sheet (laserstar, 895-945 Franell, 100062). The design was chemically etched onto a flexible copper substrate (Pyrulux, DuPont, USA). Components were then manually soldered onto the circuit. The full specification for the PPG system (probe and instrumentation) is included in Appendix A.

7.3 Combined sensor: Laser Doppler probe and monitor

A commercial titanium laser Doppler disc probe (Moor Instruments VP8c, Moor Instruments Ltd., UK) was incorporated into the sensor used in this research. Light is delivered via a central window at a right angle to the cable. Figure 7.5 shows a photograph of the probe. The laser Doppler probe is connected to a laser Doppler monitor (Moor Instruments, Ltd., U). The specification for Laser Doppler monitor and probe can be seen in Appendix B.

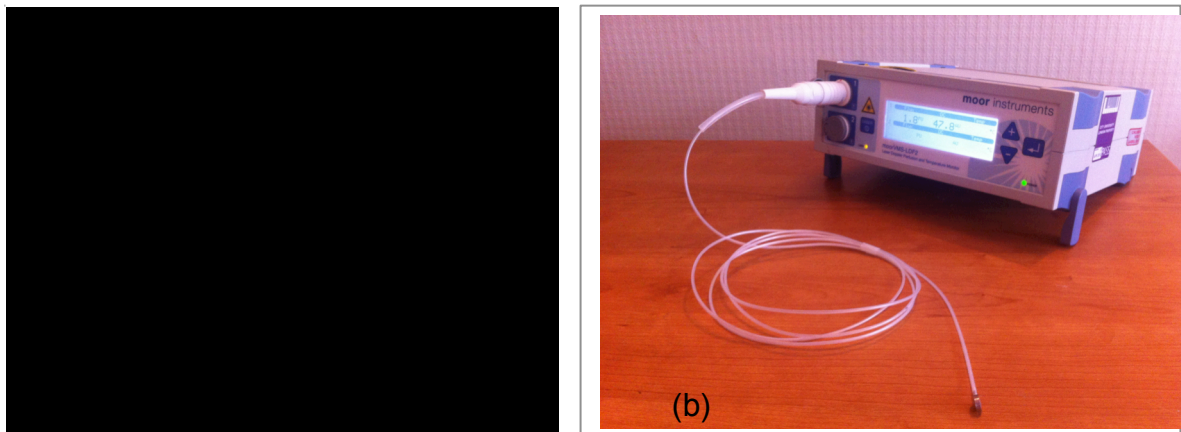


Figure 7.5: The VP8c titanium disc probe (232) (a) and the laser Doppler monitor (b)

Figure 7.6 shows a photograph of the completed combined probe. The probe connects with the instrumentation unit (Chapter 8), which interfaces with a data acquisition card and signals acquired using a LabVIEW virtual instrument (Chapter 9). The distal part of the probe connects to the instrumentation unit via a 5-core screened cable with a length of 3.9 m.

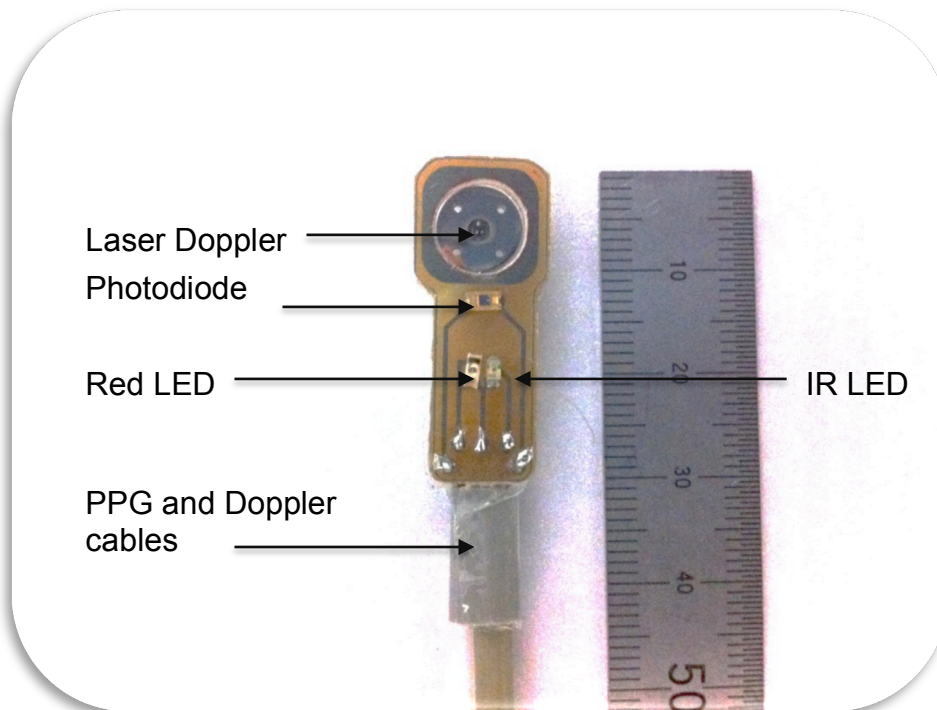


Figure 7.6: Photograph of the probe with two LEDs, one photodiode and the laser Doppler probe tip of 8mm in diameter.

7.4 Probe sheath

In order to protect patients against cross contamination during measurements, a single-use sterile latex sheath was used to protect the surgical site from contamination. A custom-made probe cover made with Palmedic (Palmedic b.v., The Netherlands) provided a perfect fit for the combined probe during intra-operatively measurements in the clinical trials. Figure 7.7 shows the custom-made probe cover used.

The maximum length of the sheath supplied by manufacture was 2.40 cm, which didn't cover the entire length of the cables from the probe to the measurement unit, so a sterile camera sleeve was used to cover the rest of the cables. These two together were able to cover enough cable length to protect the probe from possible contamination. After covering the probe, the probe was placed on a separate trolley, which was covered with a sterile sheet. Another sterile sheet was placed over the combined probe to protect that from any possible

contamination before each use. The probe was then ready to give to the surgeon for measurements.



Figure 7.7: The sterile probe ready to use for measurement.

After each trial the probe covers were removed carefully in a dirty utility room adjacent to the theatre. To test for possible contamination of the probe after each trial, the protective sheath had to be investigated to prove it had not been damaged during the trial (e.g. by puncturing when inserting the probe). Since the probe could not be cleaned, it was recommended by infection control that the sheath should be inspected before use and handled with care. After use, the integrity of the sheath could be confirmed by gently inflating it and immersing in water. After confirming of the absence of bubbles the probe was ready to use for the next trial. If the sheath was damaged after the trial there was no way of decontaminating the probe and therefore it would have to be discarded, however this event did not occur in any of the clinical studies.

7.5 Evaluation of the combined sensor

To assess the functionality of the sensor, two volunteer studies were performed in the laboratory on the finger of healthy volunteers. Note that these evaluations were conducted with using the instrumentation and software described in Chapters 8 and 9 respectively. The first study was performed to evaluate the

system's ability to differentiate between states of normal and compromised perfusion and the second study was conducted to investigate any optical interference between the PPG and LDF sensors. These studies were approved by the City University London Senate Research Ethics committee.

7.5.1 First volunteer study

This study presents evaluation of a system combining laser Doppler flowmetry and photoplethysmography (PPG) in a single probe for the simultaneous measurement of perfusion and blood flow in the finger. A cuff sphygmomanometer was used to partially occlude the arteries supplying the hand to investigate the effect of low pressure on photoplethysmographic and laser Doppler signals and also to calculate arterial blood oxygen saturation values (SpO_2). Red and infrared PPG and Doppler signals were recorded from six healthy volunteers at various pressures.

Experimental method

Six healthy volunteers (2F, 4M; mean age 25) who were not taking any regular medication and were free of any significant medical problems participated in this study. A pressure cuff attached to a manual sphygmomanometer was placed around the left arm of a volunteer while he/she was sitting on a chair. The experimental probe was attached to the left index finger. One minute of simultaneous PPG and Doppler flux measurements were taken with the cuff deflated. The cuff was then inflated in 15 mmHg steps up to 135 mmHg. Measurements of PPG and Doppler were acquired during one minute for each pressure condition. The cuff was deflated for 30 seconds between each measurement to allow re-perfusion of the hand and to avoid unnecessary discomfort for the volunteer subjects.

Data Analysis

From the PPG signals, the peak-to-peak amplitudes of the AC red (R_{AC}) and infrared (IR_{AC}) signals were calculated for each cardiac cycle (heartbeat) and the mean value of these amplitudes determined for all signals during each one-minute measurement period. DC values for red (R_{DC}) and infrared (IR_{DC})

calculated as well. The amplitudes of laser Doppler for all six volunteers were also measured during the cuff inflation process for about one minute with calculation of peak-to-peak amplitude of the laser Doppler signals. The SpO₂ values were also calculated using the following formula:

$$SpO_2 = 110 - 25 (R_R)$$

In which,

$$R_R = \frac{R_{AC}/R_{DC}}{IR_{AC}/IR_{DC}}$$

Results

PPG and Doppler signals were recorded from the index finger in all volunteer subjects. The AC red and infrared PPG and Doppler traces in one volunteer at zero, 75 mmHg and 135 mmHg pressure for 10 seconds are shown in Figures 7.8, 7.9 and 7.10 respectively. In all Figures AC infrared (IR_{AC}) PPG is shown in the first graph, AC red (R_{AC}) PPG is the middle graph and the last graph is related to laser Doppler. By comparing Figures 7.8, 7.9 and 7.10, it is clear that there are marked differences between IR_{AC} and R_{AC} PPG and Doppler signals at each of the cuff pressures represented by the graphs. In fact at 75 mmHg, the finger PPG signals are noticeably reduced for all subjects compared to the signals obtained at zero pressure and with a further increase of the cuff pressure to approximately 120 mmHg all signals ceased due to no blood flow to the finger (see Figure 7.12 at pressure 120 mmHg). In Figures 7.11, 7.12 and 7.13, the amplitude of AC red and infrared signals along with the Doppler signal at various pressures in all subjects is shown. As the cuff is gradually inflated, the brachial artery will be occluded gradually. As a result, less blood reaches the finger, producing low amplitude signals for all measurements. This effect is obvious in changes in the amplitude of IR_{AC} and R_{AC} PPG and Doppler signals from the finger probe. The IR_{AC} and R_{AC} amplitude reduced by 58.96% and 37.58% respectively at 75 mmHg compared to zero cuff pressure. The laser Doppler amplitude fell by 60.14% at 75 mmHg cuff pressure compared to zero cuff pressure. Figure 7.14 shows the calculated SpO₂ at different cuff pressures. It can be seen the values of SpO₂ become erratic at cuff pressures greater than 75 mmHg, with all but one subject showing apparent desaturation at high cuff pressures.



Figure 7.8: (a) IR_{AC} , (b) R_{AC} and (c) laser Doppler signals at zero mmHg for 10 second.

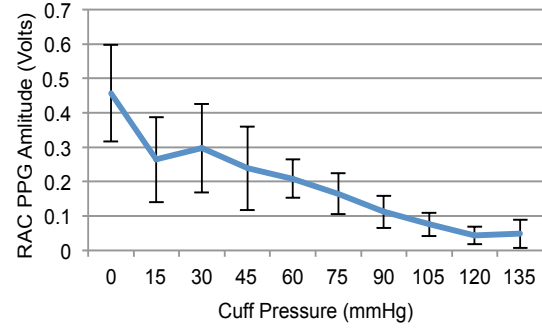


Figure 7.11: R_{AC} amplitude (\pm SD) at various pressure from zero to 135 mmHg.

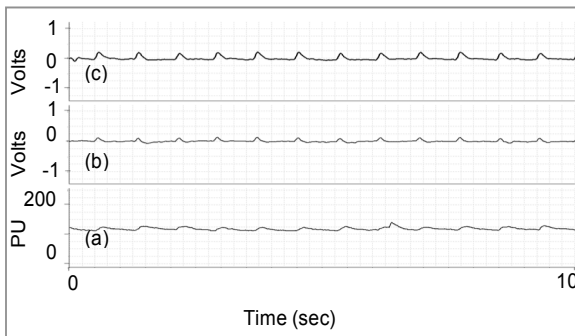


Figure 7.9: (a) IR_{AC} , (b) R_{AC} and (c) laser Doppler signals at 75 mmHg for 10 second.

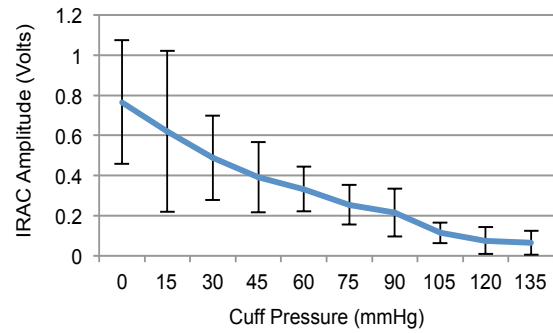


Figure 7.12: IR_{AC} amplitude (\pm SD) at various pressure from zero to 135 mmHg.

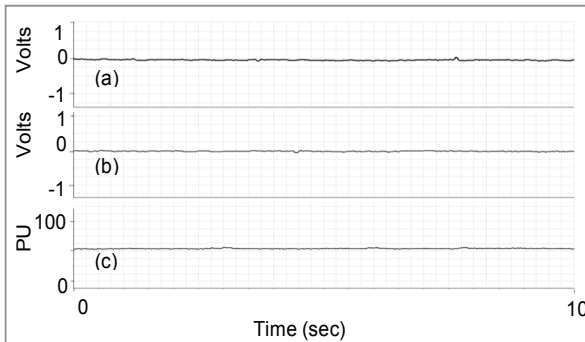


Figure 7.10: (a) IR_{AC} , (b) R_{AC} and (c) laser Doppler signals at 135 mmHg for 10 second.

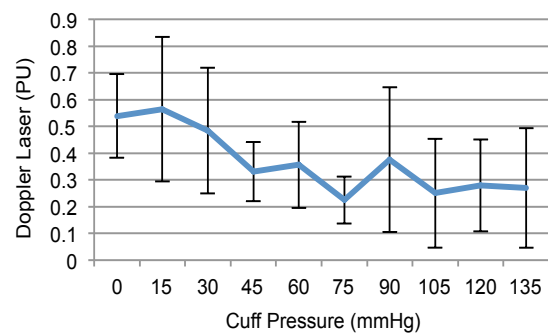


Figure 7.13: Laser Doppler amplitude (\pm SD) at various pressure from zero to 135 mmHg.

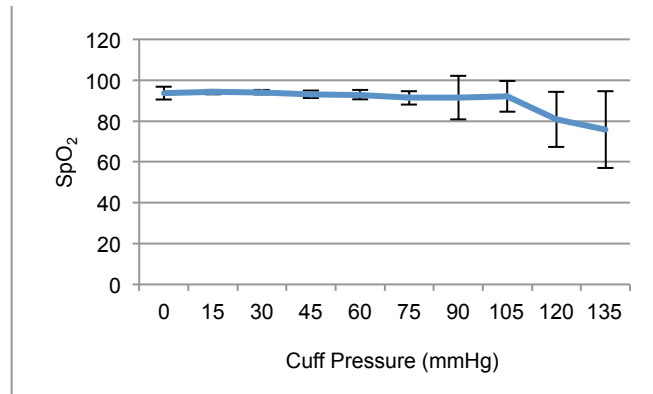


Figure 7.14: Blood oxygen saturation (SpO₂) (±SD) during hypoperfusion from zero to 135 mmHg.

Discussion and conclusion

Finger PPG and Doppler signals were measured in six volunteers in various pressures from zero to 135 mmHg. Clear signals were recorded in all subjects at low cuff pressures; however both PPG and Doppler signals showed a gradual decrease in amplitude at higher pressures. During hypoperfusion the amplitude of the PPG and Doppler signals decreased with increasing cuff pressure as expected due to occlusion of the brachial artery. From the signals obtained at different pressures, it can be seen that the mean AC red and infrared PPG and Doppler amplitude is considerably reduced in states of simulated ischaemia in the finger tissue. The decrease in the amplitude of the PPG signals and Doppler coincides with the observed changes in blood oxygen saturation in all subjects. These findings suggest that both PPG and LDF individually are sensitive indicators of ischaemia although the percentage fall in amplitude of the Doppler signals was greater than PPG between zero and 75 mmHg cuff pressure. This result suggests that PPG is more sensitive to ischemia than Doppler in peripheral tissue.

7.5.2 Second volunteer study

Red and infrared PPG and Doppler signals were recorded from a healthy volunteer in three studies at different distances between LDF and the photodiode in PPG. Clear photoplethysmographic (PPG) and Doppler signals were detected simultaneously using the probe from the skin of the finger. The influence of the PPG light sources on LDF measurements was investigated; also the influence of

the LDF light sources to the PPG measurements was studied. For this study, one healthy subject participated. In vivo evaluation of the PPG and Doppler system was done on the left index finger at rest in room temperature conditions.

Experimental method

To minimize stray light, the study was conducted in a dark room with lights off. Room temperature was 20–22°C. In order to minimize motion induced artefacts the subjects remained silent and still during the measurement. In order to evaluate the effect of interference between PPG and LDF, three studies were evaluated in which two experiments were performed. In the first study the LDF fibre tip was placed 7 mm from the photodetector (the distance used in the probe design). In the second and third studies the LDF fibre was placed 20 mm and 40 mm from the photodetector respectively.

a. First study

For the first study, the LDF fibre tip was placed at 7 mm from the photo detector.

The first measurement was performed to evaluate the influence from LDF on the PPG. This measurement was first recorded for PPG with only the PPG activated for 60 seconds and then with the PPG and LDF activated for another 60 seconds.

To assess the influence from PPG on the LDF, the second measurement was performed in which LDF was switched on while PPG was off for 60 seconds and then with the LDF and PPG active for another 60 seconds.

b. Second study

All measurements in the first study were repeated with different placement for the LDF probe: 20 mm from the photodiode.

c. Third study

All measurements again were repeated but this time the LDF probe was placed 40 mm from photodiode.

Data analysis

The mean value of the LDF was calculated for each measurement. The PPG amplitude was taken as the peak-to-peak value of the AC-part of the signal. A

custom made LabVIEW VI was used to extract the peak-to-peak value from the acquired PPG signals. The mean PPG amplitude of each 60-second segment was then calculated.

Results

Clear PPG and Doppler signals were detected from the combined probe from all six experiments. The results for mean value for the measurements from the first, second and third studies are presented in Table 7.4 (a), (b) and (c) respectively.

Table 7.4: Mean value from measurements in the first study (a), second study (b) and in the third study (c)

Measurement		Average AC Amplitude (V)		Mean DC (V)		Average LDF Flux (PU)
PPG	LDF	IR	R	IR	R	
ON	OFF	4.560	0.683	1.502	0.391	---
OFF	ON	---	---	---	---	38
ON	ON	4.753	0.740	1.526	0.416	43.6

(a)

Measurement		Average AC Amplitude (V)		Mean DC (V)		Average LDF Flux (PU)
PPG	LDF	IR	R	IR	R	
ON	OFF	2.738	0.460	1.081	0.301	---
OFF	ON	---	---	---	---	51.2
ON	ON	2.799	0.469	1.220	0.330	57

(b)

Measurement		Average AC Amplitude (V)		Mean DC (V)		Average LDF Flux (PU)
PPG	LDF	IR	R	IR	R	
ON	OFF	1.774	0.329	1.088	0.322	---
OFF	ON	---	---	---	---	38.6
ON	ON	1.778	0.334	1.127	0.338	42.4

(c)

The 60-second average IR_{AC} in the first measurement in the first study increased slightly when the LDF was switched on. This suggests that switching on the laser source results in more light being detected by the PPG photodetector, an increase in amplitude of 4.07% was seen. The average for R_{AC} with PPG on and LDF off

increased by 7.66%. This shows that the R PPG is affected proportionally more by LDF than IR PPG. The average for LDF flux was seen to increase by 14.7% when the PPG light sources were turned on.

From the results of the second experiment it was found that by switching the PPG emitters on and off had less effect on the laser Doppler signal than the first experiments. The average for IR_{AC} and R_{AC} increased by 2.18% and 1.99% respectively when the LDF laser was switched on. Switching on the PPG light sources in the second study caused an increase of 11.3% in average laser Doppler flux.

From the results of the third experiment it was found that by switching the PPG emitters on and off, this had the least effect on the LDF. The average for IR_{AC} and R_{AC} increased by 0.23% and 1.40% respectively. Switching on the PPG light sources in the second study caused an increase of 9.84% in the average laser Doppler flux.

The IR_{DC} and R_{DC} are also affected by LDF and their amplitude increased by switching the LDF on between in all three measurements as it can be seen from the Table 7.4 (a), (b) and (c). The average for IR_{DC} and R_{DC} in the first study increased by 1.57% and 6.01% respectively. The average for IR_{DC} and R_{DC} in the second study increased by 1.14% and 8.79% respectively and the average for IR_{DC} and R_{DC} in the third study increased by 3.46% and 4.73% respectively.

Discussion and Conclusion

This study was performed to evaluate optical interference between PPG and LDF in a combined system. From all the results of this experiment it was found that the PPG is not greatly affected by LDF; in the worst case the change in AC amplitude when the LDF system is switched on was less than 8%.

Results from this trial study showed that by increasing the distance between the LDF and the photodiode, the effect of optical interference from LDF on both red and infrared PPG signals decreased. Also it was found that R PPG is proportionally more affected by LDF light than IR PPG. The results also show that the effect on reported LDF flux from the PPG light sources is more marked. In the

worst case the change in LDF flux amplitude when the PPG system is switched on was less, just over 14.7%. Like the PPG amplitudes, it was found that increasing the distance between the LDF and the photodiode had the effect of reducing the optical interference from PPG light sources on the LDF flux values.

The observed changes in AC amplitude and LDF flux were considered small enough to not disrupt the measurements and overall assessment of bowel viability.

7.6 Thermal evaluation on the combined sensor

7.6.1 Thermal Safety Testing

The red and infrared emitters are low power components with operating currents of 50 mA. The laser Doppler output power is 2.5 mW and this is further affected by the optical fibre. All optical components are also thermally insulated from the tissue by the approximately 1 mm thick sterile latex sheath. Despite the fact that the operating current of the emitters and the output from laser Doppler was well below the maximum rated value, it was still necessary to confirm that these sources would not cause any direct thermal damage to the tissue. So temperature tests were performed to assess the likely thermal effect of placing the optical probe in contact with tissue during measurements.

A thermal sensor; LM35 (National Semiconductor, USA) was used to measure the temperature produced by light sources while the probe was on. LM35 is a precision IC temperature sensor with its output proportional to the temperature (in °C). LM35 possesses low thermal effects and does not cause a rise above 0.1 °C in ambient temperatures (233).

To convert the output voltage to temperature, the following equation was used:

$$\text{Temp in } ^\circ\text{C} = (\text{Volt in mV}) / 10$$

7.6.2 Experimental methods

An *in vivo* experiment was carried out on the forearm of a female volunteer. The thermal sensor was placed directly adjacent to the combined probe. It was connected to one analogue input of a data card (USB 600, National Instruments, USA). Data was recorded at a rate of 100 Hz by the use of a virtual instrument implemented in LabVIEW (National Instruments, USA). The probe was placed on the forearm for 30 minutes to reach a steady thermal state. Then the temperatures of the thermocouples were continuously recorded for 40 minutes while the circuit was switched on, so both PPG and Laser Doppler light sources were emitting continuously. The drive current (as stated on the LEDs datasheet) used for switching the red and infrared LEDs was 50 mA using a current-limiting resistor of value $R=220\ \Omega$ and a voltage supply of 12 V. The PPG and Laser Doppler light sources were then switched off and the temperatures recorded for another 20 minutes. In order to confirm and average out results the experiment was repeated twice more.

7.6.3 Results

Figure 7.15 shows a graph of changes in temperature against time.

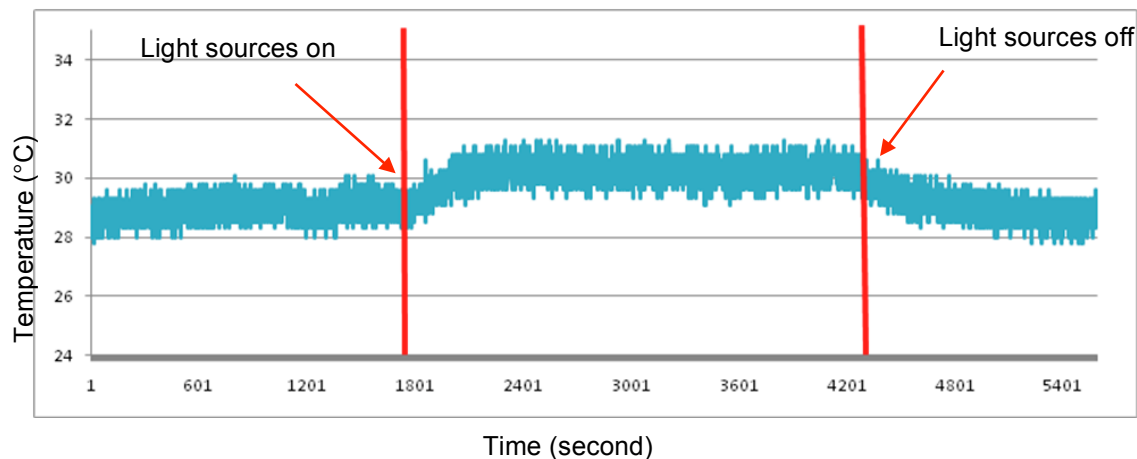


Figure 7.15: Graph showing changes in temperature induced on skin by the combined probe.

After the light sources were switched on, the temperature increased and after approximately 2 minutes it reached to a steady state (mean temperature 30.2 °C), as shown in Figure 7.15, where the temperature is plotted against time. Monitoring was continued for a further 38 minutes. When the light sources were

switched off, again a steady state temperature was achieved after approximately 2 minutes. The mean temperature with light sources off was 29.0 °C. See Table 7.5.

Table 7.5: Temperature change with LEDs of and on.

LEDs status	Mean Temperature
LEDs off 30 minutes baseline	29.2
LEDs on 40 minutes	30.2
LEDs off 20 minutes	29.0

The mean observed temperature rise was no greater than 1.2 °C with light sources emitting continuously. The rise in temperature would not be expected to result in tissue damage and therefore, it was concluded that there would be negligible risk of thermal injury to the tissue using the proposed probe.

7.7 Sensor design and safety test summary

Good results from the both studies along with the thermal test have determined that the use of this sensor for bowel operation would be very unlikely to cause any injury during intraoperative measurements in theatre.

The following chapter describes the design and development of the instrumentation system for acquisition of signals from the probe.

Development and Evaluation of the Combined PPG/LDF Measurement System

8.1 Introduction

The aim of this research is to develop a new system for simultaneous measurement of blood flow and pulsation for intraoperative evaluation of perfusion in intestinal tissue. This approach requires the combination of two different optical methods. Chapter 7 describes the design and manufacture of the combined photoplethysmography (PPG) and laser Doppler (LDF) sensor for the monitoring of pulsatile blood in bowel tissue. To drive the optical combined probes, a custom-made hardware PPG processing system was developed. The new combined PPG/LDF system was designed and developed in order to detect the red and infrared (AC and DC) PPG signals along with laser Doppler flowmetry signals. It then pre-processes the acquired signals and displays them, analysed and stored on a laptop computer for further analysis. Figure 8.1 shows a simple block diagram of the whole PPG/LDF processing system.

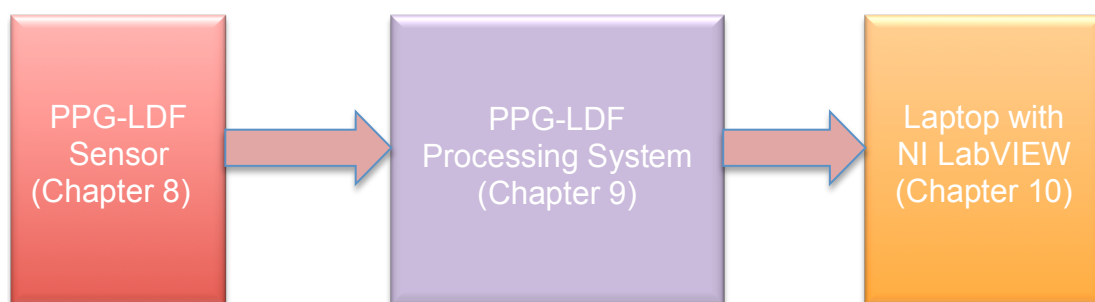


Figure 8.1: A simple block diagram of the PPG/LDF processing system.

8.2 Instrumentation

As mentioned, the measurement system comprises a combined probe, PPG instrumentation unit (PPG unit) and laser Doppler flux monitor (LDF monitor).

PPG unit

This unit consists of a small box (30 x 28 x 9 cm) weighing 3.44 kg, containing a power supply unit (two 12 V 2.2 Ah sealed lead-acid batteries), LED current sources and a custom-made signal processing circuit to separate the photoplethysmographic signals into AC (rapidly varying or 'pulsatile') and DC (slowly varying) components and to amplify each component together with the associated combined probe and a laptop computer (see Figure 8.2). The laptop computer was also powered by an internal battery comprising two 12 V 1.2 Ah sealed lead-acid batteries.

The unit also contained a data acquisition card (National Instruments Inc., Austin, TX, USA) which samples (at 100 samples per second) and converts the analogue output of the PPG measurement system into a digital signal then feeds it to a notebook computer via a USB connection. (Note: The data acquisition card also connects to the LDF monitor via a cable between the PPG unit and LDF monitor. This arrangement enables simultaneous recording of the LDF signal on the notebook computer).

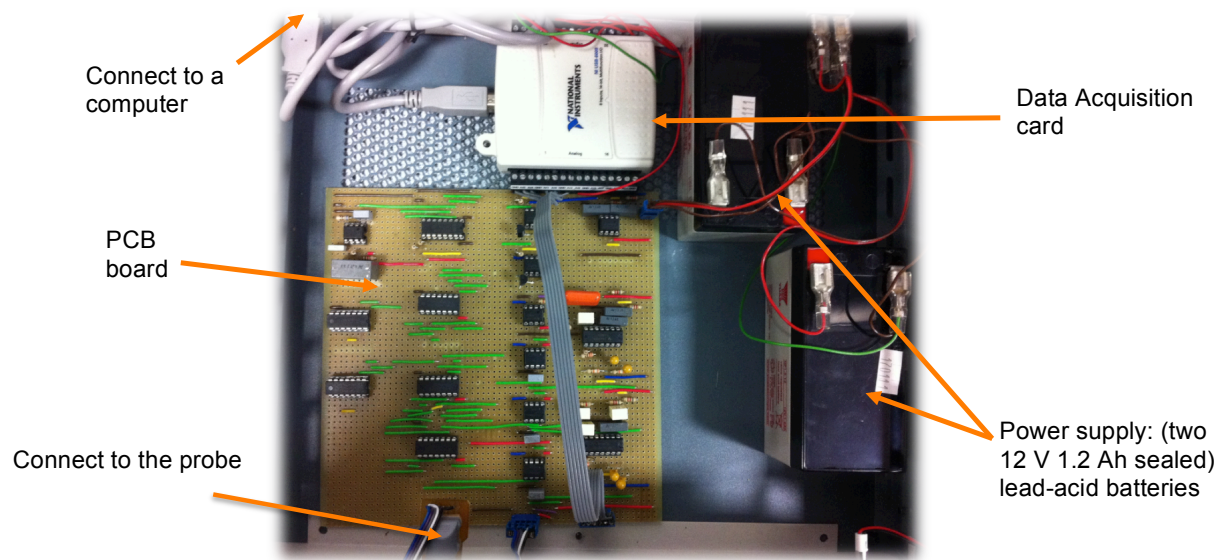


Figure 8.2: Instrumentation: unit containing Data acquisition card, PCB board, power supply unit and the connection to the computer and probe.

Photographs of the front and rear panel of the monitoring system used in this study are presented in Figures 8.3 and 8.4 respectively.

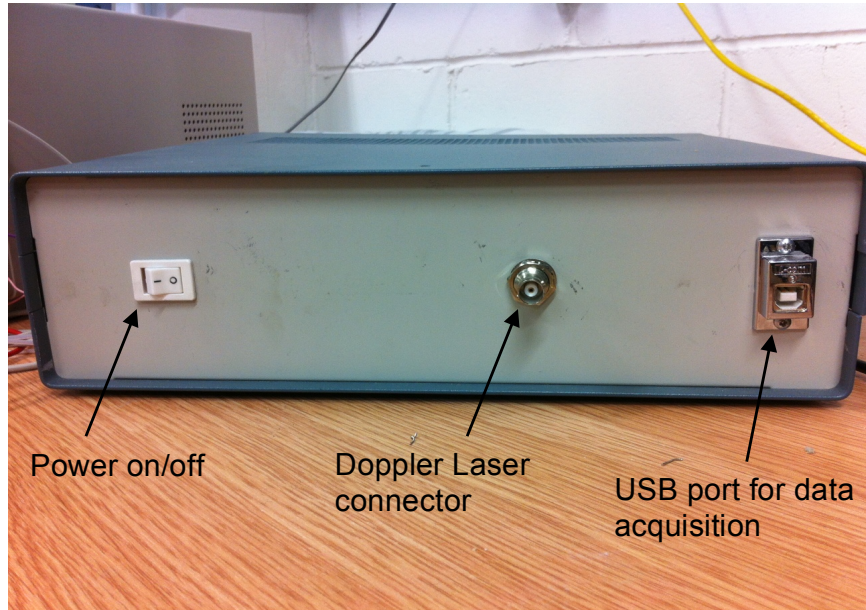


Figure 8.3: Photograph of the rear panel of monitoring system.

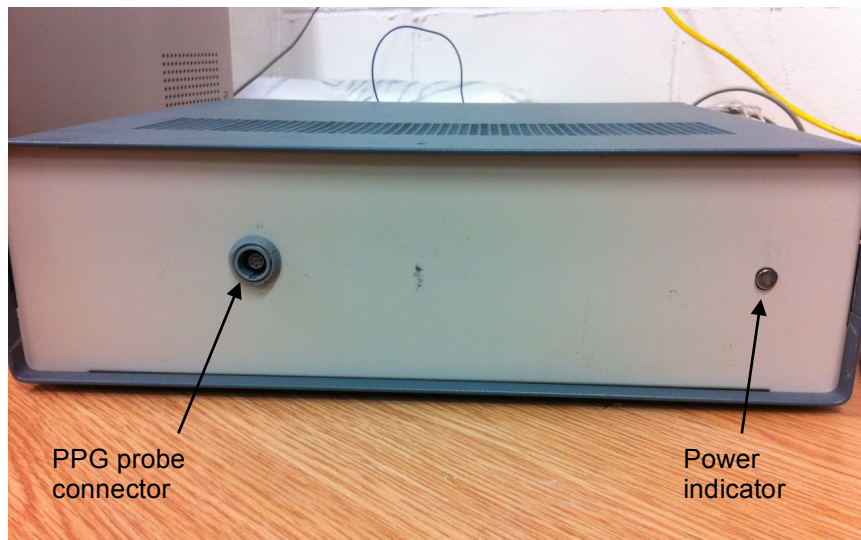


Figure 8.4: Photograph of the front panel of monitoring system.

Block Diagram of the System

This circuit contains a timer circuit, LED driver circuit, photodiode detector circuit, amplifier circuit, de-multiplexer (sample and hold) circuit and a filter circuit. Figure 8.5 shows a photograph of the circuit used in this study. Figure 8.6 presents a block diagram of the PPG/LDF system. The block diagram consists of eight parts, starting from timer, multiplexer, LEDs driver, sensor, photodiode detector, amplifier, de-multiplexer and band pass filter circuit.

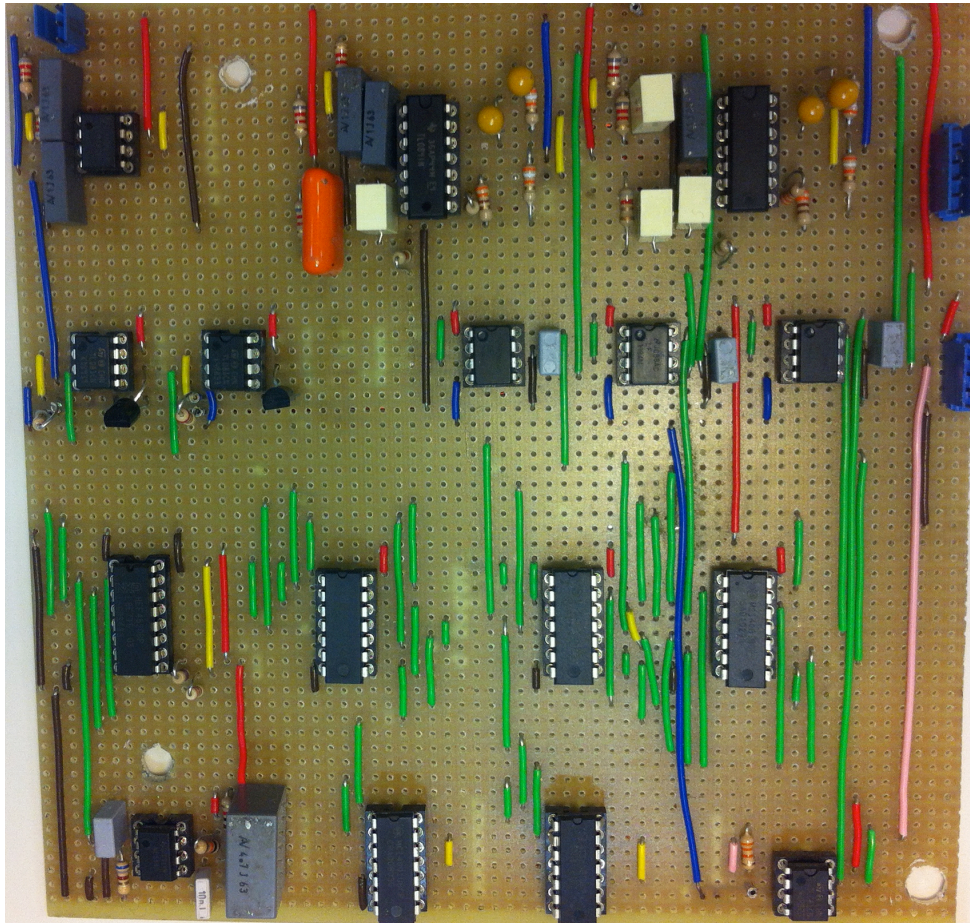


Figure 8.5: The circuit of PPG measurement system.

The red and infrared signals, which comprise AC and DC parts (Section 4.4) are demultiplexed in order to separate them into two different signals; red and infrared. The red (AC and DC) and infrared (AC and DC) are digitised and sent to the notebook computer for analysis.

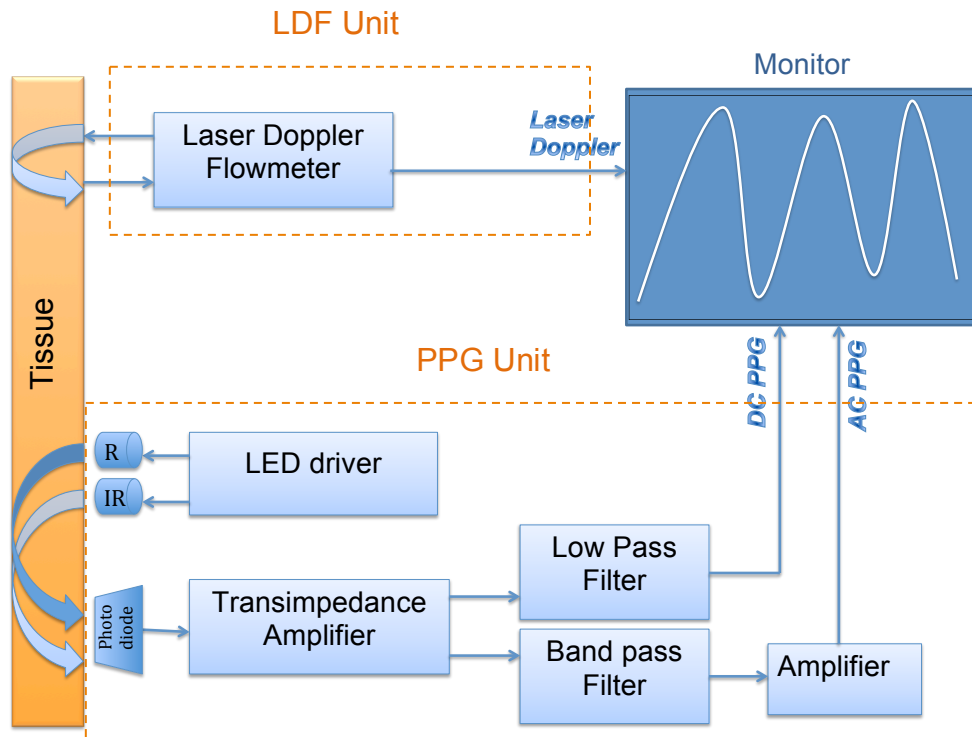


Figure 8.6: The block diagram of the PPG/LDF system.

A schematic diagram of the entire measurement system is shown in Figure 8.7. Detailed descriptions of each segment are presented in the following sections.

Timing Circuit

In this study an NE555 timer was used to generate stable and accurate timing pulses. It is an 8-pin timer IC and has mainly two modes of operation: monostable and astable. In this study, the astable mode is used to generate a continuous series of pulses (monostable mode can be used to make a one-shot or monostable circuit). The circuit of the 555 timer used in this study is shown in Figure 8.8.

The frequency or repetition rate of the output pulses is determined by the values of two resistors, R_1 and R_2 and the capacitor C using the Equation 8.1 and 8.2 (234).

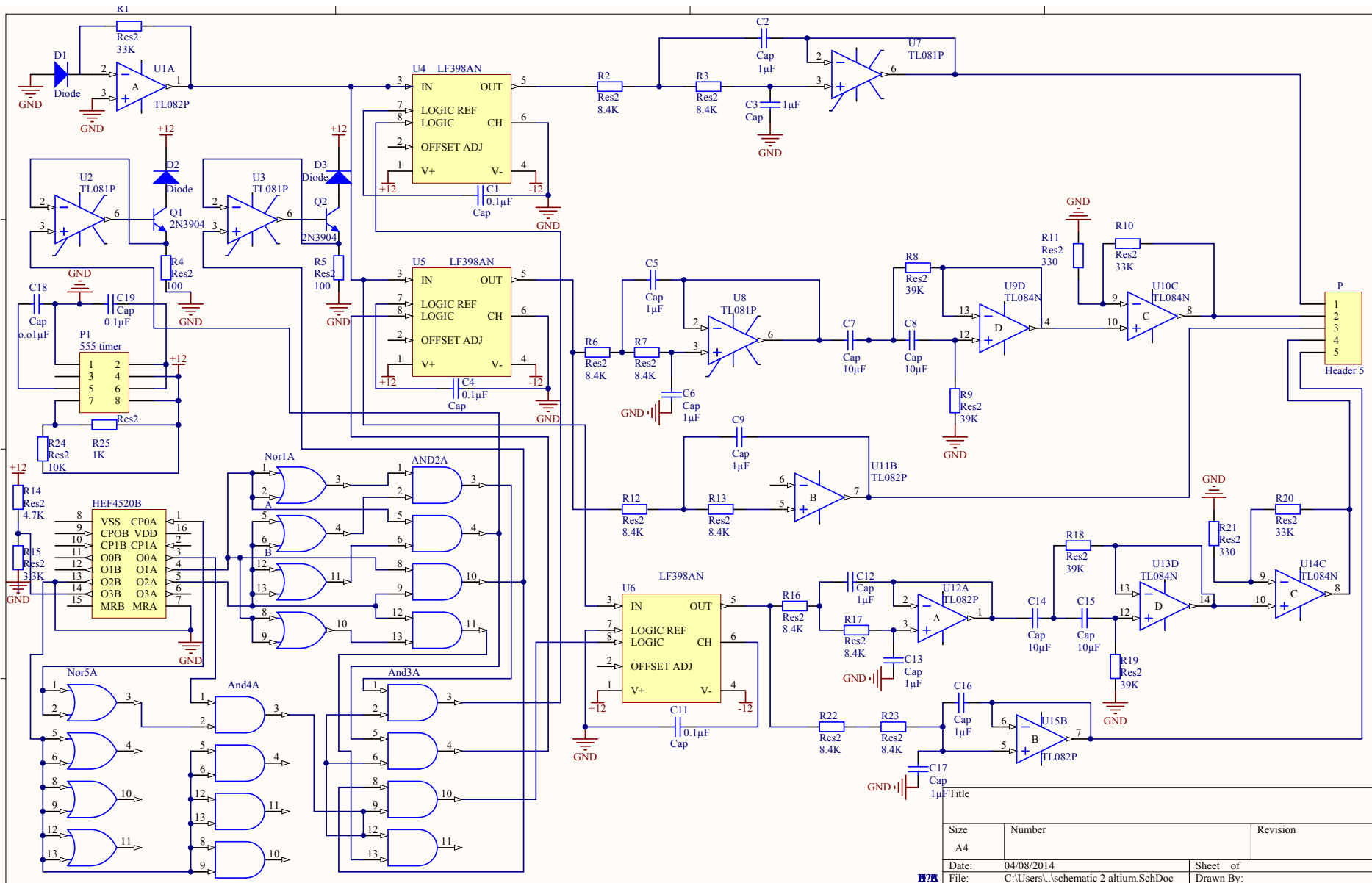


Figure 8.7: A schematic of the entire measurement system.

$$T = \frac{1}{f} \quad \text{Equation 8.1}$$

$$f = \frac{1.44}{(R_1 + 2R_2) \times C} \quad \text{Equation 8.2}$$

T = Time period in seconds (s)

f = Frequency in hertz (Hz)

R_1 = Resistance in ohms (Ω)

R_2 = Resistance in ohms (Ω)

C = Capacitance in farads (F)

With $R_1 = 1 \text{ K } \Omega$, $R_2 = 10 \text{ K } \Omega$ and $C = 100 \text{ nF} = 0.1 \text{ } \mu\text{F}$:

$f = 680 \text{ Hz}$

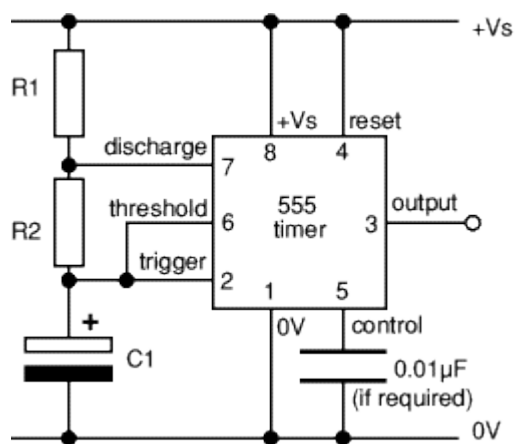
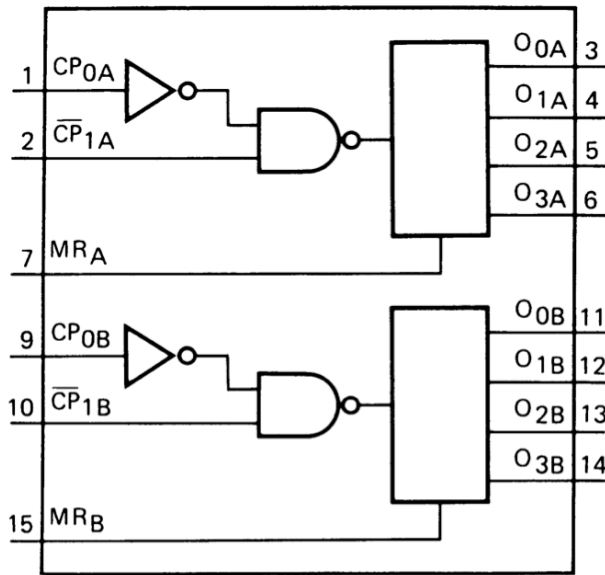


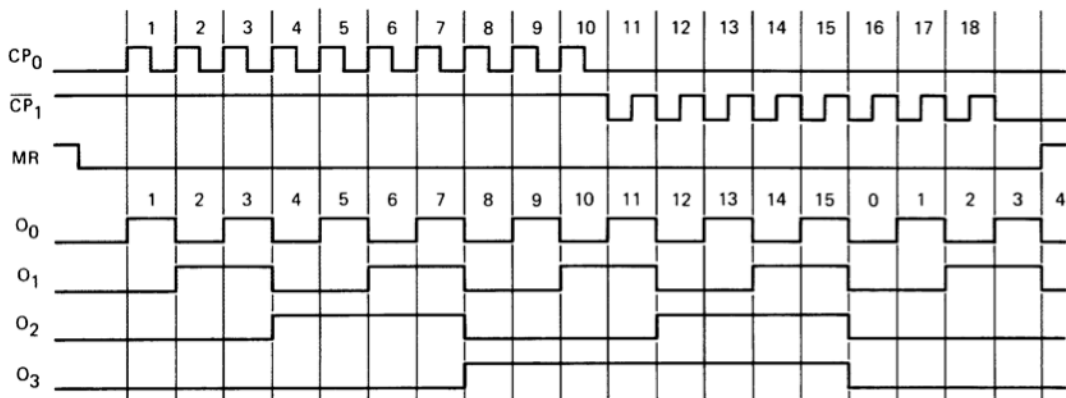
Figure 8.8: Generating the timing pulses for pulse oximeters using 555timer (235).

Multiplexer/Driver of two Wavelengths

The counter provides the timing signal for the multiplexed LED driver circuits and for the demultiplex circuit. In this study a dual 4-bit counter (HEF4520B, Philips Semiconductors) was used, see the functional and timing diagram for HEF4520B in Figure 8.9 (a) and (b). By inputting a clock signal provided by the 555 timer (CP1), the counter produces three signals at different frequencies: half, one quarter and one eighth the frequency of the timer signal (Q1, Q2 and Q3 respectively) as shown in Figure 8.10.



(a): Functional diagram for HEF4520B



(b): Timing diagram

Figure 8.9: (a) Functional and (b) timing diagram for HEF4520B.

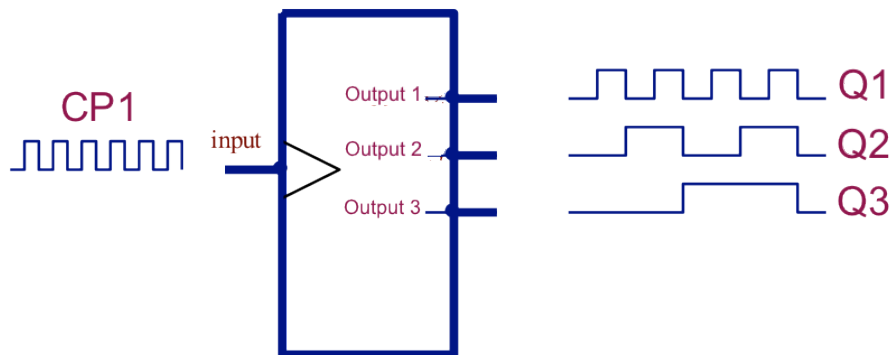


Figure 8.10: HEF4520B 4-bit binary counter was used in this circuit, CP1 is the clock signal (frequency = f_{CP1}) as the input and counter produces three signals Q1, Q2 and Q3. Q1 has frequency $f_{CP1}/2$, Q2 has frequency $f_{CP1}/4$ and Q3 has frequency $f_{CP1}/8$.

Figure 8.11 shows the LED driver circuit, which comprises a basic multiplexing logic circuit based on two AND gates, a pair of current sources consisting of a low power operational amplifier (TL081, Texas Instruments, Dallas, Texas, USA) and a NPN transistor (2N3904).

The timing signal provided by HEF5420B, drives the current sources. The output of the first AND gate is connected to the input of the R LED driver switches on the R LED when Q1 and Q2 are both high, see the timing diagram in Figure 8.12. The output of the second AND gate is connected to the input of the IR LED driver. To drive the IR LED, one of the inputs of the AND gate is inverted. The IR LED is thus switched on when Q1 is high and Q2 is low. The red and infrared LEDs therefore switch on alternately, with periods in between when both emitters are off.

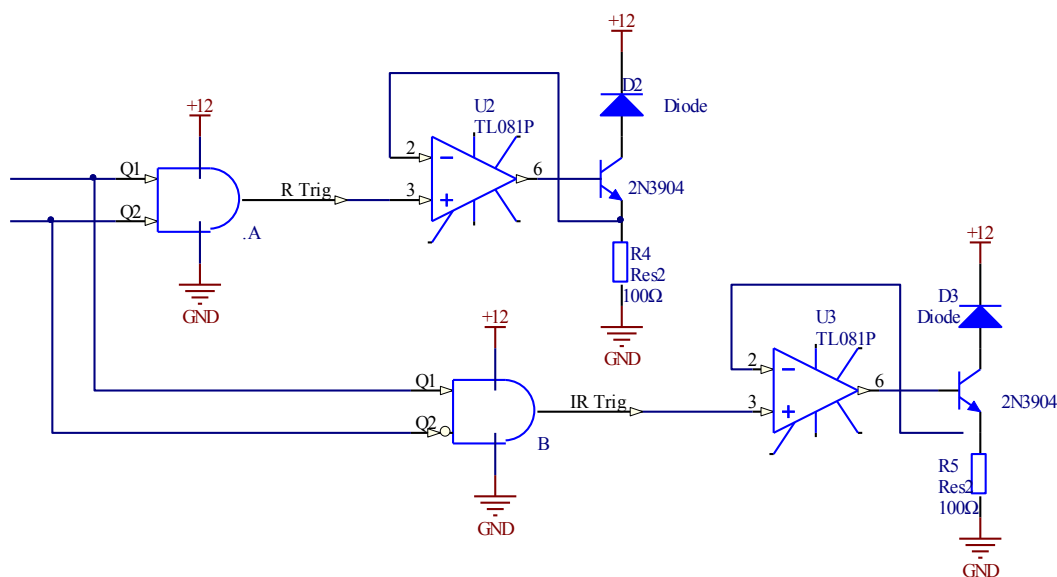


Figure 8.11: Schematic drawing of the LEDs current driver circuit.

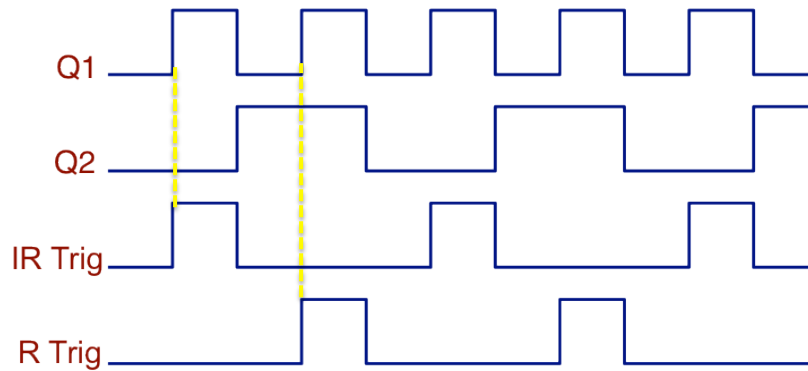


Figure 8.12: Light source timing diagram. Q1 and Q2 are the outputs from the counter. The R LED switches on when Q1 and Q2 are both high while the IR LED is switched on when Q1 is high and Q2 is low.

Transimpedance Amplifier

Many biomedical and analytical applications require the detection of light. A photodetector is able to detect the light transmitted through the part of the target tissue and convert light into an electrical signal. There are several basic technologies including: photomultiplier tubes (PMTs), avalanche photodiodes (APDs), and photodiodes. Photodiodes were chosen for this project as they produce current linearly proportional to the intensity of the detected light. Using a transimpedance amplifier this current can be then converted to voltage.

Positive-intrinsic-negative (PIN) photodiodes have been used in the majority of commercial pulse oximeters as detectors mostly due to their rapid response times, favourable spectral response at red and infrared wavelengths and also relative insensitivity to temperature variation. The photodiode used in this application is a silicon PIN photodiode operating with reverse bias applied to the p-n junction (photoconductive mode). Electron-hole pairs are created when light falls on the junction area of the photodiode. Due to the reverse bias, i.e. (increased depletion region) the hole sweeps towards the p-material and the electron towards the n-material. The output light current can be seen as a large increase in the reverse current. The photocurrent is effectively transformed into a voltage using the circuit shown in Figure 8.13. This circuit is known as a transimpedance amplifier or I-V converter. The output voltage of the circuit is given by:

$$V_o = -I R_f$$

where R_f is the feedback resistor and the output V_o is proportional to the light intensity I .

A very large feedback resistance is usually required as the output current from the photodiode is very small (values as high as several tens of M Ω are typical). Note that the gain of the transimpedance amplifier is equal to the value of the feedback resistor in ohms.

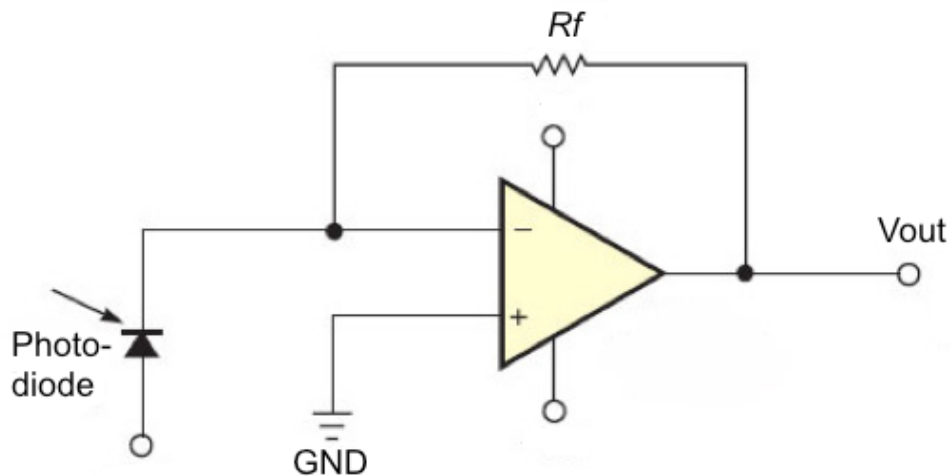


Figure 8.13: Transimpedance amplifier circuit.

The output from the photodetector is passed into an analogue circuit in order to amplify and filter the signal.

De-multiplexer

The output of the transimpedance amplifier consists of mixed (multiplexed) signals so in order to separate the detected signals into its components, a de-multiplexer was used. In this circuit a sample and hold circuit (LF398) was used to de-multiplex three signals detected from the detector circuit corresponding to the red, the infrared and the ambient light (measurable during periods when both LEDs are off). See Figure 8.14. These signals then were passed to the filters and the AC post-amplifier.

The mixed signals from the transimpedance amplifier are fed into a de-multiplexer to separate the signals into independent channels as shown in Figure 8.15. The de-multiplexing circuit comprised of a logic circuit connected to three LF398 sample and hold circuits. (National Semiconductor Inc., Santa Clara, CA, USA). The logic circuit composed of a combination of AND gates and NOR gates. The signals from the counter (CP1 and Q1–3) were used as the inputs for the logic circuit. Figure 8.16 shows a timing diagram for the de-multiplexer. As shown in this diagram, Q2 and Q3 determine which LF398 is triggered, while triggering only occurs when CP1 is low and Q1 is high.

The logic circuit was designed to trigger each LF398 to sample the signals at appropriate times so the first LF398 samples the output signal from photodiode when both R and IR emitters are off (i.e. the ambient light level is sampled). The timing diagram (Figure 8.16) shows that the sampling time occurs at the mid-point of the period when the LEDs are off, thereby avoiding interference from the light sources in the event of switching delays. Two other LF398s were sampled when the infrared and red light sources were on, at the mid-points of each period of illumination which allows time for the LEDs to reach full brightness before sampling.

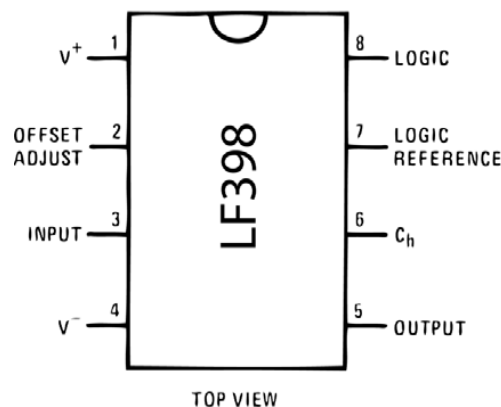


Figure 8.14: Sample and hold IC pin out diagram.

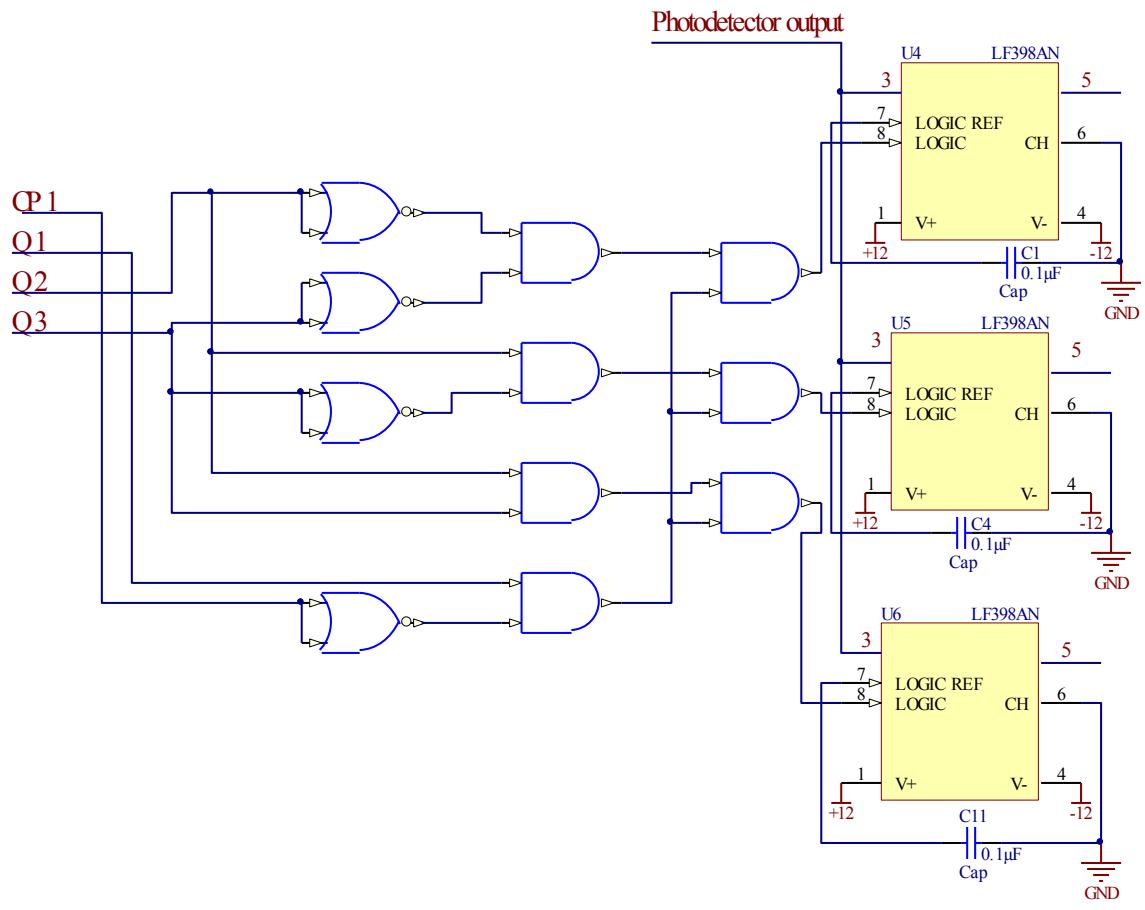


Figure 8.15: The de-multiplexer circuit. The pins on the LF398 sample-and-hold chip are: pin 3 (photodiode output/analogue input), pin 8 (logic input) and pin 5 (analogue output).

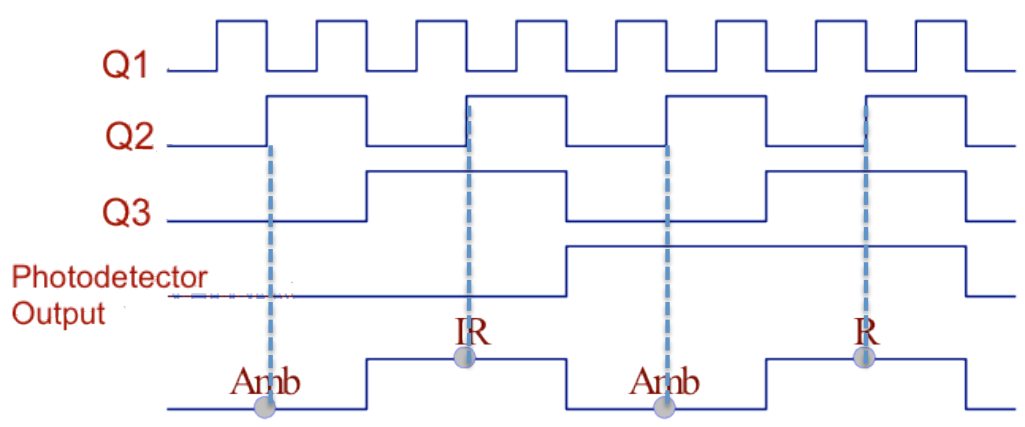


Figure 8.16: Timing diagram for the de-multiplexer. The dotted lines indicate the times when sampling of the photodetector output occurs.

Band-pass Filter (Low and High Pass Filter)

The output coming from the multiplexing stages are the raw signals consisting of the sum of the AC and DC components. These signals are then passed through an array of filters (described below) to separate the AC and DC components and to remove unwanted frequencies.

In this study a pair of band-pass active second-order Butterworth filters (see Figure 8.15) were used to separate the red and infrared (AC) photoplethysmographic signals from the total (DC) detected signal levels and remove high frequency noise. The value of the cut off frequency of the high pass filter stage was 0.4 Hz and for the low pass filter stage it was 19 Hz to ensure that the pulsatile portion of the PPG signals were preserved. The red and infrared DC signals were filtered to remove high frequency noise using a low-pass second-order active Butterworth filter (see Figure 8.7) with cut off frequency 0.15 Hz.

Amplifier

To amplify the AC signals detected from the photodiode detector an amplifier was used. In this study an inverting amplifier was used with a gain of 100. Two amplifiers were required in this circuit, one for each of the red and infrared signals.

8.3 Laser Doppler Monitor

The LDF monitor is a commercial *VMS-LDF* laser Doppler monitor (Moor Instruments Ltd, Exmoor, UK), a fully certified CE-marked medical device. See Figure 8.17. The LDF monitor is connected to the PPG unit via a coaxial cable.



Figure 8.17: Photograph of Laser Doppler Flowmetry monitor.

Figure 8.18 shows a photograph of the entire measurement system. As can be seen, the probe is connected via a Y-shaped cable to the PPG unit and the laser Doppler monitor. The laser Doppler monitor is connected to the PPG unit via an analogue connection which represents the flux value as an analogue voltage where 1 V is equal to 100 perfusion units (PU). The PPG unit is connected to a personal computer (a laptop computer for this clinical study) via a USB connector.

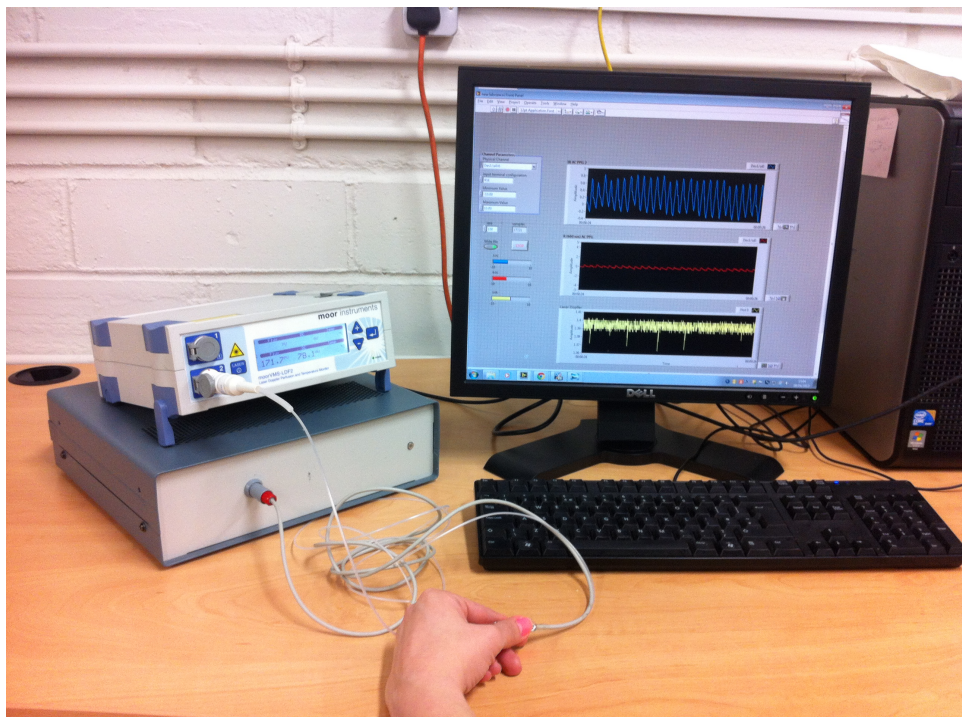


Figure 8.18: Photograph of measurement system. Note: in the photograph the distal tip of the probe is being held between thumb and forefinger.

The PPG signals (AC and DC), and the perfusion signal from the laser Doppler flowmeter were acquired and recorded with a 14-bit data acquisition card (USB6009, National Instruments, TX, USA) at a sampling frequency of 100 Hz using a specially developed LabVIEW program (National Instruments Inc. Austin, TX, USA). The data acquisition card is a bus-powered device; which is attached to a laptop computer via a USB connection. The laptop computer runs a 'Virtual Instrument' (VI) software application for acquisition and displays signals acquired from the probe and instrumentation, which is covered in Chapter 9.

Data Acquisition and Development of the Virtual Instrument (VIs) for Signal Processing, Data Storage and Display

9.1 Introduction to LabVIEW

A Virtual Instrument (VI) created in LabVIEW (National Instruments, Austin, Texas, USA), reads the digitised signals at a rate of 100 samples per second, displays the signals to the operator and writes them to a tab-delimited text file for future analysis. The processing system in this study provides six output signals including AC PPG (pulsatile arterial component) for red and infrared wavelengths, DC PPG signals (non-pulsatile PPG component from venous, skin and bone) for red and infrared wavelengths, ambient and also laser Doppler signals. These acquired PPG and LDF output signals from the sensor are digitised using a data acquisition card (National Instruments) incorporating an analogue to digital convertor (ADC). The Data acquisition (DAQ) card is connected to a computer via a USB cable so that the digitised PPG and LDF signals can be saved to the computer's hard disk drive. Figure 9.1 illustrates the main functions of the developed VI and the connection with the processing system.

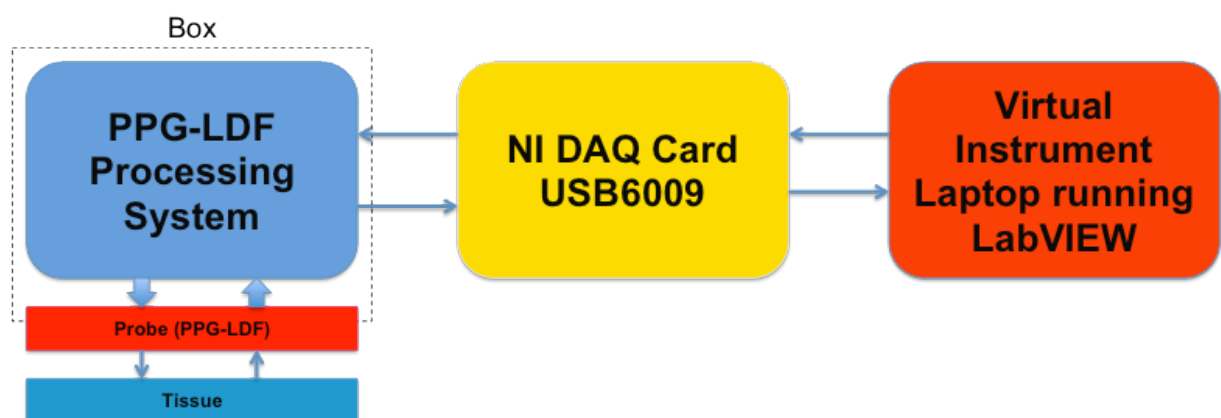


Figure 9.1: Block diagram of the PPG-LDF processing system and the connection with the VI.

LabVIEW, which stands for Laboratory Virtual Instrument Engineering Workbench, is a development environment designed by National Instruments (National Instruments, Austin, Texas, USA). Programs developed in LabVIEW are referred to as Virtual Instruments (Vis) due to their visible and functional resemblance to hardware instruments. LabVIEW uses a graphical programming language called “G”. Using a workspace known as the ‘block diagram’, a program can be created in G, in contrast to most other programming systems that use text-based lines of code. In fact, this software relies on graphical symbols instead of textual language to create applications.

Each VI comprises three main parts, including the ‘front panel’ a graphical user interface for operating the VI when it is running and the block diagram representing the program, which contains multiple functions, some of which are also represented on the front panel.

The front panel: The front panel may consist of controls and indicators. Controls are knobs, buttons, dials and other input devices, while indicators are graphs, LEDs and other displays. The user interfaces with the running VI via the front panel.

The block diagram: The block diagram consists of functions connected together by virtual ‘wires’ represented by lines. Functions (also known as sub-Vis) can be selected from a library or created by the programmer. In this way they are similar to subroutines used in text-based programming languages. All front panel objects are represented on the block diagram, so may be connected to other front panel objects (or just to block diagram objects). Other functions used in text-based languages are available such as while loops, for loops etc.

Wires perform a similar function to variables in text-based programming and can be of different types including integer, floating point and string. One or two dimensional array variables of these types can also be used. Data acquired through a DAQ card may be processed using simple or advanced mathematical functions and the results displayed numerically or on a graph. Data may also be read from and saved to text files.

9.2 Two Wavelengths and Laser Doppler Signal Acquisition VI

In order to use the data acquisition hardware described in Chapter 8, a VI was created in LabVIEW (Version 8.5), shown schematically in Figure 9.2. This VI was designed to acquire all signals, displays AC and DC PPG, ambient and also LDF signals in a graphical format, calculate SpO₂ value and at the end, save the data in a spreadsheet format for further analysis.

The following sections will describe each part of this VI.

NI-DAQmx is a set of drivers, which are a connection between the data acquisition card (DAQ) and a laptop. Figure 9.3 shows the basic DAQmx, which has been used in the VI developed to continuously acquire all PPG and LDF signals in this current study, which will be explained in detail.

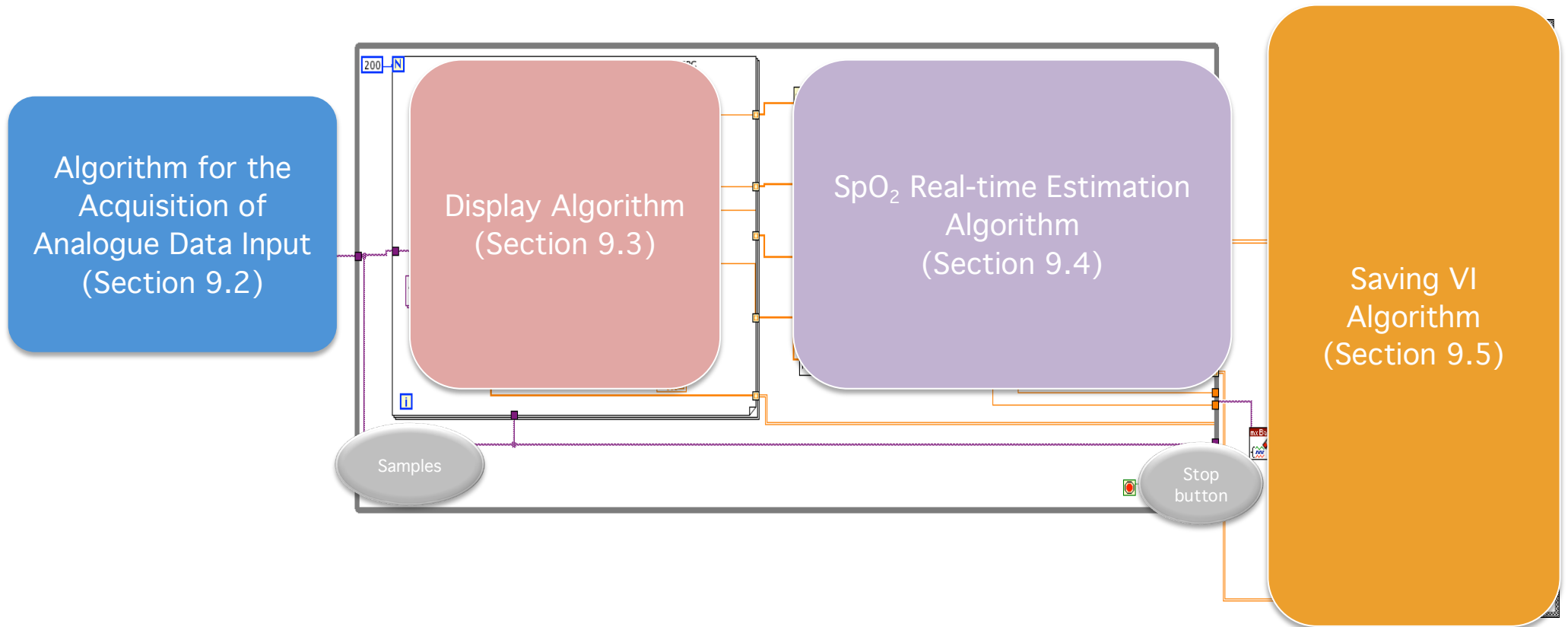


Figure 9.2: Simple diagram of the virtual instrument (VI).

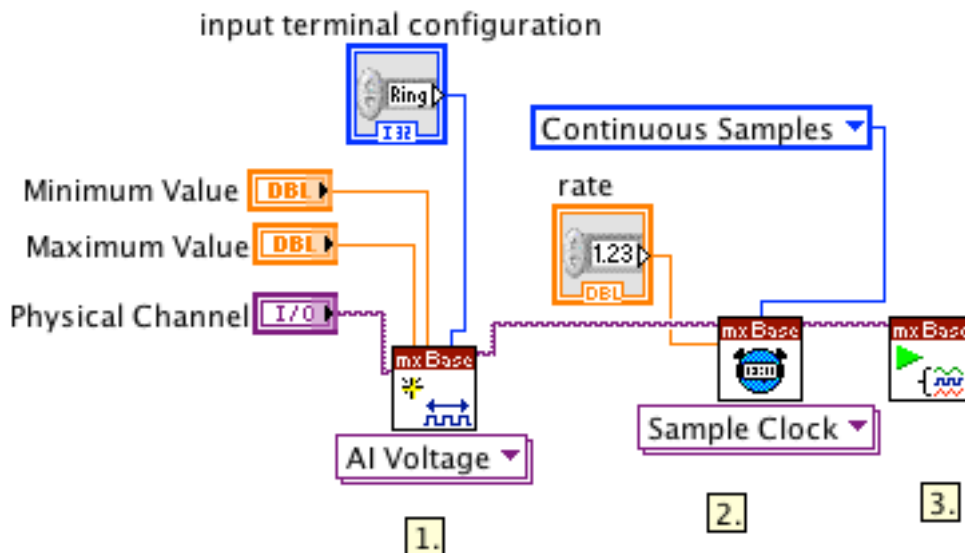


Figure 9.3: Basic DAQmx functions used in the VI developed to continuously acquire PPG and LDF signals.

DAQmx create Channel: uses the Physical Channel to create and set up an Analogue Input Voltage virtual channel, which has six virtual channels to measure the voltage output from the PPG/LDF processing system. As mentioned before the DAQ card used in this study (USB6009) has 8 analog inputs, six of them (*ai0-ai5*) have been connected to the output of the PPG/LDF processing system, the virtually created channels correspond to these six physical terminals on the DAQ card. Maximum and minimum voltages may be set according to the requirements of the data acquisition but the default range is +10 v to -10 v, the input terminal configuration are set for RSE (Referenced Single Ended) mode. See Figure 9.4.

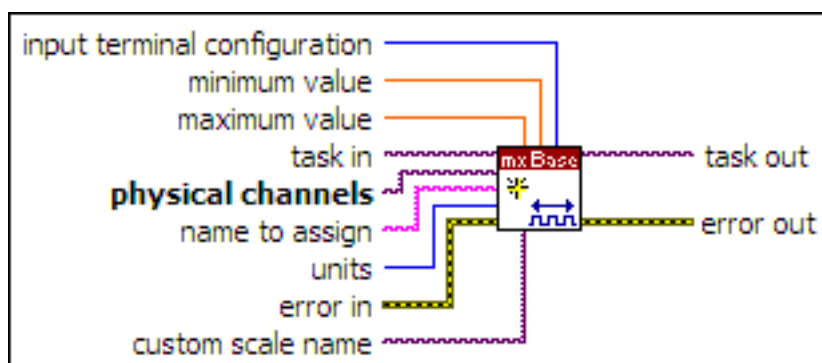


Figure 9.4: Diagram of DAQmx Create Virtual Channel.

DAQmx Timing (Sample Clock): To controls the number of and rate at which samples are acquired DAQmx Timing is added. The sample mode is on the continuous mode, which acquires samples continuously until the VI is stopped, sampling rate of 100 Hz is also set. See Figure 9.5.

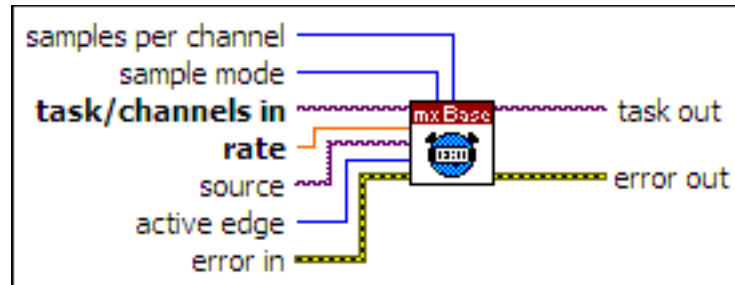


Figure 9.5: Diagram of DAQmx Timing.

DAQmx Start Task: To start and run the measurement (acquiring the samples). See Figure 9.6.

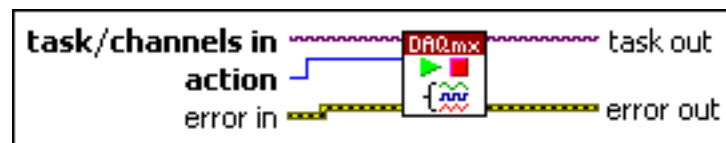


Figure 9.6: Diagram of DAQmx Start Task.

9.3 Algorithm for continuous signal display

While-Loop: The task (acquired data) is then passed into a while-loop, which incorporates most of the VI's functions, which contains a for-loop, which will be explained in the next section. Within the while-loop the acquisition and all codes will be executed continuously until a condition occurs and the user stops the program by pressing the stop button on the front panel of the VI, in fact it executes the sub diagram until the conditional terminal  receives a specific Boolean value ("TRUE"). As soon as the TRUE condition is received the while-loop will finish executing all codes. The while-loop always executes at least once. The iteration terminal  contains the number of completed iterations. Figure 9.7 shows the block diagram representation of a while-loop.



Figure 9.7: While-loop

As explained, the VI is based on a repeating loop. The user sets the number of samples per cycle on the front panel, then during each loop the VI acquires that number of samples from each channel. At the end this number of acquired samples is written onto a spreadsheet file for further analysis, which will be explained later in this chapter.

For-Loop: A for-loop executes a sub diagram within it, N times. A for-loop differs from the while-loop, as the for-loop executes at a set number of times (N) however a while-loop stops executing the sub diagram only if specific values at the conditional terminal occurs. Figure 9.8 shows the block diagram representation of a for-loop. As it can be seen in Figure 9.9 the DAQmx Read function is placed inside a for-loop, which is in turn inside a while-loop. Details of this function will be explained in the next section.

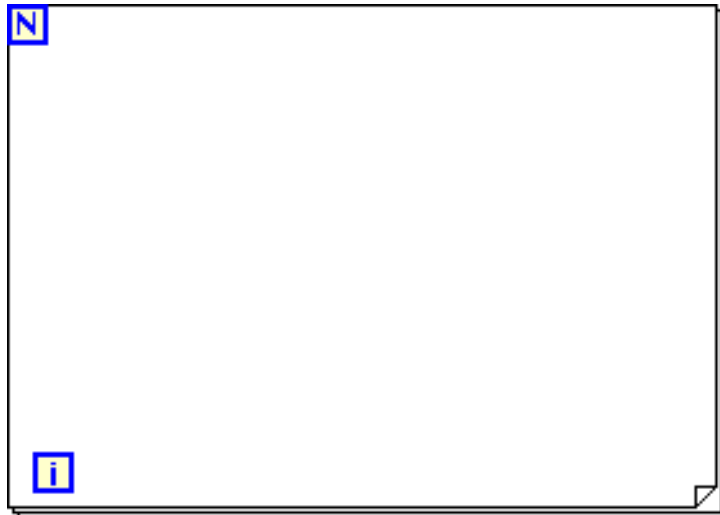


Figure 9.8: For-loop

DAQmx Read: using this function inside the while-loop the signals that have been sampled by the DAQ card can be read for each specified channel. After the creation of an analogue output signal, the while-loop along with the *DAQmx Read* function generates an output voltage continuously. The DAQmx Read VI reads one sample from a single channel. The format of sampling is set for analogue “1D DBL NChan NSamp” so single samples from multiple channels can be read and the output is a one-dimensional array. Figure 9.10 shows a diagram of a DAQmx Read.

The VI is designed to run continuously to obtain one sample as set in the DAQmx Read, so that one sample for each iteration may be acquired. The for-loop is set to execute continuously 200 times. Therefore, after 200 iterations of the for-loop, 200 samples can be acquired. The while-loop continuously repeats, runs the process and keeps scanning the data until the conditional terminal receives the Boolean value corresponding to a ‘stop’ command (TRUE). When the user presses the stop button on the front panel of the VI the while-loop stops acquiring data.

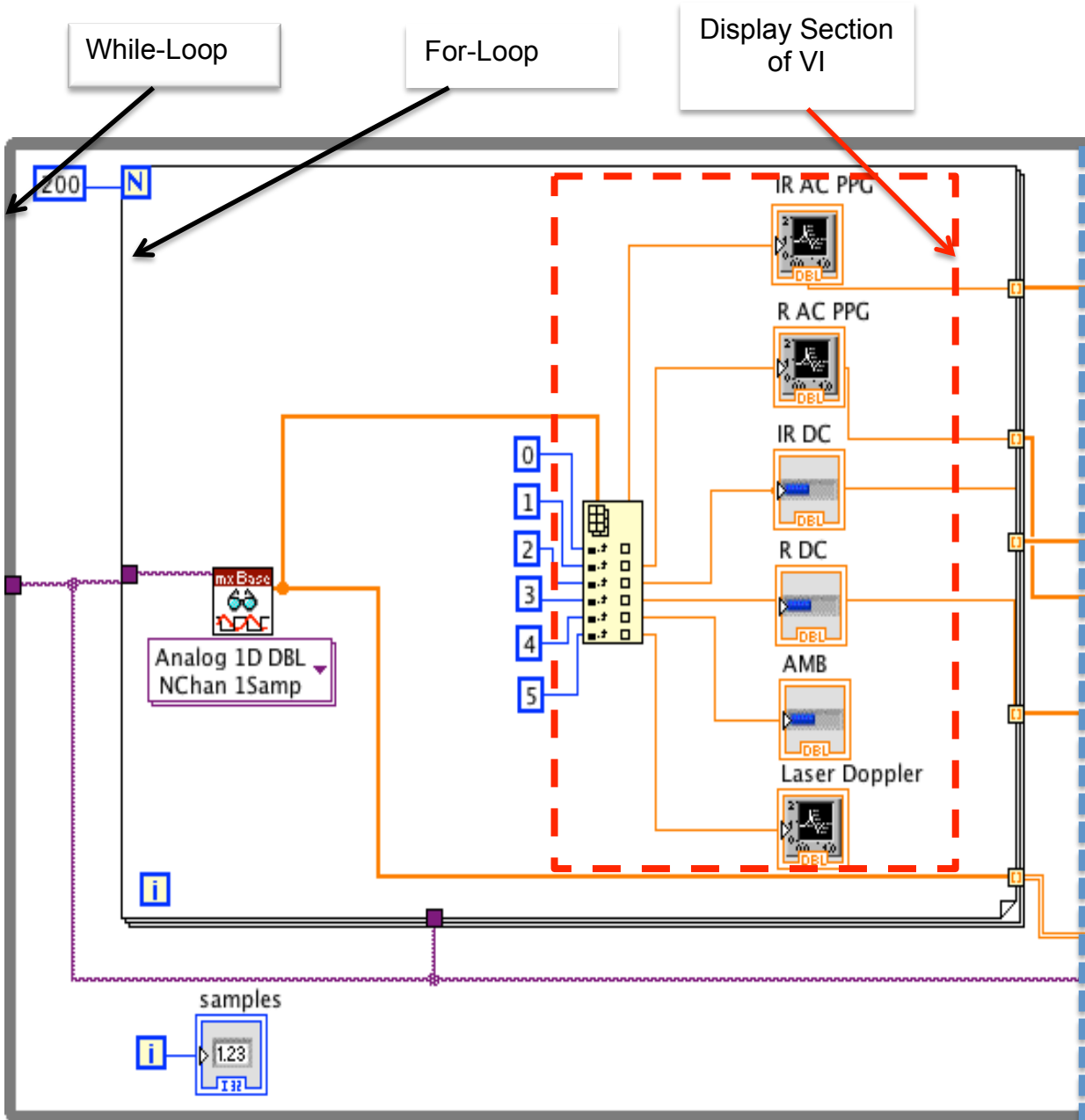


Figure 9.9: Algorithm for continuous signal display.

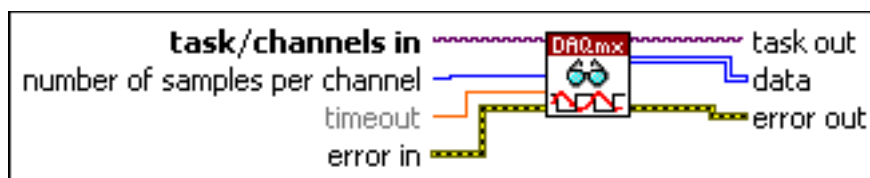


Figure 9.10: Diagram of DAQmx Read.

The output of the DAQmx Read function is fed into an “Index Array” function. Using this function, any of the columns representing each channel at the voltage data output of the DAQmx Read function may be extracted. This function can resize automatically when wired to an array, and displays an index input for

dimension in the array. Also more elements or subarray terminal can be added by resizing the function (See Figure 9.11). The output of this function is six separated acquired channels.

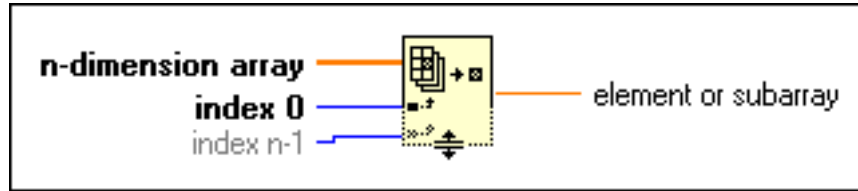


Figure 9.11: Index Array function.

9.4 Estimation of the bowel tissue SpO₂

The arterial blood oxygen saturation (SpO₂) values were also calculated from the incoming raw PPG signals using a developed VI. To derive estimations for SpO₂ values, initially the ratio (R_R) of the quotients of the AC and DC amplitudes of the red and infrared wavelengths are calculated using:

$$R_R = \frac{R_{AC}/R_{DC}}{IR_{AC}/IR_{DC}} \quad \text{Equation 9.1}$$

The outputs of the formula are displayed on the front panel.

The arterial oxygen saturation is then computed using the formula below:

$$SpO_2 = 110 - 25 (R_R) \quad \text{Equation 9.2}$$

A VI was designed and implemented to calculate the R_R and the SpO₂ of the bowel tissue using Equations 9.1 and 9.2. These details will be explained in the following section.

In order to find the peak-to-peak amplitude of the pulsatile R and IR PPG components of the required signals, the difference between the maximum and minimum values of a short segment of the acquired signal is found. Note that the acquisition time of two seconds ensures that at least one heartbeat is

represented by the acquired segment of data.

Following the separation of the raw acquired signals by Index Array function, the output (comprising 200 samples, or 2 seconds of data) then passes outside the for-loop. Among them the R_{AC} and IR_{AC} and also R_{DC} and IR_{DC} signals pass through “Array Max and Min” functions (Figure 9.12), which returns the maximum and minimum values of all elements in the array.

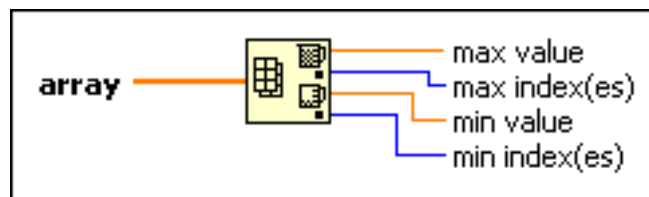


Figure 9.12: Array Max and Min functions.

The peak-to-peak amplitude is then calculated from the difference between the maximum and minimum values.

The mean of the values for the DC component of the PPG for both R and IR wavelengths is calculated using two “Mean” functions (see Figure 9.13).

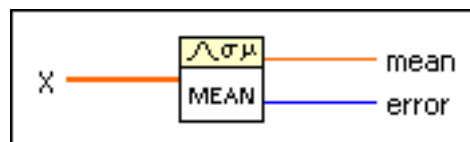


Figure 9.13: Mean function

Following calculations of the amplitude of the AC PPG for both R and IR wavelength and also the mean values for DC PPG, all the outputs from the array functions are then sent into a formula node, so now the ratio of R_{AC} / R_{DC} and IR_{AC} / IR_{DC} can be obtained using “division numeric” functions. At the end another division numeric function needs to be used to compute the ratio-of-ratios (R_R) value by dividing the obtained values in the Equation 9.1. The calculated R_R used to calculate the SpO_2 value using Equation 9.2. The whole block diagram for calculation of R_R and SpO_2 is illustrated in Figure 9.14.

DAQmxBase Clear Task VI: After the VI is stopped by pressing the STOP button, the VI commands the DAQ card commands to stop acquiring data using DAQmxBase Clear Task VI. This allows the DAQ card to clear the previous set up parameters and reset itself. See the diagram of DAQmxBase Clear Task in Figure 9.15.

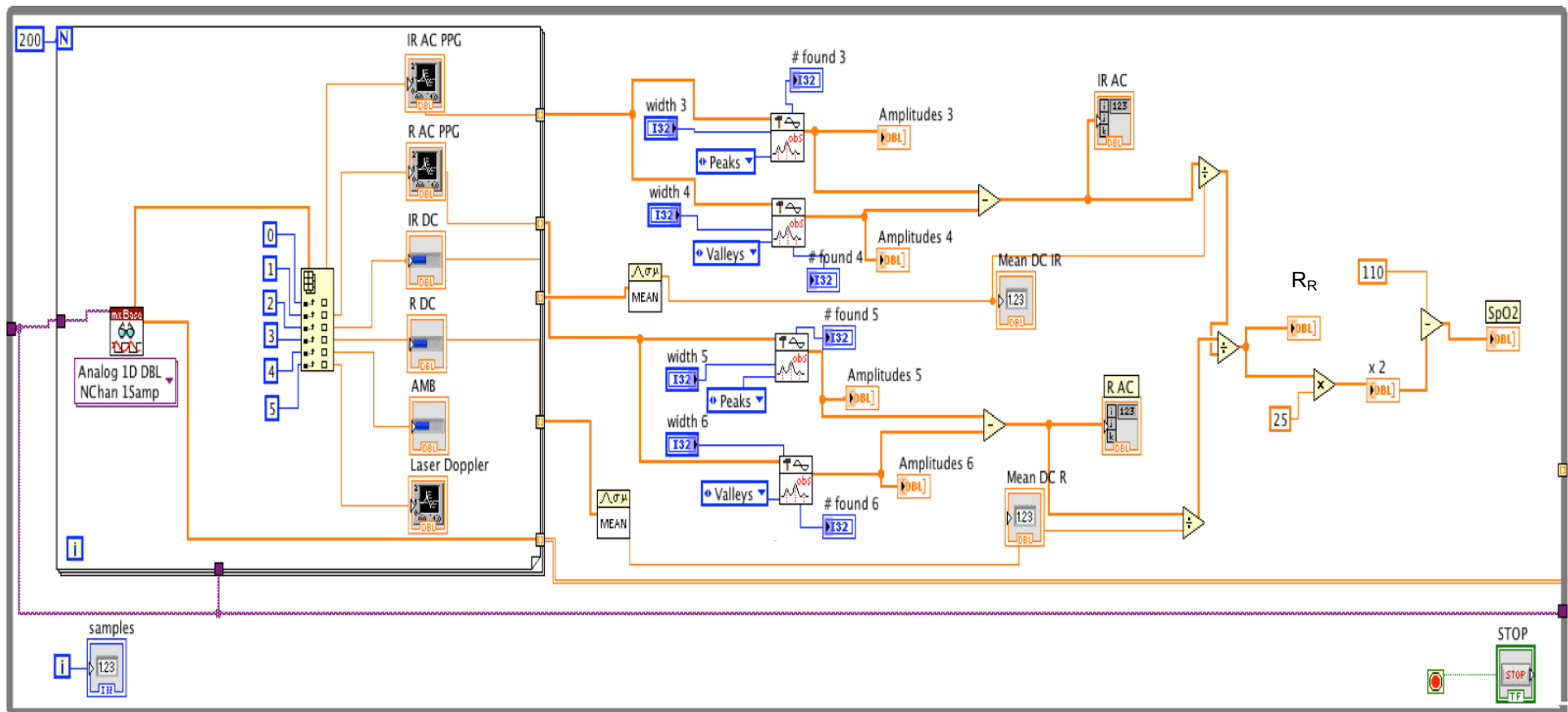


Figure 9.14: Illustration of the block diagram, used for calculating R_R and SpO_2 for the PPG.



Figure 9.15: Diagram of DAQmx Base Clear Task VI.

9.5 VI for Data Storage

The acquired data must be saved and stored in a text file for further analysis. All PPG and LDF signals are saved into a file in a tab-delimited text format.

The 'DAQmx Read' VI produces a 2-dimensional array, which is then formatted and saved.

The data in the 2D array first needs to be converted to a table in string form, which is accomplished with an "Array to Spreadsheet String" function (Figure 9.16).

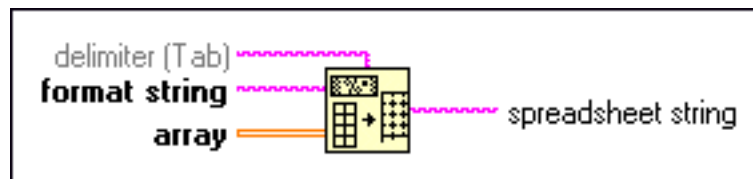


Figure 9.16: Array To Spreadsheet String Function.

After generating the spreadsheet string, the data is saved in the specified file, using a 'Write File' function (Figure 9.17). All the acquired data can thus be saved in memory continuously while the VI is running. The date and time of the measurement is also saved using the "Get Date/Time String" Function (Figure 9.18).



Figure 9.17: Write to Text File Function.

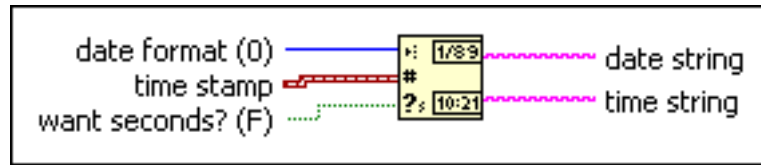


Figure 9.18: Get Date/Time String Function.

At the end of the measurement by pressing the stop button on the front panel of the VI, the file is transferred to a text file saved to the computer hard disk. The VI used to save all the acquired analogue signals is shown in Figure 9.19.

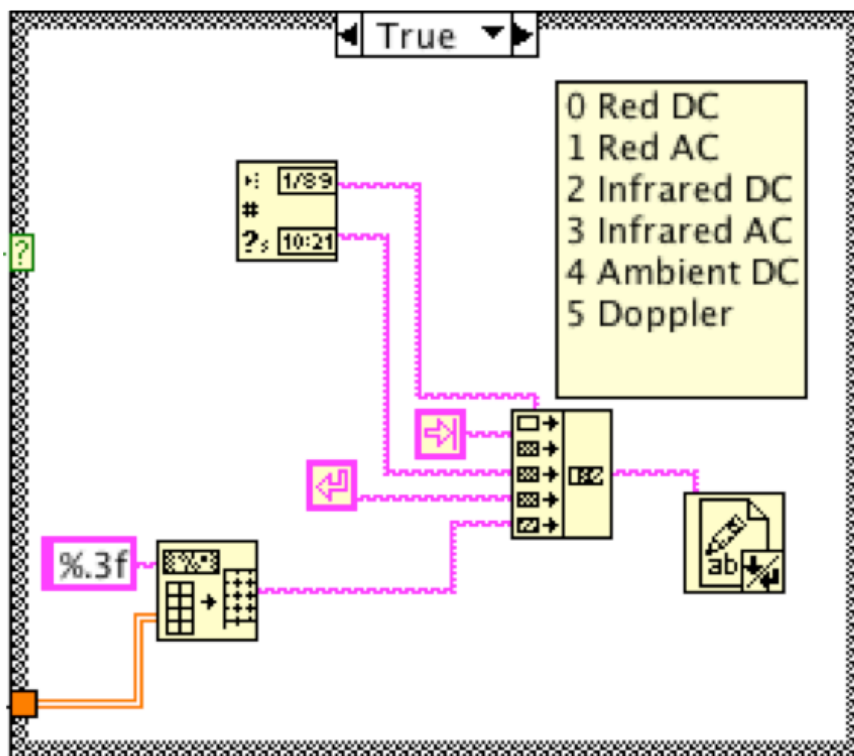


Figure 9.19: The VI used to save all the acquired analogue signals.

9.6 Front panel of the VI

All six signals including photoplethysmographic, laser Doppler and ambient light are displayed on the front panel using three chart indicators for IR_{AC} , R_{AC} and LDF, also three bar indicators for IR_{DC} , R_{DC} and ambient light outputs in real time. As mentioned before the user can observe these output signals, also their amplitude and morphology can be monitored during acquisition of data as a way of verifying the quality of the signals. Figure 9.20 shows the Front panel of the

Virtual Instrument, as it can be seen the first chart on the right top side of the front panel shows the IR_{AC} PPG, the second chart shows R_{AC} PPG and the third chart shows LDF. In all three charts amplitude is plotted versus time in seconds. The waveform chart is a graphical representation of the output data to display the PPG and LDF signals.

On the left side of the front panel there are three bar indicators for IR DC, R DC and ambient outputs. These three horizontal coloured bar displays, show the output voltages corresponding to the total detected signal level acquisition phase (infrared and red signal levels (AC+DC)). Bar indicators are chosen for DC displays since they give a quick and easy visual interpretation of DC level in the PPG processing signals. Also the set up parameters are placed on the left side of the front panel in order to control and adjust the parameters if required. All the controls of the system including offset control of the waveforms, sampling frequency of the acquisition, R_R , and SpO_2 are placed on the front panel of the VI and can be seen and controlled by the user.

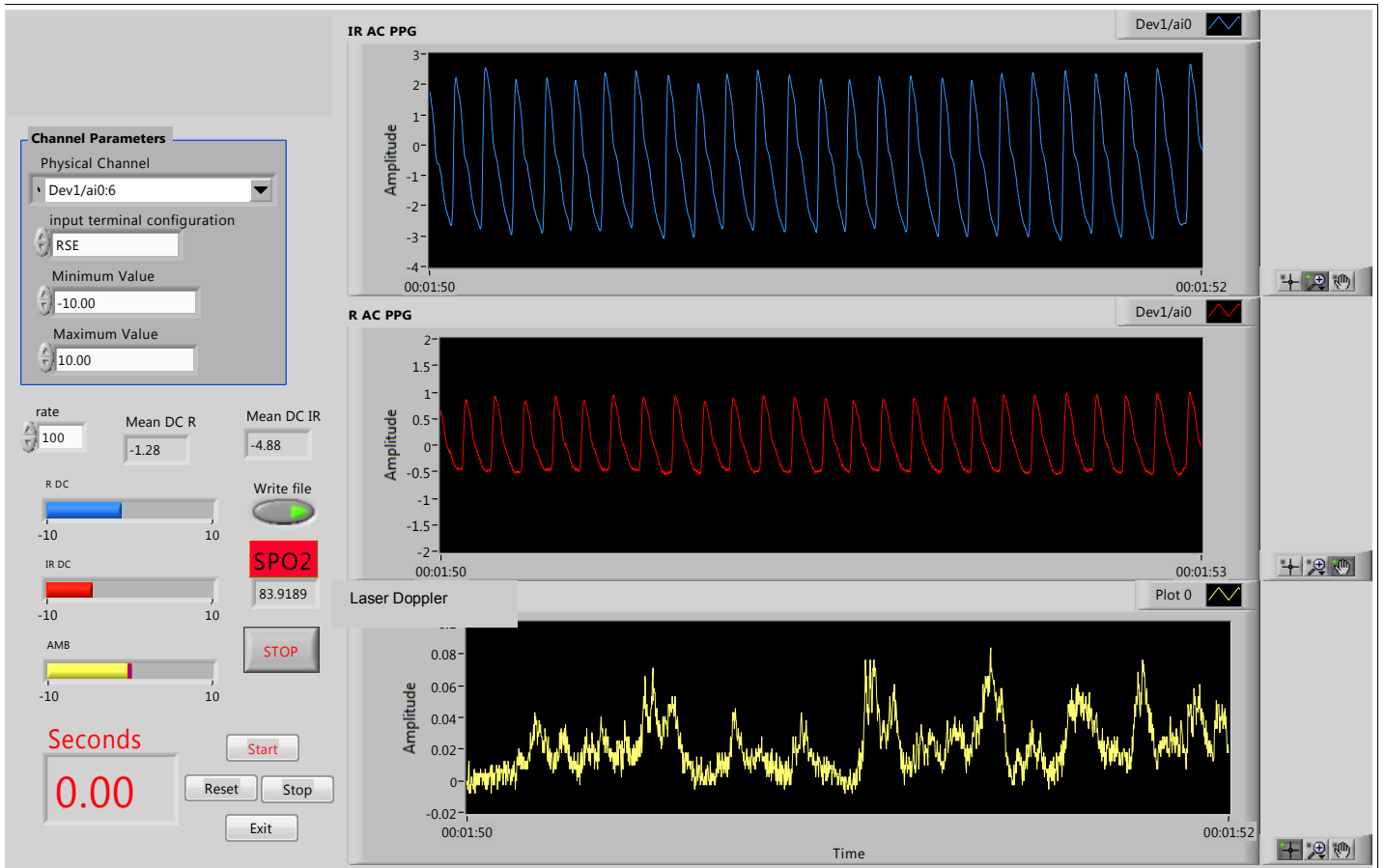


Figure 9.20: Front panel of the Virtual Instrument.

Intra-operative PPG/LDF Assessment of Bowel Tissue Viability

Following the design of the probe and instrumentation and the successful evaluation, clear PPG and LDF signals through two different volunteer studies were obtained in Chapter 7. The functionality of the developed PPG/LDF system was then discussed in Chapter 8 and the virtual instrument presented in Chapter 9. With these three chapters, sufficient confidence was acquired to allow the system and probe to commence the preliminary clinical measurements. The recruitment process for selecting potential patients who met the inclusion criteria for the trial and the procedure by which the PPG and LDF signals that were acquired *in vivo* will be presented in this chapter. This chapter also explains the methodology used to analyse the acquired data followed by a detailed discussion of the results.

10.1 Introduction

The aim of this evaluation was to determine if clear PPG and LDF signals could be obtained from the surface of the large bowel at different stages in bowel resection intra-operatively, also to compare differences in PPG amplitude and LDF flux obtained from different stages during the operation. Arterial blood oxygen saturation was also estimated from the large bowel at each stage.

The PPG/LDF instrumentation system was inspected by the Clinical Physics Department of Barts and the London, NHS Trust, London and was deemed safe for use on patients in the clinical environment. Ethical approval (Appendix D) was written and obtained for this study in June 2013 by the National Research Ethics Service (NRES) Research Ethics Committee London: City & East. The study was approved by the Barts and Queen Mary Joint Research Office in September 2013.

10.2 Methods

10.2.1 Patients

Written informed consent from each patient was obtained prior to recruitment to the study. In total, 24 patients undergoing bowel resection with/without anastomosis (Chapter 3) that met the inclusion criteria and were due for colorectal surgery at the Royal London Hospital from January 2014 to September 2014 were entered into this study. 11 volunteers were male and 13 were female with average age (\pm SD) of 66 (\pm 15.6) (range 33 - 91). These preliminary clinical measurements were performed on patients undergoing bowel resection both laparotomy (4 cases) and laparoscopy (20 cases). Table 10.1 summarises the patients' details, which included age, sex, type of measurements and number of measurements obtained from each patient. It was decided by the surgeons that the evaluation should focus on the measurements at eight different stages during each operation (if possible), see Section 10.3. In order to avoid delaying the surgical procedure, the length of the recording for each measurement was limited to about one minute. A Case Report Form (CRF) was also prepared for each patient, where patient information such as the patient's date of birth, weight, date of surgery, medical history, reason for the operation, etc. were documented.

10.2.2 Measurements

As mentioned in chapter three, the most common procedure in this study was the removal of a cancerous segment of the large intestine, which can be done through laparoscopy or laparotomy. To perform a laparoscopy, three or four small incisions are commonly made, (in order to prevent a large incision), to insert the laparoscope and small surgical tools. While in laparotomy, the operation is carried out through a large incision on the abdomen.

After administration of general anaesthesia, the patient was intubated and mechanically ventilated. This research was planned so as not to interfere with the operation so the PPG/LDF probe was placed on a separate sterile trolley near the patient's bed to be used later by the surgeon. Since this was a research study, care was taken to ensure that the recorded data was not available to the surgeons during the measurements in case it could be interpreted as a reliable

indicator of tissue viability and possibly contribute to clinical decision making. Prior to any measurements, the combined sensor was inserted into the sterile probe cover (Section 7.4) and was placed on the sterile covered trolley beside the surgeon and operating table. For each measurement, at an appropriate time, the processing system was switched on and the sensor was passed to the surgeon with caution and inserted through the Trocar¹ (size 12-mm) in laparoscopy and applied over the surface of the bowel or applied directly and gently onto the surface of the bowel in laparotomy. For each recording the surgeon tried to put the sensor over a suitable place on the surface of the bowel to obtain a clear signal but sometimes the probe position needed adjusting slightly by the surgeon until a clear signal could be observed on the laptop screen.

Signal acquisition then commenced using the LabVIEW program (Chapter 9) on the laptop. The sensor was held as steadily as possible over the investigation site by the surgeon during the recording period. To ensure no interference with the light from the combined sensor during the measurements in laparoscopy, the laparoscopic light was turned off. During the laparotomy procedure, the overhead operating theatre lights were turned off. Simultaneous AC and DC PPG and LDF signals were then acquired using the PPG/LDF processing system and recorded for approximately one minute for each measurement.

Once satisfied with the signal detected from the investigation site, the signal acquisition was stopped and the acquired signals were saved. Any additional information such as surgical events, during the measurements was recorded on a separate notebook for future analysis, if required. In order to compare the recorded values obtained by custom made PPG/LDF sensor with those from routine commercial measurements, the data such as blood oxygen saturation, heart rate, systolic and diastolic blood pressures and temperature from the theatre monitors, were also noted right after each measurements separately. After each measurement the surgeon would remove the sensor from the measurement site (in the case of laparoscopy, the sensor would be withdrawn

¹ A sharp-pointed surgical instrument used a means of introduction for cameras and laparoscopic hand instruments, such as scissors, graspers, etc.,

from the trocar) and put back with caution on to the sterile trolley for the next measurement and the operation continued as planned. Sometimes the investigation site was in a very low location in the abdomen, this happened mostly for post anastomosis or over tumour measurements, so the measurement from these locations could not be monitored.

Table 10.1: Details of all patients recruited to the study including the measurements for each trial. Reference; 1: Mobilisation, 2: Over Tumour, 3: Pre Ligation, 4: Post Ligation, 5: Pre Anastomosis Proximal, 6: Pre Anastomosis Distal, 7: Post Anastomosis Proximal, 8: Post Anastomosis Distal measurement (Measurements will be explained in detail in the following section).

Patient	Sex	Age	Type of Operation	Reason for Operation	Measurement								
					1	2	3	4	5	6	7	8	
1	M	82	Laparoscopy	Tumour	✓	x	✓	✓	✓	✓	✓	✓	✓
2	F	56	Laparoscopy	Tumour	x	x	x	✓	✓	x	x	x	x
3	F	61	Laparoscopy	Tumour-Right side	✓	✓	✓	x	✓	x	✓	x	x
4	F	54	Laparoscopy	Rectal Tumour	✓	x	x	x	✓	x	x	x	x
5	M	33	Laparoscopy	Tumour-left side	x	x	x	x	✓	✓	✓	✓	✓
6	F	61	Laparoscopy	Tumour-left side	✓	✓	✓	✓	x	x	x	x	✓
7	M	52	Laparoscopy	Right Hemi-colectomy	✓	✓	✓	x	✓	x	✓	✓	✓
8	M	85	Laparotomy	Hernia repair/closure of colostomy	x	x	x	x	✓	✓	✓	✓	✓
9	M	72	Laparoscopy	Anterior Resection	x	x	x	x	✓	x	✓	✓	x
10	M	75	Laparoscopy	Anterior Resection of rectum	✓	x	✓	✓	✓	x	✓	✓	x
11	M	38	Laparoscopy	Hemi-colectomy	x	✓	x	✓	✓	✓	✓	✓	x
12	F	82	Laparotomy	Rectum tumour	x	x	x	x	✓	✓	✓	✓	✓
13	F	77	Laparoscopy	Anterior Resection	✓	✓	✓	✓	✓	x	✓	✓	x
14	F	61	Laparoscopy	Anterior Resection	x	x	✓	✓	✓	✓	✓	✓	x
15	F	56	Laparotomy	Open Anterior Resection	✓	x	✓	✓	x	x	✓	✓	x
16	F	74	Laparoscopy	Anterior Resection	✓	x	x	✓	x	x	✓	✓	x
17	F	35	Laparoscopy	Right Hemi-colectomy	✓	✓	x	✓	x	x	✓	✓	✓
18	F	72	Laparoscopy	Low Anterior Resection	x	x	✓	✓	✓	x	✓	✓	✓
19	M	80	Laparoscopy	Hartmann's	✓	✓	✓	✓	✓	x	✓	✓	x
20	F	91	Laparoscopy	Tumour-left side	✓	x	x	✓	x	x	x	x	x
21	M	59	Laparoscopy	Anterior Resection	✓	x	x	✓	✓	✓	✓	✓	✓
22	F	81	Laparoscopy	Anterior Resection	✓	x	x	✓	x	x	x	x	x
23	M	72	Laparoscopy	Anterior Resection	✓	x	✓	✓	x	x	✓	✓	✓
24	M	68	Laparoscopy	Anterior Resection	x	x	x	x	x	x	x	x	x
N=	---	---	---	---	15	7	11	16	16	7	18	10	

10.3 Intraoperative Measurements

With the agreement by the surgeon, intraoperative measurements were made through eight measurements made at the following times:

1. Mobilisation
2. Over tumour
3. Pre- Ligation
4. Post-Ligation
5. Pre-Anastomosis, Proximal
6. Pre-Anastomosis, Distal
7. Post-Anastomosis, Proximal
8. Post-Anastomosis, Distal

Each measurement is explained in brief below.

10.3.1 Mobilisation

The first surgical step in bowel resection is mobilisation of the colon and its mesentery, i.e. separation of the colon from the wall of the bowel. Once mobilisation is complete, the first measurement can be performed as explained. In total, 15 mobilisation measurements were performed.

10.3.2 Over Tumour

The second measurement was planned to be performed on the tumour, in which the probe was placed over the cancerous site, although in many cases the tumour was very small or located very low and couldn't be monitored. In total, seven measurements over tumours were acquired.

10.3.3 Pre-Ligation

After mobilisation of the bowel vascular ligation takes place, in which the blood vessels, which are providing blood supply to the area, must be stapled in order to stop feeding the region of colon to be removed. In this step of the operation the appropriate recipient vessels must be identified in the area by the surgeon in preparation for clamping. Before ligation, a measurement ('pre-

ligation') was performed. In total, 11 pre-ligation measurements were performed.

10.3.4 Post-Ligation

Following vascular ligation, post ligation measurement could be carried out. In total, 16 post-ligation measurements were performed.

10.3.5 Pre Anastomosis Proximal and Distal

After ligation of the blood vessel in the area to be removed, the cancerous segment is ready to be removed followed by anastomosis of the healthy segments. At this point of the procedure in laparoscopy a section of colon that includes the cancerous segment is passed through one of the small incisions (which needs to be enlarged to 3–4 cm) (Chapter 3), so anastomosis is performed while the colon is out of the abdomen (Figure 10.1). Anastomosis is performed by joining the edges of the healthy parts together along with rejoining the arterial and venous blood vessels of the proximal sites of the anastomosis area. Pre-anastomosis measurements were made before rejoining two segments together. The measurements were performed on the proximal and distal ends of the anastomosis edge. In total, 16 pre-anastomosis proximal and seven pre-anastomosis distal measurements were performed. After the anastomosis, the colon was then placed back into the abdomen.

10.3.6 Post Anastomosis, Proximal and Distal

After the anastomosis, in order to capture the reperfusion of the anastomosis site, PPG amplitude, LDF flux and arterial blood oxygen saturation measurements at the proximal and distal ends of the anastomoses were performed. In total, 18 post-anastomosis proximal and ten post-anastomosis distal measurements were performed. Figure 10.1 shows a picture of the PPG/LDF recording at an anastomosis measurement in which the surgeon applied the sensor on the surface of the colon, outside of the abdomen.

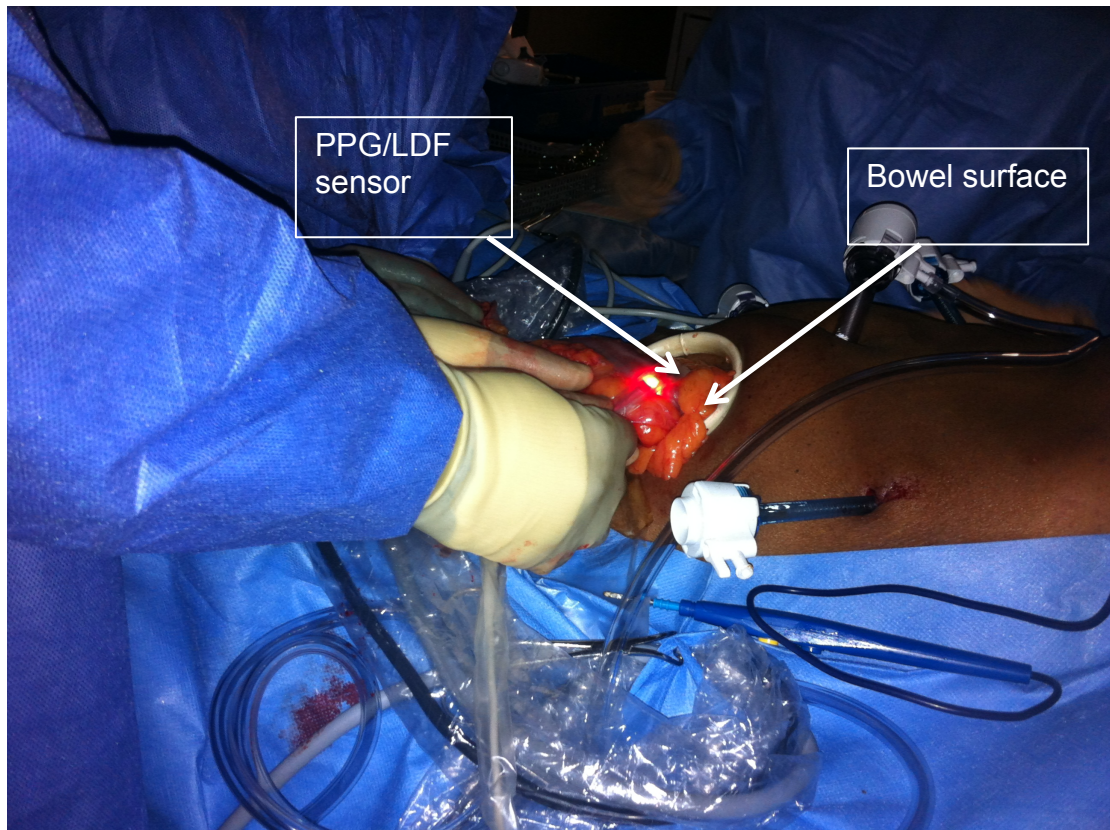


Figure 10.1: *In vivo* monitoring for anastomosis measurement during laparoscopy.

At the end of the surgery, after construction of the anastomosis, the abdomen was then closed with sutures.

The total numbers of measurements in all investigated sites was 100 (15 mobilisation, 7 over tumour, 11 pre-ligation, 16 post-ligation, 16 pre-anastomosis proximal, 7 pre-anastomosis distal, 18 post anastomosis proximal and 10 post anastomosis distal investigations). To facilitate the comparison between the results obtained with the combined sensor, the results were divided into four groups: *mobilisation*, *over tumour*, *ligation* and *anastomosis*.

10.4 Methods of Analysis of Acquired Data

In the 24 patients; 20 anastomosis and 4 non-anastomosis, 100 recordings were made. Clear red and infrared PPG and laser Doppler signals were acquired in most attempts from various measurements: mobilisation (n=15),

over tumour (n=7), Pre-ligation (n=11), post-ligation (n=16), Pre-anastomosis-proximal (n=16), pre-anastomosis-distal (n=7), post-anastomosis-proximal (n=18) and post-anastomosis distal (n=10). The PPG signals on the laptop screen appeared to show morphology typical of PPGs measured in other sites (71). As mentioned, it was planned to get all the eight measurements in each trial but this wasn't possible in all subjects for one or more of the following reasons:

- The operation didn't include anastomosis, resulting in fewer measurements.
- The measurement site was very low in the bowel or in a place that wasn't easy to access
- The surgeon was too busy (or forgot) to take the measurement
- The surgeon decided that there was insufficient time to complete the measurements without unacceptably delaying the operation.
- The processing system failed to detect clear PPG or LDF signals due to poor contact with tissue surface, or other technical reason.

In the next section, the results will be presented and compared between measurement sites.

In each group (mobilisation, over tumour, ligation and anastomosis) typical samples of acquired signals from one patient are shown. Also a table with the mean normalised amplitude for ac PPG for both red and infrared and also the mean LDF flux values for each patient in all measurements is included. An explanation of the normalisation method is given in Section 10.4.1. At the bottom of the table, the mean amplitude and flux averaged for all patients, and standard deviation (\pm SD) in all measurements is shown. Data analysis for the calculation of the average amplitude for ac PPG and LDF fluxes and the mean DC PPG were computed using LabChart 7 software (ADInstruments). The mean peak-to-peak amplitude of the AC PPG was automatically calculated and displayed by the software. The mean of the DC PPG and LDF flux selected data were also calculated automatically by the software. 10 to 20

second periods of each measurement were selected for the data analysis. For this calculation, periods with the fewest artefacts for three signals (R and IR PPGs and LDF) simultaneously were chosen, identified by visual inspection. A 43 second period is shown in Figure 10.2 from which a 10 second part was selected for the data analysis. In some measurements the acquired data couldn't be analysed and was excluded from the data analysis process. These cases were due to insufficient duration of clear signals as a result of motion artefacts caused by the surgeon while holding the sensor over the surface of the colon.

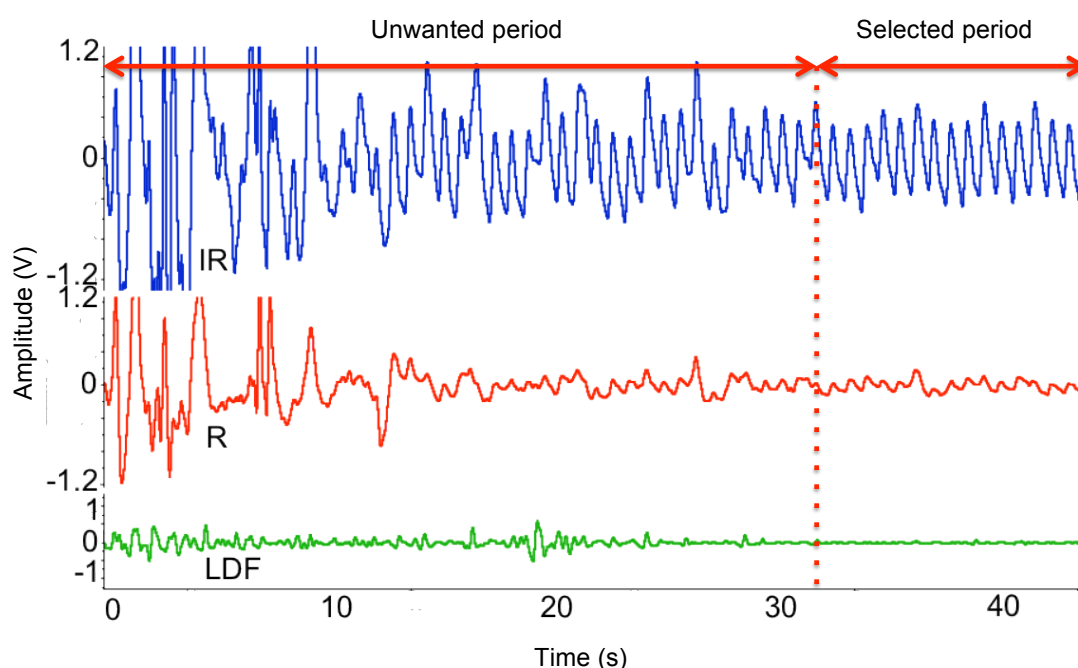


Figure 10.2: Selected period of the data for analysis.

The average laser Doppler flowmeter signal for the corresponding time, which was calculated by LabChart, then converted to conventional perfusion units (PU; 1 PU=10 mV) (66), values are given as mean PU (\pm SD) in the table along with the PPG values for each measurement.

10.4.1 Filtering and Normalisation of the Acquired Signals

To perform the analysis, the raw detected signals firstly had to be filtered to remove and eliminate the unwanted noise using LabChart. All detected

signals were filtered before any data analysis. In order to filter AC and DC a band-pass filter with a cut-off at 0.2 and 10 Hz and a low-pass filter at cut-off at 0.125 Hz were used respectively. Figure 10.3 shows a sample of signal before and after filtering.

The red and infrared AC PPG signals were normalised to remove the effect of non physiological variables from the signal. Normalisation is performed by dividing each AC component by its respective DC component (235). This removes the effect of variations in light intensity emitted by the LEDs, differences in sensitivity of the photodiode to each of the two PPG wavelengths and other non-physiological effects. Normalisation thus allows more meaningful comparison between measurements from different subjects.

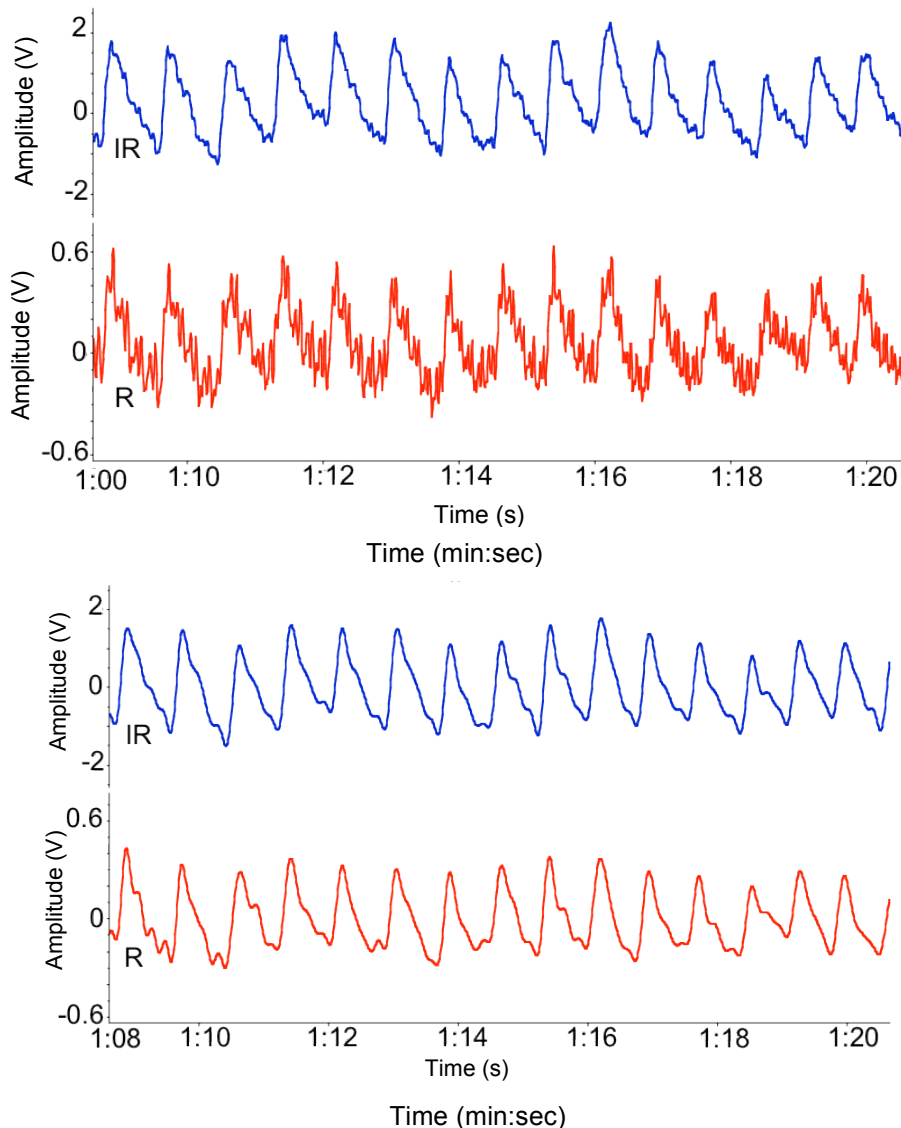


Figure 10.3: Raw signals with noise artefact (a) and after filtering (b).

10.5 Results of Analysis of Acquired Data

10.5.1 Mobilisation Measurements

Figure 10.4 illustrates a typical 10-second sample of the infrared and red AC PPG along with LDF signals obtained at mobilisation from one patient. Table 10.2 shows the mean normalised amplitudes for the red and infrared AC PPG and the mean flux for LDF from all patients at mobilisation (both values averaged over each measurement period). The mean (\pm SD) values averaged for all patients also are presented. In total, 15 measurements in mobilisation were acquired, among them 13 measurements for IR, 10 R and 11 LDF were included in the analysis (two measurements for IR, five for R and four from LDF were excluded from the analysis due to insufficient duration of clear signals). The mean (\pm SD) IR and R AC amplitudes averaged for all subjects were 433 (\pm 238) mV and 409 (\pm 255) mV respectively, and the mean LDF flux averaged for all subjects was 80.8 (\pm 76.3) PU.

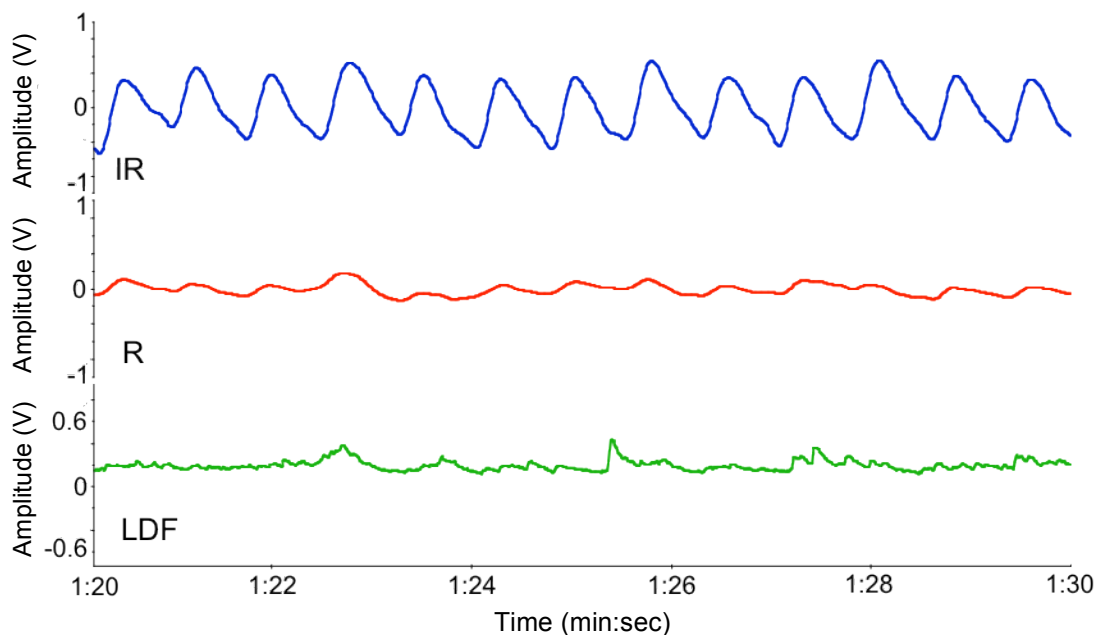


Figure 10.4: 10-second sample of red and infrared AC PPGs and LDF obtained at typical mobilisation measurements (case No. 6).

Table 10.2: Mean normalised AC PPG amplitudes and LDF flux from all subjects at mobilisation.

Patient	AC IR normalised (mV)	AC Red normalised (mV)	LDF (PU)
1	---	---	---
2	---	---	---
3	224	507	---
4	523	247	---
5	----	---	---
6	326	379	21.3
7	458	372	23.3
8	---	---	---
9	---	---	---
10	494	---	11.3
11	---	---	---
12	---	---	---
13	466	---	22
14	----	---	---
15	222	220	20.3
16	339	289	30.6
17	---	---	---
18	---	---	---
19	995	---	92
20	230	260	175
21	575	673	129
22	94	151	232
23	687	991	130
24	---	---	---
Mean	433	409	80.8
±SD	238	255	76.3

10.5.2 Over Tumour Measurements

Figure 10.5 shows a typical 10-second period measurements of the infrared, red PPG and LDF signals obtained in an over tumour measurement from one patient. Table 10.3 shows the mean normalised amplitudes for the red and infrared AC PPG and the mean flux for LDF from all patients from the over tumour measurements; the mean (\pm SD) values averaged for all patients are also presented. In total, seven measurements over tumour were acquired, among them six measurements for IR, three R and seven LDF were included in the analysis. The mean IR AC amplitude was 550 (\pm 361) mV, for R it was 431 (\pm 218) mV and 32.4 (\pm 31.5) PU for LDF, averaged for all subjects.

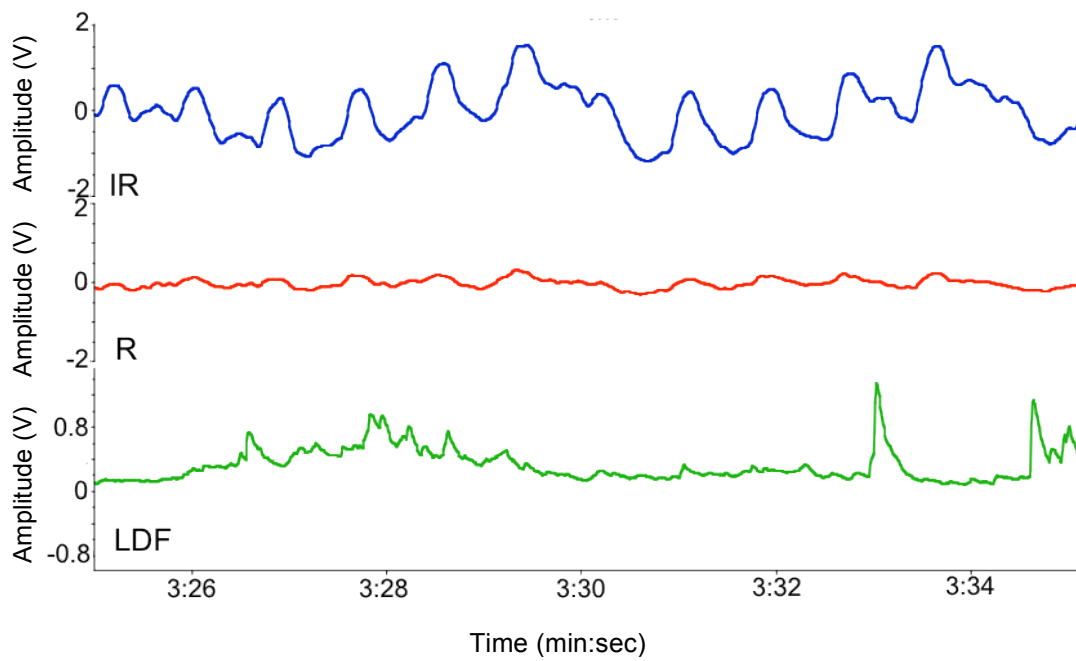


Figure 10.5: 10-second sample of typical red and infrared AC PPGs and LDF obtained at over tumour measurements (case No. 7).

Table 10.3: Mean normalised PPG AC amplitudes and LDF flux from all subjects at over tumour.

Patient	AC IR normalised (mV)	AC Red normalised (mV)	LDF (PU)
1	---	---	---
2	---	---	---
3	177	192	0.52
4	---	---	---
5	----	---	---
6	---	---	---
7	547	620	15
8	---	---	---
9	---	---	---
10	---	---	14.9
11	424	---	36
12	---	---	---
13	467	---	15.7
14	----	---	---
15	---	---	---
16	---	---	---
17	442	481	51.9
18	---	---	---
19	1.24	---	92.9
20	---	---	---
21	---	---	---
22	---	---	---
23	---	---	---
24	---	---	---
Mean	550	431	32.4
±SD	361	218	31.5

10.5.3 Pre and Post Ligation Measurements

Figures 10.6 and 10.7 show a typical 10-second sample of the infrared, red PPG and LDF signals obtained in pre and post ligation from one patient. Table 10.4 shows the PPG AC normalised amplitudes and the mean flux LDF from all patients at pre and post ligation and the mean (\pm SD) values averaged for all subjects. In total, 27 measurements at pre and post ligation, among them 26 measurements for IR, 18 R and 20 LDF were performed. The mean IR AC amplitude in pre-ligation was 394 (\pm 152) mV, for R it was 349 (\pm 265) mV and 80.4 (\pm 71.1) PU for LDF. The mean IR AC in post ligation was 293 (\pm 161) mV, for R it was 286 (\pm 152) mV and 71.2 (\pm 49.2) PU for LDF.

Figure 10.8 is a bar graph of the mean (\pm SD) normalised AC amplitudes for red and infrared averaged for all patients at pre and post ligation.

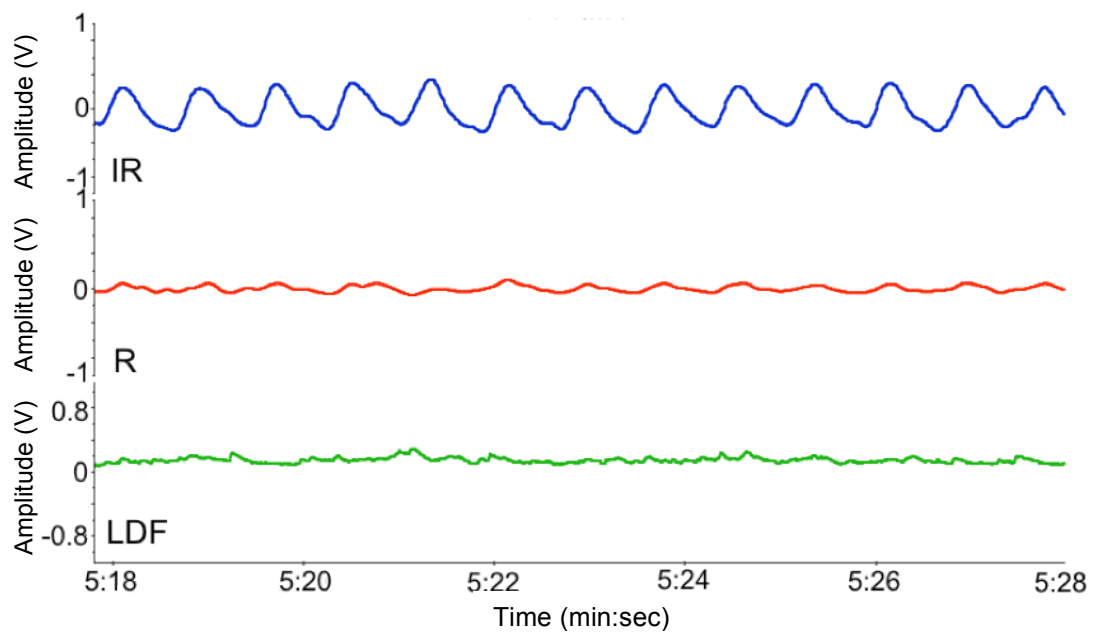


Figure 10.6: 10-second sample of typical red and infrared AC PPGs and LDF at pre ligation measurements (case No. 6).

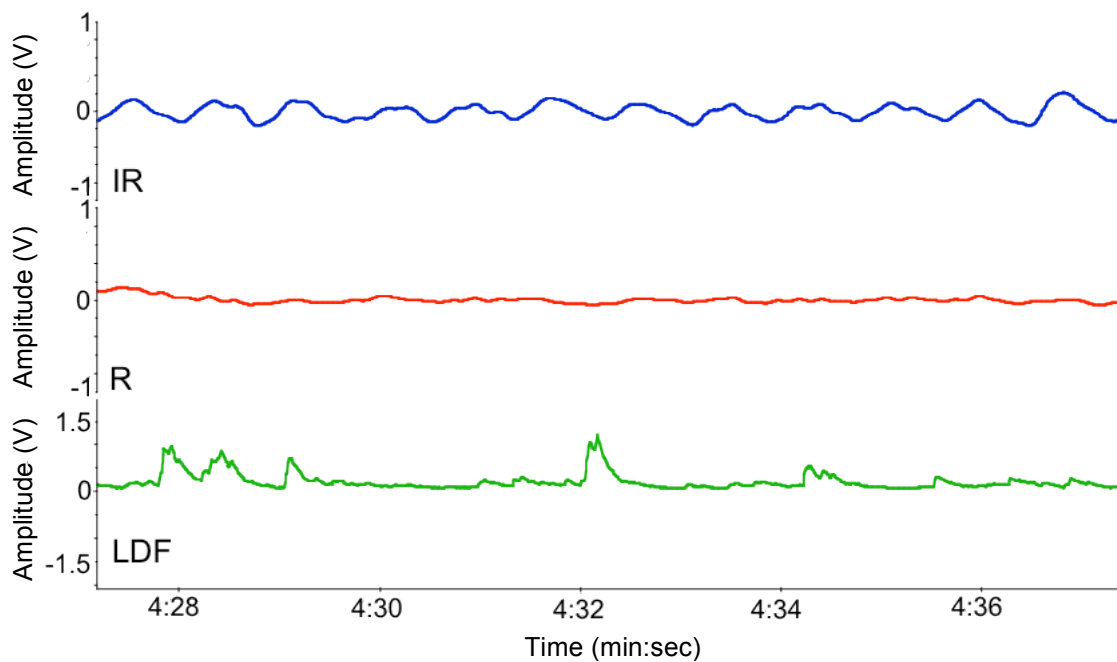


Figure 10.7: 10-second sample of typical red and infrared AC PPGs and LDF at post ligation measurements (case No. 6).

Table 10.4: Mean normalised PPG AC amplitudes and LDF flux from all subjects at pre and post ligation.

Patient	Pre Ligation			Post Ligation		
	AC IR normalised (mV)	AC Red normalised (mV)	LDF (PU)	AC IR normalised (mV)	AC Red normalised (mV)	LDF (PU)
1	---	---	---	---	---	---
2	---	---	---	329	196	37.1
3	302	858	---	213	268	---
4	---	---	---	---	---	---
5	---	---	---	---	---	---
6	302	224	29.7	103	180	21.4
7	458	372	---	---	---	---
8	---	---	---	---	---	---
9	---	---	---	---	---	---
10	674	---	28.9	763	688	---
11	---	---	---	294	---	81.2
12	---	---	---	---	---	---
13	466	---	---	139	---	89
14	427	---	74.1	471	---	28.9
15	119	109	57.9	168	132	16.9
16	---	---	---	124	171	---
17	---	---	---	352	---	31.4
18	295	223	25.5	270	235	43.2
19	525	---	127	291	---	108
20	---	---	---	217	260	146
21	---	---	---	267	306	135
22	---	---	---	202	369	39.5
23	372	304	220	402	336	148
24	---	---	---	---	---	---
Mean	394	349	80.4	293	286	71.2
±SD	152	265	71.1	161	152	49.2

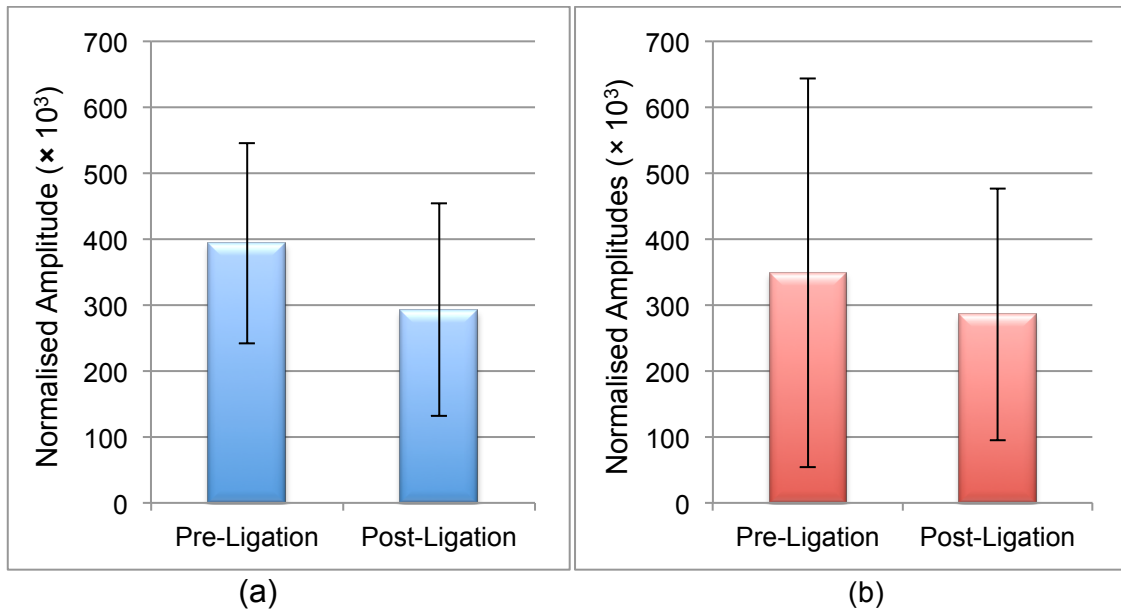


Figure 10.8: Mean (\pm SD) of normalised AC IR PPG amplitudes averaged for all patients for (a) pre-ligation IR (n=10), post-ligation IR (n=16), (b) pre-ligation R (n=6), and post-ligation R (n=12).

10.5.4 Pre and Post Anastomosis Measurements

Figures 10.9 to 10.12 depict AC PPGs and LDF signals for a 10 second sample at pre and post anastomosis, at proximal and distal sites from one patient. Tables 10.5 and 10.6 show the mean normalised amplitudes for the red and infrared AC PPG and the mean flux for LDF from all patients at pre and post anastomosis measured from the proximal end, and pre and post anastomosis measured from the distal end respectively; the mean (\pm SD) values averaged for all patients were also presented. In total 51 measurements at pre and post anastomosis were acquired, among them 43 measurements for IR, 30 R and 42 LDF were included in the analysis. The mean IR AC in pre anastomosis at the proximal site was 300 (\pm 149) mV, for R it was 333 (\pm 174) mV and for LDF it was 69.1 (\pm 49.3) PU. The mean IR AC amplitude at post-anastomosis from the proximal site for IR, R, and LDF was 350 (\pm 230) mV, 325 (\pm 189) mV and 44.1 (\pm 4.7) PU respectively. These values for pre anastomosis at the distal site for IR, R and LDF were 351 (\pm 168) mV, 583 (\pm 389) mV and 48.0 (\pm 37.2) PU respectively. The mean IR AC amplitude at post-anastomosis from the distal site was 432 (\pm 244) mV, for R it was 361 (\pm 91) mV and 66.1 (\pm 69.8) PU for LDF. A bar graph of the mean (\pm SD) amplitude at pre and post anastomosis from both sites for R and IR has been illustrated in Figures 10.13 and 10.14 respectively.

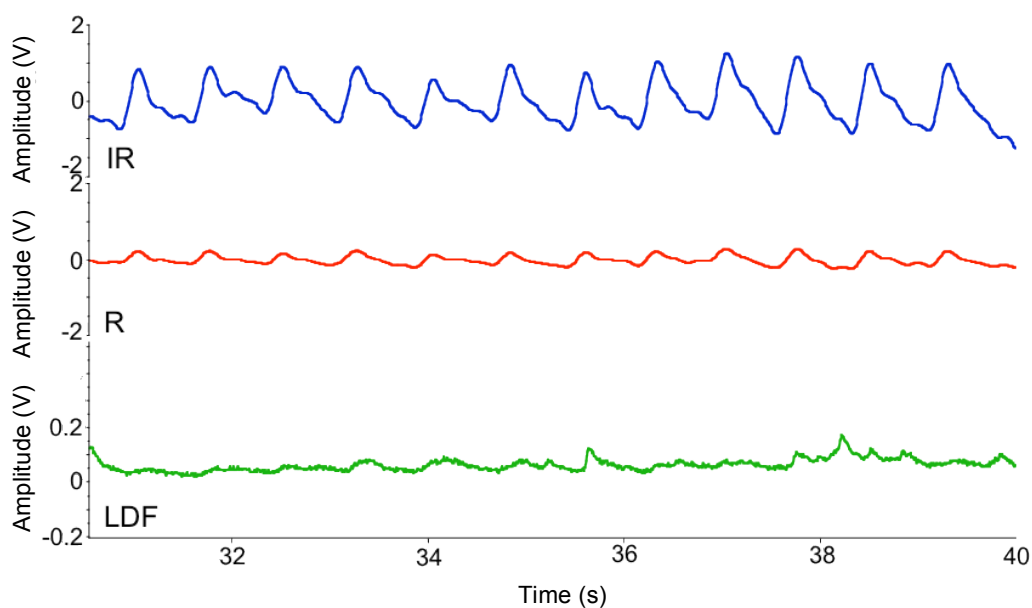


Figure 10.9: 10-second sample of typical PPG and LDF signals at pre anastomosis measurement at the proximal end (case No. 5).

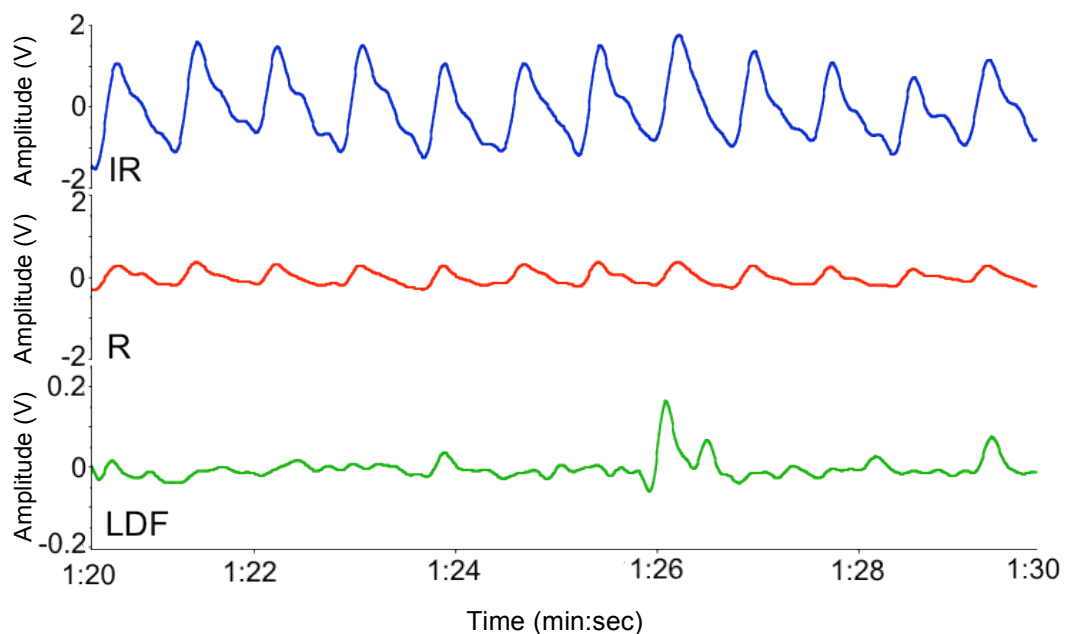


Figure 10.10: 10-second sample of typical PPG and LDF signals at pre-anastomosis measurement from the distal end (case No. 5).

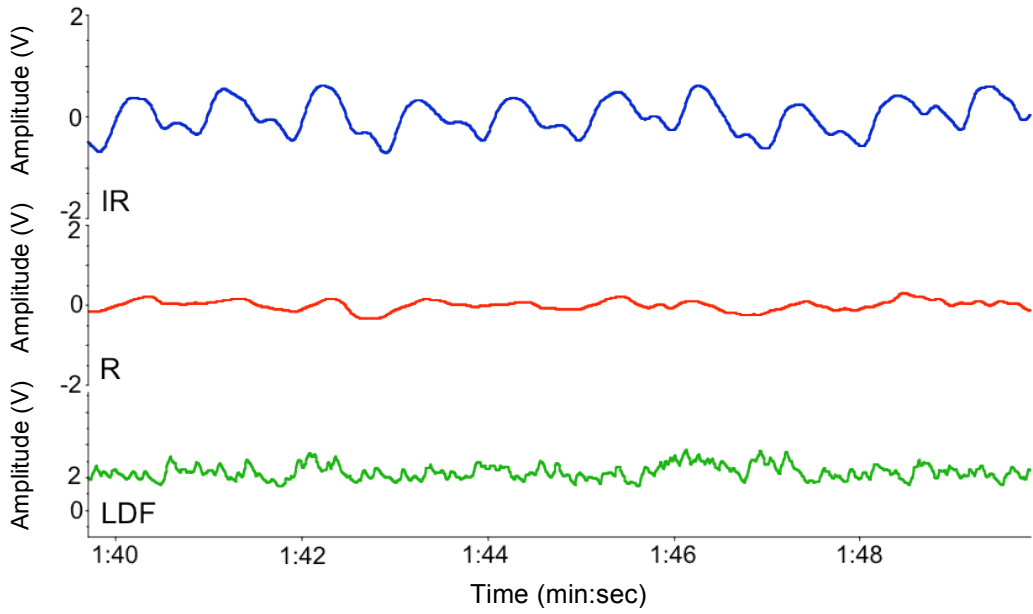


Figure 10.11: 10-second sample of typical PPG and LDF signals at post-anastomosis measurement from the proximal end (case No. 21).

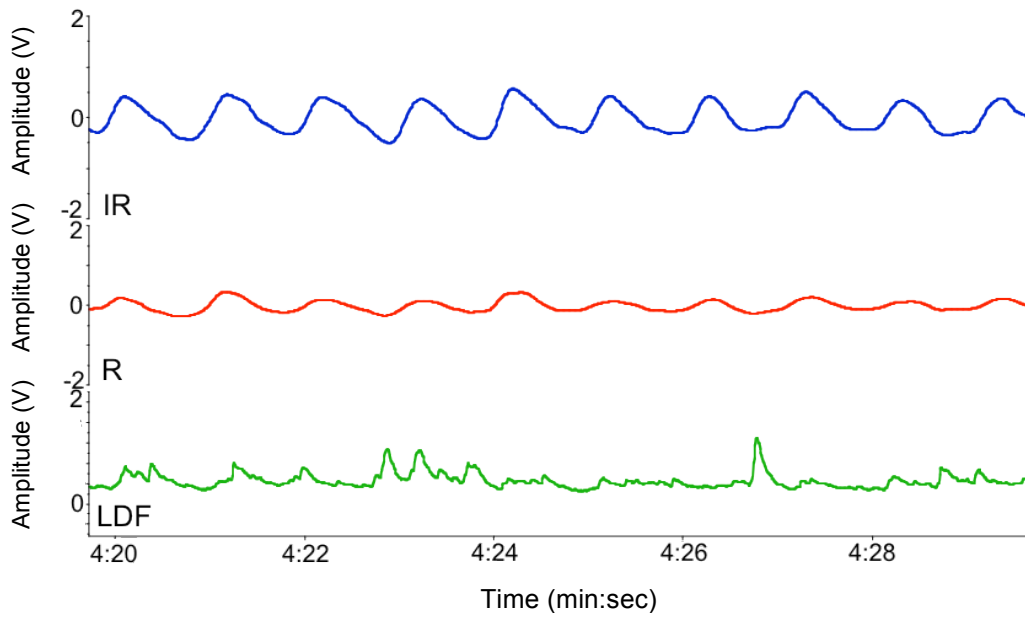


Figure 10.12: 10-second sample of typical PPG and LDF signals at post-anastomosis measurement from the distal end (case No. 21).

Table 10.5: Mean normalised PPG AC amplitudes and LDF flux from all subjects at pre and post anastomosis (proximal).

Patient	Pre-Anastomosis Proximal			Post-Anastomosis Proximal		
	AC IR normalised (mV)	AC Red normalised (mV)	LDF (PU)	AC IR normalised (mV)	AC Red normalised (mV)	LDF (PU)
1	---	---	---	---	---	---
2	247	243	---	---	---	---
3	213	268	---	---	262	---
4	705	---	---	---	---	---
5	492	640	96.5	120	162	10.3
6	238	321	147	242	320	11.1
7	---	---	---	214	646	17.1
8	461	307	162	191	175	16.4
9	226	---	26	229	---	19.4
10	351	---	24.1	154	298	5.7
11	294	---	---	289	---	45.9
12	355	---	18.7	889	---	40
13	259	---	75.9	495	---	68.3
14	193	---	68.1	482	---	24.7
15	---	---	---	390	442	24.9
16	124	171	49	129	295	139
17	---	---	---	732	575	28.6
18	156	163	23.9	---	---	11.1
19	165	---	105	---	---	92
20	---	---	---	---	---	---
21	262	610	33.9	352	360	151
22	---	---	---	---	---	---
23	---	---	---	---	---	---
24	---	---	---	---	---	---
Mean	300	333	69.1	350	325	44.1
±SD	149	174	49.3	230	189	45.7

Table 10.6: Mean normalised PPG AC amplitudes and LDF flux from all subjects at pre and post anastomosis (distal).

Patient	Pre-Anastomosis Distal			Post-Anastomosis Distal		
	AC IR normalised (mV)	AC Red normalised (mV)	LDF (PU)	AC IR normalised (mV)	AC Red normalised (mV)	LDF (PU)
1	---	---	---	---	---	---
2	---	---	---	---	---	---
3	---	---	---	---	---	---
4	----	---	---	---	---	---
5	549	655	77.5	354	355	9.22
6	---	---	---	---	---	---
7	---	---	---	287	330	22.1
8	316	224	9.45	215	172	13.4
9	---	---	---	---	---	---
10	---	---	---	---	---	---
11	---	---	---	449	---	165
12	393	---	10.1	959	---	22
13	----	---	---	---	---	---
14	---	---	89.5	---	---	---
15	146	---	---	---	---	---
16	---	---	---	---	---	---
17	---	---	---	597	391	191
18	---	---	---	126	431	14.5
19	---	---	---	---	---	---
20	---	---	---	---	---	---
21	---	996	53.5	498	427	59.8
22	---	---	---	---	---	---
23	---	---	---	405	417	97.6
24	---	---	---	---	---	---
Mean	351	583	48.0	432	361	66.1
±SD	168	389	37.2	244	91	69.8

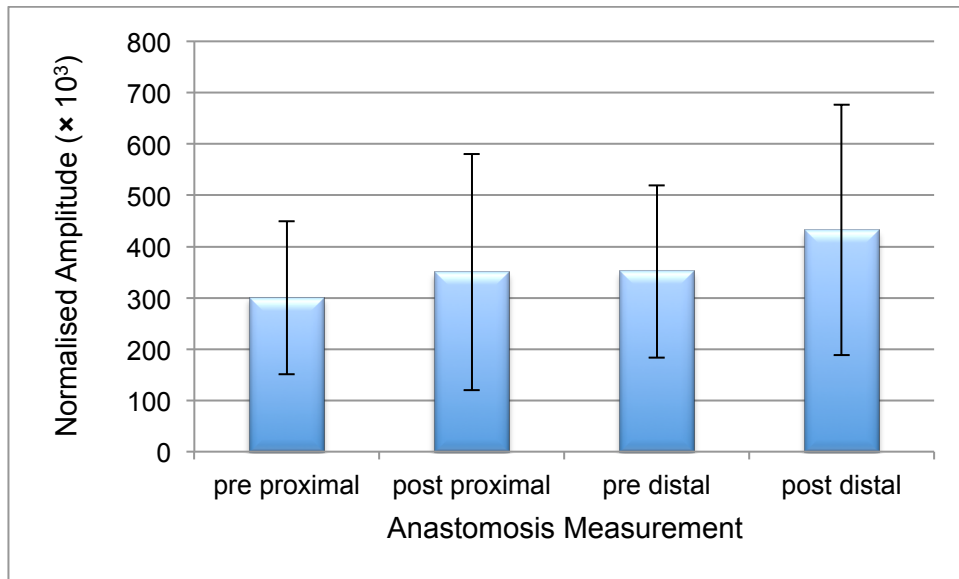


Figure 10.13: Mean (\pm SD) for normalised AC IR PPG amplitudes averaged for all patients in pre-anastomosis-proximal (n=16), pre-anastomosis-distal (n=4), post anastomosis-proximal (n=14) and post-anastomosis distal (n=9).

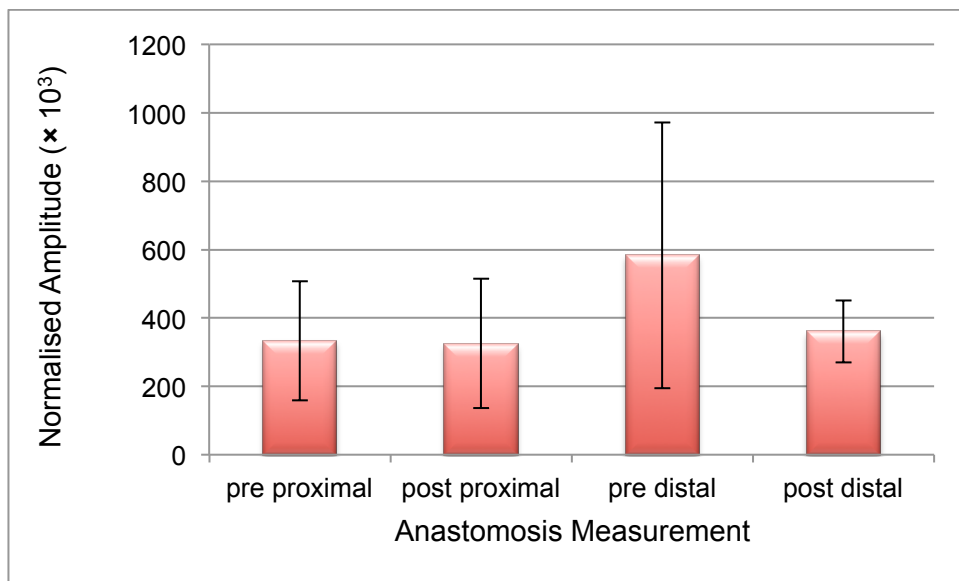


Figure 10.14: Mean (\pm SD) for normalised AC R PPG amplitudes averaged for all patients in pre anastomosis-proximal (n=10), pre-anastomosis-distal (n=3), post anastomosis-proximal (n=10) and post-anastomosis distal (n=7).

10.6 Comparison of PPG amplitude between all measurements

In order to provide an indication of how PPG amplitudes differ between different measurements in all patients, a bar graph of mean (\pm SE) for IR and R PPG amplitudes for all 24 patients are presented graphically in Figure

10.15. Figure 10.16 presents the percentage change from baseline (with measurement made during mobilisation) for normalised IR PPG amplitudes across all measurements.

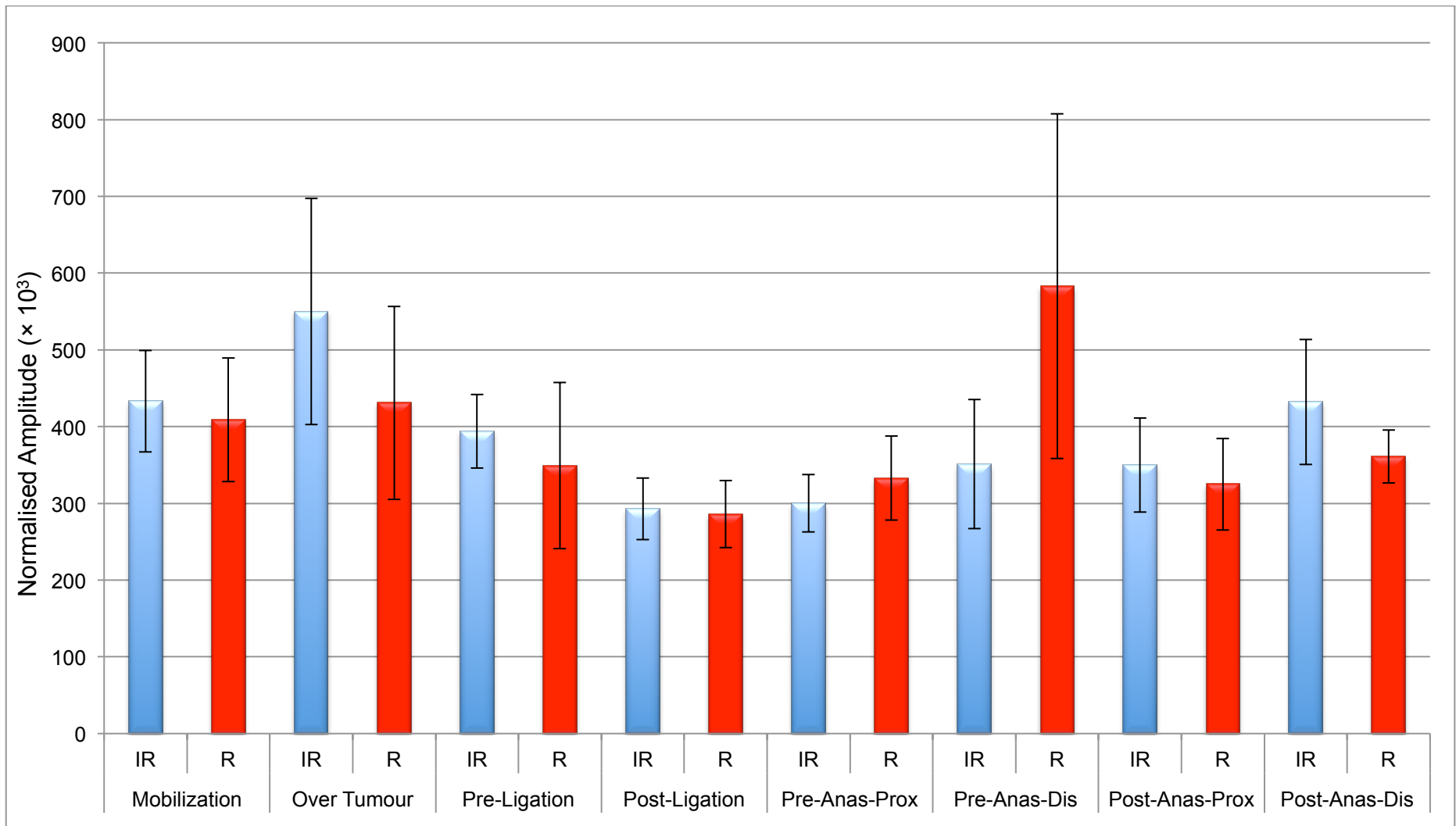


Figure 10.15: Standard error of the mean normalised R and IR across all the measurements averaged for all patients.

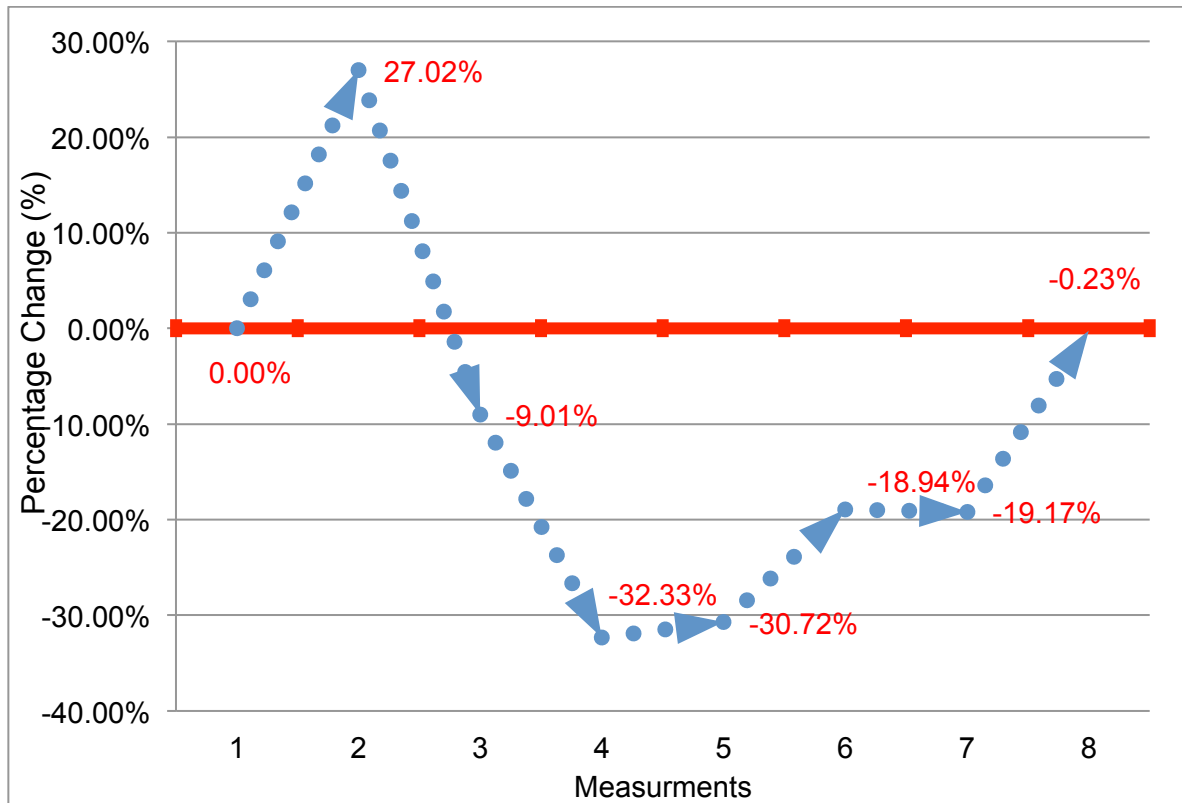


Figure 10.16: Percentage change for IR PPG amplitudes for all measurements in all patients. Reference; 1: Mobilisation, 2: Over Tumour, 3: Pre-Ligation, 4: Post-Ligation, 5: Pre-Anastomosis Proximal, 6: Pre-Anastomosis Distal, 7: Post-Anastomosis Proximal, 8: Post-Anastomosis Distal.

The percentage change in all measurements for R amplitude is presented in Figure 10.17, and in Table 10.7 the values for the percentage change between R and IR was compared.

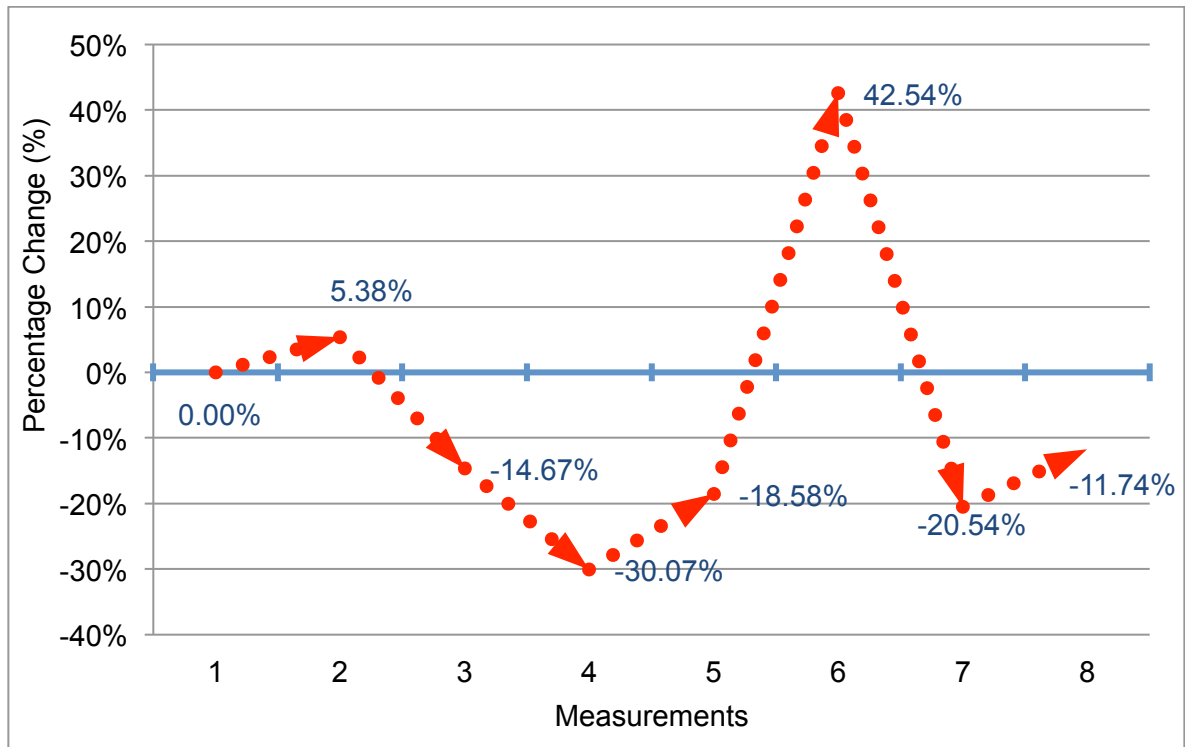


Figure 10.17: Mean R PPG amplitudes with the percentage change for all measurements in all patients. Reference; 1: Mobilisation, 2: Over Tumour, 3: Pre-Ligation, 4: Post-Ligation, 5: Pre-Anastomosis Proximal, 6: Pre Anastomosis Distal, 7: Post-Anastomosis-Proximal, 8: Post-Anastomosis Distal.

Table 10.7: The percentage change in all measurements for R and IR. Reference; 1: Mobilisation, 2: Over Tumour, 3: Pre-Ligation, 4: Post-Ligation, 5: Pre-Anastomosis Proximal, 6: Pre-Anastomosis Distal, 7: Post-Anastomosis Proximal, 8: Post-Anastomosis Distal.

Measurement	1	2	3	4	5	6	7	8	
Percentage change	IR	0	+27.0	-9.01	-32.3	-30.7	-18.9	-19.2	-0.23
	R	0	+5.38	-14.7	-30.1	-15.9	+42.5	-20.5	-11.7

Figure 10.18 illustrates the percentage change in R and IR amplitude in pre and post ligation. The reduction at post-ligation in both R and IR is apparent: the amplitude of IR fell by -25.6% and the amplitude for R PPG fell by -18.0% from pre ligation.

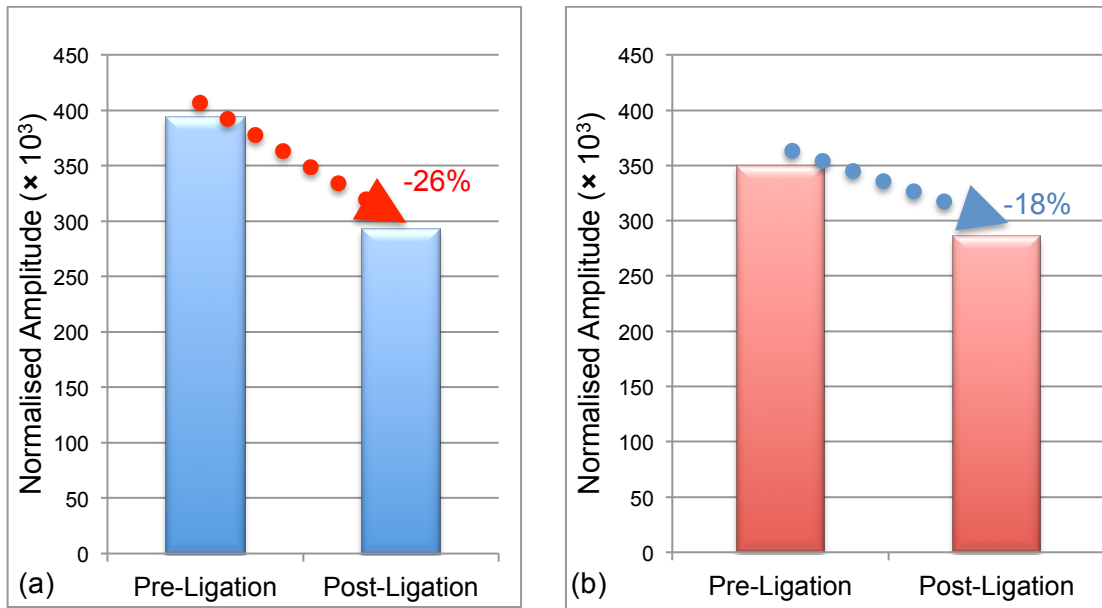


Figure 10.18: Percentage change in amplitude for (a) normalised IR and (b) normalised R PPG in pre and post ligation.

In Figure 10.19 the percentage change in amplitude for normalised IR PPG in pre and post anastomosis in both proximal and distal sites can be observed. Values at post-anastomosis from the proximal site for IR PPG increased by 17% from pre anastomosis, and by 23% for the distal site.

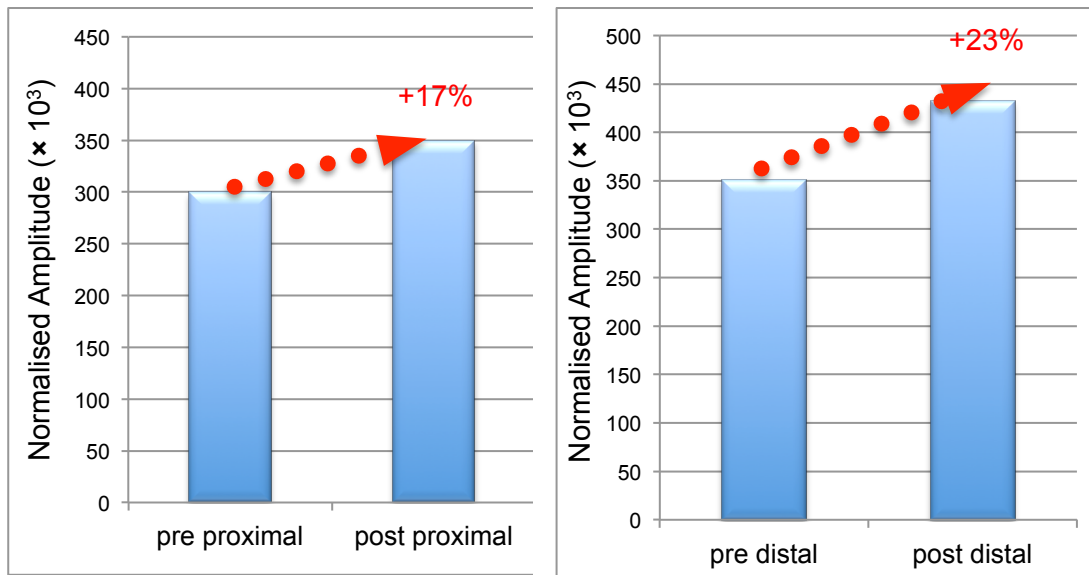


Figure 10.19: Percentage change in amplitude for normalised IR PPG in pre and post anastomosis in proximal and distal site.

At the proximal site, the amplitude of the R PPG decreased by 6% from pre to post-anastomosis as shown in Figure 10.20. At the distal site there was a decrease of 38% from pre- to post-anastomosis.

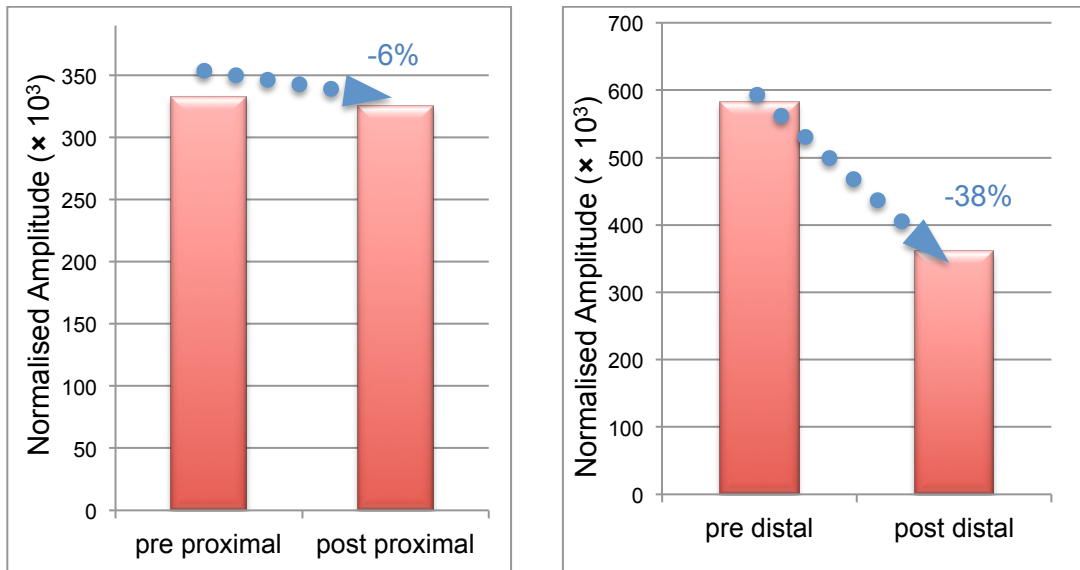


Figure 10.20: Percentage change in amplitude for normalized R PPG in pre and post anastomosis in proximal and distal site.

Figure 10.21 shows the amplitude of DC IR in all measurements, which is an indicator of blood volume, the lower value of DC IR indicates greater blood volume, due to higher absorption of light due to increased haemoglobin density (236). As can be seen, the lowest DC IR value is observed for the over tumour measurements, which also shows the largest PPG amplitude (Figure 10.15).

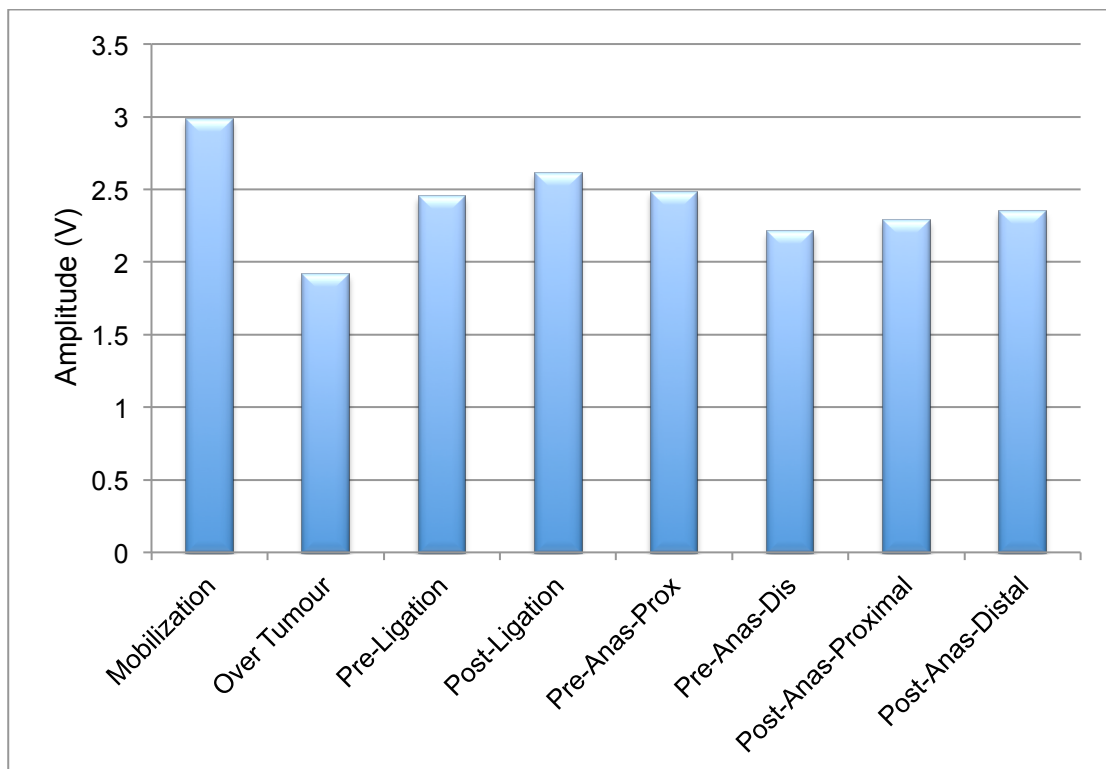


Figure 10.21: Amplitude of DC IR in all measurements showing the blood volume.

10.7 Comparison of LDF Flux between all measurements

The laser Doppler signal was more sensitive to artefact than PPG, as several spikes were observed across most of the measurements, an example of that can be seen in Figure 10.22. These are most likely due to motion of the probe relative to the tissue.

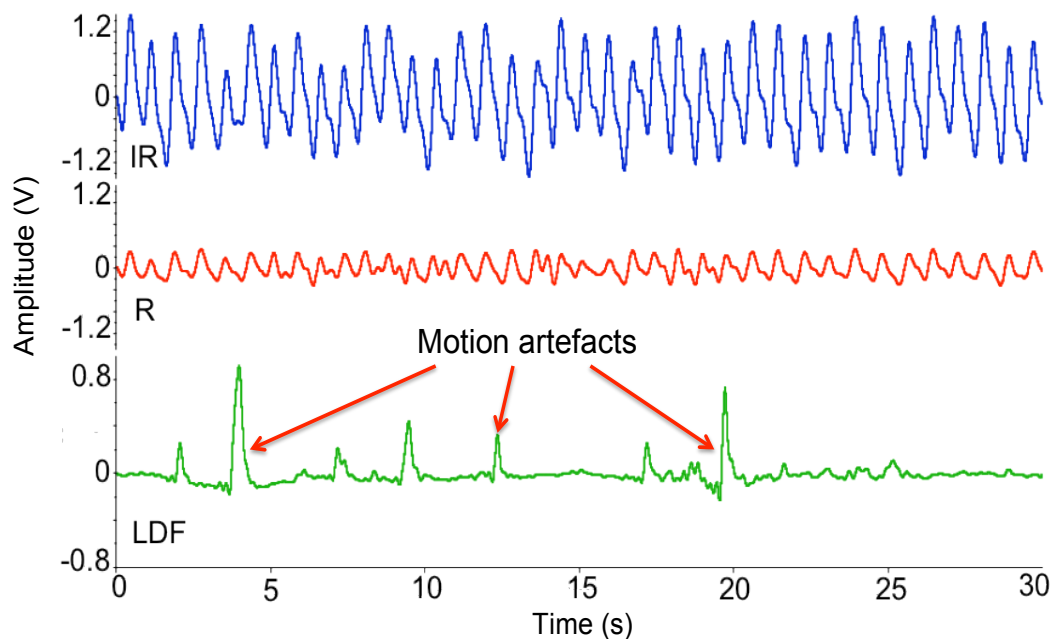


Figure 10.22: Detected signals, showing that LDF was more sensitive to motion artefacts than PPG.

The mean (\pm SD) LDF flux was obtained and in order to show how the values change between measurements, a bar graph is illustrated in Figure 10.23.

As can be seen in Figure 10.23 at mobilisation, the mean flux has the lowest value (31.6 PU) of all the measurements. Also the flux at pre-ligation (80.4 PU) decreases at post-ligation (71.2 PU). Figure 10.23 also shows that the LDF flux before and after the anastomosis for both proximal and distal ends changed. As Figure 10.23 shows, an increase from pre-anastomosis to post-anastomosis in the flux at the distal end (48.0 PU to 66.1 PU) is observed. In contrast, the flux values are reduced at the proximal site from 69.1 PU to 44.1 PU after anastomosis.

The percentage change from baseline in all measurements for LDF flux is presented in Figure 10.24.

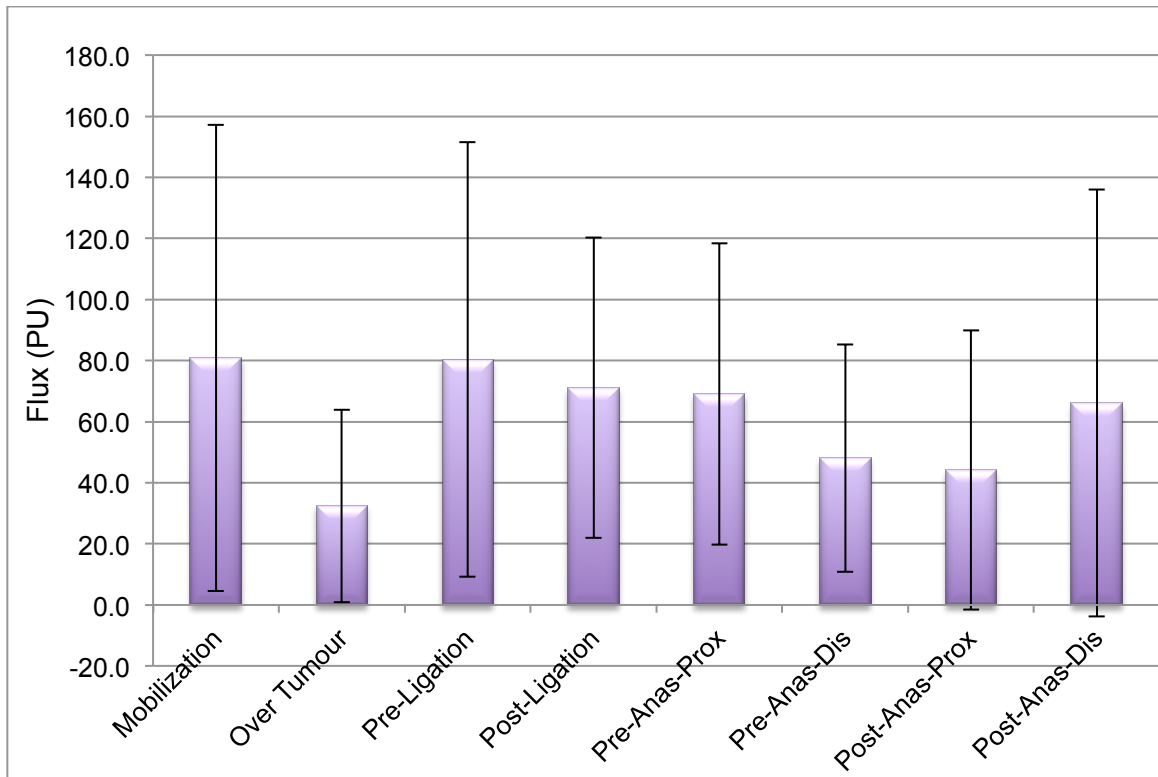


Figure 10.23: Mean (\pm SD) LDF flux for all measurements averaged for all patients.

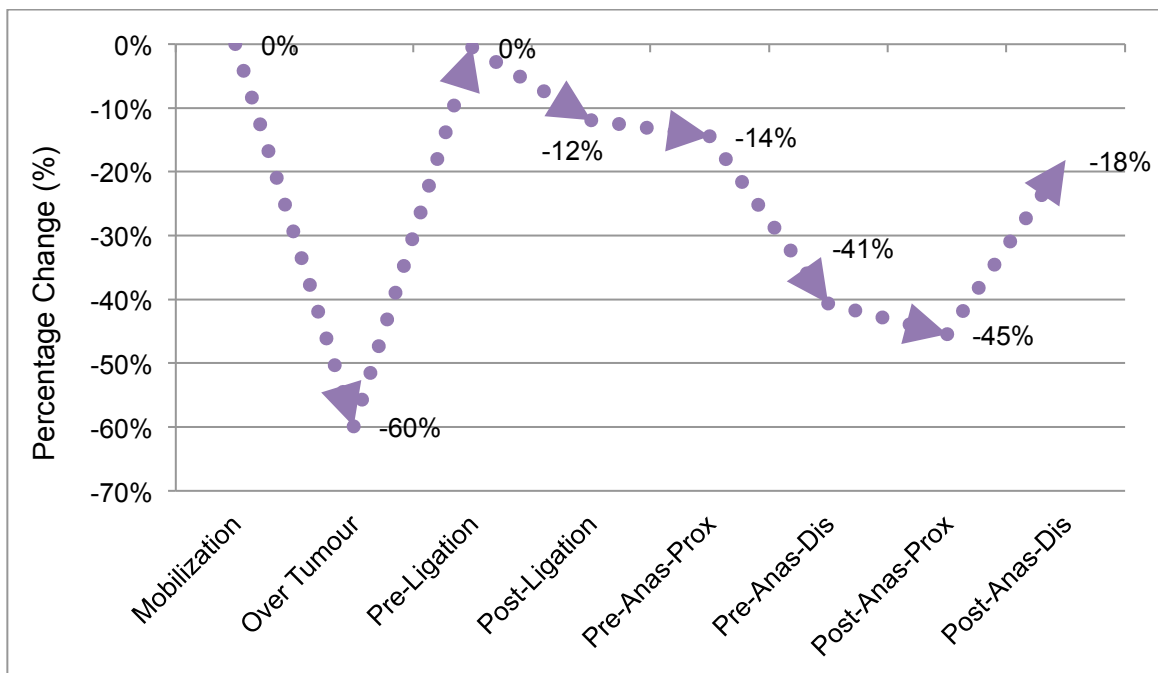


Figure 10.24: Percentages change in PU across all the measurements.

10.8 Arterial Blood Oxygen Saturation (SpO₂) Estimations

As explained in Chapter 8, using AC and DC components for both red and infrared PPG signals, blood arterial oxygen saturation can be estimated from the various periods of measurements, which can be an indicator of the system's ability to estimate arterial blood oxygen saturation. Preliminary estimated SpO₂ values were estimated for each measurement and the results are presented in the Table 10.8.

Table 10.8: The estimated SpO₂ values in all measurements. Reference; 1: Mobilisation, 2: Over Tumour, 3: Pre Ligation, 4: Post Ligation, 5: Pre Anastomosis Proximal, 6: Pre Anastomosis Distal, 7: Post Anastomosis Proximal, 8: Post Anastomosis Distal.

Patient No.	Measurement							
	1	2	3	4	5	6	7	8
1	---	---	---	---	---	---	---	---
2	---	---	---	95.1	---	---	---	---
3	53.4	82.9	39.1	78.5	78.5	---	---	---
4	98.2	---	---	---	100	---	---	---
5	---	---	---	---	77.4	85.9	76.5	84.9
6	80.9	---	91.5	66.2	76.3	---	106	---
7	89.7	81.7	89.7	---	---	---	34.5	81.2
8	---	---	---	---	93.4	92.3	87.1	90.1
9	---	---	---	---	---	---	---	---
10	---	---	---	87.5	---	---	61.5	---
11	---	---	---	---	---	---	---	---
12	---	---	---	---	---	---	---	---
13	---	---	---	---	---	---	---	---
14	---	---	---	---	---	---	---	---
15	85.2	---	87.1	90.4	---	---	81.6	---
16	88.7	---	---	75.5	75.5	---	52.8	---
17	---	82.8	---	---	---	---	90.3	93.6
18	---	---	91.1	88.2	83.8	---	---	24.4
19	---	---	---	---	---	---	---	---
20	81.8	---	---	80.1	---	---	---	---
21	80.8	---	---	81.4	51.7	---	84.4	88.6
22	69.7	---	---	78.4	---	---	---	---
23	73.9	---	89.6	89.1	---	---	---	84.2
24	---	---	---	---	---	---	---	---
Mean	80.2	82.5	81.3	82.8	79.6	89.1	75.0	78.2
±SD	12.4	0.69	20.7	8.2	14.4	4.52	19.4	24.0

In order to provide an indication of how SpO₂ values change between different measurements in all patients, the mean (±SD) SpO₂ values is presented in a bar

graph in Figure 10.25. As mentioned before, the commercial SpO₂ values obtained from the finger were recorded manually immediately after each measurement in all the trials. The mean SpO₂ was calculated and the results are shown in Figure 10.25 along with SpO₂ values obtained from the bowel.

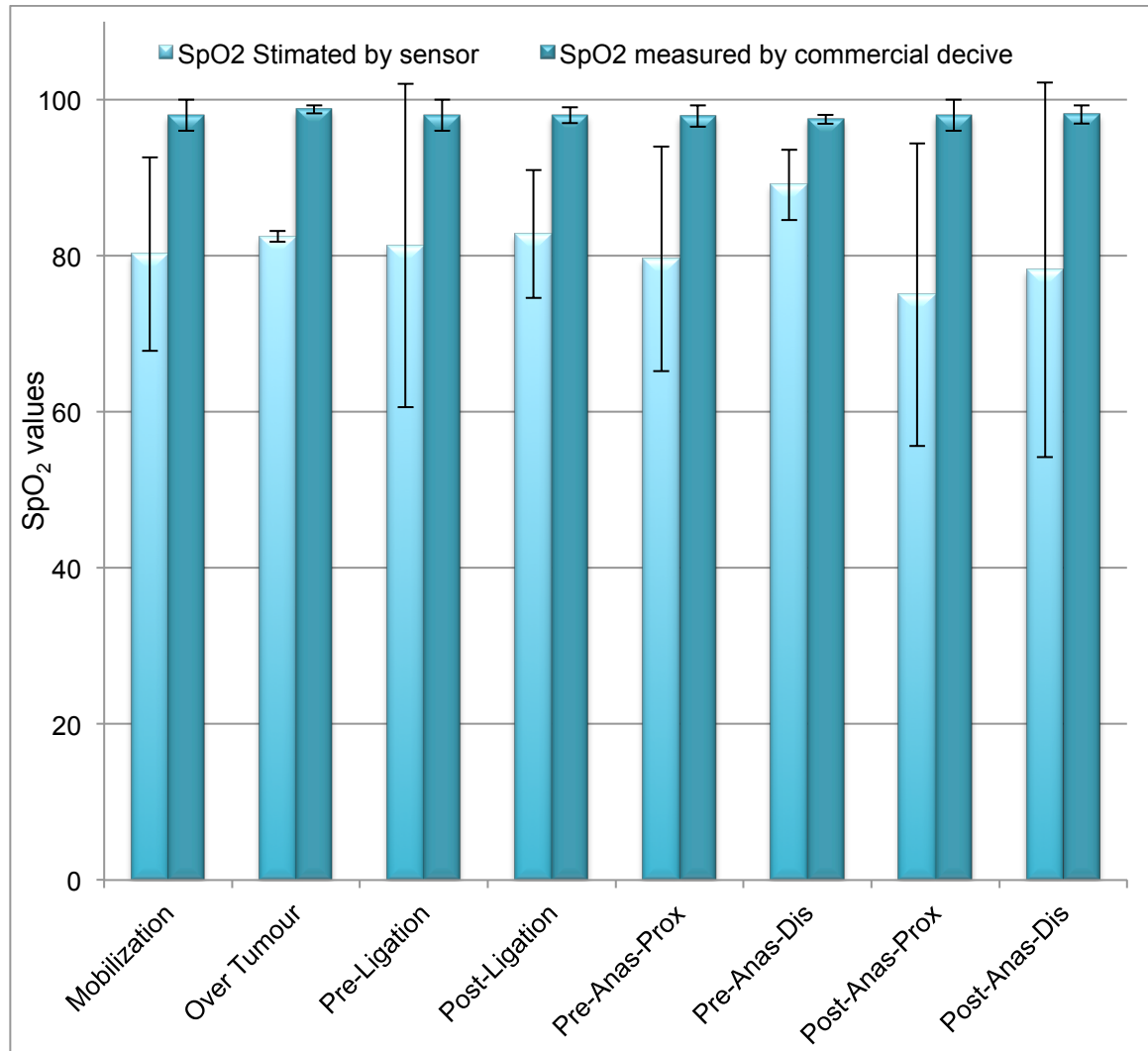


Figure 10.25: Mean (\pm SD) SpO₂ estimated values by sensor from bowel compared to the values measured with the commercial device, from the finger for all measurements averaged for all patients.

10.9 Statistical Analysis

Statistical analysis was performed on the results from the measurements. A two-tailed paired t-test was performed to test whether or not there is a significant difference between PPG amplitudes and LDF flux in different measurements ($P < 0.05$ was considered as the limit at which there is a statistically significant difference between measurements). The results are presented in Tables 10.9 to

10.16, however these results did not reveal any statistically significant difference between different measurements although a marked change in the amplitudes of PPGs was observed in some measurements (e.g. between pre and post ligation) (Figure 10.18). The reason for the lack of significance is probably because of inadequate data since the study group was too small for any statistically significant differences to be detected.

Table 10.9: Paired t-test between pre and post ligation for AC R and IR amplitudes.

Paired t-test	Pre ligation R	Post ligation R	Pre ligation IR	Post ligation IR
Pre ligation R		0.397		
Post ligation R	0.397			
Pre ligation IR				0.172
Post ligation IR			0.172	

Table 10.10: Paired t-test between pre and post anastomosis in proximal and distal for AC IR amplitudes.

Paired t-test	Pre anastomosis proximal	Post anastomosis proximal	Pre anastomosis distal	Post anastomosis distal
Pre anastomosis proximal		0.720	0.636	0.473
Post anastomosis proximal	0.720		0.764	0.117
Pre anastomosis distal	0.636	0.764		0.743
Post anastomosis distal	0.473	0.117	0.743	

Table 10.11: Paired t-test between pre and post anastomosis in proximal and distal for AC R amplitudes.

Paired t-test	Pre anastomosis proximal	Post anastomosis proximal	Pre anastomosis distal	Post anastomosis distal
Pre anastomosis proximal		0.107	0.730	0.540
Post anastomosis proximal	0.107		0.175	0.621
Pre anastomosis distal	0.730	0.175		0.323
Post anastomosis distal	0.540	0.621	0.232	

Table 10.12: Paired t-test between pre and post ligation for DC R and IR amplitudes.

Paired t-test	Pre ligation R	Post ligation R	Pre ligation IR	Post ligation IR
Pre ligation R		0.524		
Post ligation R	0.524			
Pre ligation IR				0.576
Post ligation IR			0.576	

Table 10.13: Paired t-test between pre and post anastomosis in proximal and distal for DC IR amplitudes.

Paired t-test	Pre anastomosis proximal	Post anastomosis proximal	Pre anastomosis distal	Post anastomosis distal
Pre anastomosis proximal		0.904	0.183	0.890
Post anastomosis proximal	0.904		0.072	0.914
Pre anastomosis distal	0.183	0.072		0.224
Post anastomosis distal	0.890	0.914	0.224	

Table 10.14: Paired t-test between pre and post anastomosis in proximal and distal for DC R amplitudes.

Paired t-test	Pre anastomosis proximal	Post anastomosis proximal	Pre anastomosis distal	Post anastomosis distal
Pre anastomosis proximal		0.299	0.414	0.442
Post anastomosis proximal	0.299		0.516	0.503
Pre anastomosis distal	0.414	0.516		0.402
Post anastomosis distal	0.442	0.503	0.402	

Table 10.15: Paired t-test between pre and post ligation for LDF flux.

Paired t-test	Post ligation
Pre ligation	0.171

Table 1.16: Paired t-test between pre and post anastomosis in proximal and distal for LDF flux.

Paired t-test	Pre anastomosis proximal	Post anastomosis proximal	Pre anastomosis distal	Post anastomosis distal
Pre anastomosis proximal		0.146	0.379	0.187
Post anastomosis proximal	0.146		0.409	0.207
Pre anastomosis distal	0.379	0.409		0.564
Post anastomosis distal	0.187	0.207	0.564	

The discussion, conclusion and future work will be discussed in the next chapter.

Discussion, Conclusions and Future Work

11.1 Discussion and Conclusions

The aim of this research was to assess bowel viability using photoplethysmography (PPG) and laser Doppler flowmetry (LDF) in patients undergoing bowel resection utilising custom-made combined sensors and instrumentation. Reflectance mode PPG along with LDF sensors have been successfully designed, constructed and tested for thermal safety (Chapter 7) and placement on the bowel tissues allowing monitoring of perfusion in the tissue. In order to verify the suitability of the probe for use in a clinical environment, volunteer studies were performed in which clear PPGs and LDF signals were obtained from the fingers (Section 7.5).

Clinical trials were performed at the Royal London Hospital, London, UK for patients undergoing bowel resection to monitor changes in PPG amplitude and LDF flux during surgery. Eight stages of surgery including; mobilisation, over tumour, pre and post ligation, pre and post anastomosis for both proximal and distal ends, were investigated during each trial (unless measurements were not technically possible or were not performed by the surgical team for any reason). For each measurement, PPG and LDF signals were acquired simultaneously for approximately one minute. It was shown that clear PPG and LDF signals could be obtained in most cases.

The total number of measurements in all investigated sites was 100 (15 mobilisation, 7 over tumour, 11 pre-ligation, 16 post-ligation, 16 pre-anastomosis proximal, 7 pre-anastomosis distal, 18 post anastomosis proximal and 10 post anastomosis distal investigations). Data analysis was conducted on all acquired signals to examine the difference in AC and DC PPG amplitude and also LDF flux between different signals acquired from different measurements. Blood arterial oxygen saturation (SpO_2) was calculated from the AC and DC components of the

PPG signal for both red and infrared for all measurements and compared to the values obtained from a commercial device.

The results from the data analysis were presented in the previous chapter. Figures 10.8, 10.13 and 10.14 show that there were large standard deviation values across all the measurements, due to a large variability in PPG amplitudes for all patients. The reason for this variability was possibly due to differences in the density of blood vessels beneath the probe from one patient to another. This variability highlights the need to take baseline measurements from which subsequent measurements may be compared. Although special care was taken to try to place the probe in the same position for each measurement, this was often difficult in the conditions of the operating theatre. Furthermore, differences in surgical procedures also prevented subsequent measurements from the same location.

As can be seen in Figure 10.15, the PPG amplitude (R and IR) from the over tumour measurement had the highest normalised amplitude (550 mV for IR and 431 mV for R) of all the measurements. This was possibly due to a higher concentration of blood vessels in tumour tissue compared to healthy tissue. Since cancer cells have a high oxygen requirement (as their metabolic rate is high), large tumors generate their own vasculature, a process known as angiogenesis (237). These blood vessels differ from normal blood vessels, in fact, they are highly irregular, chaotic, and leaky leading to uneven delivery of oxygen (238). This could explain the non-typical shape of the PPG waveforms, an example is shown in Figure 10.5. Also there was a large standard deviation for IR (± 361 mV) compared to other measurements (Tables 10.2–10.6), possibly also due to the different vascular structure within the tumour.

Furthermore, it is obvious from Figure 10.15 that there was a considerable difference in IR AC amplitude between pre-ligation (394 mV) and post-ligation (293 mV). After ligation a noticeable reduction in amplitude was observed, and a similar decrease was seen in the R AC signal (349 mV and 286 mV). This was expected due to the reduction in blood supply in the area as a result of vascular ligation.

Figure 10.15 shows that the PPG amplitude before and after the anastomosis for both proximal and distal ends had changed. An increase in amplitude (300 mV to 350 mV for IR in proximal end and 351 mV to 432 mV for IR in distal end) was observed after anastomosis. This increase in amplitude after anastomosis was expected as the blood vessels had been rejoined and the blood volume most likely increased in this area. The increase of amplitude could thus be an indication of improved blood volume to the area after anastomosis.

The equivalent increase was not seen in R PPG amplitude at both proximal and distal sites after anastomosis, as seen in Figure 10.20, probably due to insufficient sample size (measurements for pre anastomosis at distal site totaled only three).

The percentage change in amplitude for IR PPG from baseline in mobilisation at both pre and post anastomosis seen in Figure 10.16 was greater at the proximal compared to the distal sites. This was expected since the removal of a tissue segment can impair the local blood flow at the edge of the anastomoses (proximal end). Less effect was seen on the distal ends.

Also as it can be seen in Figures 10.15, the amplitude of IR PPG in post-anastomosis (432 mV) was similar to the amplitude of mobilisation (433 mV) suggesting that the blood volume after post-anastomosis (last step of the procedure) was recording the same value as that during mobilisation (first step of the procedure), this result suggests that this sensor has the capability to show changes in blood perfusion in the tissue intraoperatively.

By observing Figure 10.23 which shows a bar graph of mean flux for all the measurements, it can be seen that the flux at post-ligation decreased from pre-ligation by 11%, which was expected due to the reduction in blood flow in the area as a result of vascular ligation. However this decrease in flux after ligation, seen in Table 10.15, is not significant ($P=0.171$), possibly due to the high sensitivity of LDF to motion. As can be seen in Figure 10.23 an increase of 38.0% in flux at the distal end after anastomosis was observed. This could be an indication of improved blood flow to the area after anastomosis. The equivalent

increase was not seen however at the proximal site. In fact after anastomosis the flux reduced by 36.0%, possibly due to the removal of tissue segments which may have impaired the local blood flow at the edge of the anastomoses (proximal end). The changes in flux measured by LDF during each surgical stage did not follow the pattern of the changes seen in PPG amplitude, and were more difficult to interpret in terms of expected physiological changes. This is possibly due to the high sensitivity to movement of the LDF. As mentioned in Section 10.7, the LDF signals showed significant artefact that was attributed to movement (see Figure 10.22) and explains the large standard deviations observed in the LDF measurements (Figure 10.23). Although PPG is also sensitive to movement, such artefacts were not seen on the simultaneously recorded PPG signals.

By comparing the differences between the commercial and estimated SpO₂ values presented in Figure 10.25, it can be seen that across all the measurements, the mean of SpO₂ values obtained with the custom combined probe from the bowel area underestimated the arterial blood oxygen saturation compared to the commercial SpO₂ values from the finger. The values were found to be lower than those obtained simultaneously from the commercial device: between 13.4% lower in pre anastomosis distal and 31.1% lower in post anastomosis distal. Also the obtained standard deviations between measurements appeared to be large (Figure 10.25). These differences may be due to a number of reasons: firstly the algorithm used for calculating oxygen saturation was based on one derived from measurements using a finger probe in volunteer subjects and was intended for calibrating commercial finger probes. The composition of bowel tissue differs from finger tissue in terms of the relative abundance of different absorptions as well as the density of blood vessels, and the geometry of the reflectance probe differs from commercial finger probes.

Statistical analysis showed that there was no significant difference between pre and post ligation for IR ($P = 0.172$) and pre and post ligation for R ($P = 0.397$). The results for all other measurements are presented in Tables 10.9 to 10.17. As can be seen these results did not reveal any statistically significant difference between different measurements. Although an evident change in the amplitudes of PPGs was observed in some measurements (e.g. between pre and post

ligation) (Figure 10.18).

In conclusion, the results from this preliminary *in vivo* investigation demonstrated, that a combined PPG and LDF system is capable of acquiring clear PPG and LDF signals from the surface of the bowel intraoperatively in laparoscopy or laparotomy in bowel resection operations in most cases.

The results have confirmed that the custom made PPG/LDF system and sensor might has the potential to be used as an alternative technique for monitoring perfusion in various stages of the bowel operation, and may provide a useful tool for surgeons during the bowel resection.

The results form the *in vivo* investigation has indicated that there is a difference between PPG and LDF signals acquired from different stages. Obtaining the same amplitude at the last step of operation (post anastomosis), as the value of the first step of the operation (mobilisation) suggests that the probe can assist the surgeon's decision making in critical anastomosis. This could lead to a reduction in anastomotic leak thus having an important impact on the clinical outcome in bowel resection.

11.2 Future Work

This pilot study aimed to evaluate the feasibility of the proposed probe and system to acquire LDF and PPG signals simultaneously. The signals were interpreted to see if there was any correlation between changes from baseline in the results from the eight measurements in each patient and predictions made for each of them by the surgeon.

Subject to funding availability, the next stage (*'Initial study'*) will be to evaluate if the probe and system can detect any compromise in blood supply and therefore possibly predict anastomotic leak. As mentioned in Section 6.1 the most important surgical complications following bowel resection with anastomosis are anastomotic leaks. Major consequences of the anastomotic leakage are postoperative morbidity and mortality (239). Therefore detecting the anastomotic

leak intraoperatively has a significant impact on improving the outcome of operations. The initial study aims to achieve further meaningful information from the signals in order to identify the possible relation between the acquired signals and the results of the operation (anastomotic healing/failing). The influence of anaesthetic and analgesic drugs (including those epidurally administered) will also be considered to see how these factors might cause intestinal hyperaemia or hypoperfusion.

The '*Follow-up Study*' will be considered after the initial study. Once enough information from the initial study has been obtained, the probe will be used to detect possible complications and leakages in specific diseases.

The last stage is the '*Final Study*', which will focus on bowel ischaemia and to utilise the probe to detect early diagnosis of ischaemia in the small or large intestine.

Each part of the proposed future study will be explained in the following sections.

A: Initial Study

1. Longitudinal Study: the next clinical study will be initially a longitudinal study, which will include taking measurements from a number of patients (approximately 50), then following the patients' progress post operatively. It would explore long term data to see how many patients had complications and whether this was predicted by the probe. This exploration could draw conclusions as to the correlation between anastomotic healing or anastomotic failing and the results from the probe measurements.

2. Temperature sensing: knowledge of temperature differences between a tumour and the surrounding area may be valuable. It has been suggested that tumours have a different temperature in comparison to their surrounding area. It is proposed that tumours tend to be higher in temperature, possibly because of the need for more blood supply to them and also the fact that tumours continuously reproduce. Such a process continuously draws and releases energy

leading to an increase in local temperature (240). Therefore, designing a sensor with the ability to measure temperature may be of some value towards a better understanding of the tumour and possible diagnose of its existence.

3. A Larger Pool of Candidates: more laparotomy cases would be needed to obtain the correlation between laparoscopy and open surgery (laparotomy) (in this pilot study there were only 4 laparotomy cases).

4. More Data Regarding LDF Signals: since the LDF was found to be very sensitive to artefact in the first study, future work is needed to confirm whether the system could improve post-operative patient outcome.

5. A New Design for the Probe: providing a measurement tool that is impervious to motion artefacts would be an advantage. It has been suggested by the surgical team that if the probe could be inserted in a hard thin tube, that the fiberoptic LDF cable would not be subject to bending and therefore this might result in a greater reduction in motion artefacts.

B: Follow-up Study

1. Colon Interposition for Oesophageal Replacement and Gastric Pull-up: this is where the colon or gastric is used as an oesophageal substitute in patients with malignant oesophageal disease. The outcome of this operation depends strongly on the maintenance of adequate perfusion between the colon and the oesophagus. Currently there is no easy to use device available to show the viability of the tissue at the edge of the anastomosis. Using the combined probe could be of great value and help to reduce possible complications and leakages.

2. Colon Pull-through: in patients undergoing tumour resection of the rectum, the large intestine often needs to be replaced and reattached to the pelvis and anastomosis with the distal end of the rectum or anal canal has to be performed. The most common cause of the anastomotic failure is ischaemia at the edge of anastomosis. Using the combined probe for monitoring the viability of the tissue at the edges of anastomosis may help to reduce possible complications and

anastomosis leakages.

C: Final Study

Bowel Ischaemia: Surgery to remove sections of ischaemic bowel is a necessary and life-saving operation. Monitoring of the circulation intraoperatively is a very important issue especially at early diagnosis and the start of the treatment. The probe can monitor the process and give a prediction of the blood perfusion in the area possibly leading to an early diagnosis of the ischaemic tissue.

Other future work

Other alternative future work could be planned in the following areas: intraluminal measurements, Crohn's Disease, perineal blood supply and measuring the stiffness of the tumour and the surrounding tissues, pre and post treatment. These pathologies have specific and involved treatments, and monitoring is not fully developed, so further research is needed to improve diagnosis, guide therapy and improve prognosis.

REFERENCES

- 1 Karliczek A., Benaron D. A., Baas P. C., Zeebregts C. J., Wiggers T., Van Dam G. M., (2010) *Intraoperative assessment of microperfusion with visible light spectroscopy for prediction of anastomotic leakage in colorectal anastomoses*. *Colorectal Dis*, 12(10): 1018-25.
- 2 Servais E. L., Rizk N. P., Oliveira L., Rusch V. W., Adusumilli P. S., (2011) *Real-time intraoperative detection of tissue hypoxia in gastrointestinal surgery by wireless pulse oximetry*. *Surg Endosc*. 25(5): 1383-9.
- 3 XRayCeRT, (2014) *Understanding Ionizing Radiation and Protection*. Page 79.
- 4 <http://www.uahealth.com/library/sections/article/stomach-cancer-0>.
- 5 McGuire M., Beerma K., (2012) *NUTR*. Chapter 5.
- 6 Marx J. A., Hockberger R. S., et al., (2010) *Rosen Emergency Medicine*. 7th Edition, Section 5, Chapter 88. Pages 1137-1153.
- 7 O’Rahilly R., Muller F., Carpenter S., Swenson R., (2008) *Basic Human Anatomy, a regional study of human structure*. Chapter 26.
- 8 Redwine D., (2004) *100 Questions & Answers About Endometriosis*. 1st Edition, Chapter 1.
- 9 Brunicaudi C., Andersen D. K., Timothy R., (2009) *Schwartz’s Principles of Surgery, Small intestine*. 9th Edition, Chapter 28, Pages 979-1013.
- 10 <http://www.webmd.com/digestive-disorders/picture-of-the-abdomen>
- 11 Raja S. G., (2010) *MRCS Part A: Paper 1 SBAs in Applied Basic Science*. PasTest Ltd, Page 176.
- 12 <http://www.britannica.com/bps/media-view/68634/1/0/0>
- 13 Tortora G. J., Evans R. L., Anagnostakos N. P., (1987) *Principles of Human Physiology*. Harper & Row Limited, Chapter 24, Page 608.
- 14 Messmann H., (2011) *Atlas of Colonoscopy: Examination Techniques and Diagnosis*. Page 46.
- 15 <http://www.medicalartstudio.com>.
- 16 http://www.daviddarling.info/encyclopedia/S/small_intestine.html.
- 17 <http://www.stockmedicalart.com/stockimages/detail/655-Colon-anatomy.html>.
- 18 Ashalatha P. R., Deep G., (2012) *Textbook of Anatomy and Physiology for Nurses*. Chapter 13, Page 213.

- 19 Ferguson M. K., (2011) *Difficult Decisions in Thoracic Surgery: An Evidence-Based Approach*. Chapter 33.
- 20 http://www.hopkinscoloncancercenter.org/CMS/CMS_Page.aspx?CurrentUDV=59&CMS_Page_ID=1F7C07D4
- 21 Fleshman J. W., Wolff B. G., (2007) *The Ascrs Textbook of Colon And Rectal Surgery*. American Society of Colon and Rectal Surgeon, Chapter 2, Page 23.
- 22 Shaw A., Smith B., Howlett D. C., (2011) *FRCR Part 1 Anatomy Mock Examinations*. Cambridge University Press, Pages 227-228.
- 23 Kim K. H., Korean J., (2011) *Clinical Characteristics of Ischemic Colitis According to the Localization*. Soc Coloproctol, 27(6): Pages 275-275.
- 24 Meyers M. A., (1976) *Griffiths' point: critical anastomosis at the splenic flexure. Significance in ischemia of the colon*. AJR Am J Roentgenol, 126 (1), Pages 77-94.
- 25 Van Tonder J. J., Boon J. M., Becker J. H., Van Schoor A. N., (2007) *Anatomical considerations on Sudeck's critical point and its relevance to colorectal surgery*. Clin Anat. 20(4), Pages 424-7.
- 26 Longo D. L., Fauci A. S., Kasper D. L., Hauser S. L., Jameson J. L., Loscalzo J., Harrison's *Principle of Internal Medicine*. 18th Edition, Page 140.
- 27 Snell R. S., M.D., PhD, (2000) *Clinical Anatomy for medical students*. Forth edition, Chapter 5, Pages 240-246.
- 28 Rubin G. D., Rofsk N. M., (2008) *CT and MR Angiography: Comprehensive Vascular Assessment*. Chapter 19.
- 29 Tortora, G. and Grabowski, S., (2003) *Principles Of Anatomy And Physiology*. 10th ed.
- 30 McMurrich J.P., Sobotta J., (1906) *Atlas and Textbook of Human Anatomy*. Pages 50-55.
- 31 Goldie R., (1994) *Immunopharmacology of Epithelial Barriers*. Elsevier, Page 48.
- 32 Fry R. D., Mahmoud N., Maron D. J., Bleier J. I. S., (2012) *Colon and rectum*. In: *Townsend CM, Sabiston Textbook of Surgery*. 19th ed. Philadelphia, PA: Elsevier Saunders, Chap 52.
- 33 Dozois E. J., (2004) *Clinics in Colon and Rectal Surgery: Proctocolectomy and Brooke Ileostomy for Chronic Ulcerative Colitis*. 17(1): 65–70.
- 34 Tayeb M., Mohammad Khan F., Rauf F., and Mumtaz Khan M., (2011) *Phytobezoar in a jejunal diverticulum as a cause of small bowel obstruction: a case report*. J Med Case Reports, 5: 482

- 35 Evans M. D., Escofet X., Karandikar S. S., and Stamatakis J. D., (2009) *Outcomes of resection and non-resection strategies in management of patients with advanced colorectal cancer*. *World J Surg Oncol*, 7: 28
- 36 Brae G. R., (2011) *Essentials of Emergency Medicine*. Gastrointestinal disorders, 6th edition, Chapter 26.
- 37 <http://www.webmd.com/digestive-disorders/bowel-obstructions>
- 38 Soriano A., Davis M. P., (2011) *Malignant bowel obstruction: Individualized treatment near the end of life*. *Cleveland Clinic Journal of Medicine*, vol. 78 3:197-206.
- 39 Maglinte D. D. T., Kelvin F. M., Rowe M. G., Bender G. N., and Rouch D. M., (2001) *Small-Bowel Obstruction: Optimizing Radiologic Investigation and Nonsurgical Management*. *Radiology*, 218:39–46.
- 40 Parent S., Tortuyaux J. M., Deneuille M., Bresler L., Boissel P., (1996) *What are the small bowel obstructions to operate and how to do it?* *Acta Gastroenterol Belg*, 59(2): 150-1.
- 41 Silva A. C., Pimenta M., Guimarães L. S., (2009) *Small Bowel Obstruction: What to Look For*. *radiographics jou*, 29(2):423-39.
- 42 Nazhat CA., Nezhat F., Nezhat CE., (2008) *Nezhat's Operative Gynecologic Laparoscopy and Hysteroscopy*. Chapter 11, Page 304.
- 43 <http://www.drugs.com/health-guide/bowel-obstruction.html>
- 44 Neff M., and Schmidt B., (2010) *Laparoscopic Treatment of a Postoperative Small Bowel Obstruction*. *JLS*, 14(1): 133–136.
- 45 Everhart J. E., *Digestive Diseases in the United States: Epidemiology and Impact*. Abdominal wall hernia, Pages 475-476.
- 46 Benjelloun El. B., Ousadden A., Ibnmajdoub K., Mazaz K. and Taleb K. A., (2009) *Small bowel intussusception with the Meckel's diverticulum after blunt abdominal trauma: a case report*. *World Journal of Emergency Surgery*, 4:18.
- 47 Cruz C. J., Minagi H., (1994) *Large bowel obstruction resulting from traumatic diaphragmatic hernia*. *AJR*: 162.
- 48 Lamah M., Mathur P., Mckeown B., Blake H. and Swift R. I., (1998) *The use of rectosigmoid stents in the management of acute large bowel obstruction*. *j. R. Coll. Surg. Edinb*, 43, 318-321.
- 49 Márquez-Díaz A. and Ramírez-Ortega MA., (2010) *A right sided colon volvulus with necrosis in a young patient. A case reported*. 48(2): 209-14.
- 50 <http://www.columbiasurgery.org/pat/colorectal/colectomy.html>
- 51 Tursi A., (2010) *Diverticular disease: A therapeutic overview*. *World J Gastrointest Pharmacol Ther*, 1(1): 27–35.

- 52 Gearhart S., Ahuja N., (2010) *Early Diagnosis and Treatment of Cancer Series: Colorectal Cancer*. Elsevier Health Sciences, Medical, Page 272.
- 53 Brosens R. P. M., Haan J. C., Buffart T. E., et al., (2011) *Deletion of chromosome 4q predicts outcome in Stage II colon cancer patients*. *Cell Oncol (Dordr)*, 34(3): 215–223.
- 54 Rutter C. M., and Savarino J. E., (2011) *An Evidence-Based Microsimulation Model for Colorectal Cancer: Validation and Application*. *Cancer Epidemiol Biomarkers Prev*. Author manuscript.
- 55 Adrouny A. R., (2002) *Understanding Colon Cancer*. Univ. Press of Mississippi, Medical, Page 146.
- 56 Cappell M. S., MD, PhD, FACP, (2005) *The pathophysiology, clinical presentation, and diagnosis of colon cancer and adenomatous polyps*. *Med Clin N Am* 89: 1–42.
- 57 Park S. and Lee Y. S., (2011) *Analysis of the Prognostic Effectiveness of a Multivisceral Resection for Locally Advanced Colorectal Cancer*. *J Korean Soc Coloproctology*, 27(1): 21–26.
- 58 Wong S. L., (2009) *Lymph Node Counts and Survival Rates After Resection for Colon and Rectal Cancer*. *Gastrointest Cancer Res*, 3(2 Suppl 1): S33-S35.
- 59 Young A., Hobbs R. and Kerr D., (2011) *ABC of Colorectal Cancer*. Second edition.
- 60 Tajima T., Mukai M., Yamazaki M., Higami S., Yamamoto S., Hasegawa S., Nomura E., Sadahiro S., Yasuda S., And Makuuchi H., (2014) *Comparison of hand-assisted laparoscopic surgery and conventional laparotomy for colorectal cancer: Interim results from a single institution*. *Oncol Lett*, 8(2): 627–632.
- 61 Lin KM. and Ota DM., (2000) *Laparoscopic colectomy for cancer: an oncologic feasible option*. *Surg Oncol*, 9(3): 127-34.
- 62 Mukai M., Kishima K., Tajima T. and et al., (2009) *Efficacy of hybrid 2-port hand-assisted laparoscopic surgery (Mukai's operation) for patients with primary colorectal cancer*. *Oncol Rep*, 22:893–899. [PubMed].
- 63 Wang Z., Zhang X. M., Zhou H. T., Liang J. W., Zhou Z. X., (2014) *New technique of intracorporeal anastomosis and transvaginal specimen extraction for laparoscopic sigmoid colectomy*. *Asian Pac J Cancer Prev*, 15(16): 6733-6.
- 64 Mortensen N. J. and Ashraf SH., (2008) *Intestinal anastomosis*. *Gastrointestinal tract and abdomen*, ACS Surgery.

- 65 JOHNS HOPKINS medicine, colon cancer center; http://www.hopkinscoloncancercenter.org/CMS/CMS_Page.aspx?CurrentUDV=59&CMS_Page_ID=1F7C07D4-268D-4635-8975-70A594870CC8.
- 66 Kim WR., Baek SJ., Kim CW., Jang HA., Cho MS., Bae SU., Hur H., Min BS., Baik SH., Lee KY., Kim NK. and Sohn SK., (2014) *Comparative study of oncologic outcomes for laparoscopic vs. open surgery in transverse colon cancer*. *Ann Surg Treat Res*, 86(1): 28-34.
- 67 Milsom JW., Trencheva K., Sonoda T., Nandakumar G., Shukla PJ. and Lee S., (2014) *A prospective trial evaluating the clinical performance of a novel surgical energy device in laparoscopic colon surgery*. *Surg Endosc*.
- 68 Berencsi A., Bezsilla J., Sikorszki L., Temesi R., Bende S., (2013) *Laparoscopic sigmoid resection in total situs inversus*. *Magy Seb.*, 66(1): 30-3.
- 69 Guenaga KF., Lustosa SA., Saad SS., Saconato H., Matos D., (2007) *Ileostomy or colostomy for temporary decompression of colorectal anastomosis*. *Cochrane Database Syst Rev*, (1): CD004647.
- 70 Yik-Hong Ho., (2006) *Techniques for restoring bowel continuity and function after rectal cancer surgery*. *World J Gastroenterol*, 12(39): 6252-6260.
- 71 Mitsuru K., et al., (1993) *Survival and recurrence after low anterior resection and abdominoperineal resection for rectal cancer: The results of a long-term study with a review of the literature*. *Surgery Today*, Volume 23, Issue 1, Pges 21-30.
- 72 Gamagami R. A., Liagre A., Chiotasso P., Istvan G., Dr. Lazorthes F., (1999) *Coloanal anastomosis for distal third rectal cancer*. *Diseases of the Colon & Rectum* October, Volume 42, Issue 10, Pages 1272-1275.
- 73 Daams F., Wu Z., Lahaye M. J., Jeekel J., Frederik Lange J., (2014) *Prediction and diagnosis of colorectal anastomotic leakage: A systematic review of literature*. *World J Gastrointest Surg*, 6(2): 14-26.
- 74 Yasumura M., Mori Y., Takagi H., Yamada T., Sakamoto K., Iwata H. and Hirose H., (2003) *Experimental model to estimate intestinal viability using charge-coupled device microscopy*. *British Journal of Surgery*, 90: 460–465.
- 75 Karliczeka A., Benarond D. A. et al., (2008) *Intraoperative Assessment of Microperfusion with Visible Light Spectroscopy in Esophageal and Colorectal Anastomoses*. *Eur Surg Res*, 41:303–311.
- 76 Shah S. D., Andersen C. A., (1981) *Prediction of Small Bowel Viability Using Doppler Ultrasound*. *Ann. Surg* vol 194, no 1, 97-99.
- 77 Urbanavičius L., Pattyn P., de Putte D. V. and Venskutonis D., (2011) *How to assess intestinal viability during surgery: A review of techniques*. *World J Gastrointest Surg*, 3(5): 59-69.

- 78 Cooperman M., Martin E. W. Jr., and Carey L. C., (1980) *Determination of intestinal viability by Doppler ultrasonography in venous infarction*. Ann Surg. 191(1): 57–58.
- 79 Alós R., Garcia-Granero E., Calvete J., Uribe N., (1993) *The use of photoplethysmography and Doppler ultrasound to predict anastomotic viability after segmental intestinal ischaemia in dogs*. Eur J Surg., 159(1): 35-41.
- 80 Holmes N. J., (1993) *Intraoperative Assessment of Bowel Viability*. Journal of investigative Surgery, Volume6, pp. 211-221.
- 81 Andaz S., Shields D.A., Scurr J.H., Coleridge Smith P.D., (1993) *Thrombolysis in acute lower limb ischaemia*. European Journal of Vascular Surgery, Volume 7, Issue 6, November, Pages 595-603.
- 82 Murakami M., et al., (1999) *Additional microvascular anastomosis in reconstruction after total esophagectomy for cervical esophageal carcinoma*. The American journal of surgery, Pages 263-266.
- 83 Yanar H., Taviloglu K., et al., (2007) *Planned second-look laparoscopy in the management of acute mesenteric ischemia*. World J Gastroenterol, 13(24): 3350-3053.
- 84 Kudzus S., Roesel C., Schachtrupp A., Höer J. J., (2010) *Intraoperative laser fluorescence angiography in colorectal surgery: a noninvasive analysis to reduce the rate of anastomotic leakage*. Langenbecks Arch Surg, 395:1025-1030.
- 85 Almendros I., Montserrat J. M., Torres M., González C., Navajas D. and Farré R., (2010) *Changes in oxygen partial pressure of brain tissue in an animal model of obstructive apnea*. Respiratory Research, 11:3.
- 86 Sheridan W. G., Lowndes R. H., Young H. L., (1987) *Tissue oxygen tension as a predictor of colonic anastomotic healing*. Dis Colon Rectum, 30: 867-871.
- 87 Jacobi C. A., Zieren H. U., Zieren J., Müller J. M., (1998) *Is tissue oxygen tension during esophagectomy a predictor of esophagogastric anastomotic healing?* J Surg Res 74: 161-164.
- 88 Cooperman M., Martin E. W. Jr., Carey L. C., (1980) *Evaluation of ischemic intestine by Doppler ultrasound*. Am J Surg 139: 73- 77.
- 89 Cooperman M., Martin E. W. Jr., Keith L. M., Carey L. C., (1979) *Use of Doppler ultrasound in intestinal surgery*. Am J Surg 138: 856- 859.
- 90 Ambrosetti P., Robert J., Mathey P., Rohner A., (1994) *Left-sided colon and colorectal anastomoses: Doppler ultrasound as an aid to assess bowel vascularization. A prospective evaluation of 200 consecutive elective cases*. Int J Colorectal Dis 9:211-214.
- 91 Yasumura M., Mori Y., Takagi H., Yamada T., Sakamoto K., Iwata H., Hirose H.,

- (2003) *Experimental model to estimate intestinal viability using charge-coupled device microscopy*. Br J Surg 90: 460-465.
- 92 Rotering R. H. Jr., Dixon J. A., Holloway G. A. Jr., McCloskey D. W., (1982) *A comparison of the He Ne laser and ultrasound Doppler systems in the determination of viability of ischemic canine intestine*. Ann Surg. 196(6): 705-8.
- 93 Lynch T. G., Hobson R. W., Kerr J. C., Brousseau D. A., Silverman D. G., Reilly C. A., Tseng H., (1988) *Doppler ultrasound, laser Doppler, and perfusion fluorometry in bowel ischemia*. Arch Surg. 123(4): 483-6.
- 94 Mishima Y., Shigematsu H., Horie Y., Satoh M., (1979) *Measurement of local blood flow of the intestine by hydrogen clearance method; experimental study*. Jpn J Surg 9: 63-70.
- 95 Young W., (1980) *H2 clearance measurement of blood flow: a review of technique and polarographic principles*. Stroke, 11(5): 552-64.
- 96 Leung F. W., (1990) *Comparison of Blood Flow Measurements by Hydrogen Gas Clearance and Laser Doppler Flowmetry in the Rat Duodenum*. Scand J Gastroenterol, 25, 429- 434.
- 97 Wheelless C. R., Smith J. J., (1983) *A comparison of the flow of iodine 125 through three different intestinal anastomoses: standard, Gambee, and stapler*. Obstet Gynecol 62: 513-518.
- 98 Prinzen F. W., Bassingthwaight J. B., (2000) *Blood flow distributions by microsphere deposition methods*. Cardiovascular Research, 45:13–21.
- 99 Brolin R. E., Bibbo C. et al., (1997) *Comparison of Ischemic and Reperfusion Injury in Canine Bowel Viability Assessment*. Gastrointest surg 1: 511-516.
- 100 MacDonald P. H., Dinda P. K., Beck I. T., Mercer C. D., (1993) *The use of oximetry in determining intestinal blood flow*. Surg Gynecol Obstet., 176(5): 451-8.
- 101 Gardner G. P., Lamorte W. W., Obi Tabot E. T., Menzoian J. O., (1994) *Transanal intracolonic pulse oximetry as a means of monitoring the adequacy of colonic perfusion*. The journal of surgical research, vol. 57, no5, pp. 537-540.
- 102 La Hei E. R., Shun A., (2001) *Intra-operative pulse oximetry can help determine intestinal viability*. Pediatr Surg Int, 17:120-121.
- 103 Phillips J. P., Kyriacou P. A., Jones D. P., Shelley K. H., Langford R. M., (2008) *Pulse oximetry and photoplethysmographic waveform analysis of the esophagus and bowel*. Curr Opin Anaesthesiol, 21: 779-783.
- 104 Hadley G. P., Mars M., (2003) *Limitations of oximeters*. Pediatr Surg Int, 19: 130.
- 105 Dyess D. L., Bruner B. W., Donnell C. A., Ferrara J. J., Powell R. W., (1991) *Intraoperative evaluation of intestinal ischemia: a comparison of methods*. South Med J, 84: 966-99, 974.

- 106 Benaron D. A., Parachikov I. H., Friedland S., Soetikno R., et al., (2004) *Continuous, Noninvasive, and Localized Microvascular Tissue Oximetry Using Visible Light Spectroscopy*. *Anesthesiology*, 100:1469–75.
- 107 Benaron D. A., Parachikov I. H., Cheong W. F., Friedland S., Rubinsky B. E., Otten D. M., Liu F. W., Levinson C. J., Murphy A. L., Price J. W., Talmi Y., Weersing J. P., Duckworth J. L., Horchner U. B., Kermit E. L., (2005) *Design of a visible-light spectroscopy clinical tissue oximeters*. *J Biomed Opt*, 10(4): 44005.
- 108 Hirano Y., Omura K., Tatsuzawa Y., Shimizu J., Kawaura Y., Watanabe G., (2006) *Tissue oxygen saturation during colorectal surgery measured by near-infrared spectroscopy: pilot study to predict anastomotic complications*. *World J Surg*, 30: 457-461.
- 109 Karliczek A., Benaron D. A., Baas P. C., Zeebregts C. J., Wiggers T., van Dam G. M., (2010) *Intraoperative assessment of microperfusion with visible light spectroscopy for prediction of anastomotic leakage in colorectal anastomoses*. *Colorectal Dis*, 12: 1018-1025.
- 110 Düchs R., Foitzik T., (2008) *Possible pitfalls in the interpretation of microcirculatory measurements. A comparative study using intravital microscopy, spectroscopy and polarographic Po₂ measurements*. *Eur Surg Res.*, 40(1): 47-54.
- 111 Horgan P. G., Gorey T. F., (1992) *Operative assessment of intestinal viability*. *Surg Clin North Am.*, 72(1): 143.
- 112 Lynch T. G., et al., (1988) *Doppler Ultrasound, Laser Doppler, and Perfusion Fluorometry in Bowel Ischemia*. *arch surg*, vol123.
- 113 Toens C., Krones C. J., et al., (2005) *Validation of the ICview fluorescence videography in a rabbit model of mesenteric ischemia and reperfusion*. *Int J Colorectal Dis*, 19: 1–7.
- 114 Moss A. A., Kressel H. Y., Brito A. C., (1978) *Thermographic assessment of intestinal viability following ischemic damage*. *Invest Radiol*, 13(1): 16-20.
- 115 Brooks J. P., Perry W. B., Putnam A. T., Karulf R. E., (2000) *Thermal imaging in the detection of bowel ischemia*. *Dis Colon Rectum*, 43(9): 1319-21.
- 116 Roberts W. W., Dinkel T. A., Schulam P. G., Bonnell L., Kavoussi L. R., *Laparoscopic infrared imaging*. *Surg Endosc* 1997; 11: 1221-1223.
- 117 Cadeddu J. A., Jackman S. V., Schulam P. G., (2001) *Laparoscopic infrared imaging*. *J Endourol*, 15(1): 111-6.
- 118 Nishikawa K., Matsudaira H., Suzuki H., Mizuno R., Hanyuu N., Iwabuchi S., Yanaga K., (2006) *Intraoperative thermal imaging in esophageal replacement: its use in the assessment of gastric tube viability*. *Surg Today*, 36: 802-806.
- 119 Shussman N., Abu Gazala M., Schlager A., Elazary R., Khalaileh A., Zamir G.,

- Kushnir D., Rivikind A. I., Mintz Y., (2011) *Laparoscopic infrared imaging-the future vascular map*. J Laparoendosc Adv Surg Tech A. 21(9): 797-801.
- 120 Redaelli C. A., Schilling M. K., Carrel T. P., *Intraoperative assessment of intestinal viability by laser Doppler flowmetry for surgery of ruptured abdominal aortic aneurysms*. World J Surg 1998; 22: 283-289.
- 121 Vignali A., Gianotti L., Braga M., Radaelli G., Malvezzi L., Di Carlo V., (2000) *Altered microperfusion at the rectal stump is predictive for rectal anastomotic leak*. Dis Colon Rectum, 43: 76-82.
- 122 Nakatsuka M., (2002) *Assessment of gut mucosal perfusion and colonic tissue blood flow during abdominal aortic surgery with gastric tonometry and laser Doppler flowmetry*. Vasc Endovascular Surg; 36: 193-198.
- 123 Seike K., Koda K., Saito N., Oda K., Kosugi C., Shimizu K., Miyazaki M., (2007) *Laser Doppler assessment of the influence of division at the root of the inferior mesenteric artery on anastomotic blood flow in rectosigmoid cancer surgery*. Int J Colorectal Dis, 22: 689-697.
- 124 Matthiessen P., (2006) *Rectal Cancer Surgery Defunctioning stoma, anastomotic leakage and postoperative monitoring*. Department of Surgery Orebro University Hospital, No. 940 Sweden.
- 125 Kaser S. A., Glauser P. M., Maurer C. A., (2012) *Venous small bowel infarction: intraoperative laser Doppler flowmetry discriminates critical blood supply and spares bowel length*. Case Rep Med, 195926.
- 126 Djavani K., Wanhainen A., Valtysson J., Björck M., (2009) *Colonic ischaemia and intra-abdominal hypertension following open repair of ruptured abdominal aortic aneurysm*. Br J Surg., 96(6): 621-7.
- 127 Millan M., García-Granero E., Flor B., García-Botello S., Lledo S., (2006) *Early prediction of anastomotic leak in colorectal cancer surgery by intramucosal pH*. Dis Colon Rectum, 49: 595-601.
- 128 Hernandez G., Lopez F., Castillo L., et al., (1996) *“Postoperative ischemia after gut transplantation: role of different monitoring systems,”* Transplantation Proceedings. Vol. 28, no. 5, Pages 2631–2632.
- 129 Ugras B., et al., (2008) *Early prediction of anastomotic leakage after colorectal surgery by measuring peritoneal cytokines: Prospective study*. International Journal of Surgery, 6: 28-35.
- 130 Kamiya K., Suzuki S., Mineta H., Konno H., (2007) *Tonometer pH_i monitoring of free jejunal grafts following pharyngolaryngoesophagectomy for hypopharyngeal or cervical oesophageal cancer*. Dig Surg, 24: 214-220.
- 131 Tenhunen J. J., Kosunen H., Alhava E., Tuomisto L., and Takala J. A., (1999)

- "Intestinal luminal microdialysis: a new approach to assess gut mucosal ischemia"*. *Anesthesiology*, vol. 91, no. 6, pp. 1807–1815.
- 132 Birke-Sorensen H., and Andersen N. T., (2010) *"Metabolic markers obtained by microdialysis can detect secondary intestinal ischemia: an experimental study of ischemia in porcine intestinal segments"*. *World Journal of Surgery*, vol. 34, no. 5, Pages 923–932.
- 133 Deeba S., Corcoles E. P., Hanna B.G., et al., (2008) *Use of Rapid Sampling Microdialysis for Intraoperative Monitoring of Bowel Ischemia*. *Disease of colon and rectum*, Vol 51, no 9, Pages 1408-1413.
- 134 Paydar, K., et al., (2010) *Implantable Venous Doppler Monitoring in Neck Free Flap Reconstruction Increases the Salvage Rate*. *Journal of Plastic and Reconstructive Surgery*, Volume 125, Issue 4, Pages 1129-1134.
- 135 Rosato E., Molinaro I., Rossi C., Pisarri S., Salsano F., (2011) *The combination of laser Doppler perfusion imaging and photoplethysmography is useful in the characterization of scleroderma and primary Raynaud's phenomenon*. *Scand J Rheumatol*, First article: 1–7.
- 136 Bergstrand S., Lindberg LG., Ek AC. and Lindgren M., (2009) *Blood flow measurements at different depths using photoplethysmography and laser Doppler techniques*. *Skin Research And Technology*, (15), 2, Pages 139-147.
- 137 Hagblad J., (2011) *Non-Invasive Techniques for Assessment of Peripheral Blood Flow at Different Vascular Depths*. Mälardalen University Press Licentiate Theses, No. 131.
- 138 Avino A. J., Oldenburg A., Gloviczki P., et al., (1995) *Inferior mesenteric venous sampling to detect colonic ischemia: A comparison with laser Doppler flowmetry and photoplethysmography*. *Journal of Vascular Surgery*, Vol 22, No. 3.
- 139 Webster J. G., (1997) *Design of Pulse Oximeters*. Chapter 5, Page 56.
- 140 Allen J., (2007) *Photoplethysmography and its application in clinical physiological measurement*. *Phys meas*, 28:R1-R39.
- 141 Sadaka F., Aggu Sher R., Krause K., et al., (2011) *The effect of red blood cell transfusion on tissue oxygenation and microcirculation in severe septic patients*. *Ann intensive care*, 1 (1): 46.
- 142 Hertzman, A. B. & Flath, F. (1963) *The Continuous Simultaneous Registration of Sweating and Blood Flow in a Small Skin Area*. *Aerospace Medicine*, 34, 710-713.
- 143 Wong DM., Alcott CJ., Wang C., Bornkamp JL., Young JL., Sponseller BA., (2011) *Agreement between arterial partial pressure of carbon dioxide and saturation of haemoglobin with oxygen values obtained by direct arterial blood measurements*

- versus noninvasive methods in conscious healthy and ill foals.* J Am Vet Med Assoc., 239(10): 1341-7.
- 144 Oliver N. and Flores-Mangas F., (2007) *HealthGear: A Real-time Wearable System for Monitoring and Analysing Physiological Signals.* Journal Of Communications, Vol. 2, No. 2.
- 145 Lindberg LG., Öberg PA., (1991) *Photoplethysmography: Part 2. Influence of light source wavelength.* Med Biol Eng Comput 29:48–54.
- 146 Alnaeb M. E., Alobaid N., Seifalian A. M., Mikhailidis D. P., and Hamilton G., (2007) *Optical Techniques in the Assessment of Peripheral Arterial Disease.* Current Vascular Pharmacology, 53, 5:53-59.
- 147 Hertzman, A. B. (1937) *Photoelectric Plethysmography of the Nasal Septum in Man.* Proceedings of the Society for Experimental Biology and Medicine. Society for Experimental Biology and Medicine (New York, N.Y.), 37, 290-292.
- 148 Hertzman, A.B., Dillon, J.B. (1940) *Reactions of Large and Small Arteries in Man.* Am. J. Physiol. 130:56.
- 149 Phelps J. A., Sass D. J., (1969) *A Portable Battery-Powered Instrument for Visualizing the Peripheral-Pulse Waveform and Pulse Rate.* VOL.48, No.4, Pages 582-586.
- 150 Muralidhar K., (2002) *Central Venous Pressure And Pulmonary Capillary Wedge Pressure Monitoring.* Indian Journal of Anaesthesia, 46 (4): 298-303.
- 151 <http://academy.cba.mit.edu/2013/students/contonente.javier/week16/week16.html>
- 152 Zheng YP., et al., (2010) *Comparison between reflection-mode photoplethysmography and arterial diameter change detected by ultrasound at the region of radial artery.* Blood Pressure Monitoring, Volume 15 - Issue 4 - Pages 213-219.
- 153 Rhee S., Yang BH., and Asada H. H., (2001) *Finger-Ring Plethysmographic Sensors.* IEEE Transactions On Biomedical Engineering, VOL. 48, NO. 7, 795.
- 154 Feng Z., Smith M., *Measuring heart rate and blood oxygen levels for portable medical and wearable devices.* embedded-computing.com.
- 155 Severinghaus JW. (2001) *The History of Anesthesia: Proceedings of the Fifth International Symposium on the History of Anesthesia; Santiago, Spain.* p. 115.
- 156 Millikan G. A., (1942) *The oximeter, an instrument for measuring continuously the arterial saturation of arterial blood in man.* Rev. Sci., Instrum, vol. 13, Pages 434 – 444.
- 157 Wood E. H. and Geraci J. E., (1949) *Photoelectric determination of arterial oxygen saturation in man.* J. Lab. Clin. Med, vol 34, Pages 387-401.

- 158 Brinkman R. and Zijlstra W. G., (1949) *Determination and continuous registration of the percentage oxygen saturation in clinical conditions*. Vol. 1, Pages 177-183.
- 159 Sekelj P., Johnson A. L., Hoff H. E. and Scherch P. M., (1951) *A photoelectric method for the determination of arterial oxygen saturation in man*. Amer. Heart. J., vol. 42, Pages 826-848.
- 160 Landsman M. L. J., Knop N., Mook G. A., Zijlstra W. G., (1978) *A fiberoptic reflection oximeters*, Pflügers Archiv, Volume 373, Issue 3, pp 273-282.
- 161 Merrick E. B. and Hayes T. J., (1976) *Continuous, non-invasive measurements of arterial blood oxygen levels*. Hewlett-packard J., vol. 28, no. 2, Pages 2-9.
- 162 Cohen A. and Wardsworth N. A., (1972) *Light emitting diode skin reflectance oximeters*. Med. Biol. Eng., vol. 10, Pages 385-391.
- 163 Takatani S. and Ling J., (1994) *Optical oximetry sensors for whole blood and tissue*. IEEE Eng. Med. Biol. Mag., Pages 347-357.
- 164 Falconer R. J. and Robinson B. J., (1990) *Comparison of pulse oximeters: accuracy at low arterial pressure in volunteers*. BJA, vol. 65, no. 4, Pages 552-557.
- 165 Epstein B. S., (2003) *The American Society of Anesthesiologist's Efforts in Developing Guidelines for Sedation and Analgesia for Nonanesthesiologists*. Anesthesiology, 98:1261– 8.
- 166 Richards-Kortum R., Sevick-Muraca E., (1996) *Quantitative Optical Spectroscopy For Tissue Diagnosis*. Annu. Rev. Phys. Chem, 47:555–606.
- 167 Mourant J. R., Johnson T. M., Los G. and Bigio I. j., (1999) *Non-invasive measurement of chemotherapy drug concentrations in tissue: preliminary demonstrations of in vivo measurements*. J Bigio, Phys. Med. Biol. 44, Pages 1397–1417.
- 168 Webster J.G., (1997) *Design of pulse oximeters*. Chapter 7, Page 98.
- 169 Hsiu H., Hsu CL., Wu TL., (2011) *Effects of different contacting pressure on the transfer function between finger photoplethysmographic and radial blood pressure waveforms*. Proc Inst Mech Eng H., 225 (6): 575-83.
- 170 MacDonald PH., Dinda PK., Beck IT., Mercer CD., (1993) *The use of oximetry in determining intestinal blood Flow*. Surg Gynecol Obstet, 176(5): 451-8.
- 171 Kamat V., (2002) *PULSE Oximetry*. Indian Journal Of Anaesthesia, 46 (4): 261-268.
- 172 Tremper K. K., Barker S. J., (1989) *Medical Intelligence Article: Pulse Oximetry*. Anesthesiology, Volume 70-Issue 1-PPG 98-108.
- 173 Ingram G., Munro N., (2005) *The use (or otherwise) of pulse oximetry in general practice*. British Journal of General Practice, Br J Gen Pract, 55(516): 501–502.
- 174 Moyle J., (2002) *Pulse oximetry*. J.T.B., 2nd ed., London: BMJ. viii, 182 p.

- 175 Hermeling E, Reesink KD, Kornmann LM, Reneman RS, Hoeks AP. J Hypertens, (2009) *The dicrotic notch as alternative time-reference point to measure local pulse wave velocity in the carotid artery by means of ultrasonography*. 27(10): 2028-35.
- 176 Rubin AS., (1988) *Nail polish colour can affect pulse oximeter saturation*. Anesthesiology, volume, 68-issue- Pages 825.
- 177 DeMeulenaere S., (2007) *Oximetry: uses and limitation*. The Journal for Nurse practitioners-JPN.
- 178 Riva C. E., Geiser M. and Petrig B. L., (2010) *Ocular blood flow assessment using continuous laser Doppler flowmetry*. Acta Ophthalmol, 88: 622–629.
- 179 Goode T. L. and Klein H. J., (2002) *Miniaturization: An Overview of Biotechnologies for Monitoring the Physiology and Pathophysiology of Rodent Animal Models*. ILAR Journal, Volume 43.
- 180 Forrester A.T., R.A. Gudmundsen, and P.O. Johnson, (1955) *Photoelectric Mixing of Incoherent Light*. Physical Review. 99(6), 1691 LP - 1700.
- 181 Forrester A.T., (1961) *Photoelectric Mixing As a Spectroscopic Tool*. Journal of the Optical Society of America. 51(3), Pages 253-259.
- 182 Cummins H.Z. and Swinney H.L., Wolf E., (1970) *Light Beating Spectroscopy*. In Progress in optics, 135-200, North-Holland.
- 183 Stern M.D., (1975) *In vivo evaluation of microcirculation by coherent light scattering*. Nature, 254, Pages 56-58.
- 184 Holloway G.A., and Watkins D.W., (1977) *Laser Doppler measurement of cutaneous blood flow*. The Journal of Investigative Dermatology, 69(3), Pages 306-309.
- 185 Nilsson G.E., Tenland T., and Berg P., (1980) *A new instrument for continuous measurement of tissue blood flow by light beating spectroscopy*. IEEE Transactions on Biomedical Engineering, 27(1), 12-9.
- 186 Nilsson G.E., Tenland T., and Öberg P.Å., (1980) *Evaluation of a laser Doppler flowmeter for measurement of tissue blood flow*. IEEE Transactions on Biomedical Engineering, 27(10), Pages 597-604.
- 187 Nilsson G.E., (1984) *Signal processor for laser Doppler tissue flowmeters*. Medical and Biological Engineering and Computing, 22(4), 345-8.
- 188 Nilsson G.E., Jakobsson A., and Wårdell K., (1989) *Imaging of tissue blood flow by coherent light scattering in Engineering in Medicine and Biology Society, Images of the Twenty-First Century*. Proceedings of the Annual International Conference of the IEEE Engineering.
- 189 Leitao Ferreira A. I., (2007) *Laser Doppler Flowmetry*. Departamento de Fisica da

- Universidade de Coimbra, Project Report.
- 190 Rajan V., Varghese B., Leeuwen T. G. V., Steenbergen W., (2009) *Review of methodological developments in laser Doppler flowmetry*. Lasers, Med Sci, 24:269–283.
 - 191 Vongsavan N., and Matthews B., (1993) *Review Article Some Aspects Of The Use Of Laser Doppler Flow Meters For Recording Tissue Blood Flow*. Experimental Physiology, 78, Pages 1-14.
 - 192 Nilsson GE., (1984) *Signal processor for laser Doppler tissue flowmeters*. Med Biol Eng Comput, 22(4): 343-5.
 - 193 Colantuoni A., Bertuglia S., (1997) *Correlation between laser Doppler perfusion monitoring and hematocrit in hamster cheek pouch microcirculation*. Int J Microcirc Clin Exp 17:33–40.
 - 194 Kvernebo K. and Larsen S., (1988) *Evaluation of Endoscopic Laser Doppler Flowmetry for Measurement of Human Gastric Blood Flow: Methodologic Aspects*. Scandinavian Journal of Gastroenterology, Vol. 23, No. 9, Pages 1072-1078.
 - 195 Riva C., Ross B., Benedek GB., (1972) *Laser Doppler measurements of blood flow in capillary tubes and retinal arteries*. Invest Ophthalmol, 11(11): 936-44.
 - 196 Iabichella M.L., Melillo E., and Mosti G., (2006) *A review of microvascular measurements in wound healing*. The International Journal of Lower Extremity Wounds, 5(3), 181-99.
 - 197 Devgan L., Bhat S., Aylward S., and Spence R.J., (2006) *Modalities for the assessment of burn wound depth*. Journal of Burns and Wounds, 5, e2.
 - 198 Stücker M., Esser M., Hoffmann M. et al., (2002) *High-resolution laser Doppler perfusion imaging aids in differentiating between benign and malignant melanocytic skin tumours*. Acta Dermato-Venereologica, 82(1), 25-29.
 - 199 Lantsberg L. and Goldman M., (1991) *Laser Doppler flowmetry, transcutaneous oxygen tension measurements and Doppler pressure compared in patients undergoing amputation*. European Journal of Vascular Surgery, 5(2), 195-7.
 - 200 Ray S.A., Buckenham T.M., Belli A.M., Taylor R.S., and Dormandy J.A., (1997) *The predictive value of laser Doppler fluxmetry and transcutaneous oximetry for clinical outcome in patients undergoing revascularisation for severe leg ischaemia*. European Journal of Vascular and Endovascular Surgery, 13(1), 54-9.
 - 201 Wardell K., Blomstedt P. et al., (2007) *Intracerebral microvascular measurements during deep brain stimulation implantation using laser Doppler perfusion monitoring*. Stereotactic and Functional Neurosurgery, 85(6), Pages 279-286.
 - 202 Leahya M. J., Enfielda J. G., et al., (2007) *Biophotonic methods in microcirculation imaging*. Medical Laser Application, Volume 22, Issue 2, Pages 105-126.

- 203 Forrester K., Doschak M., Bray R., (1997) *In vivo comparison of scanning technique and wavelength in laser Doppler perfusion imaging: measurement in knee ligaments of adult rabbits*. Med,Bio Eng. Comput, 35, Pages 581-586.
- 204 Fredriksson I., *Quantitative Laser Doppler Flowmetry*. Department of Biomedical Engineering, Link.ping University, SE-581, 85 Link.ping, Sweden.
- 205 Koelink M. H., De Mul F. F. M., Greve J., Graaff R., Dassel A. C. M., Aarnoudse J. G., (1994) *Laser Doppler blood flowmetry using two wavelengths: Monte-Carlo simulations and measurements*. Appl Opt 33:3549–3558.
- 206 Jakobsson A., Nilsson G., (1993) *Prediction of sampling depth and photon pathlength in laser Doppler flowmetry*. Med Biol Eng Comput, 31: 301–307.
- 207 Faber D. J., Aalders M. C. G., Mik E. G., Hooper B. A., van Gemert M. J. C., van Leeuwen T. G., (2004) *Oxygen saturation-dependent absorption and scattering of blood*. Phys Rev Lett, 93 (2):028102.
- 208 Gush R. J., King T. A., (1991) *Discrimination of capillary and arterio-venular blood flow in skin by laser Doppler flowmetry*. Med Biol Eng Comput, 29:387–392.
- 209 Higurashi E., Sawada R., and Ito T., (2003) *An integrated laser blood flowmeter*. J Lightwave Technol 21:591–595.
- 210 Serov A.N., Steenbergen W., De Mul F.F.M., and Lasser T., (2003) *Quasi-parallel laser-Doppler perfusion imaging using a CMOS image sensor*. Laser Physics and Photonics, Spectroscopy, and Molecular Modeling III; Coherent Optics of Ordered and Random Media III. SPIE.
- 211 Serov A. and Lasser T., (2006) *Full-field high-speed laser Doppler imaging system for blood-flow measurements*. Advanced Biomedical and Clinical Diagnostic Systems IV. San Jose, CA, USA: SPIE.
- 212 Tindholdt T. T., Saidian S., Pripp A. H., Tønseth K. A., (2011) *Monitoring microcirculatory changes in the deep inferior epigastric artery perforator flap with laser Doppler perfusion imaging*. Ann Plast Surg, 67(2): 139-42.
- 213 Serov A., Steenbergen W., and De Mul F. F. M., (2002) *Laser Doppler perfusion imaging with a complimentary metal oxide semiconductor image sensor*. Opt Lett 25:300–302.
- 214 Serov A., Steinacher B., Lasser T., (2005) *Full-field laser Doppler perfusion imaging and monitoring with an intelligent CMOS camera*. Opt Express, 13:3681–3689.
- 215 Lohwasser R., Soelkner G., (1999) *Laser-Doppler frequency spectra of a tissue like model of a human head with capillaries*. Experimental and theoretical, Appl Opt, 38:2128–2137.
- 216 Binzoni T., Leung T. S., Boggett D., Delpy D. T., (2003) *Non-invasive Laser*

- Doppler perfusion measurements of large tissue volumes and human skeletal muscle blood RMS velocity.* Phys Med Biol, 48:2527–2549.
- 217 Tenland T., Salerud E. G., Nilsson G. E., Öberg P. A., (1983) *Spatial and temporal variations in human skin blood flow.* Int J Microcirc Clin Exp, 2:81–90.
- 218 Caspary L., Creutzig A., Alexander K., (1988) *Biological zero in laser Doppler fluximetry.* Int J Microcirc Clin Exp, 7:367–371.
- 219 Fagrell B., Shepherd A. P., Öberg PÅ. (eds), (1990) *Laser-Doppler blood flowmetry Perimed's LDV flowmeter.* Kluwer Academic Publishers, Boston.
- 220 Nilsson G. E., Shepherd A. P., Öberg PÅ. (eds), (1990) *Laser-Doppler blood flowmetry Peripheral vascular diseases.* Kluwer Academic Publishers, Boston.
- 221 Abbot N. C., Swanson-Beck J., (1993) *Biological zero in laser Doppler measurements in normal, ischaemic and inflamed human skin.* Int J Microcirc Clin Exp 2:89–98.
- 222 Fagrell S., Nilsson G., (1995) *Advantages and limitations of one point laser Doppler perfusion monitoring in clinical practice.* Vasc Med Rev 6:97–101.
- 223 Kernick D. P., Tooke J. E., Shore A. C., (1999) *The biological zero signal in laser Doppler fluximetry origins and practical implications.* Pflugers Arch 437:624–631.
- 224 Gush R. J., King T. A., (1987) *Investigation and improved performance of optical fibre probes in laser Doppler blood flow measurement.* Med Biol Eng Comput, 678:29–36
- 225 Öberg PÅ., (1999) *Tissue motion a disturbance in the laser-Doppler blood flow signal?.* Technol Health Care, 7:185–192.
- 226 Karlsson MGD., Larsson M., Strömberg T., Wårdell K., (2002) *Influence of tissue movements on laser Doppler perfusion imaging.* SPIE, 4624:106–114
- 227 Alves A., Panis Y., Pocard M., Regimbeau J. M., Valleur P., (1999) *Management of anastomotic leakage after nondiverted large bowel resection.* J Am Coll Surg, 189: 554-559.
- 228 CR 60 R, PerkinElmer, Datasheet
- 229 AP2012F3C, Kingbright Datasheet
- 230 BPW 34 S R18R-Z Datasheet
- 231 <http://gb.moor.co.uk/product/vp8c-vp8c/43>
- 232 <http://www.engineersgarage.com/sites/default/files/LM35.PDF>
- 233 Grampian M., (1976) *Electronic Engineering.* Volume 48, Issues 575-586
- 234 <http://www.doctronics.co.uk/555.htm>.
- 235 Firbank M., Okada E. and Delpy D. T., (1997) *Investigation of the effect of discrete absorbers upon the measurement of blood volume with near-infrared spectroscopy.* Physics in Medicine & Biology, 42, Pages 465-577.

- 236 Jain R. K., (2002) *Tumor angiogenesis and accessibility: role of vascular endothelial growth factor*. *Semin Oncol.*, 29(6 Suppl 16): 3-9.
- 237 Baish J. W., Stylianopoulos T., Lanning R. M., Kamoun W. S., Fukumura D., Munn L. L., and Jain R. K., (2011) *Scaling rules for diffusive drug delivery in tumor and normal tissues*. *PNAS* vol. 108, no. 5, 1799–1803.
- 238 Yueh TC., et al., (2010) *The Risk Factors of Anastomotic Leakage and Influence of Fecal Diversion after Resection of Rectal Cancer*. *J Soc Colon Rectal Surgeon*, Vol. 21, No. 1.
- 239 Baronzio G. F., Gramaglia A., Baronzio A., and Freitas I., (2000) *Influence of Tumor Microenvironment on Thermoresponse: Biologic and Clinical Implications*. Madame Curie Bioscience Database.

Appendix A

Technical Specifications for Photoplethysmographic system

A: Custom-made Probe

Manufacturer	Biomedical Engineering Research Group, School of Engineering and Mathematical Sciences, City University London
Optoelectronics: Sources	1 x 628 nm (red) LED (SMT), max power output = 25 mW 1 x 880 nm (infrared) LED (SMT), max power output = 20 mW
Optoelectronics: Photodetector	1 x 1mm ² PIN Photodiode (SMT)
Connections	3.9 m 5-core coaxial cable to locking DIN- style 8-pin plug
Dimensions	29(L) x 12(W) x 1.5(D) mm

B: Instrumentation unit

Manufacturer	Biomedical Engineering Research Group, School of Engineering and Mathematical Sciences, City University London
Measurement Parameters [†]	perfusion index PI (ratio or %) arterial oxygen saturation SpO ₂ (%) tissue oxygenation index (TOI%) Change in deoxyhaemoglobin concentration (Δ Hb) Change in oxyhaemoglobin concentration (Δ O ₂ Hb) Change in total functional haemoglobin (Δ Hb + Δ O ₂ Hb)
Signal Processing	Bandwidth: High pass 0.4 Hz Low pass 16 Hz Sample rate: 100-400 Hz
Output	USB connection to PC LabVIEW™ virtual instrument displaying red

	and infrared PPG signal, Doppler signal and calculated parameters ([†] see above). Anonymous raw data saved to tab-delimited text file.
Safety features	Battery power, low voltage Splash proof case On-off switch on front panel
Power supply	2 x 12 V 1.2 Ah lead-acid cells
External connections	Inputs: Probe connection (8 pin locking DIN-style plastic); Laser Doppler analog BNC. Outputs: USB type-B data
Dimensions	30(L) x 28(W) x 9(D) cm

Appendix B

Technical Specifications for laser Doppler monitor and probe

A: Specifications for monitor: moor *VMS-LDF*

Quality Control	Moor Instruments is certified to ISO 13485: 2003. The moor <i>VMS-LDF</i> is CE certified.
Measurement Parameters	Flux (tissue perfusion). Conc* (blood cell concentration). DC (mean intensity). Temperature.
Measurement Channels	Moor <i>VMS-LDF2</i> Dual channel.
Reliability	Assured by our 3 year basic warranty or 5 year extended warranty for the Moor <i>VMS-LDF</i> modules.
Optics	Temperature stabilised output laser diode; 785nm. Maximum output power 2.5mW.
Laser Safety Classification	Class 1 per IEC 60825-1:2007. Class 1 per 21 CFR 1040.10 and 1040.11.
Laser Doppler Signal Processing	Bandwidth: High pass 20Hz. Low pass 3kHz*, 15kHz, 22kHz*. Flux smoothing time constants: 0.1s*, 0.5s*, 1.0s, 3.0s* and unfiltered*. Automatic gain control and zeroing.
Output	LCD screen providing display of flux, DC and temperature. USB Interface for connection to PC. Analogue outputs: BNC sockets, 0-5V. Moor <i>VMS-LDF2</i> 2x flux, 2x temperature/DC (selectable). All outputs have independent user selectable scaling.
Classification	Medical devices directive 93/42/EEC: Class IIa, Active device for diagnosis. Laser classification: Class 1 per IEC 60825-1:2007. Type of protection against electric shock: Class I. Degree of protection against electric shock: Type BF applied parts. Protection against harmful ingress of water: IPX0 (not protected).

	Not suitable for use in an oxygen rich atmosphere. Not suitable for use in the presence of flammable anaesthetics.
Safety standards	Complies with: IEC 60601-1:2005, IEC 60601-1-2:2007, IEC 60825-1:2007. ISO 10993-1:2003, Medical devices directive 93/42/EEC. FDA Laser Notice No. 50; dated July 26, 2001.
Temperature Measurement	Range: 5°C to 50°C. Resolution: 0.1°C, accuracy +/- 0.3°C.
General	Power source: Universal voltage, 100-230V AC, 30VA, 50 to 60Hz. Dimensions: W x H x D mm, Weight: Kg Moor <i>VMS-LDF2</i> : 235 x 80 x 200, 1.5kg. Operating environment: Clinic or laboratory, excluding domestic. Operating temperature: 15-30°C.
References	A.P. Shepherd, P. Å. Öberg, Laser-Doppler Blood Flowmetry, 1990, ISBN 0-7923-0508-6, Kluwer Academic Publishers.

B: Specification for Probe: moor *VMS-LDF* probe, *VP8C*

Probe	Low profile disk probe
General	The <i>VP8c</i> titanium disc probe has a 2.1mm outside diameter flexible nylon sleeve with a titanium disc probe head
The probe head	8mm outside diameter and 2.5 mm high

Moor Instruments – Millwey, Axminster, Devon. EX13 5HU
Telephone +44 (0) 1297 35715

Appendix C: Ethical Approval Confirmation



NRES Committee London-City & East

Bristol Research Ethics Committee Centre
Whitefriars
Level 3, Block B
Bristol
BS1 2NT
Telephone:01173421386
Facsimile:01173420445

14 May 2013

Dr Justin Phillips
Senior Lecturer in Biomedical Engineering City University London
Northampton Square London
EC1V 0HB

Dear Dr Phillips

Study title: Evaluation of a combined laser Doppler and photoplethysmographic system for intra-operative monitoring of bowel tissue viability.

REC reference: 13/LO/0738
Protocol number: BERG-ZA-13/01
IRAS project ID: 130982

The Research Ethics Committee reviewed the above application at the meeting held on 02 May 2013. Thank you for attending to discuss the application.

Issues Discussed

- The Committee requested you to confirm that all the cases in the study will be planned routine cases and no emergency cases will be included. You agreed to provide a written confirmation for the same.
- The Committee advised that the surgeons involved in the study should be blinded to all the data collect during the study. You agreed to comply.

Ethical opinion

The members of the Committee present gave a favourable ethical opinion of the above research on the basis described in the application form, protocol and supporting documentation, subject to the conditions specified below.

We plan to publish your research summary wording for the above study on the NRES website, together with your contact details, unless you expressly withhold permission to do so.

Publication will be no earlier than three months from the date of this favourable opinion

letter. Should you wish to provide a substitute contact point, require further information, or wish to withhold permission to publish, please contact the Co-ordinator Mr Rajat Khullar, nrescommittee.london-cityandeast@nhs.net.

Ethical review of research sites

NHS Sites

The favourable opinion applies to all NHS sites taking part in the study, subject to management permission being obtained from the NHS/HSC R&D office prior to the start of the study (see “Conditions of the favourable opinion” below).

Non NHS sites

The Committee has not yet been notified of the outcome of any site-specific assessment (SSA) for the non-NHS research site(s) taking part in this study. The favourable opinion does not therefore apply to any non-NHS site at present. I will write to you again as soon as one Research Ethics Committee has notified the outcome of a SSA. In the meantime no study procedures should be initiated at non-NHS sites.

Conditions of the favourable opinion

The favourable opinion is subject to the following conditions being met prior to the start of the study.

1. Please provide confirmation that all the cases in the study will be planned routine cases and no emergency cases will be included.
2. The surgeons involved in the study should be blinded to all the data collect during the study.

You should notify the REC in writing once all conditions have been met (except for site approvals from host organisations) and provide copies of any revised documentation with updated version numbers. The REC will acknowledge receipt and provide a final list of the approved documentation for the study, which can be made available to host organisations to facilitate their permission for the study. Failure to provide the final versions to the REC may cause delay in obtaining permissions.

Management permission or approval must be obtained from each host organisation prior to the start of the study at the site concerned.

Management permission (“R&D approval”) should be sought from all NHS organisations involved in the study in accordance with NHS research governance arrangements.

Guidance on applying for NHS permission for research is available in the Integrated Research Application System or at <http://www.rdforum.nhs.uk>.

Where a NHS organisation’s role in the study is limited to identifying and referring potential participants to research sites (“participant identification centre”), guidance should be sought from the R&D office on the information it requires to give

permission for this activity.

For non-NHS sites, site management permission should be obtained in accordance with the procedures of the relevant host organisation.

Sponsors are not required to notify the Committee of approvals from host organisations

It is responsibility of the sponsor to ensure that all the conditions are complied with before the start of the study or its initiation at a particular site (as applicable).

Approved documents

The documents reviewed and approved at the meeting were:

<i>Document</i>	<i>Version</i>	<i>Date</i>
Covering Letter		25 April 2013
Evidence of insurance or indemnity		17 August 2012
Investigator CV - Justin Phillips		
Other: Peer Review - Rupert Pearse		11 September 2012
Participant Consent Form: Consent Form	1	23 April 2013
Participant Information Sheet	1	23 April 2013
Protocol	1	23 April 2013
REC application		24 April 2013

Membership of the Committee

The members of the Ethics Committee who were present at the meeting are listed on the attached sheet.

Statement of compliance

The Committee is constituted in accordance with the Governance Arrangements for Research Ethics Committees and complies fully with the Standard Operating Procedures for Research Ethics Committees in the UK.

After ethical review

Reporting requirements

The attached document “After ethical review – guidance for researchers” gives detailed guidance on reporting requirements for studies with a favourable opinion, including:

- Notifying substantial amendments
- Adding new sites and investigators
- Notification of serious breaches of the protocol
- Progress and safety reports
- Notifying the end of the study

The NRES website also provides guidance on these topics, which is updated in the light of changes in reporting requirements or procedures.

Feedback

You are invited to give your view of the service that you have received from the National Research Ethics Service and the application procedure. If you wish to make your views known please use the feedback form available on the website.

Further information is available at National Research Ethics Service website > After Review

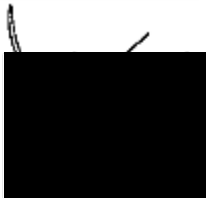
13/LO/0738

Please quote this number on all

We are pleased to welcome researchers and R & D staff at our NRES committee members' training days – see details at <http://www.hra.nhs.uk/hra-training/>

With the Committee's best wishes for the success of this project.

Yours sincerely



pp Dr Arthur T. Tucker
Chair

Email: nrescommittee.london-cityandeast@nhs.net

*Enclosures: List of names and professions of members who were present at the meeting and those who submitted written comments
"After ethical review – guidance for researchers"*

*Copy to: Ms Anna Ramberg
Mr Gerry Leonard, Barts Health - QMUL Joint Research Management Office*

NRES Committee London - City & East
Attendance at Committee meeting on 02 May 2013

Committee Members:

<i>Name</i>	<i>Profession</i>	<i>Present</i>	<i>Notes</i>
Dr Louise Abrams	Pharmacology (Vice Chair)	Yes	
Dr Chandan Alam	Experimental Pathology	Yes	
Dr Marie E Bardsley	Director	Yes	
Ms Jane Batchelor	Centre Administrator, Advanced Cardiovascular Imaging	No	
Dr Ayse Baxter	Independent Consultant Pharmaceutical Physician	Yes	
Mr Frank Cross	Consultant General and Vascular Surgeon	No	
Dr Miran Epstein	Senior Lecturer Medical Ethics	No	
Ms Janelle Hill	Non-medical lay member	No	
Professor Atholl Johnston	Professor of Clinical Pharmacology	No	
Professor Malcolm Law	Epidemiologist	No	
Mr John Lynch	Lay Member	Yes	
Mr Roger Maran		Yes	
Dr Eleni Palazidou	Consultant Psychiatrist & Honorary Senior Lecturer	Yes	
Professor Kim Piper	Consultant Histopathologist/Professor of Oral Pathology	Yes	
Dr Melanie Powell	Consultant Clinical Oncologist	No	
Dr Arthur T. Tucker	Principal Clinical Scientist & Honorary Reader, (REC Chairman)	Yes	
Ms Brigid Tucker	Non-Medical Lay Member	Yes	
Professor David Wingate	Gastroenterologist	Yes	
Dr Ariel Zosmer	Honorary Senior Clinical Lecturer	No	

Also in attendance:

<i>Name</i>	<i>Position (or reason for attending)</i>
Mr Rajat Khullar	Committee Coordinator

1. Z. Abdollahi, J. P. Phillips, P. A. Kyriacou; Evaluation of the optical interference in a combined measurement system used for assessment of tissue blood flow, SPIE BiOS, 7 - 12 February 2015, San Francisco, California, United States.
2. Z. Abdollahi, J. P. Phillips, P. A. Kyriacou; Evaluation of a combined photoplethysmography (PPG) and laser Doppler flowmetry (LDF) measurement system for simultaneously monitoring blood flow at different pressure; 35th Annual International IEEE EMBS Conference, July 3-7, 2013, Osaka, Japan.

Evaluation of the optical interference in a combined measurement system used for assessment of tissue blood flow

Zahra Abdollahi, Panayiotis A. Kyriacou, *Senior Member, IEEE* and Justin P. Phillips, *Member, IEEE*

Abstract— A dual-wavelength pulse oximetry system combined with laser Doppler was developed for the assessment of perfusion. Red and infrared PPG and Doppler signals were recorded from a healthy volunteer in three studies at different measurement sites to investigate the interference between PPG and laser Doppler flowmetry (LDF). Good quality photoplethysmographic (PPG) and Doppler signals were detected simultaneously using this combined probe from the skin of the finger. The influence of the PPG light sources on LDF measurements was investigated; also the influence of the LDF light sources to the PPG measurements was studied.

I. INTRODUCTION

Assessment of tissue perfusion can be achieved with various techniques including photoplethysmography and laser Doppler flowmetry (LDF). In photoplethysmography, changes in transmission of light through tissue due to pulsation of small arteries can be monitored while in laser Doppler flowmetry (LDF) microcirculatory blood cell velocity and flux can be studied [1].

The results presented here are part of a wider study in which a combination of LDF and PPG methods is used for assessment of perfusion in bowel tissue for patients undergoing bowel resection. Determination of bowel viability following bowel resection is essential in gastrointestinal surgery [1, 2, 3]. Monitoring blood flow in abdominal surgery especially intra and post-operatively would be a valuable tool for prevention of intestinal ischemia and necrosis, often requiring surgical re-exploration, resulting in significant postoperative morbidity and increased length of hospital stay. Although various monitoring techniques have been proposed to assess intestinal viability, none of these techniques have been proven reliable enough to replace visual observation [4]. The aim of the main study is to combine the established techniques, laser Doppler flowmetry (LDF) and Photoplethysmography (PPG), into one flexible probe intended for assessment of perfusion in abdominal tissue during bowel operation. Such a probe could alert the surgeon immediately of any compromise in blood flow so further investigation and if necessary, therapeutic steps can be applied immediately to prevent severe consequences. However in the present study, evaluation of optical interference between the two measurements was investigated.

B. Photoplethysmography (PPG)

Photoplethysmography, (PPG) a non-invasive electro-optical technique used mainly to determine and register the variation in blood volume or blood flow in the body caused by cardiovascular pulsations in the bed of tissue [5–6].

A photoplethysmographic signal is obtained by illuminating a region of tissue containing a vascular bed and acquiring either the reflected or transmitted light. Photoplethysmography (PPG) involves two basic optoelectronic components: an emitter such as a light emitting diode (LED) which illuminates the tissue and a photodiode for collecting the backscattered or transmitted. The intensity of light that reaches the photo detector can be measured which represent blood volume changes synchronous with the cardiac cycle [7].

The PPG signal consists of two components: a pulsatile ('AC') part, which is modulated by pulsations of (primarily) arterioles and a static ('DC') part which represents the light scattered from non-pulsing arterial blood, the venous and capillary blood and other static tissues. Two main PPG operational configurations include transmission and reflection mode. In transmission mode operation the tissue sample (e.g. fingertip) is placed between the source and detector while in reflection mode the LED and detector are positioned adjacently [8].

C. Laser Doppler flowmetry (LDF)

LDF is an optical and non-invasive method for monitoring microvascular blood flow and is currently used in a variety of fields in medicine [7], assessment of burn wound depth [9], skin tumor characterization [8], amputation level determination [10,11], neurosurgery [12], and breast reconstruction [13]. It has been used also for ocular, cerebral, cutaneous, auricular, splanchnic, and renal blood flow in a wide range of laboratory animal species [14].

Laser Doppler flowmetry (LDF) and photoplethysmography (PPG) are both well-established non-invasive optical methods for measuring blood flow changes in skin [12]. As they register perfusion effects at different tissue layers, application of both these methods infers a useful overall assessment of perfusion. Laser Doppler flowmetry can investigate the more superficial blood flow [13] while PPG can assess vessel pulsation deeper in the tissue [14]. Therefore the combination of LDF and PPG techniques into a single probe for estimating the degree of perfusion at different depths simultaneously would provide a new, improved method of assessing tissue viability.

II. MATERIALS AND METHODS

A. Evaluation of the system

Three main parts of the measurement system were developed and used in this study. These include the probe, instrumentation and a data acquisition system. A custom-made signal processing circuit separates the photoplethysmographic signals into its AC and DC components and amplifies each component. The AC PPG

Z. Abdollahi, P.A. Kyriacou and J. P. Phillips are with the School of Engineering and Mathematical Sciences, City University London, EC1V 0HB, UK (e-mail: zahra.abdollahi.1@city.ac.uk)

Evaluation of a combined reflectance photoplethysmography and laser Doppler flowmetry surface probe

Zahra Abdollahi, Justin P. Phillips, *Member, IEEE* and Panayiotis A. Kyriacou, *Senior Member, IEEE*

Abstract— this study presents evaluation of a system combining laser Doppler flowmetry and photoplethysmography (PPG) in a single probe for the simultaneous measurement of perfusion and blood flow in the finger. A cuff sphygmomanometer was used to partially occlude the arteries supplying the hand to investigate the effect of low pressure on photoplethysmographic and laser Doppler signals and also on calculated arterial blood oxygen saturation values (SpO₂). Red and infrared PPG and Doppler signals were recorded from six healthy volunteers at various pressures. Good quality signals were recorded in all subjects at low cuff pressures; however both PPG and Doppler signals showed a gradual decrease in amplitude at higher pressures. SpO₂ values calculated from the PPG signals showed higher deviation from measurements made on the contralateral hand using a commercial pulse oximeter at higher cuff pressures.

I. INTRODUCTION

Blood oxygen saturation level is very important in clinical physiological monitoring. In medicine, oxygen saturation indicates the percentage of haemoglobin binding sites in the bloodstream occupied by oxygen [1]. Various techniques measure the skin blood flow including Photoplethysmography and laser Doppler flowmetry (LDF). Photoplethysmography is a method of monitoring changes in transmission of light through tissue due to pulsation of small arteries while laser Doppler flowmetry (LDF) measures microcirculatory blood cell velocity and flux [2].

The results presented here are part of a wider study to combine LDF and PPG into a surface probe intended for evaluation of peripheral blood flow in abdominal tissue during bowel operations. Bowel viability assessment is essential in gastrointestinal surgery, and must be evaluated frequently during and after abdominal operation otherwise it can lead to intestinal ischemia and necrosis associated with an increased length of hospital stay, significant postoperative morbidity and mortality. Although numerous techniques of intraoperative bowel viability assessment like pulse oximetry, Polarographic measurement of oxygen tension, near-infrared and visible light spectrophotometry (NIRS & VLS) and intravital microscopy are available, only a few are applicable in bowel surgery. The majority of methods are still far from ideal [2]. Combination of these methods can be advantageous for bowel viability assessment. An optical sensor for assessment of the perfusion of the bowel has been proposed which may be placed on the bowel allowing the perfusion status and blood oxygen level before and after rejoining two parts of bowel

together to be assessed. The sensor could indicate the presence and magnitude of the circulation so allow early warning of ischaemia to the surgeon before damage occurs.

A. Photoplethysmography (PPG)

Photoplethysmography, (PPG) a non-invasive electro-optic method provides information on the blood volume changes in the body caused by cardiovascular pulsations in the bed of tissue [3]. A photoplethysmogram is obtained by illuminating a part of the body of interest and acquiring either the reflected or transmitted light. Photoplethysmography (PPG) involves two basic forms of optoelectronic which one for emitting monochromatic light into tissue and the other for collecting the light reflected back, or through, and not absorbed by tissue and blood. The intensity of light from emitter, which reaches the photodiode detector, will be measured to determine the blood volume changes. Variation in the signal correlates to several parameters of which pulsative changes in blood flow and blood volume are regarded as most important [4]. Typically PPG is a non-invasive technique and operates at red and infrared wavelength [5].

The PPG signal consists of two types of waveforms including a dominating DC-part and a pulsatile AC-part. AC component is a pulsatile waveform, which represents the pulsing of the blood in the arteries while DC component is a comprised of the absorption from the non-pulsing arterial blood, the venous and capillary blood. The AC-part is usually filtered out and amplified.

There are two main PPG operational configurations; the first one is transmission mode operation where the tissue sample (e.g. fingertip) is placed between the source and detector. And the second one is reflection mode operation where the LED and detector are placed side-by-side [6].

B. Laser Doppler flowmetry (LDF)

The Doppler Effect is utilised in laser Doppler flowmeters for measuring microvascular blood flow. In brief, a beam of laser light, carried by a fiber-optic probe attached to or inserted into the investigated tissue, interacts with moving components of tissue such as red blood cells [7] and is Doppler shifted while light interacting with static objects is unchanged. The light is then scattered and partly absorbed by the tissue to be investigated. The light is picked up by a returning fiber, converted into an electrical signal that is processed to provide an estimation of blood flow, called flux, which is the product of the velocity and the number of red cells in the volume of tissue interrogated by the probe [8]. Laser Doppler flowmetry (LDF) and photoplethysmography (PPG) are both well-established non-invasive optical methods for measuring changes in skin blood flow [9]. Through application of both these methods, the tissue blood flow in different tissue layers can be inferred. As laser Doppler flowmetry can study the more superficial blood flow [10] and

Z. Abdollahi, J. P. Phillips and P.A. Kyriacou are with the School of Engineering and Mathematical Sciences, City University London, London, EC1V 0HB, UK (e-mail: zahra.abdollahi.1@city.ac.uk)